Caractérisation structurale de protéines membranaires par échange hydrogène/deutérium spectrométrie de masse

Shahid Mehmood

THÈSE

Pour obtenir le grade de

DOCTEUR DE L'UNIVERSITÉ DE GRENOBLE

Spécialité : **Biologie Structurale et Nanobiologie**

Arrêté ministériel : 7 août 2006

Présentée par

Shahid MEHMOOD

Thèse dirigée par **Eric FOREST** et
codirigée par **Jean-Michel JAULT**

préparée à **l'Institut de Biologie Structurale Jean-Pierre Ebel**
dans **l'École Doctorale Chimie et Sciences du Vivant**

Caractérisation structurale protéines membranaires par échange hydrogène/deutérium spectrométrie de masse

Thèse soutenue publiquement le **28 février 2012**,
devant le jury composé de:

M. Patrice CATTY
Chercheur, CEA, Président
Mme. Sandrine SAGAN
Directeur de Recherche, CNRS, Rapporteur
M. Attilio DI PIETRO
Directeur de Recherche, CNRS, Rapporteur
Mme. Jeanine TORTAJADA
Directeur de Recherche, CNRS, Membre
M. Eric FOREST
Directeur de Recherche, CEA, Directeur de thèse
M. Jean-Michel JAULT
Directeur de Recherche, CNRS, Co-directeur de thèse

To

my beloved parents
my brothers Sohail,
Ayaz & Zahid bhai
& my sweetest sister
for their love, support and encouragement

Thanks

I am very much thankful to Eric & Jean-Michel for their encouraging attitude and supportive behavior during my PhD. For their immediate availability, whenever I had any question to ask they were always there to respond it. I am particularly thankful to them for their input to improve the thesis manuscript.
Eric & Jean-Michel thanks a lot!
Many thanks to Dr. Sandrine SAGAN and Dr. Attilio DI PIETRO for their kindness to accept the responsibility of thesis reviewer and preparing the reports in short time.
I wish to thank Dr. Patrice CATTY for accepting the responsibility of jury president and review the work. Thanks to Dr. Jeanine TORTAJADA for her presence and examining the thesis work.
I would like to thank members of my thesis committee: Prof. Winfried WEISSENHORN, Dr. Sandrine SAGAN and Dr. Elisabeth Le RUMEUR. The valuable comments and assessment by thesis committee during my PhD thesis was very helpful for me to carry on my research in a better way.
Many thanks to former mates in mass spectrometry group Julien, Izabel, Martial, Sophie and Benjamin. Julien was very kind to explain me the HDX-MS data analysis.
Thanks to members of Jean-Michel's team:
Hien-Anh, Ben, Bastien, Catherine, Anne-Emmanuelle and others.
Jonathan thank you very much for preparing the protein samples;
I wish you good luck for your thesis.
I am grateful to Petr Man for the support he provided from Prague to perform the MS/MS experiments. He was very kind to accommodate me in his lab for one week and provided me an opportunity to work on FT-ICR MS.

I would take this opportunity to thank all my Pakistani friends living in Grenoble specially Zahid Ishaque who made my stay in Grenoble more pleasant. Many thanks to other Pakistani friend living in different cities of France specially Usman, Ahsan, Sajjad, Shariq, Abdullah & AQ.
Thanks to administrative staff of IBS, Ecole Doctorale CSV and College Doctorale of UJF and particularly to Magali POUTIER for helping me on every step of the thesis preparation required by University.

Last but not least I am grateful to Higher Education Commission of Pakistan for awarding me the fellowship to carry out PhD in France.

Contents

List of Figures

List of Tables

List of Abbreviations

ABC	ATP-binding cassette
ADP	Adenosine diphosphate
AMP-PNP	5′-adenylyl-β-γ-imidodiphosphate
ATP	Adenosine-5’-triPhosphate
BCRP	Breast cancer resistance protein
BmrA	Bacillus multidrug resistance *ATP*
BSA	Bovine Serum Albumin
°C	Celsius Degree
CFTR	Cystic Fibrosis Transmembrane Conductance Regulator
Da	Dalton
DDM	n-dodecyl β-D-maltoside
DNA	Deoxyribonucleic acid
ECL	Extracellular loop
EDTA	Ethylene diamine tetra acetic acid
Emr	Escherichia coli multidrug resistance
ESI	Electrospray ionization
FT-ICR	Fourier-transform ion cyclotron resonance
H/DX	Hydrogen/deuterium exchange
HDX-MS	Hydrogen/deuterium exchange mass spectrometry
Hly	Haemolysin
ICD	Intracellular domain
ICL	Intracellular loop
IPTG	Isopropyl-Beta-thio-galactoside
kDa	kilo Dalton
LB	Luria-Bertani
MALDI	Matrix-assisted laser desorption/ionization
MATE	Multidrug and toxic compound extrusion
MDR	Multi drug resistance
mRNA	Messenger ribonucleic acid
MFS	Major facilitator superfamily
MRP	Multidrug resistance-associated protein

MS	Mass spectrometer
NBD	Nucleotide-binding domain
OD	Optical density
PAGE	Poly acrylamide gel electrophoresis
PDB	Protein data bank
Pi	Inorganic phosphate
PMSF	Phenyl methane sulphonyl fluoride
RNA	Ribonucleic acid
RND	Resistance-nodulation division
SBP	Substrate binding protein
SDS	Sodium dodecyl sulfate
SMR	Small multidrug resistance
TAP	Transporter associated with antigen processing
TEMED	N,N,N',N'-tetra methyl ethylene diamine
TMD	Transmembrane domain
ToF	Time-of-flight
tRNA	Transfer ribonucleic acid
(v/v)	Volume/volume
(w/v)	Weight/volume

Introduction

Membrane proteins perform vital functions like import of nutrients, binding site for ligands and export of harmful substances out of the cell.

ABC transporter is one of the largest families of membrane proteins and some ABC exporters are known to be involved in efflux of antibiotics. The acquisition and transport mechanism of these substrates by the exporters has been a question to address. High resolution X-ray structures of ABC exporters showed two extreme conformations: inward facing and outward facing conformations. In both structures the interaction between intracellular part of transmembrane domain and nucleotide-binding-domains was conserved. X-ray structures showed the conformation of exporters in a static manner and using a dynamic technique could provide information about the intrinsic flexibility of exporters. This flexibility might be essential in order to bind the drug substrates.

Hydrogen deuterium exchange in combination with mass spectrometry (HDX-MS) has been used during last two decades to probe the dynamics of proteins. The technique is now expanding its application to membrane proteins dynamics and conformational changes. HDX-MS requires less sample amount, is tolerant to the presence of solubilizing agents as in the case of membrane proteins. Recently it was shown that the technique can be used to probe the dynamics of membrane proteins in near physiological condition.

In the presented study HDX-MS is applied to probe the dynamics of three membrane proteins: BmrA, BmrC/BmrD and GLIC, a pentameric channel.

BmrA is a homodimeric ABC exporter from *Bacillus subtilis*. Limited proteolysis show that the exporter adopts two different conformations: apo form less resistant to protease and an ATP bound form which is much more resistant to protease digestion. With limited proteolysis but also using global HDX kinetics it was shown that in detergent or in membrane the global behavior of BmrA is similar. Using local HDX kinetics we show that ICDs of BmrA are highly dynamic in apo conformation but not in the closed form.

The local HDX kinetics of BmrA Walker ‘A’ mutant, K380R, show that in presence of ATP/Mg this mutant is unable to close but adopts a conformation in between apo state and closed state.

BmrC/BmrD is a heterodimeric ABC exporter from *Bacillus subtilis*. For BmrC/BmrD again HDX-MS kinetics are determined in apo and closed states. The exporter is found dynamic in apo state but closed form of the transporter is not as tight as that found for BmrA homodimer.

GLIC is a ligand gated ion channel recently identified from *Gloeobacter violaceus*. The effect of change in pH on different regions of channel is studied by HDX-MS. Local HDX kinetics show five monomers of GLIC are arranged in symmetrical manner. The kinetics difference between pH 4 and pH 7 clearly show that the channel adopts different conformation due to its closure at physiological pH. The main difference of HDX kinetics is found on the transmembrane and extracellular domain interacting regions.

Literature Review

Chapter 1. Antibiotics:

The influence of bacteria and other microorganisms in our daily life is at very large scale. It is considered that bacteria are present everywhere in our surroundings and a number of biological processes are occurring due to their presence. The number of microbes found on the body of a healthy adult is several times more than the total number of its own cells. But disease is produced by some specific bacteria which are categorized as pathogenic. These pathogenic bacteria normally do not inhabit in host body except when the target is affected. Antibiotics were introduced to counteract against these bacteria.

Antibiotics are chemical compounds, administered to kill pathogenic bacteria. The idea to introduce the antibiotic and increase the life expectancy was highlighted in 1940s and provided a sense of security which was proved false in the coming years.

The bacteria came out with unique strategies against these administered antibiotics and minimize or in some cases nullify their effectiveness, what we call now antibiotic resistance. The hallmark feature of the antibiotic resistance is multidrug resistance (MDR) means that a cell resists to the drugs which are structurally and functionally unrelated. Sometimes, this resistance is based upon the experiences, cells had already learnt from previous drugs contact.

Before we go to further details of MDR, let's recall about antibiotics and their mode of action.

Antibiotics can be classified into different groups based on their functional group or mode of action. Bacteria wherever they are present grow and divide to continue producing more and more colonies of their offspring. Hence, antibiotic can be also divided into two types, those which stop bacteria growth and those which can kill the bacteria. The first one does not kill the bacteria but has proven very effective as they stop the spreading of the infection and provide enough 'time' to host immune system to react against infection.

Antibiotics can be further classified into different types based on their mode of action. In addition to their mode of action antibiotics are also classified based upon their diversity of target.

Table 1. Common examples of antibiotics and targeted microorganisms

Target Diversity	Targeted Bacterial Organisms	Common Examples
Narrow Spectrum	Gram-positives (*Actinomyces*, *Corynebacteria*, *Bacillus*, *Clostridium*, Pyogenic cocci, Spirochetes)	Macrolides (Erythromycin) Polypeptides (Polymyxin)
Moderate Spectrum	Gram-positives plus systemic, enteric and urinary tract Gram-negatives	Sulfonamides,Aminoglycosides (Streptomycin, Gentamycin, Tobramycin)
Broad Spectrum	All prokaryotes except *Mycobacteria* and *Pseudomonas*	Chloramphenicol,Tetracycline
Anti-mycobacterial	*Mycobacteria*	Isoniazid,Ethambutol,Streptomycin Rifampin

1.1. Antibiotics mode of action:

The antibiotics used to control bacterial growth are of different types, targeting various sites with versatile mode of actions (Figure 1).

1.1.1. Antibiotics altering cytoplasm membrane:

Cell membrane wraps around the cytoplasm is the hallmark feature of living organisms. It keeps the cell protected and unaffected from their surroundings. It is believed that this membrane is a complex mixture of lipids carrying protein molecule and these protein molecules provide the passage for the substances to cross the membrane. Furthermore there are protein molecules covalently linked with carbohydrates and lipids with diverse functions.

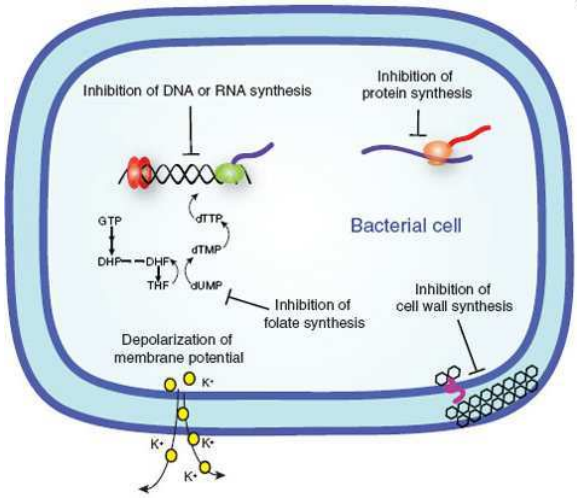

Figure 1. Antibiotics mode of actions: The different strategies adopted against bacterial growth in a nutshell (Clatworthy, Pierson et al. 2007).

Some antibiotics destabilize the lipid bilayer, distorting the regular cell structure of bacteria leading to their death (Figure 2). The antibiotics affecting the bacterial cytoplasm membrane are toxic for mammalian organisms and apparently they can not be used to target the bacteria inside the living organism. The action of these compounds are limited to Gram-negative

bacteria only, these are high molecular weight positively charged molecules which displace the negatively charged phospholipids on the surface of bacteria (Dixon and Chopra 1986).

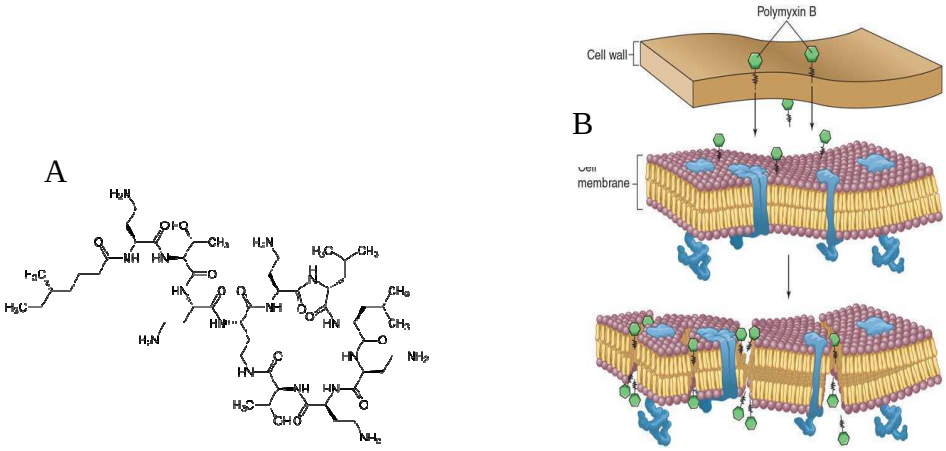

Figure 2. A. Colistin is one of the antibiotics effecting cell membrane. The drug is able to cross the cell wall and destabilize the lipid bilayer. B. Polymyxin is able to cross the cell wall and then destabilize cytoplasmic membrane (Web link: http://quizlet.com/6100231/chc-micro-150-exam-5-final-redux-flash-cards/).

1.1.2. Antibiotics inhibit bacterial cell wall synthesis:

Bacterial cell wall provides the first line of defense to bacteria in severe conditions; it maintains the shape of the cell and keeps the cell alive in case of water loss. The properties of bacterial cell wall are mainly attributed to the peptidoglycan. The peptidoglycans are made up of carbohydrates chains and these chains are linked by peptides comprising of unusual D-amino acids (van Heijenoort 2001). Since peptidoglycans are the most important components of bacterial cell wall, some antibiotics target peptidoglycan synthesis which eventually leads to death of bacteria.

The synthesis of peptidoglycan takes place in three steps and there are antibiotics targeting these particular steps. The first and irreversible step is the transfer of phosphoenolpyruvate to the hydroxyl moiety of UDP-N-acetyl glucosamine catalyzed by MurA enzyme (UDP-N-actetylglucosamine-3-enolpyruvyltransferase) (El Zoeiby, Sanschagrin et al. 2003).

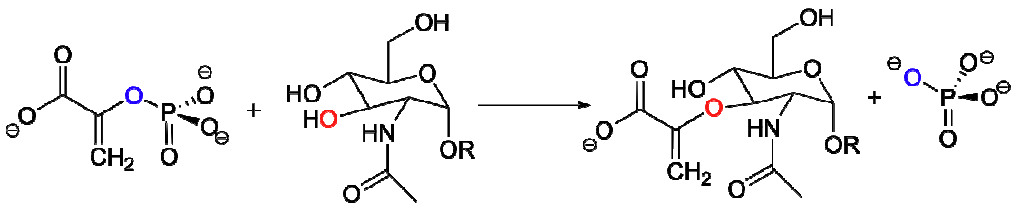

phosphoenolpyruvate (PEP) UDP-*N*-acetylglucosamine

Fosfomycin halts first step of peptidoglycan synthesis by inactivating MurA enzyme. It has a broad spectrum of target and it is effective against both Gram-positive and Gram-negative bacteria. Since mammalian cell enzymes are not affected by fosfomycin, it has been used as potent antibacterial agent to treat infection (Marquardt, Brown et al. 1994).

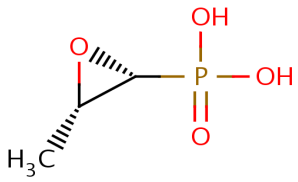

Fosfomycin

Once the precursor of peptidoglycan is synthesized, it must be transported outside the cytoplasm to the growing peptidoglycan. This transfer of the precursor is catalyzed by enzymes linked to the membrane. The enzymes modify the precursor into GlcNAc-ß-(1,4)-MurNAc-(pentapeptide)-pyrophosphoryl-undecaprenol and transfer this hydrophilic molecule across the hydrophobic membrane. It is also believed that this transfer is also accompanied by flip flop of lipid molecules but no biochemical evidence ha been obtained so far (Scheffers and Pinho 2005).

1.1.3. Protein synthesis and antibiotics:

Proteins are essential molecules found within living organisms along with lipids, carbohydrates and nucleic acids. Production of new proteins transcribed by the mRNA is essential for metabolism and growth of organism. Ribosomes are the machines of protein production and shutting down these machines will stop protein synthesis. In bacteria, protein synthesis is carried out on 70S ribosome (30S and 50S ribosomal subunit) with help of some proteins. Hence, any compound that can bind to the ribosomes or protein can be used as antibiotic. The protein synthesis is divided into three steps initiation; elongation and termination; some antibiotics target initiation and elongation steps (Figure 3).

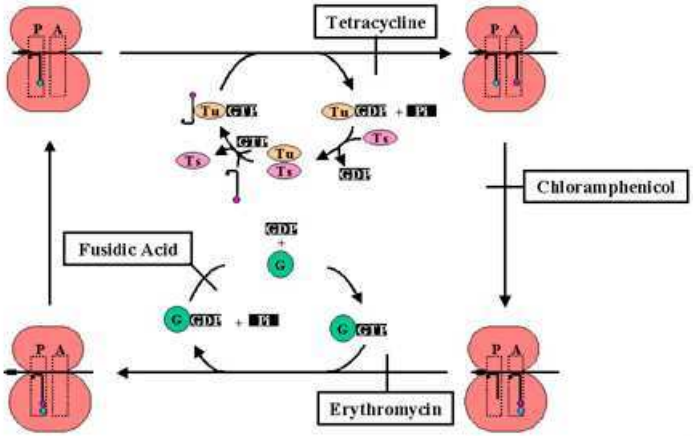

Figure 3. The steps of protein synthesis and antibiotics acting to halt the protein synthesis (Web link: *pathmicro.med.sc.edu/mayer/antibiot.htm).*

1.1.3.1. Antibiotics action on 30S ribosomal subunit:

The antibiotics affecting the 30S ribosomal subunit can be divided into three classes of compounds: Aminoglycosides , tetracyclines and spectinomycin.

Aminoglycosides:

The initiation of protein synthesis requires the 30S ribosomal subunit, mRNA and tRNA. Amnioglycosides target the complex of protein synthesis initiation and bind to the 30S ribosomal subunit and stop the initiation of protein synthesis. The antibiotic is also affected for the blockage of protein chain elongation. Since the binding is irreversible, the effect on bacteria is bactericidal (Shakil, Khan et al. 2008; Durante-Mangoni, Grammatikos et al. 2009). Kanamycin, neomycin, streptomycin and tobramycin are some examples of aminoglycosides.

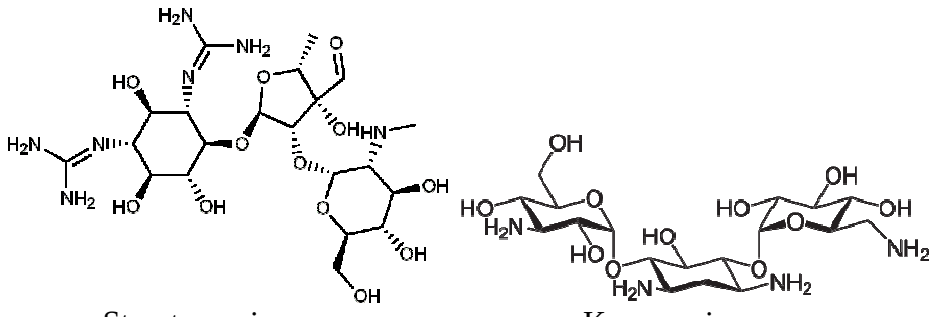

Streptomycin Kanamycin

Streptomycin and Kanamycin target protein synthesis in bacteria. These two antibiotics are widely used in molecular biology for screening of resistant strain and for overproduction of recombinant proteins.

Spectinomycin :

Spectinomycin share structural similarity with aminoglycosides but its binding to the 30S-mRNA-tRNA complex is reversible and therefore classified as bacteriostatic. Like other aminoglycosides, spectinomycin is also used in combination with penicillin and proved useful to overcome the resistance developed by bacteria against the drug (Boslego, Tramont et al. 1987).

Tetracyclines:

Tetracyclines are another class of compound binding to the 30S ribosomal subunit, they target the mRNA and ribosomal unit complex and stop the protein synthesis by inhibiting the binding of tRNA. The binding to the 30S subunit is reversible and therefore effect is bacteriostatic. This class of antibiotics targets a broad range of target bacteria (Borderie, Hernvann et al. 2001), doxycycline and minocycline are examples of tetracyclines.

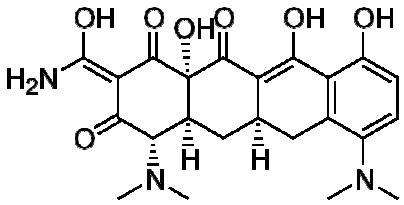

Minocycline

1.1.3.2. Antibiotics Action on 50S ribosomal subunit:

There are two groups of compounds acting on 50S ribosomal subunit: Lincosamides and Macrolides

Lincosamides:

The 50S ribosomal subunit performs enzymatic function by catalyzing the peptide linkage formation between amino acids. This aminoacyl transferase activity of the ribozyme is inhibited by the binding of lincomycin or clindamycin to the 50S ribosomal subunit (Spizek and Rezanka 2004).

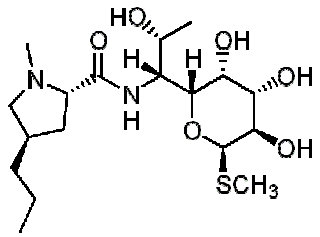

Lincomycin one of the example of Lincosamides

Macrolides:

The 50S ribosomal subunit in addition to enzymatic activity receives tRNA carrying acylated amino acid. tRNA binds on position A of the ribosome and after the peptide linkage between newly made chain and amino acid, 'free' tRNA moves onto position 'P' of 50S ribosomal unit. Macrolides compounds bind to the 'P' position of 50S subunit and inhibits the transfer of tRNA from 'A' to 'P' position. Clarithromycin and azithromycin are common examples of macrolides acting on broad spectrum of bacteria.

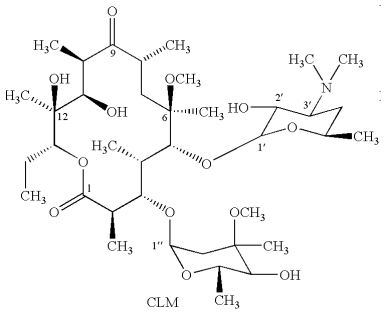

Clarithromycin

1.1.4. Antibiotics targeting nucleic acid synthesis:

The antibiotics targeting nucleic acid synthesis in prokaryotes are the most widely used antibiotics in clinical practice. This is due to the fact that the RNA and DNA synthesis enzymes in prokaryotes and eukaryotes are different and therefore provide selectivity measure for the drug action.

1.1.4.1. RNA synthesis inhibitors:

Tuberculosis is the leading cause of death due to an infectious disease worldwide and rifampicin is widely used for the treatment of tuberculosis (Dye 2006). Rifamapicin binds to the β-subunit of RNA polymerase which is responsible for initiation of RNA synthesis and elongation. Earlier biochemical data showed that the drug inhibits the RNA synthesis initiation and once synthesis is began, there is no effect conferred by the drug (Neu and Gootz 1996). But recent advancement particularly crystal structure of RNA polymerase (RNAP) in complex with rifamapicin proved that the agent blocks elongation step of RNA (Campbell, Korzheva et al. 2001). Rifamycin and rifampicin are other antibiotics acting on RNAP. The binding of the drug is tight and the effect is bactericidal (Yusibov and Streatfield 2010).

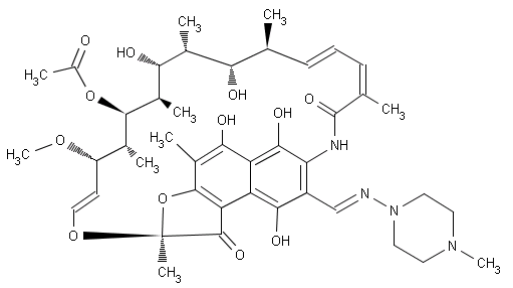

Rifampicin

1.1.4.2. DNA synthesis inhibitors:

The double stranded structure of DNA is based on the super-coiling of its anti-parallel strands. The winding and unwinding of these strands are catalyzed by a group of enzymes called the topoisomerases. Only unwound DNA can serve as template for both DNA and RNA synthesis. For newly made DNA strand, super-coiling is carried out by gyrase enzyme and this enzyme is also the target of antibiotics (Reece and Maxwell 1991). Quinolones are compounds acting on gyrase enzyme, they bind to the 'A' subunit of the enzyme and halts the super-coiling (Drlica and Zhao 1997).

Nalidixic acid is an example of quinolones.

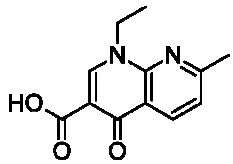

Nalidixic acid

1.1.5. Inhibition of metabolic pathways:

The antibiotics used for targeting metabolic pathways are relatively less in number and in use. Most effective antibiotics are those which alter the folic acid synthesis pathway. The end product of folic acid synthesis pathway is tetrahydrofolate which has key role in peptidoglycan, DNA and RNA synthesis (Maden 2000). The synthesis of tetrahydrofolate takes place in three steps catalyzed by different enzymes (Figure 4).

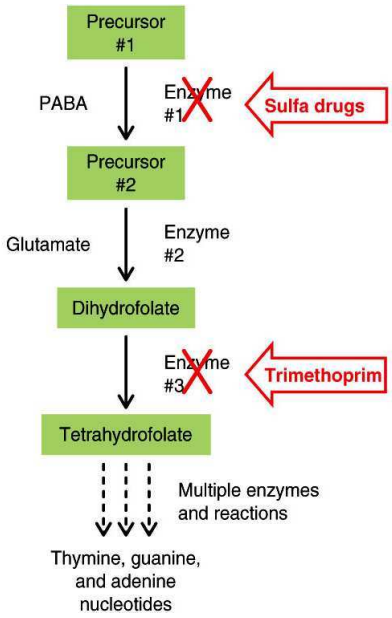

Figure 4. The biosynthesis of folic acid within bacteria can be inhibited by two different antibiotics each affecting on a different step of the synthesis.

Sulfonamides (sulfa drugs) and trimethoprim are two families of compounds acting on different steps of tetrahydrofolate synthesis. The sulfa drugs share the structural similarity with para-aminobenzoic acid (PABA), the natural substrate of enzyme. There is competitive inhibition observed between drug and substrate (Dozzo and Moser). Trimethoprim binds to the enzyme dihydrofolate reductase and inhibits the conversion of dihydrofolate to tetrahydrofolate. Like sulphonamide, the inhibition by trimethoprin is competitive against the natural substrate and results in a dead enzyme-inhibitor complex (Parry 2003; Then 2004). Trimethoprim is generally administered in combination with sulfonamide both acting on Gram-positive and Gram-negative bacteria (Antoniou and Gough 2005). The enzymes required for the synthesis of folic acid are not found in eukaryotes thus bacterial systems are specifically targeted by mentioned drugs.

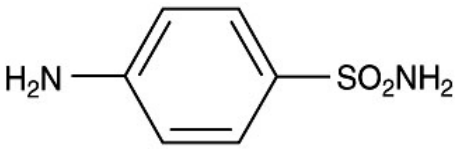

Sulfonamides

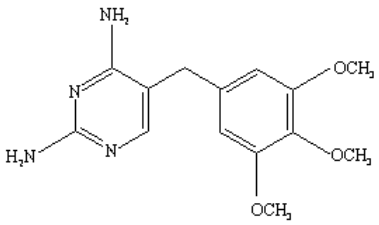

Trimethoprim

Chapter 2. Antibiotic resistance:

The wide use of antibiotic soon after their discovery and/or synthesis led to a problem which was not anticipated by the scientists. Bacteria developed some modification in their phenotype and started preparing themselves ready to combat with administered antibiotics. The modification is not limited to phenotype but also incorporated in the genotype of some species making them prepared for long battle. The pace of antibiotic resistance emergence was almost same as was of antibiotic introduction (Figure 5).

Focus of a great deal of biomedical and biochemical research has been to overcome this resistance but problem emerges more. Because in most of the cases the mechanism of drug resistance is not limited to one strategy, it has diversity, but the result is the same nullifying the action of drug.

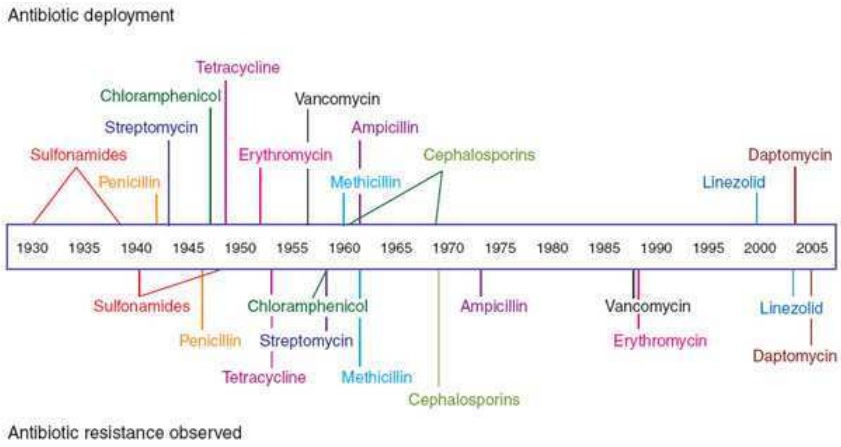

Figure 5. Time line of antibiotic administration and resistance emerged showing that the resistance was found shortly after the use of antibiotic against bacteria (Clatworthy, Pierson et al. 2007).

Different sites are targeted by various antibiotics within the bacteria using different mode of actions, in response bacteria has also shown multidimensional strategies not limited to only mean of survival. It is possible that many more ways of resistance against antibiotic by bacteria will be identified in future but three strategies are investigated in detail yet (Figure 6). The resistance of the bacteria towards a drug or compound can be either passive or active (acquired). There are number of natural shields provided by the nature to bacteria to survive in extreme conditions. These factors are equally distributed among pathogenic or non-pathogenic bacterial species. While introducing antibiotics these passive ways of resistance were in consideration by the scientists and therefore this kind of resistance was overcome easily.

The second and major mean of resistance is of active type in which bacteria acquire the genetic elements and express them in response to antibiotic encounter.

Although all the means of active resistance are potent and effective, the most important one is the active efflux of the drug by integral membrane proteins called exporters. These exporters are the main reason behind the multi-drug resistance because of their ability to export diverse arrays of compounds which are even unrelated in their structure.

Each type of active resistance will be discussed in detail:

- Enzymatic effect on the drug
- Modification of the drug target protein
- Reduced drug accumulation by active efflux and less permeability

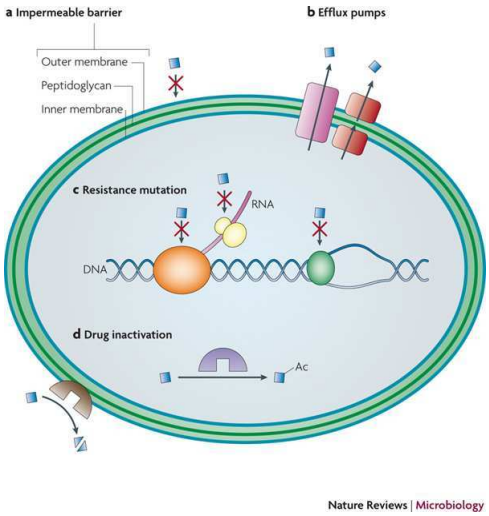

Figure 6. Summary of mechanisms of antibiotic resistance conferred by Gram-negative bacteria (Allen, Donato et al. 2010).

2.1. Enzymatic alteration of the drug

Penicillin is a group of antibiotics which are characterized and widely used around the globe. Penicillium is a fungus which serves as source for penicillin compound and many derivatives of penicillin are being used as clinical drugs. First proof of the effectiveness of the compound against bacteria lies back in 1871 when Sir John Burdon-Sanderson observed difference in turbidity of bacteria media in presence or absence of penicillium mold growth (Selwyn 1979).

The modification of the administered compound (drug) by the bacteria is one of the active types of resistance against antibiotics. The resistance is due to expression of broad spectrum of enzymes under selective pressure of an antibiotic or group of antibiotics.

The following table provides the information about different enzymes, their mode of action and plausible targeted antibiotics (Wright 2005).

Table 2. Enzymatic strategies of antibiotic inactivation (Wright 2005)

	Strategy	Type	Examples of antibiotics effected
Antibiotic Destruction	Hydrolytic	β-lactamses	β-Lactams
		Esterases	Macrolides
		Epoxidases	Fosfomycin
	Non hydrolytic	Lyases	Type B streptogramin
Antibiotic Modification	Group transfer	Acyl	Aminoglycoside
			Chloramphenicol
			Type A streptogramin
		Phosphoryl	Aminoglycoside
			Macrolide
			Rifamycin
			Peptide
		Thiol	Fosfomycin
		Nucleotidyl	Aminoglycoside
			Lincosamide
		ADP-ribosyl	Rifamycin
		Glycosyl	Macrolide
			Rifamycin
	Other	Redox	Tetracycline
			Rifamycin
			Type A streptogramin

The enzymatic action imposed by bacteria directly on the antibiotics are specific i.e. expression of a particular enzyme in response to one particular antibiotic or a class of structural similar compounds. The enzymatic effect on antibiotics can be of two types:

Destruction of the antibiotic
Chemical modification of antibiotic

There are two types of enzymatic strategies employed: hydrolytic and non-hydrolytic.

In the hydrolytic, enzyme requires no other cofactor except water. Therefore, these hydrolytic enzymes present first wall of defense and destroy the antibiotic even outside the cytosol.

β-lactamase:

Penicillin and its derivatives are recognized by the presence of β-lactam ring and hydrolysis of the ring is the target of β-lactamase enzymes. β-lactamases encoding genes are present on both bacterial chromosomes and transferable DNA content plasmid. There is a wealth of literature dedicated for the functional classification of β-lactamases including (Bush 1989;

Bush, Jacoby et al. 1995; Arakawa 1999; Bebrone 2007; Bush and Jacoby) but recent classification proposed provides an updated and detail classification (Bush and Jacoby 2010). The enzymes are classified into four groups from A to D. Briefly there are two main mode of action employed by the enzymes i.e. those mimicking serine proteases (Group A, C & D) and others like metallo proteases (Group B). With the introduction of new antibiotics the number and even the mechanism of the enzymes are evolving (Jacoby and Munoz-Price 2005).

2.2. Modification of the drug target protein:

In general bacteria lack the enzymes required for hydrolysis and /or modification of synthetic (non-natural source) antibiotics therefore alteration of drug target is a way of conferring drug resistance (Nikaido 2009). This alteration can be mutation of the target protein or in some cases bacteria adopts changes in usual metabolic pathways hence avoiding some intermediates which were possible target of the antibiotics (Perichon and Courvalin 2000; Hooper 2002). For example, the effect of fluoroquinolones is minimized by mutation of one amino acid of DNA replication enzyme however the activity of enzyme is also retained (Hooper 2000).

2.3. Active efflux of the drugs:

The most active and efficient way adopted by the bacteria to show resistance against antibiotics is the active efflux. This active efflux of compounds is carried out by membrane transporters. These membrane proteins The substrate can be caught from cytoplasm or directly from inner leaflet of phospholipid bilayer The phenomenon of MDR is attributed to these transporters as they are able to extrude variety of compounds belonging to different families with distinct structures. Since the active efflux is energy dependent process it is not surprising that there are energy sources for the functioning of these pumps. In fact basic classification is based on the energy source used.

There are primary type of MDR transporters, some of them belong to the ABC superfamily, which use ATP as energy source and secondary type of transporters those rely on other energy sources like concentration gradient of proton or sodium ion (Figure 7).

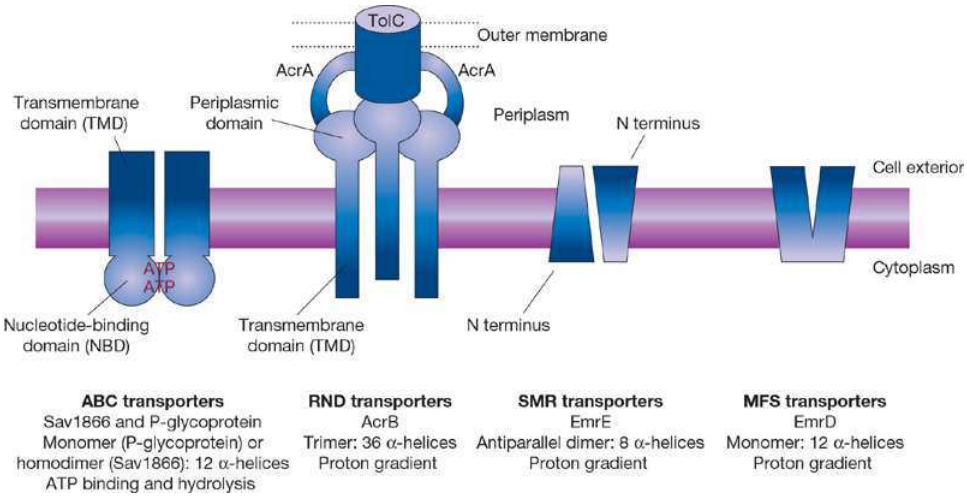

Figure 7. The transporters involved in efflux of antibiotics vary in their size and topological arrangement within cell membrane (Higgins 2007). Pink border is possible position of lipid bilayer.

2.3.1. SMR Transporters:

Small multidrug resistance or SMR is the family of integral membrane protein conferring resistance against particularly (but not exclusively) against positively charged ions such as tetraphenylphosphonium (TPP^+), cetyltrimethylammonium bromide (CTAB), and benzalkonium (Bz) (Bjorland, Sunde et al. 2001; Nishino and Yamaguchi 2001; Ubarretxena-Belandia, Baldwin et al. 2003). This is the smallest MDR transporter family both in terms of

Table 3. Examples of the members of SMR Transporters (Some are homo-dimer like EmrE and some form hetero-dimer like EmrA/EmrB)

Name of Transporter	**Organism**
EbrA	*Bacillus subtilis*
EbrB	*Bacillus subtilis*
EmrE	*Escherichia coli*
Mmr	*Mycobacterium tuberculosis*
QacE	*Gram-negative bacteria*
Smr (Emrb/QacC/QacD)	*Staphylococcus aureus*
YkkC	*Bacillus subtilis*
YkkD	*Bacillus subtilis*

protein size with 100-110 residues (12 kDa) and number of its family members (Chung and Saier 2001; Sharoni, Steiner-Mordoch et al. 2005). It consists of only transmembrane domain without any cytosolic or extracellular domain. The membrane spanning region consists of four α-helices which traverse the membrane and linked by very short intracellular and extracellular loops. The transmembrane helices provide the pathway for the substrate translocation, this

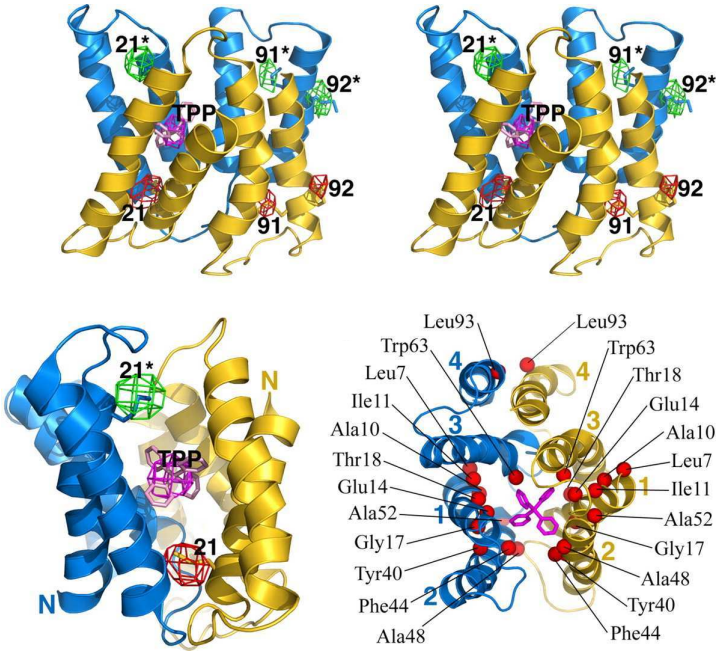

Figure 8. EmrE binds TPP as an antiparallel dimer. Stereo view of the EmrE transporter in complex with TPP. The two monomers are colored blue and yellow, and the bound TPP is pink (Chen, Pornillos et al. 2007).

pathway is achieved by the dimerisation of two monomers in antiparallel fashion (Figure 8) (Yin, He et al. 2006).

Since both monomers are aligned in an antiparallel manner the accessibility of the substrate towards the transporter is considered as unchanged. If both sides have equally affinity for substrate then how is it translocated against concentration gradient across membrane?

To answer the question, EmrE is used as a model representative of the SMR family. The structure of EmrE was solved at reasonable resolution (Chen, Pornillos et al. 2007) (Figure 8) and it remains highly stable and functionally active even in detergent solubilized state (Schuldiner 2009). Briefly, it is shown that EmrE requires two protons as energy cross for the translocation of one substrate molecule from cytoplasm to periplasmic space. The highly conserved glutamate at position 14 is considered as responsible for the binding and uphill transport of the substrate (Grinius and Goldberg 1994; Yerushalmi and Schuldiner 2000; Sharoni, Steiner-Mordoch et al. 2005).

2.3.2. Resistance-nodulation-division transporters:

Resistance nodulation division transporters are one of the key factors responsible for multidrug resistance in Gram-negative bacteria. The RND transporter such as AcrB (an integral membrane protein) acts in combination with AcrA and TolC and extrude the drug outer surface of the cell membrane (Figure 9). This mechanism of drug efflux outside the cell

membrane explains the intrinsic resistance of Gram-negative bacteria which was first thought to be only due to less permeability of the outer membrane for the drug (Vaara 1993; Nikaido, Basina et al. 1998; Murakami 2008). In addition to RND transporters, there are other RND proteins responsible for diverse cellular functions like regulation of cell cycle and organization of cytoskeleton. The RND proteins are equally distributed within prokaryotes and eukaryotes (Ko, Gordon et al. 2001; Ma, Erkner et al. 2002).

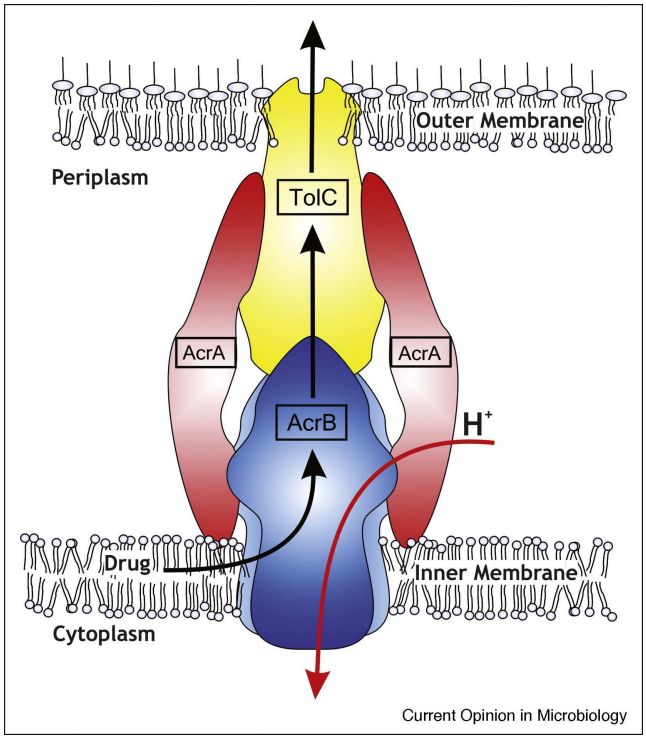

Figure 9. RND transport complex consisting of RND transporter (AcrB) which works in coordination with outer membrane pump (TolC). The intermediate role of membrane fusion protein (AcrA) in complex between AcrB and TolC is shown in schematic presentation (Blair and Piddock 2009).

2.3.2.1. AcrB:

AcrB is the integral cytoplasmic membrane part of the three member complex, responsible for extrusion of the drugs from cytoplasm. AcrB is first harboring point for drug export driven by proton motive force. As other multidrug transporters, AcrB recognizes and binds to wide array of substrates nevertheless showing priority for lipophilic compounds like ethidium bromide, cephalosporins, fusidic acid and even different detergents (Nikaido and Takatsuka 2009).

AcrB is first member of secondary type multidrug transporters whose structure became available, the structure was solved for first time in year 2002 (Murakami, Nakashima et al. 2002). In coming years release of more structures helped to explain the mechanism of AcrB

functioning (Yu, McDermott et al. 2003; Murakami, Nakashima et al. 2006; Seeger, Schiefner et al. 2006; Das, Xu et al. 2007; Tornroth-Horsefield, Gourdon et al. 2007; Drew, Klepsch et al. 2008).

The obtained structural data shows that the AcrB functions as a trimer consisting of three similar subunits. Each subunit can be divided into two parts periplasmic domain, which is involved in interaction with TolC, and transmembrane domains. The transmembrane domain consists of twelve α-helices traversing the cytoplasmic membrane (Figure 10). Each subunit carries a drug binding site (lower part) to catch the drug from cytoplasm, the captured drug is then moved to upper part of AcrB and eventually released to TolC. On any given time, only one site of the three monomers can bind with drug and sites on other monomers are potentially inaccessible. The energy required for the conformational change to transport is driven by the proton downhill concentration movement.

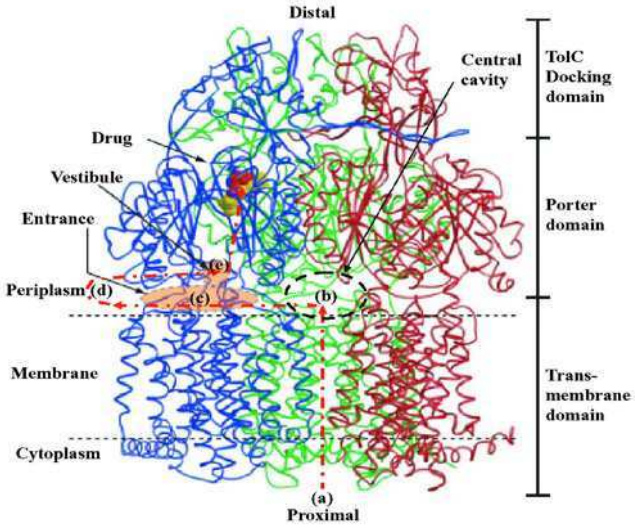

Figure 10. AcrB makes a homotrimer giving rise to a functional transporter in cytoplasmic membrane. Each monomer can be divided into three domains: Transmembrane domain, porter domain and TolC interacting domain (Murakami, Nakashima et al. 2002).

2.3.2.2. TolC:

The substrate caught by AcrB either from cytoplasm or from cytoplasm lipid bilayer is transferred to a huge outer membrane protein called as TolC. TolC interacts with AcrB and traverse the outer membrane and release the substrate on the outer surface of the Gram-negative bacteria. In addition to the drugs captured by AcrB, the drugs present in periplasmic space are also effluxed to outer cell membrane by TolC. This activity of TolC has an important role in drug efflux system because many integral membrane efflux pumps catch the drugs from cytoplasm and release in periplasmic space and target of many antibiotics also exist in periplasmic space (Blair and Piddock 2009; Eicher, Brandstatter et al. 2009).

The structure of TolC was solved in 2000 followed by another structure of its homologue OprM (Koronakis, Sharff et al. 2000; Akama, Kanemaki et al. 2004). The structure shows a trimeric arrangement of TolC which give rise to a tube like shape providing the pathway for the compounds to be exported. Each monomer of TolC can be divided into two: parts periplasmic and transmembrane. The periplasmic part is formed by six coiled-coiled helices, the arrangement of these helices give rise to a tubular structure. The transmembrane part majorly consists of β-barrels which are connected by extracellular loops (Figure11) (Koronakis, Sharff et al. 2000).

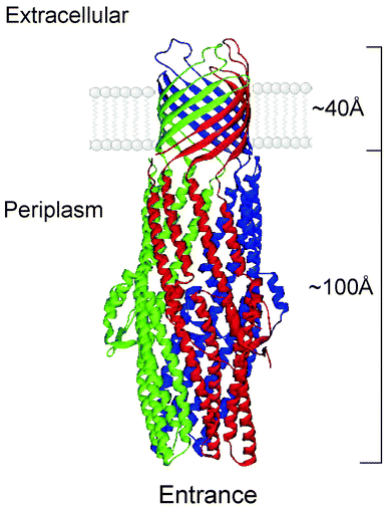

Figure 11. The x-ray structure of TolC consisting of long cyliserical shape providing the passage for the drugs to be extruded on the outer surface of the cell membrane og Gram-negative bacteria (Koronakis, Sharff et al. 2000).

Table 4: RND family multidrug efflux systems in Gram-negative bacteria (Poole 2001).

RND family multidrug efflux systems of Gram-negative bacteria [3,4•].

Organism	Efflux components			Regulatory gene(s)	Expression*	Substrates†
	MFP	RND	OMF			
B. cepacia	CeoA	CeoB	OpcM	?	wt/–; mutant/+	CM, CP, TP
B. pseudomallei	AmrA	AmrB	OprA	*amrR*	wt/+	AG, ML
E. coli	AcrA	AcrB	TolC	*acrR, marA, robA, soxS*	wt/+; *marR*/++‡; *acrR*/++	AC, BL, BS, CM, CV, EB, ER, FA, FU, NV, PO, SDS, TC, TR, TX
	AcrE	AcrF	TolC	*acrS*	wt/–; mutant/+	as for AcrAB–TolC
	?	AcrD	?	?	wt/+	AG
H. influenzae	AcrA	AcrB	?	?	wt/+	AC, CV, EB, ER, NV, RF, SDS
N. gonorrhoeae	MtrC	MtrD	MtrE	*mtrR, mtrA*	wt/+; *mtrR*/++; *mtrA*/–	AZ, CP, CV, ML, PN, RF, TX
P. aeruginosa	MexA	MexB	OprM	*mexR*	wt/+; *nalB*/+++; *nalC*‡/++	AC, AH, BL, CL, CM, CV, EB, FQ, HL, IR, NV, SM, SDS, TL, TP, TS
	MexC	MexD	OprJ	*nfxB*	wt/–; *nfxB*/++	AC, AH, BL, CL, CM, CV, EB, FQ, ML, NV, SDS, TC, TP, TS
	MexE	MexF	OprN	*mexT*	wt/–; *nfxC*‡/++	AH, CM, FQ, TP, TS
	MexX (AmrA)	MexY (AmrB)	OprM	*mexZ (amrR)*	wt/+	AG, ER, FQ, TC
P. putida	ArpA	ArpB	ArpC	*arpR*	wt/+	CB, CM, ER, NV, ST, TC
	MepA	MepB	MepC	*mepR*	?	AH, BL, ER, NV, TC
	SrpA	SrpB	SrpC	*srpR, srpS*	wt/+¶	AH
	TtgA	TtgB	TtgC	*ttgR*	wt/+	AP, CM, TC, TO
	TtgD	TtgE	TtgF	?	wt/+¶	AH
	TtgG	TtgH	TtgI	?	wt/+; induced/++††	AH, AP, CB
S. typhimurium	AcrA	AcrB	?	?	wt/+; mutant/++	AC, BL, BS, CH, CM, CV, DOC, ER, FA, NAL, NOR, NV, RF, SDS, TC
S. maltophilia	SmeA	SmeB	SmeC	*smeRS*	?	AG, BL, FQ
	SmeD	SmeE	SmeF	?	wt/+; mutant/++	EB, ER, RQ, TC

2.3.4. Major facilitator superfamily:

With more than 15000 protein sequences, major facilitator superfamily (MFS) is one of the largest families of membrane proteins characterized so far in living organisms. The members of MFS are equally distributed between prokaryotes and eukaryotes. Like many other secondary transporter, MFS members function is driven by the use of energy conserved in the electrochemical gradient of ions generally protons. Large number of MFS substrates that have been identified (e.g. sugars, neurotransmitters, drugs, amino acids, peptides and positive ions etc.) These transporters are of special interest because they exhibit three types of substrate transport, based on electrochemical gradient i.e. uniport, symport and antiport (Law, Maloney et al. 2008). (Uniport term is used for transfer of one substrate downhill the concentration gradient across the lipid bilayer. In symport and antiport transfer system, the energy obtained from downhill transfer of substrate is utilized for transfer of drug towards uphill concentration gradient. In symport and antiport, proton and drug are transferred in same or opposite direction of the proton respectively) (Chang, Lin et al. 2004; Ren and Paulsen 2005; Lewinson, Adler et al. 2006; Ren and Paulsen 2007; Lam, Lee et al. 2011).

The number of residues within different members of MFS ranges from 400 to 600. Prior to release of structures, the traditional structure prediction tools depicted different number of transmembrane helices from 6 TMHs to 24 TMHs (Saier 2003; Law, Maloney et al. 2008). Few high resolution structures of the MFS transporters have been solved providing a health of knowledge towards our understanding of transport mechanisms (Figure 12) (Abramson, Smirnova et al. 2003; Huang, Lemieux et al. 2003; Yin, He et al. 2006; Dang, Sun et al. 2010; Newstead, Drew et al. 2011).

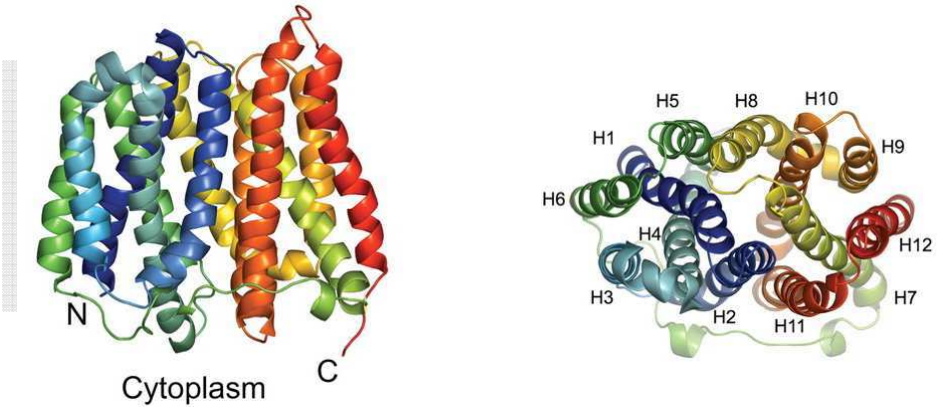

Figure 12. Top view (right) and side view (left) of a major facilitator super-family member, EmrD is shown in ribbon presentation. The transporter consists of 12 transmembrane helices each shown with different color. Number of transmembrane helices from 1 to 12 is also indicated. The substrate translocation is carried through the hydrophobic central region (Yin, He et al. 2006).

2.3.5. Multidrug and toxic compound extrusion:

All secondary type multidrug resistance transporters described so far rely on the electrochemical gradient of the protons. But presence of a reasonable amount of Na^+ ion in cytoplasm prompted scientist to look for the transporter which could use electrochemical gradient of Na^+ ions concentration and this led to recent discovery of multidrug and toxic compound extrusion family (Morita, Kodama et al. 1998; Brown, Paulsen et al. 1999; Chen, Morita et al. 2002; Begum, Rahman et al. 2005).

Members of MATE family are distributed in all forms of life from bacteria to eukaryotes including mammals and even in plants conferring multidrug resistance (Kaatz, McAleese et al. 2005; Magalhaes, Liu et al. 2007; Tsuda, Terada et al. 2009). Most of the identified substrates of the MATEs are positively charged ions like norfloxacin, ciprofloxacin, ofloxacin. Like the substrates of other MDR transporters, there is no structural similarity found within substrate of MATEs (Kuroda and Tsuchiya 2009).

The x-ray structure of NorM was very recently determined in outward facing conformation. The structure also confirms the previously predicted topology showing that NorM consists of twelve transmembrane helices (Figure 13) (He, Szewczyk et al. 2010).

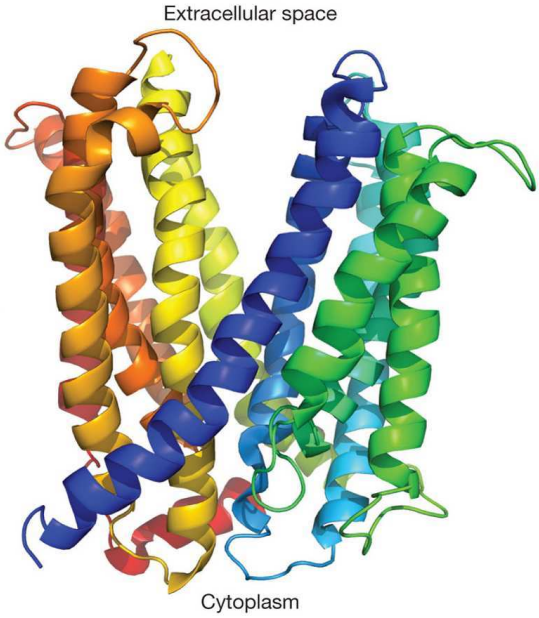

Figure 13. Front view of outward facing three dimensional structure of NorM of *Vibrio cholerae* solved at 3.6 Å (He, Szewczyk et al. 2010).

Chapter 3. ATP binding cassette transporter:

AT binding cassette (ABC) proteins are considered as the largest family of protein found in both prokaryotes and eukaryotes. Genomic analysis of *E. coli* revealed that 5% of its genome is constituted of genes potentially coding ABC proteins. The amino acid sequence of ABC proteins remains highly conserved among 13 different organisms of kingdom Archea, Eubacteria and Eukarya (Higgins 1992; Isenbarger, Carr et al. 2008). The name ABC was given due to presence of conserved Walker 'A', Walker 'B' and signature motif of this family, a stretch of few conserved amino acids usually starting on LSGGQ. Based on the functions, the ABC proteins can be classified into two classes: DNA binding proteins and ABC transporters. DNA binding proteins are soluble, found within cell to perform DNA repair functions. ABC transporters are then divided into exporters and importers both are integral membrane proteins involved in efflux and influx of substrate from and into the cell, respectively. The ABC transporters perform their respective function driven by energy from the hydrolysis of ATP. Whereas, the importers are specific to their respective substrates, exporters can be poly specific.

3.1. Structural characterization:

The minimal topology of any ABC transporter consists of four domains: two transmembrane domains and two nucleotide-binding domains. The transmembrane domains dimerize and provide the pathway for the translocation of substrate through the inner membrane. Nucleotide-binding domains bind and hydrolyze ATP molecules working as 'power engine' (Figure 14). In mammalian cells all four domains are usually expressed as one polypeptide (Aller, Yu et al. 2009) whereas in prokaryotes two polypeptides, (Ward, Reyes et al. 2007)to four polypeptides are expressed separately and then form a functional transporter as in the case of BtuCD (Hvorup, Goetz et al. 2007).

In addition to minimal subunits, additional domains are also found in ABC transporters such as regulatory domain found in Cystic fibrosis transmembrane conductance regulator (CFTR), extra N-terminal domains in transporter associated with antigen processing (TAP) TAP1/TAP2 and C- terminal domain in maltose importer. In importers substrate binding proteins are required for import of substances (Sheppard and Welsh 1999; van der Heide and Poolman 2002; Biemans-Oldehinkel, Doeven et al. 2006; Oancea, O'Mara et al. 2009).

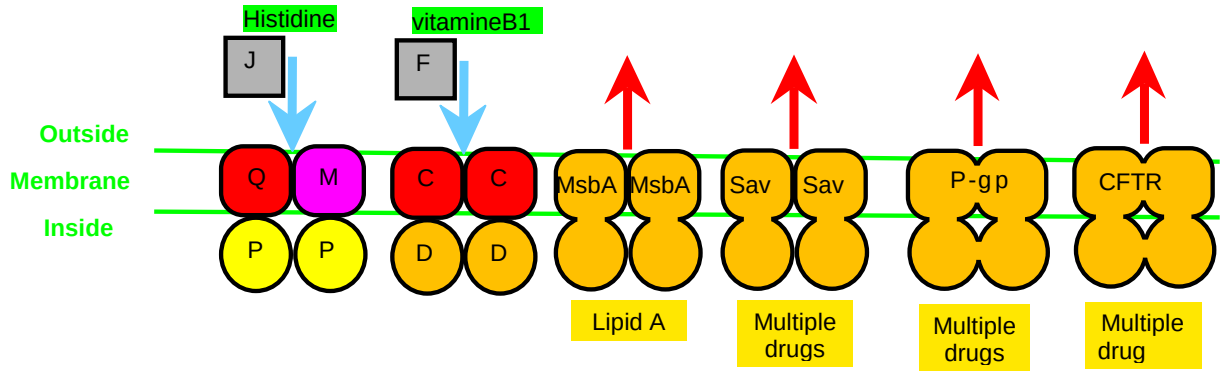

Figure 14. Core structure of ABC transporters

3.1.1. Transmembrane domains:

Since the TMDs show translocation specificity towards their respective substrates in case of importers, they share less sequence similarity as compare to NBDs within the superfamily of ABC transporters. The structural features of TM domain were unknown until the availability of first crystal structure of an ABC importer which was solved at 3.2Å resolution in year 2002 (Locher, Lee et al. 2002). The structure provided the key details characteristic which was not possible with traditional sequence based topology prediction tools (Dawson, Hollenstein et al. 2007). Later, on the basis of structural data various folds of the membrane domain were recognized (Rees, Johnson et al. 2009).

3.1.1.1. Exporter transmembrane domain fold:

The first structure of ABC exporter, Sav1866, which functions as a homodimer showed that TMD of the exporter comprises of six transmembrane helices (TMH). These helices traverse the cytoplasmic membrane and are joined by extracellular and intracellular loops (Dawson and Locher 2006). Extracellular loops are short, connecting the TMHs, whereas the intracellular loops protrude deep into the cytoplasm and make the transmission interface with NBDs. The intracellular loops are more frequently called as intracellular domains (ICDs). ICD1 provides linkage between transmembrane helices TMH2 and TMH3 making an interaction with its respective nucleotide-binding domain. ICD2 provides a link between TMH4 and TMH5. The key feature revealed by the Sav structure was the interaction of (ICD2) of *cis*- subunit with NBD of *trans*- subunit. Subsequently, the second intracellular loop of *trans*- unit was found interacting with *cis*- subunit (Figure 15). The cross over interaction of the loops and NBDs was not anticipated, and is not found in any ABC importer yet.

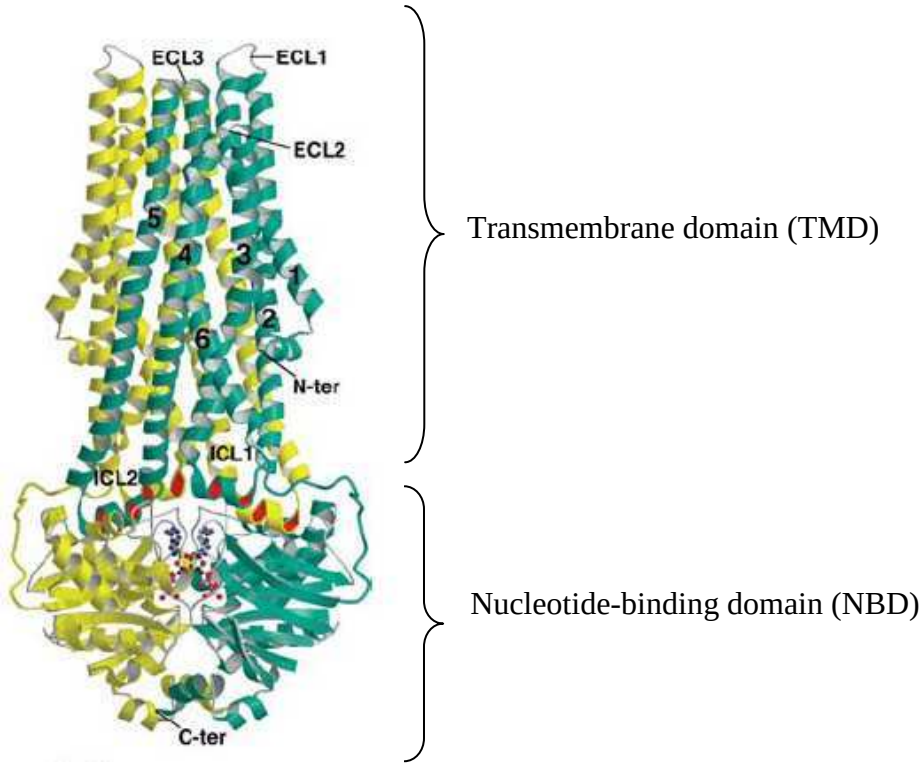

Figure 15. Ribbon presentation of Sav1866 structure. Two subunits of transporter are colored yellow and turquoise. The numbering of transmembrane helices from 1 to 6 is shown on turquoise colored subunit (Dawson and Locher 2006).

The Sav1866 structure was solved in the outward facing conform showing that the transporter is protected or closed from the cytoplasmic side and opened to the periplasmic space. The transmembrane helices group themselves from TMH1 to TMH3 and TMH4 to TMH6 giving rise to two wings within the membrane (Figure 15). Another structure of Sav1866 which was crystallized in the presence AMP-PNP showed the same structural arrangement (Dawson and Locher 2007).

Soon after the release of Sav1866, the structures of MsbA were corrected and released again (Chang, Roth et al. 2006; Petsko 2007; Ward, Reyes et al. 2007). The transporter was crystallized in three different conditions: in the presence of 5′-adenylyl-β-γ-imidodiphosphate (AMP-PNP) or Adenosine diphosphate/vanadate (ADP·Vi) separately or without any nucleotide (apo conformation). The solved structures showed three different conformations: closed in presence of (AMP-PNP or ADP-Vi), apo open and apo closed (Figure 16). The closed structure was in full accordance with Sav1866 structure for both transmembrane domain arrangement and nucleotide-biding domains. Whereas apo form yields two different conformations, apo-closed and apo-open, in both structures the NBDs are not interacting with one another but in apo-open conformation the distance between the two NBDs is higher as compared to the apo-closed. In both structures of apo conformation TMD are shown in inward

facing conformation, open towards cytoplasmic side and closed on periplasmic side. A possible conformation in which the substrate is acquired form cytoplasm.

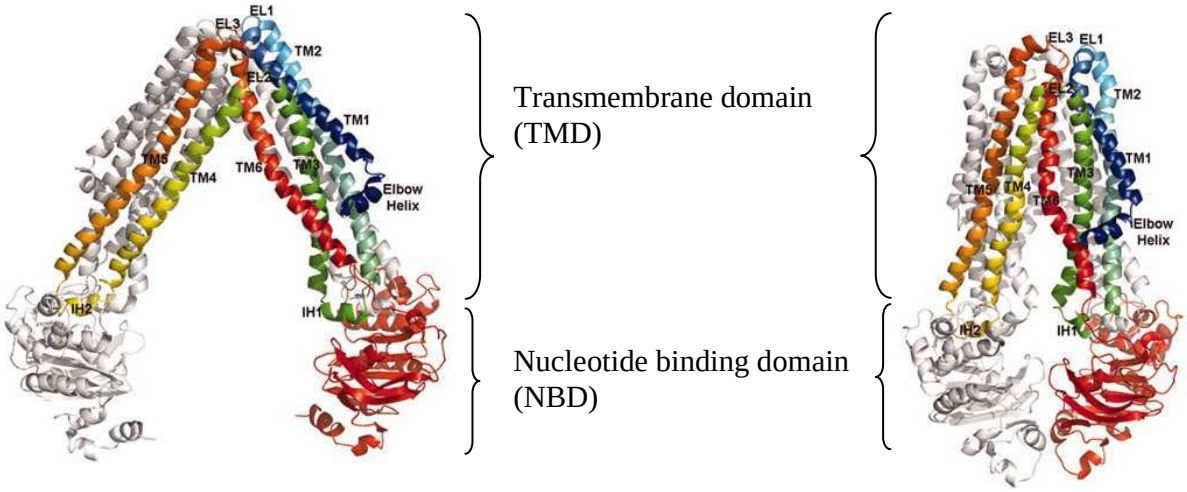

Figure 16. Two apo conformation of MsbA are shown in ribbon presentation: apo open (left) and apo closed (right). One of two subunits is colored white and other one rainbow. The transmembrane helices are also numbered from 1 to 6. In both conformation there is opening inside and extracellular side is closed. The ICD1 and ICD2 (IH1 and IH2 here) are always in contact with NBDs (Ward, Reyes et al. 2007).

Recently solved structure of eukaryotic ABC transporter P-glycoprotein from mouse extended the structural information of ABC exporters to the mammals (Aller, Yu et al. 2009). In human, P-glycoprotein in is the best characterized ABC exporter yet which has an important role in multidrug resistance in chemotherapy (Higgins 2007). P-glycoprotein was crystallized in the absence of any nucleotide or in the presence of two stereo isomers of QZ59 (Figure 17). The apo form yielded the overall same conformation as observed in the case of apo-open MsbA. With the virtue of P-glycoprotein structures solved in presence of inhibitors, the drug-binding sites were revealed showing that there is large cavity able to acquire the drug from cytoplasm or plasma membrane (Figure 17) (Aller, Yu et al. 2009).

All the ABC exporters structurally characterized so far show a similar topology i.e. six transmembrane helices connected by loops.

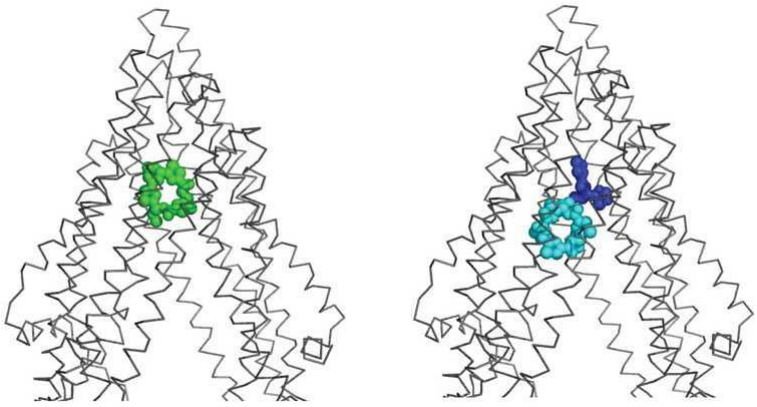

Figure 17. Binding sites of QZ59-RRR (green spheres) and QZ59-SSS (blue and cyan) inhibitors in the internal cavity of P-glycoprotein are shown in space filling model. Transmembrane helices of P-glycoprotein are shown in wire presentation (Aller, Yu et al. 2009).

3.1.1.2. Importer transmembrane domains fold:

Unlike ABC exporters the number of ABC importers helices is not constant. Based on the fold and topology of TMDs, the importers are divided into two types.

Type I importer fold and Type II importer fold

The TMD fold name given to a family is based on the historical characterization of their respective members not on the basis of sequence of their structural finding or characteristics.

3.1.1.3. Type I importer fold:

The number of transmembrane helices is not constant in type I importer fold family. The numbers of transmembrane helices vary from five to eight. The fold classification is based on the comparatively newly determined structure of MetI of Met transporter (Kadaba, Kaiser et al. 2008; Rees, Johnson et al. 2009). There are five transmembrane helices present in each monomer traversing the lipid bilayer as in the case of ABC exporters. The translocation pathway is mainly provided by the TMH-2 to TMH-5 of each subunit. The other members of type I TMD importer fold, ModB which imports molybdate possesses six transmembrane helices. MalF and MalG subunits of maltose transporter posses eight and six helices respectively (Hollenstein, Frei et al. 2007; Oldham, Khare et al. 2007; Gerber, Comellas-Bigler et al. 2008). The maltose transporter is the only ABC transporter carrying different number of helices in the two TMDs. The accessory helices of MetI or MalF and MalG are involved in the interaction between transmembrane subunits (Figure 18) (Oldham, Davidson et al. 2008).

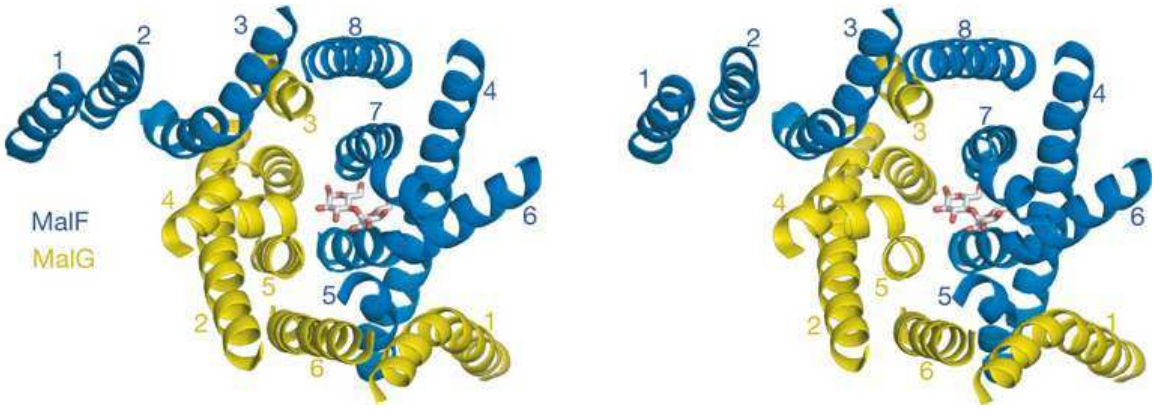

Figure 18. The arrangement of transmembrane helices within Type I ABC importer fold, the number of TMHs in both monomers are not constant but translocation pathway is provided by TMH2 to TMH5 (TMH 4 to TMH 7 for MalF subunit of maltose transporter) (Oldham, Khare et al. 2007).

3.1.1.4. Type II importer fold:

There are two homolog ABC importers characterized at structural level showing Type II importer fold for their TM domains: BtuC subunits of the vitamin B12 importer BtuCDF and HI1471 subunit of HI1470/1 transporter of *E. coli* and *Haemophilus influenzae* respectively (Locher, Lee et al. 2002; Pinkett, Lee et al. 2007). Alternatively these are also called big ABC importers because each transmembrane subunit consists of ten transmembrane helices giving rise to a complete transporter of twenty TM helices. The TMH2 is oriented in such a way that it is closer to other transmembrane helices of its own subunit. TMH4 and TMH5 of each of the subunits provide entrance, the translocation pathway and the exit for the substrate (Figure 19). The interaction between subunits is additionally maintained by the interaction between TMH10 of both subunits (Dawson, Hollenstein et al. 2007; Hollenstein, Dawson et al. 2007).

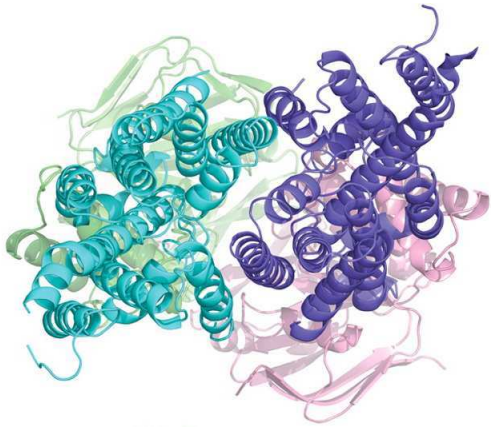

Figure 19. The transmembrane fold present within Type II ABC importers fold (Pinkett, Lee et al. 2007).

3.1.2. Nucleotide-binding-domains:

Nucleotide-binding-domains or ABC cassettes are the cytosolic subunits of ABC transporter providing the energy required for the translocation of the substrate by ATP hydrolysis. Whereas TMDs vary in their amino acid sequence; the NBDs share very high sequence similarity within ABC superfamily (Holland and Blight 1999; Geourjon, Orelle et al. 2001). First high resolution structures of separate NBDs became available in year 1998, and in coming years the structure of NBDs alone or with whole transporter showed that NBDs are highly conserved in the structural arrangement which is probably due to a common mechanism for ATP hydrolysis (Hung, Wang et al. 1998; Jones, O'Mara et al. 2009). At larger scale NBD is divided into two sub-domains: Rec-A like domain and helical domain. Within each NBD there are specific fold and regions which are critical for ATP binding and hydrolysis, interaction with intracellular loops originating from TMD and dimerization of two NBDs (see Figure 20).

Walker 'A':
Identified by the presence of a highly conserved stretch of few amino acids residues GXXGXGK(S/T) is found in many of nucleotide-binding proteins (Walker, Saraste et al. 1982). It is established that conserved lysine residue is critical for the interaction with phosphate moiety of bound nucleotide, mutating this residue leave the NBD in an incompetent state (Chen, Lu et al. 2003; Orelle, Gubellini et al. 2008).

Q loop:
Q-loop contains a conserved glutamate and found only in ABC transporter. It comprises eight residues, that makes the interaction face with ICD1 and ICD2 of *cis*- and *trans*-transmembrane domains respectively (Dalmas, Orelle et al. 2005; Zolnerciks, Wooding et al. 2007; Oancea, O'Mara et al. 2009). The Q-loop makes the connection between the ATP binding subdomain and helical subdomain of NBD. It has a role in the hydrolysis of bound nucleotide.

ABC signature:
Exclusively present in ABC transporters, the name of the superfamily is partly attributed to presence of a conserved LSGGQ motif. In monomer state the role of signature motif is not established, in dimeric state the signature motif of the *trans*- subunits comes in proximity with nucleotide bound to this *cis*- subunit by stabilizing the γ-phosphate of ATP with the help of positively charges residues (Fetsch and Davidson 2002; Jones, O'Mara et al. 2009).

Walker ‘B’:
Identified with a conserved sequence of XXXXD (where X=any aliphatic residue). Conserved aspartate is considered as interacting with Mg^{2+} required for ATP hydrolysis. The interaction between aspartate and Mg^{2+} is also thought to stabilize the ATP hydrolysis complex. The catalytic glutamate residue (XXXXDE) present just after the Walker ‘B’ motif has a central role in nucleophilic attack on the ATP. The mutation of conserved glutamate into alanine or aspartate halts the ATP hydrolysis of transporter (Orelle, Dalmas et al. 2003).

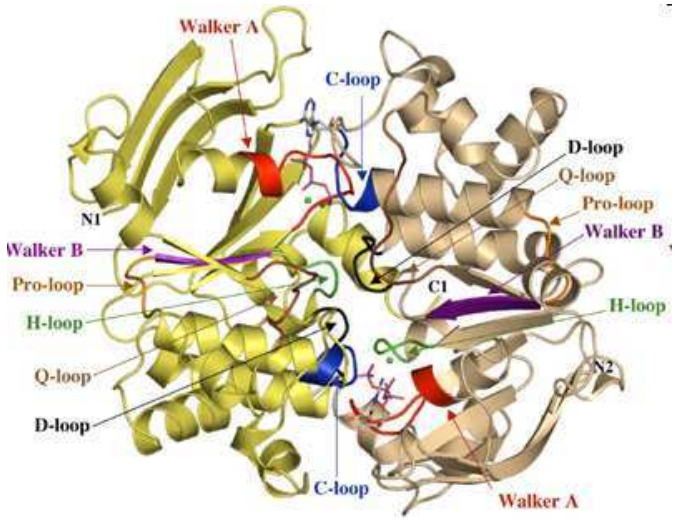

Figure 20. X-ray structure of nucleotide-binding domains of transpoter Hly. The highly conserved motif present within nucleotide-binding domains are labeled (Zaitseva, Jenewein et al. 2005).

Mechanism of ATP hydrolysis:
The ATP hydrolysis mechanism adopted by nucleotide-binding domain of ABC transporters is widely discussed and several models are proposed to explain it e.g. ATP switch model (Higgins and Linton 2004; Linton 2007). Briefly, it is described that open conformation of ABC exporter is in state of high affinity for ligand with less affinity for ATP. The binding of ligand to exporter induces affinity of NBDs for ATP leading to its binding. For ATP hydrolysis, the NBDs of two subunits form a closed dimer and this conformational change is large enough to close the transmembrane face in intracellular side and open on extracellular surface and translocation of ligand takes place. The ATP molecule(s) then hydrolyzed and returning the transporter back to its open form. This model also explains that in vivo the ABC transporters are not in utilizing the ATP but it’s the binding of ligand which triggers ATP hydrolysis. The binding of ATP occurs on Walker ‘A’ motif which is stabilized by the signature motif of NBD of other subunit. The hydrolysis is then initiated by catalytic glutamate adjacent to Walker ‘B’.

3.2. Functional classification of ABC transporters:

The ABC transporters can be classified into two major types depending on their function in vivo: ABC Importers and ABC Exporters.

3.2.1. ABC importers:

Nutrients are essential for the growth and maintain metabolic process of the cell and these nutrients are acquired from the environment by specialized membrane proteins including ABC importers.

The transporter acquires the substrate present within the periplasmic space between inner and outer cell membrane of Gram-negative bacteria. Here the acquisition is assisted by the special periplasmic proteins 'substrate binding proteins' that binds to the substrate and deliver it to ABC importer which then transfer the substrate to cytoplasm. In Gram-positive bacteria , substrate binding proteins are also found in direct contact with the outer surface of cytoplasmic membrane or with ABC importer itself (van der Heide and Poolman 2002). In large part the specificity towards the substrates is provided by substrate binding protein as SBP first bind to their respective substrate and then transfer it to transporter (Figure 21) (Wilkinson 2003; Doeven, Abele et al. 2004; Davidson, Dassa et al. 2008).

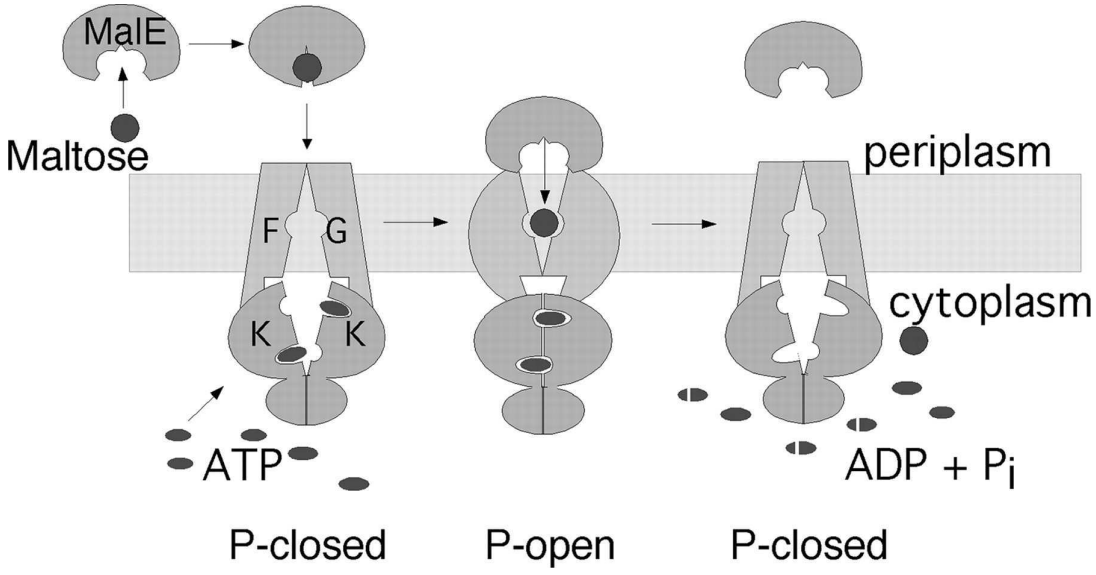

Figure 21. The mechanism of substrate capture by SBP (MalE in this case) and then import by the ABC importer (Mal FGK_2) is schematized (Davidson, Dassa et al. 2008).

Large number of substrates imported by these importers belonging to different classes of compounds including sugars, metals, peptides and amino acids etc (Davidson, Dassa et al. 2008; Eitinger, Rodionov et al. 2011).

3.2.2. ABC exporters:

The structural features of the ABC exporters are discussed in previous section; here the significance will be discussed. Exporters are found in all forms of life from bacteria to human performing their general prescribed natural function of extruding the toxic and waste substances out of the cell. In higher organism their function is also to provide the selectivity filter against harmful substances. The cytotoxic compounds are efflux out of the cells by the virtue of presence of ABC exporters. Usually showing specificity towards their substrate, the ABC exporters are also found exhibiting poly specificity towards the different compound of absolute irrelevant structural features (Higgins 2007).

3.2.3. ABC exporters and human:

The analysis of completed genome sequence of *homo sapiens* revealed the existence of 7 families of ABC exporters with a total number of 49 exporters (Dean, Rzhetsky et al. 2001). But importance of these exporters was realized long ago when it was shown that resistance towards different administered compounds is due to the active efflux by these transporters (Juliano and Ling 1976).

3.2.3.1. P-glycoprotein:

P-glycoprotein also known as ABCB1 or MDR1 is one of the best characterized proteins with vital significance in the clinical practice. The important role of P-glycoprotein in drug resistance was realized some 35 years ago when it was shown that a glycosylated protein is responsible for the drug resistance and therefore given the name of P-glycoprotein (Juliano and Ling 1976). It is a large membrane protein of 170 kDa, expressed as one polypeptide which organizes into two transmembrane and two nucleotide-binding domains, giving rise to a ‘full transporter’ (Higgins, Callaghan et al. 1997). In human, P-glycoprotein is present at various sites within body and perform extrusion of noxious substances to protect the cells from their toxicity effect. But during the development of cancer and then the treatment, P-glycoprotein becomes curse and start extruding the cytotoxic drug administered to kill the affected cells. The situation tends to worse many folds as the transporter is able to efflux wide range of structurally unrelated drugs. Owing to exposure to drugs, the cells also start overexpression of the transporter (Szakacs, Paterson et al. 2006; Hall, Handley et al. 2009). Recently solved structure of the P-glycoprotein shows that it share the structural and mechanistic features to its bacterial homologues like Sav1866 (Figure 22)(Aller, Yu et al. 2009; Gottesman, Ambudkar et al. 2009).

Table 5. Clinically relevant and atypical ABC proteins (Linton 2007).

ABC Protein	Psuedonym	Ligand(s)/Function	Associated Disease(s)
ABC1	ABCA1	Cholesterol	Tangier disease
ABCR	ABCA4	Retinal	Various eye diseases
TAP1/2	ABCB2/B3	Peptides	Bare lymphocyte syndrome
ABC7	ABCB7	Iron	Anemia and XLSA
MRP6	ABCC6	?	Pseudoxanthoma elasticum
ALD	ABCD1	vlcFA	Adrenoleukodystrophy
Sterolin1/2	ABCG5/G8	Sterols	Sitosterolemia
PGY3/MDR3	ABCB4	Phosphatidylcholine	Liver disease: PFIC3, OC
BSEP/SPGP	ABCB11	Bile acids	Liver disease: PFIC2
MRP2	ABCC2	Conjugated bilirubin	Liver disease: D-J syndrome
MDR1	ABCB1	Hydrophobic drugs	Failure of chemotherapy
BCRP/MXR	ABCG2	Hydrophobic drugs	
MRP1	ABCC1	Conjugated drugs	
MRP4	ABCC4	Conjugated nucleosides	
Atypical ABC proteins			
CFTR	ABCC7	Chloride ion channel	Cystic fibrosis
SUR	ABCC8	Regulation of K_{IR} channel	PHHI
SMC1-6		Chromosome maintenance	
Rad50		DNA, telomere repair	
Elf1p		mRNA trafficking	

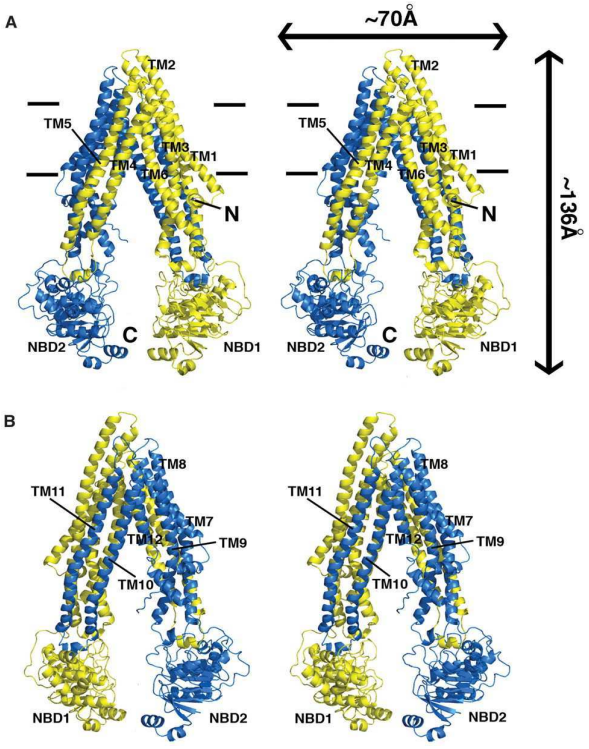

Figure 22. The structure of P-glycoprotein in apo conformation: (**A**) Front and (**B**) back stereo views of PGP. TMs 1 to 12 are labeled. The N- and C-terminal half of the molecule is colored yellow and blue, respectively. TMs 4 and 5 and TMs 10 and 11 crossover to form intertwined interfaces that stabilize the inward-facing conformation. Horizontal bars represent the approximate positioning of the lipid bilayer. The N- and C-termini are labeled in (A). TM domains and NBDs are also labeled (Aller, Yu et al. 2009).

3.2.3.2. Breast cancer resistance protein:

BCRP or ABCG2 is another human ABC exporter conferring the resistance towards the chemotherapeutic drugs in the case of breast cancer. Although the transporter is also found on other site like placenta, the name was given due to its resistance properties in cancer cell lines of MCF-7 on administration of doxorubicin and verapamil (Doyle, Yang et al. 1998; Maliepaard, Scheffer et al. 2001; Doyle and Ross 2003). Unlike P-glycoprotein, BCRP consists of only one transmembrane domain and one nucleotide domain and two subunits make a homo-dimer and eventually an active transporter (Figure 23). The transmembrane domain is considered carrying six transmembrane helices as in the case of all the ABC exporters (Wang, Lee et al. 2008). BCRP is found to be active against mitoxantrone, methotrexate and irinotecan.

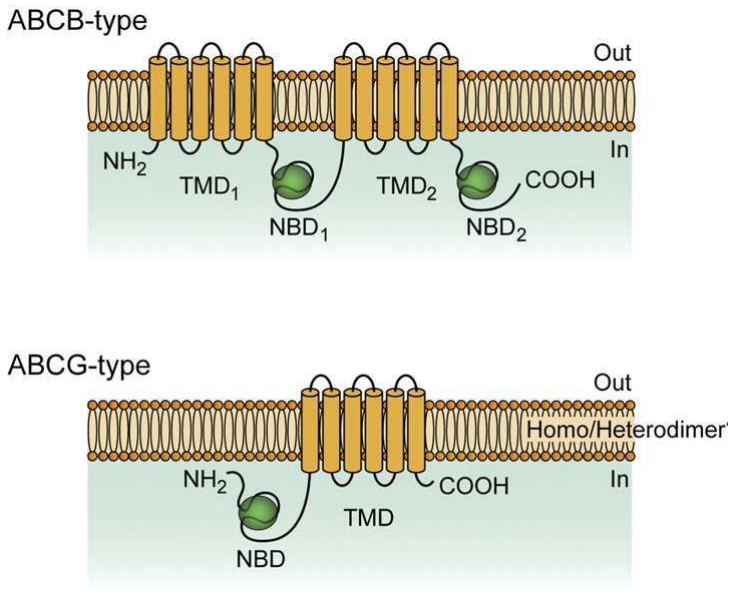

Figure 23. ABCB transporters are expressed as one polypeptide whereas ABCG dimerize to form a functional transporter (Sarkadi, Homolya et al. 2006).

3.2.4. ABC exporters and bacteria:

Multidrug resistance found in bacteria is in part due to presence of the ABC exporters. They are equally distributed in Gram-positive and Gram-negative a. There are various physiological functions of the performed by these transporters including excretion of cytotoxic compounds or rearrangement of the lipid in lipid bilayer synthesis e.g. MsbA.

3.2.5. Bacterial ABC exporter BmrA:

BmrA is a multidrug ABC exporter characterized from *Bacillus subtilis* carrying out transport of the various drugs. The genomic analysis of *Bacillus subtilis* reveals the existence of seventy eight genes coding for ABC transporters and gene *YvcC* was identified as ABC transporter. BmrA is expressed as half transporter of 66 kDa i.e. as one subunit of transmembrane domain and nucleotide-binding domain and two subunits dimerize to form a functional homo-dimer both when it is expressed or after solubilization in detergent (Dalmas, Do Cao et al. 2005; Ravaud, Do Cao et al. 2006). The half transporter shares high sequence similarity with its *lactococcus* homologue, LmrA, and each halves of P-glycoprotein.

BmrA is one of the best characterized ABC exporter from bacterial origin and *in vitro* analysis show the transport of 7-aminoactinomycin D, doxorubicin and Hoechst 33342 (Steinfels, Orelle et al. 2004). The transport activity *in vitro* was recently confirmed when it was found that *Bacillus subtilis* confers resistance towards Cervimycin C due to presence of BmrA gene (Krugel, Licht et al. 2010). The vital role of glutamate in ATP hydrolysis was first realized when it was shown that mutation of this glutamate to other amino acid leaves the transporter in an inactive form devoid of any ATPase activity. This glutamate is found just after the conserved Walker 'B' motif in ABC domain of ABC transporters (Figure 24). The position and residue is highly conserved throughout ABC super-family (Orelle, Dalmas et al. 2003) and recent structural evidence has underlined the role of this residue (Oldham and Chen 2011). The structure of BmrA is still undetermined. Low resolution structure determined with cryo-elcetron microscopy showed that the overall topology of BmrA is similar to that of Sav1866 or MsbA (Chami, Steinfels et al. 2002). It was also shown that conserved lysine of Walker 'A' motif essential for closure of two subunits to hydrolyze ATP in BmrA (Figure 24).

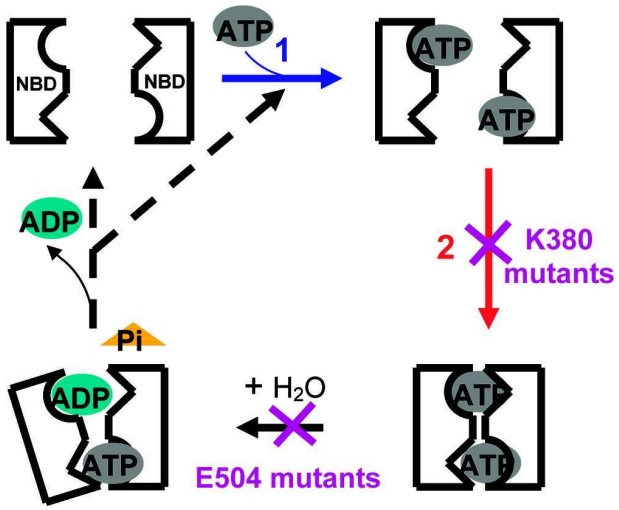

Figure 24. The effect of two mutations (Wlaker 'A' motif, K380R and catalytic glutamate) in BmrA is summarized in the schematic diagram (Orelle, Gubellini et al. 2008).

3.2.6. Bacterial ABC exporter BmrC/BmrD:

The further search for the new ABC exporters within *Bacillus subtilis* resulted in finding of another ABC exporter BmrC/BmrD. Both genes coding for this hetero-dimer are found within same opern anticipating two different ABC transporters and later characterization showed that both half transporters are capable of dimerization and giving rise to hetero-dimeric exporter (Figure 25). The over expression of both genes produced high yield of targeted genes. Overexpression of both gene showed high protein yield when expressed together or separately (Torres, Galian et al. 2009). The association between two monomers remains active during the purification and characterization steps. The BmrD subunit is bigger in size than BmrC with difference of eighty residues. Topological analysis of BmrC and BmrD based on the conventional structure prediction methods showed that each monomer can be divided into transmembrane domain and nucleotide-binding domain. In both subunits presence of six transmembrane helices in TMD is also predicted and extra eighty residues of BmrD are predicted to form a large extracellular loop between transmembrane helix 1 and 2.

The physiological function of this hetero-dimer remains yet to be determined but in vitro it is capable of transporting various antibiotics. The conserved glutamate responsible for the ATP hydrolysis is found only in the large subunit i.e. BmrD and mutation of this residue into aspartate inactivates the transporter (Carmen Galian's thesis).

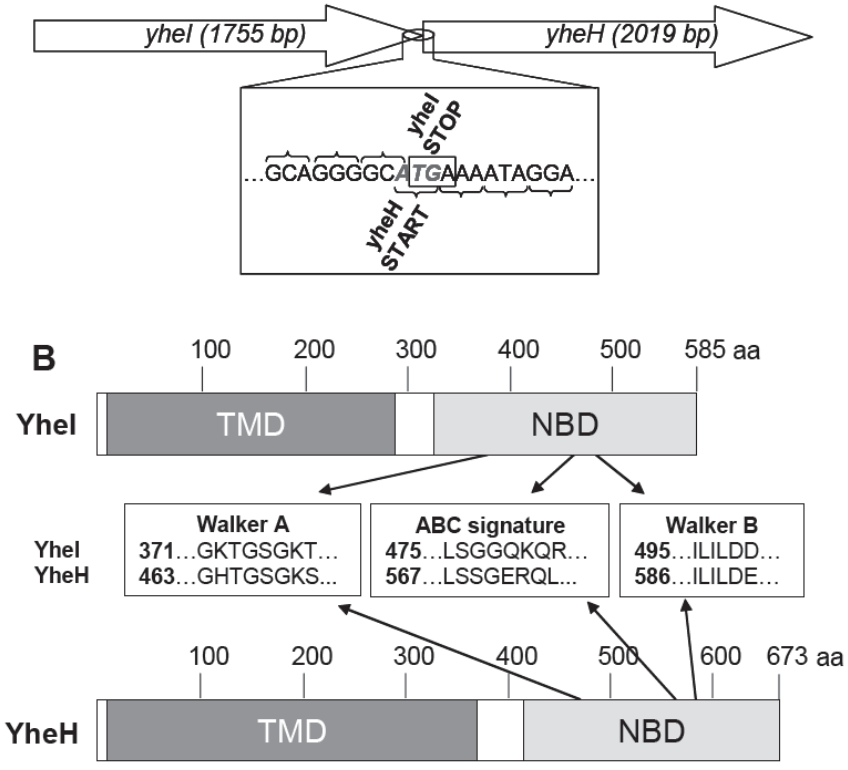

Figure 25. Gene organization of the YheI/YheH (Torres, Galian et al. 2009).

Question related to structure and function of ABC exporters:

1. The most critical feature of the ABC exporters is their poly-specificity towards the different compounds with versatile structural features. What makes ABC transporter capable to acquire these compounds from the cytosol with same transporter?
2. The mechanism of the ATP hydrolysis and transfer of the substrate by the transporter.
3. Is the distance between the two nucleotide-binding domains shown in the apo ABC exporters real?
4. The dynamics of ICDs of ABC transporters in different conformations.

We aimed to answer the third and fourth question with the help of hydrogen/deuterium exchange mass spectrometry.

Chapter 4: Mass spectrometry:

Mass spectrometers are instruments used to determine the molecular weight of molecules, atoms or isotopes in their ionic form. Once analytes are ionized within ion source their mass-to-charge ratio (m/z) is analyzed by the mass analyzer and then detected by the detector and, based upon this m/z ratio, the molecular weight is deduced (Figure 26). Mass spectrometry is one of the most highly used analytical techniques for the characterization of a broad array of analytes. The applications of the technique range from the pharmaceutical industries to petroleum analyses and from structural biology to dope tests. The effect of a drug can be monitored by the metabolites which can be analyzed with a mass spectrometer. With a high resolution mass spectrometer it has become possible to distinguish very closely related compounds within crude oil sample (Rodgers, White et al. 1998). Recent advancement in the technique has made it useful for the structural analysis of biomacromolecules (proteins, carbohydrates, etc) with prior sample preparations methods (Sharon and Robinson 2007; Harvey 2009; Benesch and Ruotolo 2011; Konermann, Pan et al. 2011).

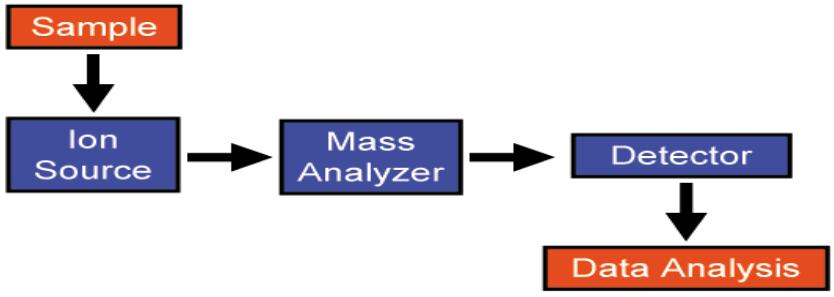

Figure 26. Scheme of a basic mass spectrometer

The principle of MS is based on the m/z determination and therefore the analyte must be charged before the analysis. A neutral molecule can be ionized by different ways such as addition of proton H^+ or Na^+ or removal of electron within the ion source. These charged species are then transferred through the mass analyzer and separated based upon their m/z ratio.

4.1. Ionization source:

There are two types of methods employed for the ionization of organic molecules:
hard or soft ionization.

Hard ionization causes the ionization and the fragmentation of the molecule, it is routinely used for compounds of low molecular weight. Electron impact (EI) belongs to this type of ionization. In EI the electron beam bombards the vaporized molecule, which causes the loss

of electron and as well as the fragmentation of the target molecule. This fragmentation is found to be useful to obtain structural information of small organic compounds (Cooks, Howe et al. 1969; Yinon and Hwang 1984).The analytes, ionized by hard ionization methods are volatile in nature and of low molecular weight. This prompted scientists to look for other ways of ionization which could be used for bio-macromolecules such as proteins, nucleic acids or carbohydrates.

Other ionization techniques are called soft because these techniques are generally not strong enough to dissociate the covalent bonds within analyte molecule but non covalent interactions are not preserved in general. Electrospray and MALDI are examples of soft ionization sources and are now widely used for the analysis of biological molecules. Both methods cause the ionization of protein molecules in the gas phase conserving their covalent linkage. In 2002 the inventors of the techniques John B. Fenn and Koichi Tanaka were awarded with Nobel prize in chemistry for the development of ESI and MALDI ionization methods, respectively (Tanaka, Waki et al. 1988; Fenn, Mann et al. 1989; Fenn 2003; Tanaka 2003).

4.1.1. Electrospray ionization:

Electrospray ionization is a soft ionization technique most widely used for the analysis of biomolecules such as proteins, peptides, nucleic acids and carbohydrates. The mass of the analytes which can be ionized by ESI ranges from some tens of Daltons to several mega Daltons (Smith, Loo et al. 1991; Griffiths, Jonsson et al. 2001). The mechanism of the technique can be divided in few steps: Nebulizer gas (nitrogen) is applied on flow of the solvent in presence of high electric voltage between 2 to 4 kV (Figure 27). The combination of nitrogen gas and electric field causes the production of highly charged droplets from the solution. The droplets are filled with the solvent of the solution and charged ions. The solvent present within droplets is evaporated by heating and/or exposing them to dry gas. The release of solvent causes the shrinkage of droplet (Kebarle and Verkerk 2009; Raut, Akella et al. 2009). The shrinkage of the droplets and repulsion of similar ions eventually leads to rupture of droplets and release of the ions (Fenn, Mann et al. 1990; Kebarle and Tang 1993). These ions are then guided towards mass analyzer. As the ions are produced directly from solution flow it is possible to couple electrospray with liquid chromatography. Normal ESI can handle the continuous flow up to 200 µl per minute with conventional capillary source (Tang, Bruce et al. 2006). A modified version of ESI, is able to work at nano-liter flow reducing the sample amount and solvent required called nano-ESI (Wilm, Shevchenko et al. 1996; Frommberger, Schmitt-Kopplin et al. 2004). Since the evaporation of the solvent is crucial to produce good

ionization of the samples, mostly but not necessarily organic evaporable solvents are used for electrospray ionization. The removal of salts or any other contamination within buffer is necessary as it can cause poor ionization of biomolecules (Garcia 2005; Cotte-Rodriguez, Zhang et al.).

In ESI, during the ionization of the analyte molecule, the phenomenon of multiple charging is also observed.

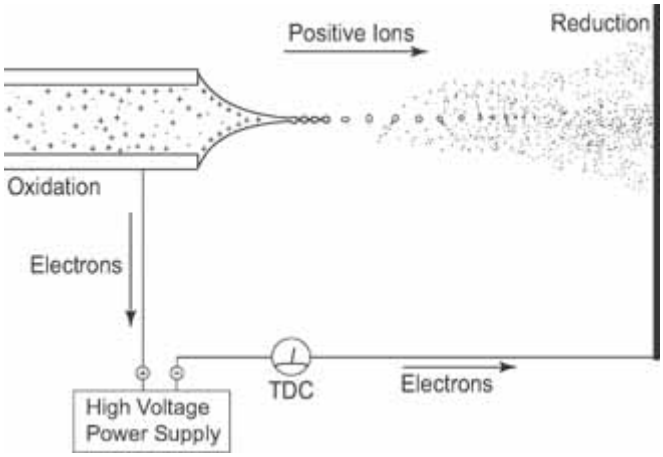

Figure 27. Ion producing process from an electrospray source (Kebarle and Verkerk 2009).

Multiple charging:

Basically, the concept of mass spectrometry is to ionize the molecule to obtain its molecular mass. But due to the electrospray ionization it was made possible to produce multiple charges on the molecule (Fenn, Mann et al. 1989). For example, for proteins or peptides which are generally positively charged at acidic pH, the number of charges on one single molecule can be from +1 to more than +100 depending on the size (Figure 28). Since in a mass spectrometer m/z is measured, the mass with higher charged states will produce m/z far smaller than the molecular weight of analyte. This m/z can then be easily analyzed by a mass spectrometer with even limited m/z range. The number of charges produced due to multiple charging is varied; the determined m/z of these charged states are then fed to computer-based program which calculates the exact molecular weight of the analyte. The phenomenon is called as multiple charging but the deduced mass is called as average mass determined (McLuckey and Stephenson 1998). Robinson's group showed that electrospray is tolerant to some kinds of detergents (like DDM) and can be used as a tool to study the protein complexes while keeping their non-covalent interactions preserved in gaseous phase (Barrera, Di Bartolo et al. 2008).

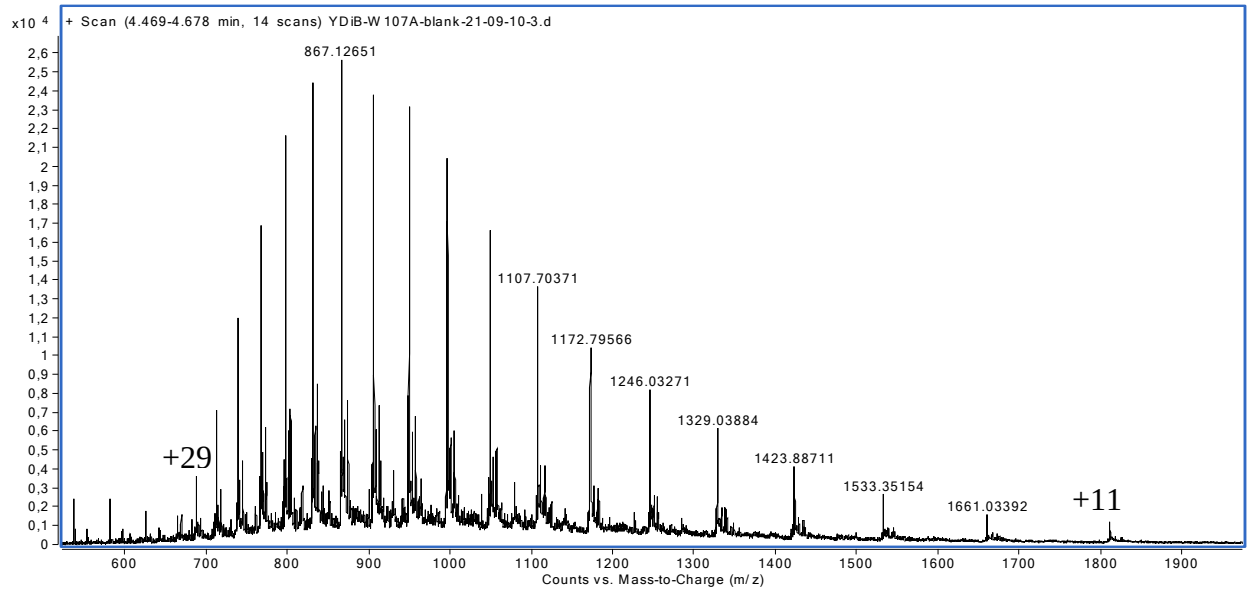

Figure 28. A typical ESI spectrum of a 19920 Da protein (YDiB). The charge states from 11 to 29 are shown.

4.1.2. Matrix-assisted laser desorption ionization:

MALDI is another soft ionization technique commonly used for peptide and protein analysis. It is a highly sensitive technique detecting femtomolar concentration and requires small sample amount. Though not as accurate as compared to ESI it is a robust technique that can be performed rather quickly.

In routine MALDI-ToF analysis, matrix solution 3,5-dimethoxy-4-hydroxycinnamic acid (sinapinic acid) and (a-cyano-4-hydroxycinnamic acid) are used for protein and peptide sample respectively in 1: 1 ratio (Beavis and Chait 1989a; Beavis and Chait 1989b). A quick sample preparation method is used for the analysis of molecules; 1-2 µl of analyte is mixed with the matrices and spot is air dried. The spot is prepared on a metal plate and this plate is then inserted into the mass spectrometer inlet source.

A laser beam is fired on the spot which causes the activation of matrix and subsequently the activated matrix ions transfer energy to analyte molecule causing their ionization. These ions are then analyzed in a time-of-flight analyzer (described later) and detected by the detector (Figure 29). Nowadays the use of MALDI is increased for the molecular imaging in combination with high resolution analyzers such as FT-ICR (Koestler, Kirsch et al. 2008). The coupling of MALDI with liquid chromatography has been also made available. With the direct coupling, the analysis of complex mixture of the peptides from proteome has become robust while using MALDI as ion source (Bodnar, Blackburn et al. 2003; Mueller, Voshol et al. 2007).

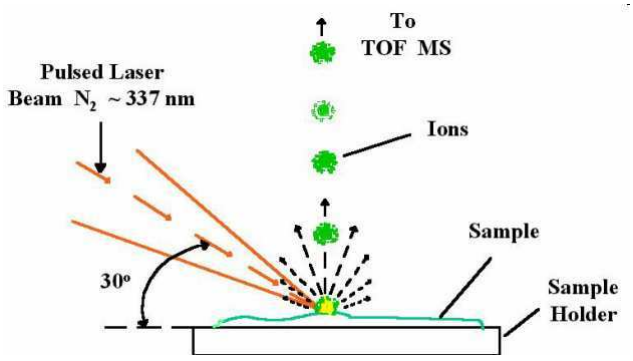

Figure 29. Mechanism of ionization of the analyte with a MALDI source.

The above mentioned method is used for soluble proteins and peptides. The presence of detergent or higher amount of salt leads frequently to failure of ionizations. Only dilution of the sample can be useful for salts but generally not for detergent as it might cause precipitation of membrane proteins. Nevertheless for intact membrane protein analysis, modified methods have been developed, facilitating the ionization and analysis (Figure 30) (Cadene and Chait 2000; Fenyo, Wang et al. 2007; Gabant and Cadene 2008).

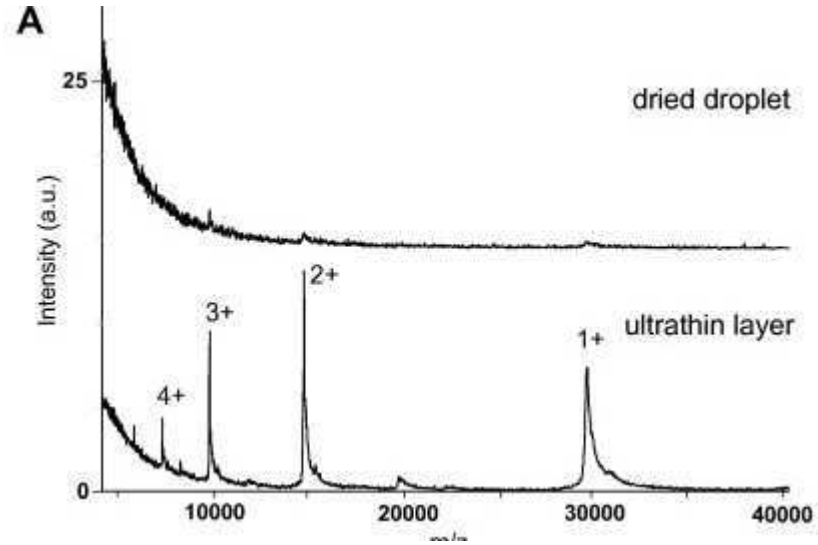

Figure 30. The difference between two MALDI-ToF spectra of a membrane protein can be appreciated after sample preparation with ultra thin layer method (Gabant and Cadene 2008). Single, double, triple and quarterly charged states can be observed with this preparation.

4.2. Ion analyzers:

Ion analyzer can be unarguably called as the heart of the mass spectrometer, the efficiency of any mass determining machine depends on the strength of its mass analyzer. The selection of the mass analyzer depends on the requirements of the sample to be analyzed and experiments to be performed. Since the generated ions carry positive or negative charge, magnetic or electric field within analyzer exploits this charge on ion and determine their m/z.

Three types of mass analyzers were used during this work and are discussed here briefly:

- 3D Ion Trap
- ToF
- FT-ICR

4.2.1. 3D ion trap:

Trap works as a mass analyzer, the ions generated by ESI are trapped under radio frequency (rf) field on constant amplitude, and the constant amplitude keeps the ions in a confined trajectory unless the amplitude is varied. The ions are trapped with the help of two electrodes of parabolic shape with application of appropriate potential on these electrodes showed as ring electrodes in Figure 31. The variation of radio frequency causes the escape of the ions from the trap and subsequently their detection by detector. The amount of known varied frequency from lower to higher range causes the escape of lower mass ion earlier and higher ions later, making their separation possible. For understanding the trap instrument it can be resemble to a bowl filled with solvents of different densities. On the tilting of the bowl the solvent with lower density will flow earlier as compare to other solvents with higher densities. The radio frequency generated by electrodes of the trap work as solvent for the ions in the gas phase keeping them “soluble” (for review (March 1997; March 2009)).

Trap is also used for MS/MS analysis for fragmentation of trapped ions and then analyzing its daughter ions varying the rf voltage again to obtain structure information on peptides.

Trap is advantageous by providing MS and MS/MS analysis of a peptide to identify. Better signal-to-noise can be obtained by keeping the ions for longer time in the space confined by two electrodes and following their motion.

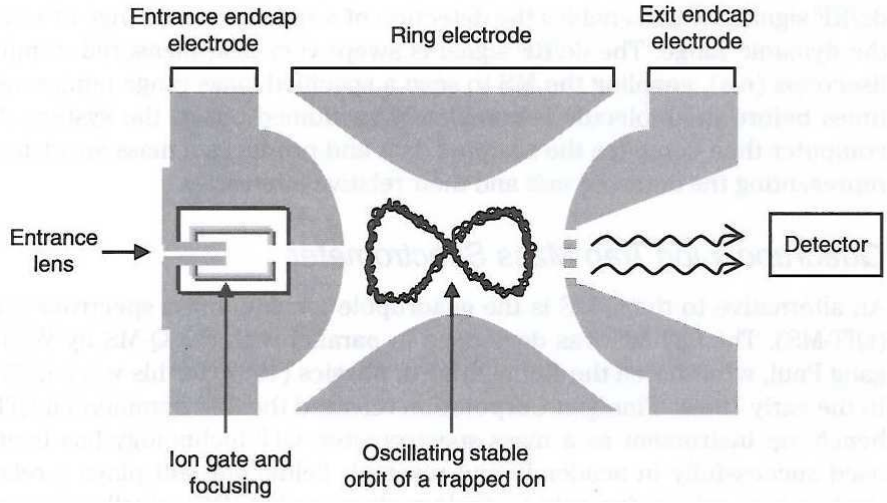

Figure 31. Schematic presentation of a 3D ion trap (Weblink: http://drugstestingbook.com/confirmation-via-contemporary-and-latest-techniques/)

4.2.2. Time-of-Flight:

The idea of the time-of-flight (ToF) was presented more than a half century ago (Wiley and McLaren 1955). This method to analyze the ions in mass spectrometry was highlighted in the 1960s but the development of the technique remained poor until the advancement of detecting and recording techniques in millisecond time scale (Guilhaus 1995). The principle of ToF analyzer is based upon the measurement of time taken by ions to travel a known distance. If ions carry identical kinetic energy, the measured time will be solely dependent on the m/z of ions.

The ions are highly dynamic species and irregularly dispersed therefore their movement and extraction is controlled by electrostatic plates. After emission from ion source, ions are focused within electrostatic plates. The function of these plates is more important in case of electrospray because electrospray produce continuous flow of ion. The ions are then released in packets to the ion analyzer.

Kinetics energy of any particle is described as:

$$KE = \frac{1}{2} mv^2$$

here, m and v correspond to molecular weight and velocity of the ions after acceleration

for a charged particle:

$$KE = zeV$$

z is charge state, e is charge on an electron and V corresponds to the amount of electric field in volts, on combining both equations:

$$\frac{mv^2}{2} = zeV$$

we know that velocity can be calculated by dividing the distance covered with time required:

$$v = l/t$$

$$\frac{1}{2} m(l^2/t^2) = zeV$$

$$T = l\left(m/2zeV\right)^{1/2}$$

distance covered by ions, charge on electron and amount of electric potential are constant values: t = (m/z) .½ . constant

hence m/z = 2.t.1/constant

In linear mode ToF analyzers, ions are analyzed by their time of flight as discussed above. An advancement of the ToF analyzers is the addition of “reflector” on end of time of flight tube rather than a detector. The reflectors are the electrostatic mirrors acting in dual way: ToF and reflector (Figure 32).

Theoretically all ions present in the source would absorb similar energy but practically this does not happen and ions with varied kinetic energies cause peak broadening, this peak leads to decrease in resolution. The electrostatic mirrors provide different energy levels for the ions of varied energies. The ions with high energy will protrude deep in the reflectron and after focusing will be released back into the time of flight tube and lower energy ion will be repelled from the surface, hence making the energy level similar within all ions so that ions reach at the same time on detector. Secondly, the presence of these electrostatic mirrors provides the longer length for the ions to fly within time of flight and enhancing the resolution of the instrument (Cornish and Cotter 1993; Cotter, Gardner et al. 2004). ToF provides good resolution and in some cases more than 50,000 depending on the instrument specifications. The difference in kinetic energy distribution of same m/z ions leads to peak broadening and decreasing the resolution (Brown and Lennon 1995).

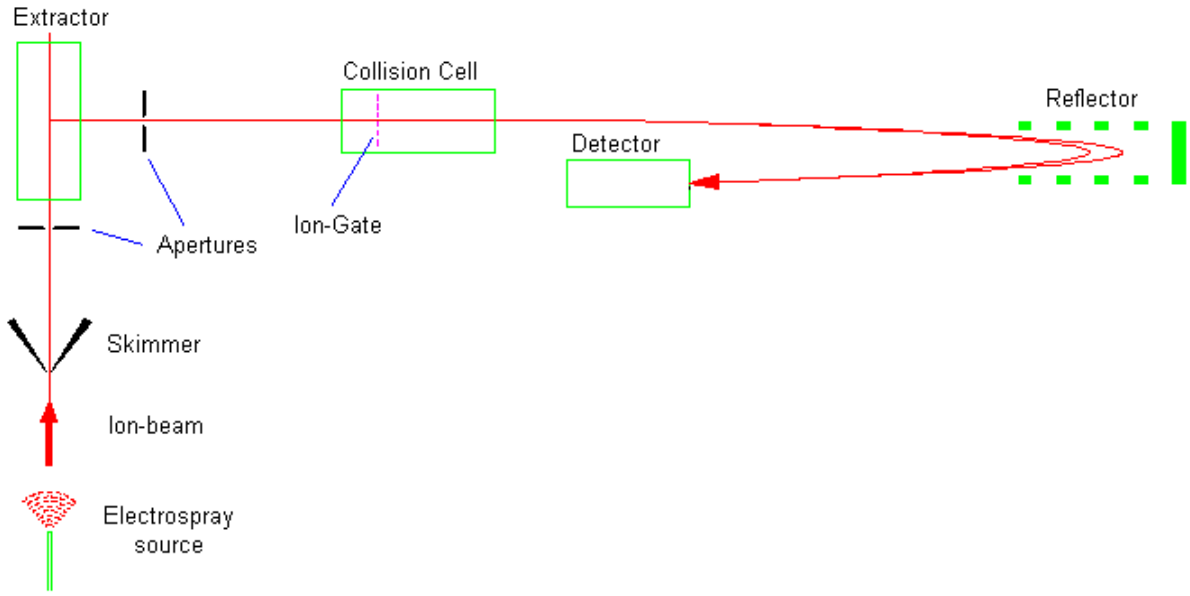

Figure 32. Main components of an ESI-ToF instrument

4.2.3. Fourier transform ion cyclotron resonance:

The FTICR mass analyzers are the highest mass resolution analyzers these days. The use of increasing magnetic field with a proportional effect on the mass resolving power was realized more than 60 years ago (Sommer, Thomas et al. 1951). During last two decades, there is big progress in development of the instrument mainly contributed by Alan G. Marshall. However, high cost and difficult maintenance of instrument explain its less frequent usage.

The mechanism of m/z determination within FTICR is different as compared to other mass analyzers both for ions analysis and detection. The analyzer operates in very strong magnetic field, generated by superconducting magnet. The magnetic field is generated when the high current is passed through the coiled electromagnetic wires. We know that ionization source like ESI continuously generates the ions, these ions are gathered within an octapole ion trap in presence of constant electro potential. The ions are then ejected by varying the potential on the ends of the octapole. The ions emitted by first octapole are then again passed through another octapole ion trap to focus the ion beam before their exit into the centre of the magnetic field. After the emission from second octapole ions enter into the cell, this is the place surrounded by constant strong superconducting magnetic field. Within the cell ions perform circular motion perpendicular to strong magnetic field and presence of trapping plates prevents escape of the ions. The force which causes the circular movement of charged particles/ions in presence of magnetic field is called as Lorentz force. The frequency of circular motion exhibited by ions depends on their respective m/z ratio. But this frequency is not strong enough to be recorded or used for m/z assignment. The ions are excited by the

voltage pulse generated by excitation plates and then their round movement within the magnetic field generates the ICR frequencies which are recorded by detector plates. The frequencies generate the spectrum in time dependent manner which are then treated according to Fourier transformation giving the m/z spectrum (Figure 33). There is no colliding of the ions with the detector as in the case of other mass spectrometer rather the generation of varied frequencies determines m/z of the ions (Marshall, Hendrickson et al. 1998).

For mathematical understanding of the mechanism we consider that if Lorentz force is denoted by F then it should be equal to:

$$F = zev * B \qquad (1)$$

Here, *e* is the ion charge, *v* is velocity of the ion and B is strength of magnetic field.

$$F = \frac{mv^2}{r} \qquad (2)$$

comparing Equation 1 & 2:

$$\frac{mv}{r} = ze\,B$$

After excitation of ions the frequency (ω_c) adopted by ions can be donated as:

$$\omega_c = \frac{ezB}{m}$$

The applied magnetic B is known and generated frequencies by the ions are recorded, hence m/z of ion can be determined:

$$m/z = \frac{eB}{\omega_c}$$

Since the principle of FTICR analyzer is based on the magnetic field, stronger the field will have better mass resolution. The FTICR mass spectrometers are unique for providing MS/MS analysis by an unusual fragmentation method for peptide/protein sequencing. The fragmentation method is called as electron capture dissociation (ECD). Though FT-ICR analyzers provide high resolution and sensitivity, one of their disadvantages is high cost and maintenance of the instrument. In contrast, with orbitrap, high resolution and mass accuracy can be achieved with comparatively lower expenses. The principle of orbitrap is to confine the ions in presence of electrostatic field in absence of any magnetic field (Hu, Noll et al. 2005).

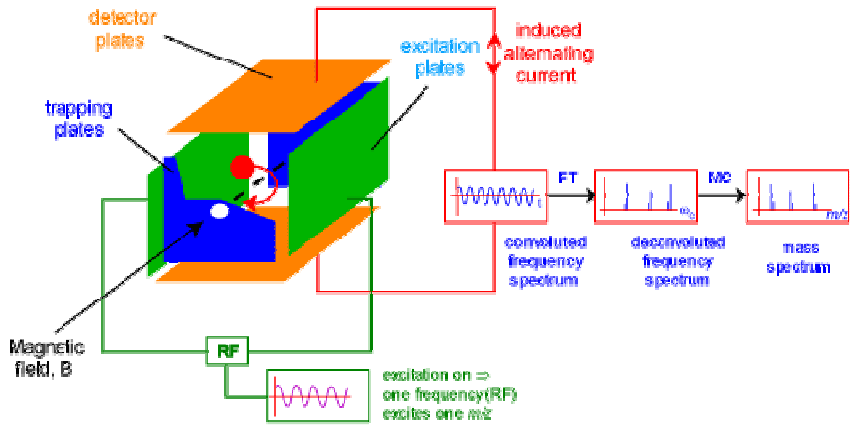

Figure 33. Schematic diagram of an FT-ICR ion analyzer (from Bristol University Website).

4.3. Protein/peptide sequencing by MS:

The sequencing of peptides or proteins in the mass spectrometer is achieved by their fragmentation. Fragmentation methods used for MS/MS sequencing can dissociate all three types of bonds within protein/peptide backbone, nevertheless fragmentation of amide/peptide bond between carbon of carbonyl and nitrogen of amide is more commonly observed O=C NH. For any sequence the fragmentation produces two products, one charged ion and a neutral specie. Decrease in m/z of charged fragmentation due to loss of H_2O, NH_3 or CO is called as neutral loss. The fragmentation of a peptide produces series of ions and the nomenclature adopted for these daughter ions is shown in the Figure 34. Depending on the bond fragmentation, six type of ions are expected (x, y, z) if identified part of the peptide belongs to C terminal or (a, b, c) if identified part matches with N-terminal. With the help of mass analyzer the molecular weight of the liberated product ions is determined and possible sequence is predicted (see Figure 34 and 35).

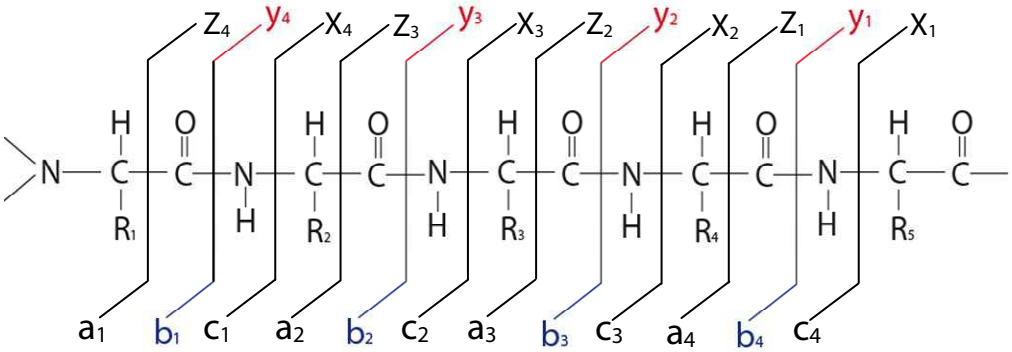

Figure 34. Daughter ions (fragments) emerging from N terminal and C terminal are given name as x, y, z ions and a, b, c ions respectively. The fragmentation of a peptide produces series of ions which are generated and the nomenclature adopted for these daughter ions as shown in the figure.

For an accurate prediction, the fragmentation pattern is searched or compared throughout the sequence database to identify the protein. For sequencing and peptide identification of a peptide mixture, arising by the digestion of a protein with known sequence, the dissociation pattern of residues is compared to theoretical dissociation database with help of database dedicated search engine like Mascot (Perkins, Pappin et al. 1999; Sadygov, Liu et al. 2004; Paizs and Suhai 2005; Xu and Ma 2006).

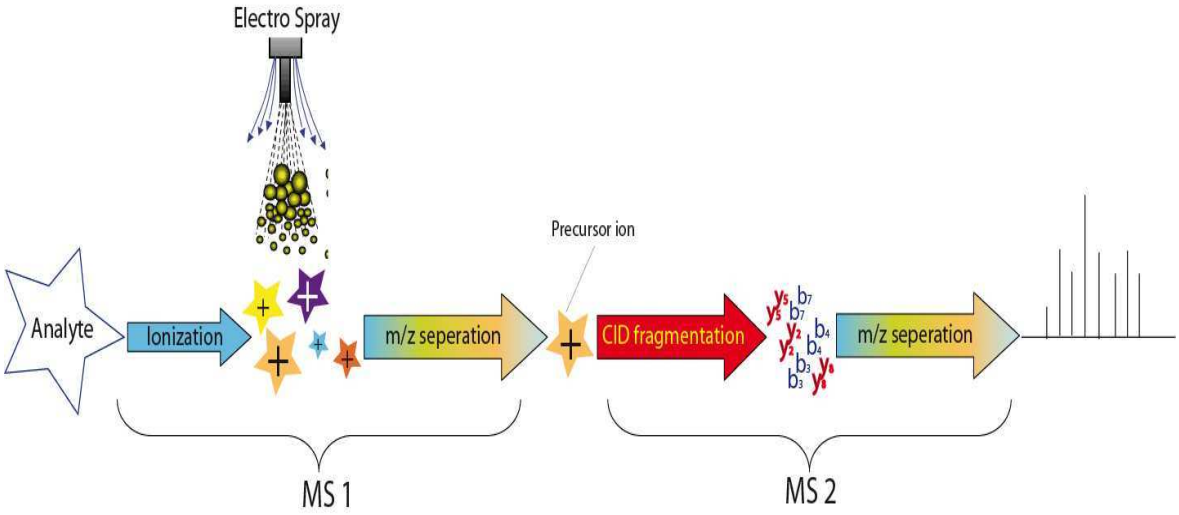

Figure 35. General scheme of MS/MS analysis

4.3.1. Fragmentation methods:

For the fragmentation of peptide different methods are in use. One possibility is the in-source decay which is used with MALDI ion source. When laser beam is fired on the analyte for ionization with extra energy, it causes the fragmentation of the analyte. The matrix used for this purpose is of particular characteristic capable of absorbing high energy like 2,5-dihydroxybenzoic acid (Reiber, Grover et al. 1998). The method is used for intact protein and as well as mixture of peptides of proteolytic digests of a protein or mixture of proteins. If peptide mixture of many proteins is under investigation, it can generate complicated MS/MS spectrum as the whole analyte will be ionized at one time. To avoid this complication MALDI is also being used in combination with liquid chromatography (Poutanen, Salusjärvi et al. 2001; Hardouin 2007).

Within post-source fragmentation there are two strategies in used depending on the time and the space: MS/MS in space and MS/MS in time

4.3.1.1. MS/MS in space:

As indicated in the name, the mass analysis and fragmentation takes place at physically distinct places. For example in triple quadrupole (QqQ) (Figure 36) or Q-ToF (QqToF) instruments first quadrupole acts as a mass filter which analyzes the m/z of the precursor ions, in the next quadrupole which acts as a collision cell, the ions are fragmented and then analyzed with the main analyzer like Time-of-flight or another quadrupole. Conventionally FTMS has been used as one of the time based MS/MS instrument but relatively recently developed new generations FT-MS are hybrid with Qq-FTMS (quadrupole mass filter and fragmentation cell and FT-MS ion analyzer)(Syka, Marto et al. 2004).

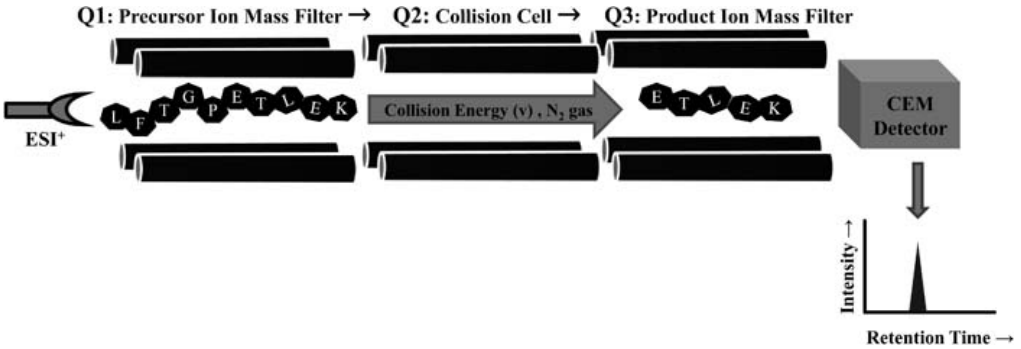

Figure 36. Three sections of a typical triple quadrupole are shown. Peptide arising from electrospray is analyzed in first quadrupole, fragmented in second and then product ions are analyzed in third quadrupole (Halquist and Thomas Karnes 2010).

4.3.1.2. MS/MS in time:

Examples of time based MS/MS include FTMS or ion trap where at the same place first the mass analysis of the peptides occurs followed by their fragmentation and subsequently mass analysis of the product ions. Since all the steps of the sequencing occur at the same physical space but in different time, the method is called as MS/MS in time.

Apart from the strategies there are several ways to fragment the peptides like:

Collision Induced Dissociation (CID)
Electron capture dissociation (ECD)
Electron transfer dissociation (ETD)
Infra red multi-photon dissociation (IRPMD)

4.3.2. Collision induced dissociation:

Employed for both MS/MS in space and MS/MS in time, collision induced dissociation is the most widely used method for the peptide fragmentation. The principle of the CID is based on the fact that the internal energy of ions in their gaseous phase is induced by colliding them

with an inert gas. The kinetic energy of the ions is increased by submitting them to electric field. The increased kinetic energy cause fasts movement of ions and their collision with inert gas. Due to continuous collision with gas, the kinetic energy tends to transform into internal energy. At certain limit the internal energy causes the breakage of the precursor ions generating daughter ions. The principle of the CID is used both for the linear triple quadrupole and 3D ion trap in presence of argon and helium gas, respectively (Wells and McLuckey 2005; Pittenauer and Allmaier 2009; Romanov, Verkerk et al. 2009). Labile post translational modifications are not conserved when CID fragmentation method is applied for peptide sequencing or for determining exact site of modification (Creese and Cooper 2007).

4.3.3. Electron capture dissociation:

Recently developed electron capture dissociation technique is based on the use of low energy electron to cleave the peptide bond. For electron bombardment, an electron gun is introduced within MS instrument. The low energy electrons emitted from the electron gun target the peptide bond within protein or peptide generating the fragments. The electron capture dissociation is mostly used with FTMS analyzers. The use of high resolution analyzers made possible the MS/MS of the intact protein without prior digestion by proteases. Another advantage of the ECD is that the fragmentation pattern only dissociates the peptide bond thereby conserving any post-translational modification on the protein like phosphorylation, glycosylation and the modified peptides are then identified indicating the exact site of the modification (Kelleher, Lin et al. 1999; Medzihradszky 2005; Peter-Katalinic 2005; Sweet and Cooper 2007; Sweet and Cooper 2009).

In proteomics the FTMS instruments with ETD are used for protein identification (Mikesh, Ueberheide et al. 2006). The use is not limited for protein identification, for HDX-MS, these tools are used for peptide mapping as for a typical HDX experiment protocol (HDX section).

Table 6. A general comparison of mass analyzers used here modified from (Siuzdak 2006).

	Ion Trap	**Time-of-Flight Reflectron**	**FT ICR**	**Orbitrap (Perry, Cooks et al. 2008)**
Accuracy	0.01% (100 ppm)	0.001% (10 ppm)	<0.00005% (<0.5 ppm)	~ 0.2 ppm
Resolution	4,000	15,000	500,000	500,000
m/z Range	4,000	100,000	>20,000	>150,000
Scan Speed	~a second	milliseconds	~a second	≤1.8 sec
Tandem MS	MS^n	MS^2	MS^n	MS^n generally with LTQ
Tandem MS Comments	Good accuracy Good resolution Low-energy collisions		Excellent accuracy and resolution of product ions	Advantageous as FT
General Comments	Low cost Ease of switching pos/neg ions Well-suited MS^n	Good accuracy Good resolution	High resolution, MS^n high vacuum, high cost, difficult expense	Low cost, easy maintenance

Chapter 5. Hydrogen/deuterium exchange:

Like other biomolecules proteins are mainly made up of carbon, nitrogen, hydrogen, sulphur and oxygen atoms. These elements perform defined roles e.g. hydrogen atoms remain constantly engaged in the exchange of hydrogen provided by the solvent keeping the molecules soluble (Kwart, Kuiin et al. 1954). In the case of proteins the exchange of the hydrogen with the solvent also depends on the global three-dimensional structure, the local spatial conformation of the protein and the protein interaction with other ligands or protein-protein interactions themselves. In protein molecules secondary structural features polypeptide are dependent on hydrogen bonding. The hydrogens involved in hydrogen bonding to form secondary structure are less susceptible to exchange the hydrogen with solvent (Kabsch and Sander 1983; Richards and Kundrot 1988). Therefore, a technique capable of measuring this hydrogen exchange can provide significant information regarding the solvent accessibility or even the dynamics of the protein. To measure this hydrogen exchange, the protein molecules are diluted in the deuteration solutions and the deuterium uptake is then monitored by nuclear magnetic resonance or mass spectrometry.

The role of mass spectrometry to determine hydrogen deuterium exchange (HDX) was first time realized by Chait's group (Katta and Chait 1991) and fundamentals advancement in the techniques was brought by David Smith's group (Zhang and Smith 1993; Yang and Smith 1997). The role of different acid proteases was used for the HDX MS technique by our group as well (Cravello, Lascoux et al. 2003; Marcoux, Thierry et al. 2009; Rey, Man et al. 2009).

5.1. General mechanism:

For a protein or peptide, three types of hydrogen atoms are found (Figure 37). First, those hydrogens which are linked to carbon atoms of main chain or side chain; these exchange very slowly with solvent and can not be used for few hours deuteration exchange experiments. Second, those hydrogens which are part of the side chains of the residues linked through functional group. Since the side chains of the amino acids are highly dynamic the exchange of these hydrogen atoms occurs at relatively high speed making it difficult to monitor. Third type of hydrogens called as amide hydrogens are considered as best candidates for HDX studies. Their exchange rate is neither too slow nor too fast to be monitored. The amide hydrogens are directly linked to the backbone of the protein therefore provide the exact information of the protein backbone dynamics (see Figure 37)(Rose and Wolfenden 1993).

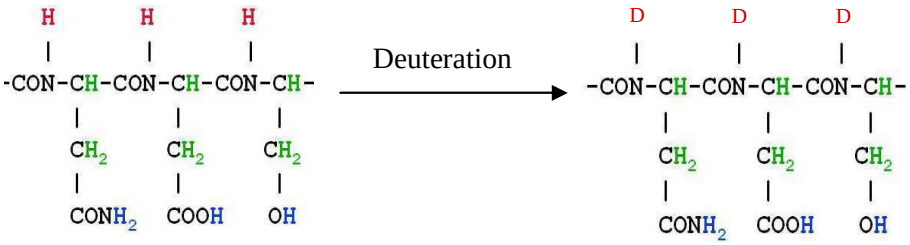

H : Do not exchange
H : Too fast to be monitored
H : Best candidates for deuterium exchange;

Figure 37: Three kinds of hydrogens found in peptides and site of deuterium exchange in lieu of hydrogen.

EX2 and EX1 kinetics:

In folded proteins, secondary structural elements are made due to hydrogen bonding of amide hydrogens. The other amide hydrogens which are not involved in secondary structure and are more likely on protein surface mainly contribute for deuterium exchange. The deuterium exchange for these regions can be explained according to equation 1.

$$F\,(H) \xrightarrow[D_20]{k_{ex}} F\,(D) \qquad (1)$$

where folded state of protein is shown as *F*, hydrogen and deuterium are shown as *H* and *D*. The rate constant for this exchange is defined as k_{ex}.

Within the proteins in a particular region or globally unfolding and folding occurs at different rates in physiological conditions. The deuterium exchange for this condition is described according to equation 2 which shows that deuterium exchange takes place only on unfolded state of protein.

$$F\,(H) \underset{k_{-1}}{\overset{k_1}{\rightleftharpoons}} U\,(H) \xrightarrow[D_20]{k_2} U\,(D) \underset{k}{\overset{k_{-1}}{\rightleftharpoons}} F\,(D) \qquad (2)$$

where *F* and *U* show the folded and unfolded state of protein and/or protein region respectively. Hydrogen and deuterium are shown as *H* and *D*, respectively. k_2 is the rate of exchange in unfolded state of protein. k_1 and $k_{-1}$are rate constant of protein unfolding and folding respectively.

$$k_{-1} >> k_2$$

Now, if rate constant of protein folding k_{-1} is higher than the rate constant of exchange k_2, low deuterium content can be observed for short deuteration times. This model of deuterium exchange kinetics is called as EX2. EX2 is the case for most protein in physiological conditions.

$$k_{-1} << k_2$$

But in some cases the unfolded states of protein exist for comparatively longer duration. In this case rate constant of exchange in unfolded state k_2 is considered higher than the rate constant of protein folding k_{-1} , this condition is called as EX1 kinetics.

It is common to observe two species of isotopic envelopes after deuteration in EX1 kinetics, Pure EX1 kinetics is identified by progressive decrease in intensity of lowered mass and increase in intensity of higher mass envelope (Figure 38)(Deng and Smith 1998; Weis, Wales et al. 2006; Kerfoot and Gross 2011). In other words, EX2 and EX1 can also be defined as deuterium exchange uncorrelated and correlated to protein unfolding.

The remaining traces of undeuterated peptides before the deuterated sample run on liquid chromatography can sometimes also lead to a false observation of EX1 kinetics as reported by *Fang et al* (Fang, Rand et al. 2011). The determination of the exact rate of folding requires precise information of the contribution of each residue exhibiting the EX1 kinetics.

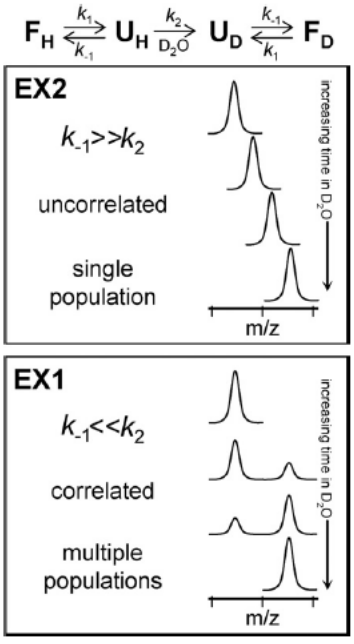

Figure 38. Exmaple of EX1 and EX2 kinetics observed in hydrogen/deuterium exchange (Weis, Wales et al. 2006).

5.2. H/D exchange is influenced by factors:

Apart from protein dynamics and conformation, three other major factors influence the deuterium exchange: the temperature and the pH of the solution and amino acid composition.

5.2.1. Temperature:

It is well established that the movement of the molecules within water or any other matter depends on the temperature of the matter itself and the surroundings. On heating the molecules absorb the energy which leads to increase in their internal energy and fast movement.

In the case of proteins we know that lowering and increasing temperature above a certain limit leads to their cold denaturation and denaturation respectively. However, changes in certain limits do not affect the protein native state but the movement and their rate of amide hydrogen exchange with solvent is affected. The rate of exchange is found to be slowed down the by 3-fold factor on lowering the temperature by 10 degrees (Zhang and Smith 1993). Most of the proteins remain soluble and functionally active at room temperature, therefore HDX experiments are performed at ambient temperature in routine. However, in some cases due the very highly dynamic nature of the protein the exchange was carried out at 0°C and significant difference in HDX was observed in presence or absence of ligand (Brier, Lemaire et al. 2004).

5.2.2. pH:

The reaction of exchange is initiated by the exchange of proton of the HOH or deuteron of DOD in case of deuterated buffer, therefore the pH or pD of the solution plays a major role. In nature mostly the protein molecules are found to be active around physiological pH i.e. between pH 7 to pH 8. Increase or decrease in the pH affects the stability and structure of the protein and as well as rate of hydrogen deuterium exchange. It was also reported that lowering the pH by one unit slows down the exchange rate by a factor of 10 (Figure 39). For example a protein sample requiring 10 seconds to exchange at pH 7 will require 1000 seconds at pH 5 and 10000 seconds at pH 4 respectively (Englander and Kallenbach 1983; Bai, Milne et al. 1993).

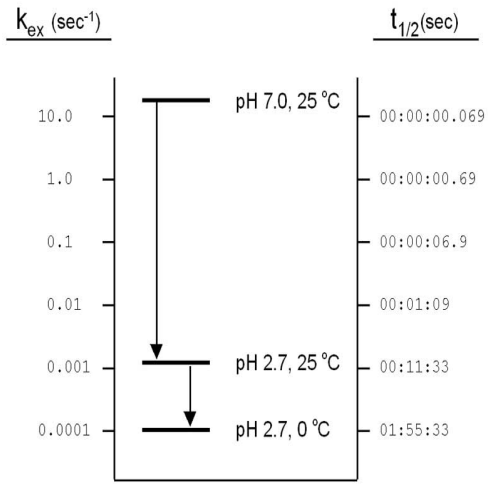

Figure 39. Effect of pH and temperature on amide hydrogen exchange (Bai, Milne et al. 1993).

5.2.3. Peptide sequence:

Soon after introduction of the technique, the influence of amino acid composition in a particular region of protein on HDX was first realized and then monitored by the Englander group (Bai, Milne et al. 1993). The HDX was monitored on the group of dipeptide considering dipeptide of alanine as reference. The effect of side chain of different residues and the absence of amide hydrogen of proline was also considered while calculating the percent deuterium exchange. The presence of acidic or basic amino acids has effect on rate of exchange depending on pH of the solution but generally not considered.

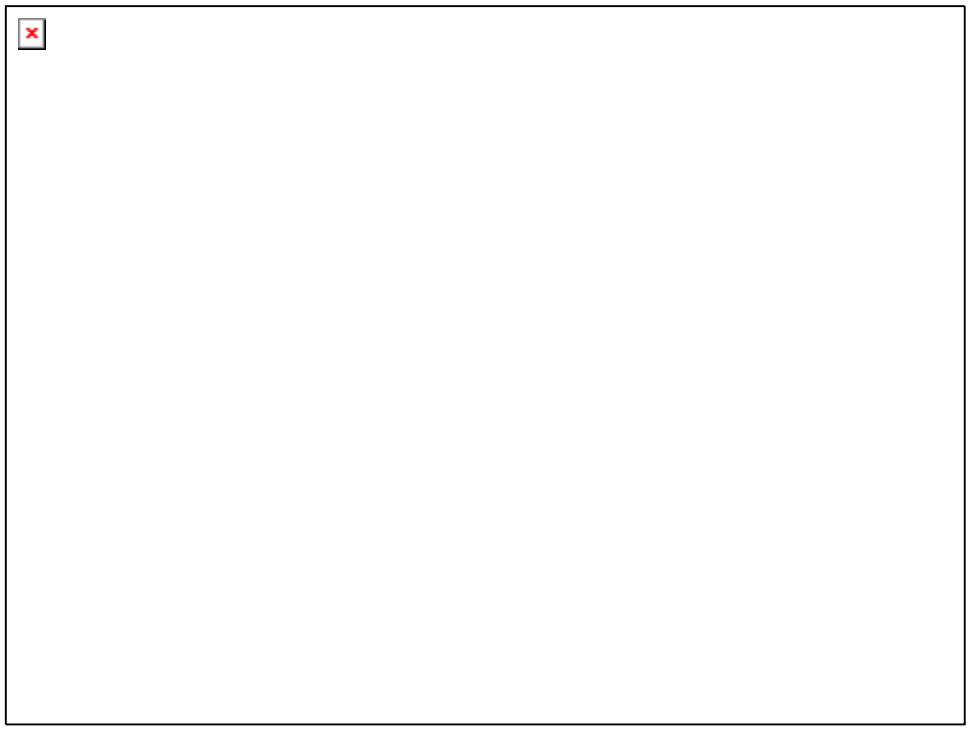

Figure 40. Steps of a typical HDX experiments are shown. The protein sample is diluted in deuterated buffer for different time intervals. The back-exchange of deuterium is avoided by decreasing pH and temperature of sample. The deuterated sample is then either proteolysed by acid proteases or directly sent to mass spectrometer.

5.3. Hydrogen deuterium exchange experiment:

Different steps in a typical hydrogen/deuterium experiment are outlined in Figure 40.

5.3.1. Peptide mapping:

The protein mapping is initial step of any HDX experiment. To acquire the knowledge about conformation change in different regions of a protein, the HDX difference is calculated after digestion of protein by acid proteases. The acid proteases are generally not specific for their cleavage site on protein and generate mixture of unidentified peptide. These peptides are identified by MS/MS and mapped on the sequence of protein.

5.3.2. Protein labeling:

The hydrogen deuterium exchange experiment starts by exchange of protein amide hydrogen with deuterium. This labeling is achieved by diluting 5 to 20 fold the protein solution in deuterated buffer. The pD of this deuterated solution is already adjusted to physiological value or varied unless required (Man, Montagner et al. 2007). For continuous labeling experiments, the concentrated protein sample diluted in deuterated buffer and after different time intervals, the aliquots are drawn, ‘quenched’ and frozen. Usually, the labeling is carried out at room temperature and quench is performed by lowering the pH to 2.2 and temperature to 0°C (Thevenon-Emeric, Kozlowski et al. 1992; Zhang and Smith 1993).

5.3.3. Global deuteration kinetics:

The deuterated sample of proteins can be directly analyzed by electrospray ionization or MALDI mass spectrometry. The mass of undeuterated protein is also determined and the difference of the determined mass between deuterated and undeuterated determines the percent deuterium intake by the protein. The mass of undeuterated protein can also be calculated from the protein sequence but use of mass spectrometer also ensures the target protein is unvaried (Maw, Kennedy et al. 1997).

5.3.4. Local deuteration kinetics:

The local deuteration kinetics is determined to identify the region of interest of the protein. Deuterated samples are digested with help of some acid proteases like pepsin, rhizopuspepsin and plasmepsin (Marcoux, Thierry et al. 2009; Rey, Man et al. 2009). Since the acid proteases are generally non specific to the cleavage site on the protein sequence, therefore the peptides are identified with the help of MS/MS. The uptake of deuterium is then followed with increasing time. The deuteration level of peptides is determined as function of deuteration

time. The deuteration level at any time (t) for example can be calculated by following expression:

$$\text{Deuteration level (t)} = \frac{m(t)-m_0}{m_{100}-m_0}$$

where m_0 is the molecular weight of undeuterated peptide and m(t) is the weight determined after deuteration of protein for duration of time (t). m_{100} corresponds to the determined molecular mass of the fully deuterated amides of the peptide. Another frequent way to determine the percentage of deuteration content is to subtract the molecular weight of undeuterated peptide from the determined molecular weight after of deuterated peptide after deuteration time (t). The value obtained is then divided with the number of amides present in the peptide. This method does not require the fully deuterated peptide as reference.

Difference of molecular weight "$m_{(d)}$" = $m_{(t)}-m_0$

$$\text{Percent deuteration} = \frac{m_{(d)}}{\text{Number of amides}} \quad X \ 100$$

5.3.5. Data analysis:

After successful completion of series of experiments, the next step is to analyze the obtained MS data. Usually manual data processing of the each peptide was in trend but nowadays successful efforts are made to make a computer program enabled of automated data analysis like Magtran, HD-Express, Hydra, Deuterator and HD Examinor etc. (Zhang and Marshall 1998; Weis, Engen et al. 2006; Pascal, Chalmers et al. 2007; Slysz, Baker et al. 2009).

5.3.6. Top-Down HDX:

Recently introduced "top down" approach in HDX MS which is based on the determination of per residue deuterium exchange is carried out by the above mentioned fragmentation method and MS instrument. The 'top down' approach is unique to the conventional HDX experiments because no prior digestion with acid proteases is carried out (Figure 41). The intact protein is exchanged with deuterium and subjected to fragmentation with ECD (Hagman, Tsybin et al. 2006; Pan, Han et al. 2009; Pan, Han et al. 2010). The technique is used for smaller proteins in general. There are few examples where CID fragmentation is also applied for Top-Down HDX but due to scrambling effect, it is not being applied extensively (Deng, Pan et al. 1999; Ferguson, Pan et al. 2006).

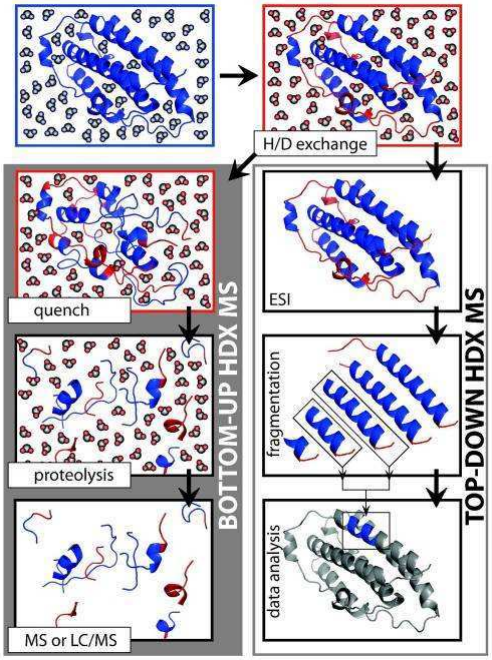

Figure 41. The conventional HDX MS experiment setup called 'Bottom-Up HDX MS is compared with recently advanced Top-Down HDX-MS (Kaltashov, Bobst et al. 2009).

5.4. HDX-MS applications:

The applications of HDX-MS are increasing with time as the development of the technique. For example, X-ray crystallography is no doubt the main source about the knowledge of any protein structure but the dynamics of the protein in solution itself and after binding with effectors is difficult to follow with the typical X-ray crystallography generated structures. Protein-ligand, protein-protein interactions and the intermediate states of the protein folding pathway from its denatured to natured state is possible to be monitored with the HDX-MS. The focus of research has been towards the membrane protein characterization during last few years by various biophysical methods. HDX-MS is also expanding its role for characterization of membrane proteins dynamics.

5.4.1. Protein folding:

The specific sequence of the amino acids and subsequently structure adopted by the proteins dictates the function of protein molecules. In cell the protein molecules are expressed as linear chain and then they are folded with help of other factors and special folding machineries "chaperones"(Rose, Fleming et al. 2006). It is also reported that misfolding of the protein can cause severe dysfunction leading to disease conditions such as Alzheimer's and Parkinson's diseases (Selkoe 2003). Therefore, it seems interesting to acquire the knowledge about the

different folding stages and protein conformation during these steps. With the help of HDX-MS it is possible to follow the folding of the protein (Konermann and Simmons 2003).

Whereas a protein has the capability to conserve its native conformation in the favorable conditions which is of course necessary for the function, on the change of pH or temperature it tends to lose the structural arrangement and we called this as denatured state. But interestingly on providing the good conditions the denatured form adopts back the native one. During this denatured to native state there are several short-lived protein conformations which are explored by deuteration of the fractions of sample for milliseconds (Figure 42). Deuteration kinetics of these fractions carries the information about the intermediate of the folding steps. The technique is called as pulse HDX (Miranker, Robinson et al. 1993; Konermann and Simmons 2003; Pan, Han et al. 2010).

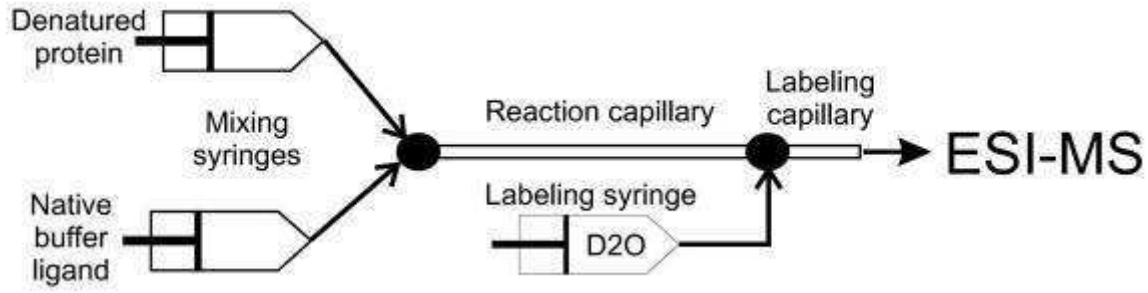

Figure 42. The scheme of the strategy used for the pulse labeling to probe the folding steps of a denatured protein (Suchanova and Tuma 2008).

5.4.2. Protein-ligand, protein-protein interaction:

Within the biological systems the interaction of protein molecules with other protein molecules and/or varied molecular weight ligands (drugs, metals, or hormones etc.) is often observed. By interacting with the regulators the mechanisms of protein functioning are regulated (Schneider, Prosser et al. 2009). The binding of DNA binding proteins to DNA is also found to be essential for its replication and super-coiling (Weber, Ashkar et al. 1996; Saiz and Vilar 2008; Tarassov, Messier et al. 2008; Schneider, Prosser et al. 2009). Therefore, these interactions are of high significance and monitoring them can provide the functional basis of these complexes.

There are few examples of high resolution structures of these complexes but to crystallize these assemblies has been challenging for the X-ray crystallographers and due to their large size nuclear magnetic resonance has been also a difficult solution (Shi and Wu 2007; Janin, Bahadur et al. 2008; Tang, Luo et al. 2010). Nevertheless, the interaction between the

subunits of these complexes can be probed by HDX-MS (Marcsisin and Engen 2010) (Figure 43.) For this purpose the HDX of intact protein in monomeric form or in apo form is monitored and compared with protein in multimeric form or after interaction with ligand respectively.

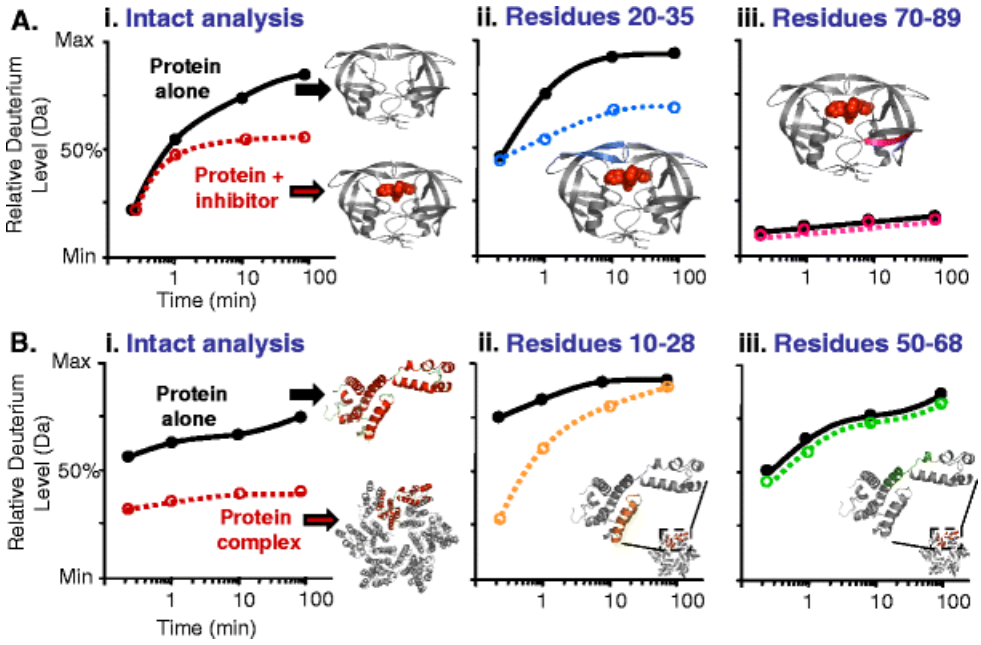

Figure 43. The strategy employed for targeting the interaction regions in case of protein-protein or protein ligand interaction is illustrated (Marcsisin and Engen 2010).

5.4.3. Membrane proteins and HDX-MS:

The importance of membrane protein in living organisms is very well established. They provide a passage across the lipid bilayer for transportation of hydrophilic substances inside and outside of the cell. Many act as receptor, bind the ligand on extracellular surface and trigger the response inside the cell. As a receptor on the cell membrane or on nuclear receptor, membrane proteins are also target of the administered drugs (Tsuchida, Yamauchi et al. 2005; Taylor, Talley et al. 2007). Within the cell their presence in the mitochondria makes sure the availability of ATP which is energy coin for the cell e.g. the mitochondrial membrane carries high number of ADP/ATP carrier(Nury, Dahout-Gonzalez et al. 2006). In eukaryotes small peptides involved in immune response and the peptides results of the protein degradation are transported with the help of membrane proteins like ABC transporters (Procko and Gaudet 2009).

Due to their presence in lipid bilayer the membrane proteins are largely composed of hydrophobic residues and in result their hydrophobic nature makes difficult dissolution in the aqueous buffer. Therefore, several agents like detergents are used for the solubilization and

extraction of these proteins; in contrast these agents produce hindrance in the analysis of target protein molecules. With the development of biophysical techniques the number of membrane proteins structures are increasing on daily basis but search within PDB with keywords of membrane proteins retrieves only 441 out of 76669 structures making only 0.5% of all the deposited entries. Even if structure is solved, it is possible that the protein is crystallized in a conformation and in presence of other ligand with other conformation the structure is never solved. Another issue frequently encountered with researchers in case of membrane proteins is their expression level is poor and therefore less sample availability for structure determination techniques.

After realizing the above mentioned problems and importance of membrane proteins, the HDX-MS is now being frequently used for the conformational analysis of membrane proteins. Due to several advantages of HDX-MS it is possible to use the technique for exploration of the mentioned class of proteins. As compared to other techniques, it requires less sample amount, more tolerant to presence of solubilization agents like detergents. Several methods have been invented for removals of the detergents before mass spectrometry analysis (Wu and Yates 2003; Everberg, Gustavasson et al. 2008; Rey, Mrazek et al. 2010).

The structure of mitochondrial ADP/ATP carrier from bovine in complex with carboxyatractyloside was solved several years ago. The structure of carrier in complex with other inhibitors couldn't be obtained. However, with the use of HDX-MS it was made possible to explore the dynamics of the carrier in complex with another inhibitor bongkrekic acid. The dynamics obtained in complex with CATR were similar to those obtained with the structure and validated the technique. Application on the bongkrekic acid carrier complex showed other possible adopted conformation (Rey, Man et al. 2010).

Another important class of membrane protein G protein-coupled receptor (GPCR) has been targeted by the scientists to obtain the information about their functioning and mechanism behind the activation of GPCR after binding the ligands (Yao, Velez Ruiz et al. 2009; Wu, Chien et al. 2010). Very recently the dynamics of the receptor was explored with the help of HDX-MS and information about the conformations in presence of different agonists and antagonists is obtained (West, Chien et al. 2011).

Furthermore, it is also recently shown that technique is suitable to probe the conformational changes of membrane proteins embedded in phospholipid bilayer nanodiscs (Hebling, Morgan et al. 2010).

Materials and Methods

1. Purification of recombinant BmrA:

The plasmid pET-23b carrying the gene for BmrA was transformed into competent *E. coli* strain C41 (DE3).

1.1. *E. coli* StrainC41 (DE3):

C41 is an expression system used for the overexpression of recombinant proteins both from prokaryotic and eukaryotic origin. It is a mutant of BL21(DE3) which is known for producing the T7 RNA polymerase after receiving the genetic information from prophage (Miroux and Walker 1996). The addition of IPTG induced the expression of cloned gene of recombinant protein by acting on lac UV5 promoter region (Studier, Rosenberg et al. 1990).

1.2. Plasmid vector pET-23b:

pET-23b is a circular DNA molecule which is transformed into the competent bacteria for overexpression of targeted protein (Figure 44). The pET-23b has dual functions: first it carries the DNA information which helps the bacteria to survive on exposure to ampicilline hence providing the selectivity for the bacteria with the transformed vector. The gene of target protein with extra His-tag of six histidine is inserted into the plasmid immediately after the region for expression by the T7 RNA polymerase. After the induction of IPTG, the bacteria tend to overexpress the T7 RNA polymerase and eventually the recombinant protein.

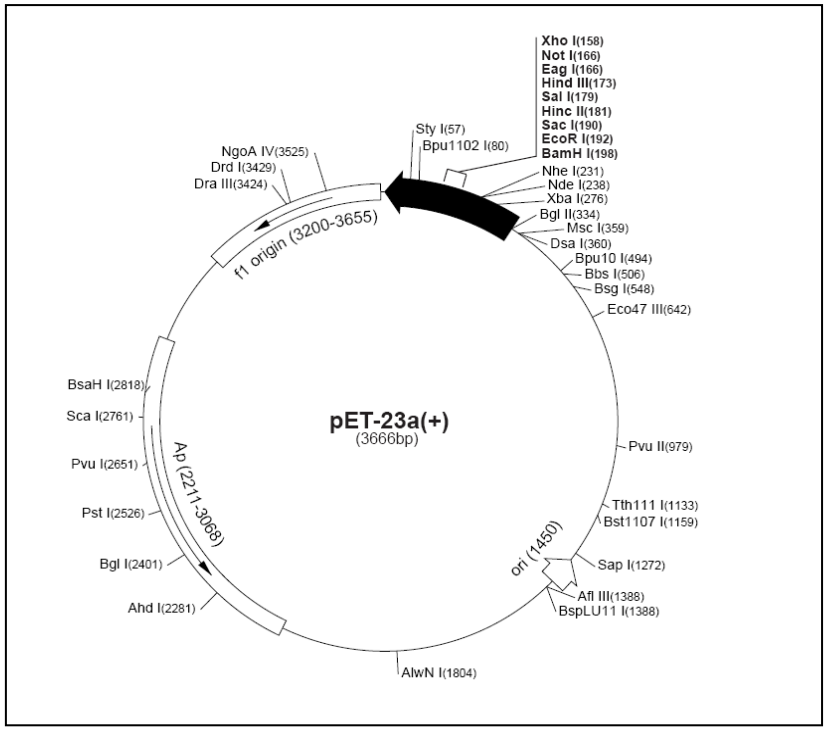

Figure 44. Map of the plasmid pET-23a(+)

1.3. Preparation of competent cells:

E. coli bacteria were grown overnight in a small amount of LB medium. In 50 ml of LB medium, 1 ml of the preculture was added and kept for incubation at 25°C. At optical density between 0.6-0.8 the cells were taken and centrifuged in a sterile tube at 5000g at 4°C. The pellet was slowly dissolved in PIPES buffer (buffer composition, page. 93). After solubilization the bacteria were kept on ice for 2-3 hours followed by another centrifugation step at 1100g at 4°C. The pallet was dissolved in same buffer with maximum volume of 2 ml. The cells were fractionated in 100 µl volume, frozen in liquid nitrogen and stored at -80°C till further use.

1.4. Plasmid vector transformation:

100 µl of the previously prepared competent bacteria strain C41 (DE3) were left on ice for 10 minutes to thaw them. Then 1 µl of vector plasmid carrying the gene for BmrA was added to the competent cells and left on ice for 20 to 30 minutes. The competent bacteria with the plasmid were submitted to a thermal shock at 42°C for 1 minute. Immediately after the heat shock the bacteria were again left on ice for another 10-15 min. Then 600 µl of autoclaved LB medium was added to the tube. The bacteria were then incubated at 37°C for one hour. This phase helps the bacteria to become active and start dividing. After one hour, 100 µl of the transformed bacteria were spread over a Petri dish. The Petri dish contained LB medium, 35 g/l of agar and 100µg/ml ampicilline. The Petri dish was then incubated overnight at 37°C.

1.5. Culture Medias:

Two culture medias; LB and 2YT were used for the transformation and production of BmrA respectively.

Composition:

	LB Medium	**2YT Medium**
Bactotyptone	16g	10g
Yeast Extract	10g	5g
Sodium Chloride	5g	10g

1.6. BmrA Overexpression:

While avoiding any satellite colony, three to four colonies of transformed *E. coli* were randomly picked up from the Petri dish and added to one liter of 2YT medium in a flask. The medium was autoclaved and then 75µg/ml ampicilline was added before the addition of colonies. The flask was then kept at 25°C in a shaking incubator overnight. Next day the absorbance of the growing culture was measured at 600 nm. As soon as the optical density reached 0.8, 700 µl of IPTG (1 M) was added into culture medium which makes the final concentration of IPTG 0.7 mM. Again the flask was incubated in a shaking incubator at 25°C for another four hours.

1.7. Preparation of inverted membrane with overexpressed BmrA:

After the induction of BmrA expression, the bacteria were centrifuged at 7500g for 20 minutes at 4°C. The pellet of bacteria was solubilized in 10 ml of buffer 'A' (see buffer composition, page 93) making sure that the entire pellet was well dissolved without leaving any solid mass. The cells were then broken with the help of microfluidizer with a pressure range between 15000 to 18000 psi.

After the breakage of the cells, EDTA was added to cell lysate at 10 mM final concentration. Microfluidizer lysis is considered one of the latest and most efficient way to lyse cell. Nevertheless, the lysate was centrifuged at 15000g for 30 minutes in order to remove cell debris (high molecular weight cytoplasmic content of the cells) and bacteria which were not broken. After centrifugation step, the solid residue at the bottom of tube was discarded and supernatant was collected. The supernatant was then subjected to ultracentrifugation at 100,000 g for one hour. This ultracentrifugation step was performed in order to collect the cell membranes. This pellet of cell membranes was dissolved in buffer 'A°' and subjected to another ultracentrifugation step at 100,000 g for one hour. After second centrifugation step, the pellet was dissolved in buffer 'B' keeping the volume as low as possible. This dissolved pellet contained inverted vesicles highly enriched in BmrA (at almost 50% of the all protein content). The protein concentration within vesicles was determined by modified Lowry's method. The vesicles were frozen in liquid nitrogen and stored at -80°C. All the steps right after the bacteria centrifugation until the preparation of vesicles were performed keeping the temperature of the sample at 4°C.

1.8. BmrA solubilization:

The inverted vesicles were thawed at 37°C and then immediately transferred onto ice. The vesicles were then diluted in buffer 'S' in such a way that final protein amount concentration remained between 1-2 mg/ml. Detergent DDM (n-dodecyl β-D-maltoside) was added to the solution (final concentration of DDM at 1%). The solution was left for mixing at slow speed for one hour to solubilize the proteins. In order to separate the membrane after solubilization, another ultracentrifugation step was added at 280,000 g for one hour. The supernatant with solubilized proteins was kept and the pellet was discarded.

1.9. Affinity chromatography:

As it is described earlier, BmrA was overexpressed with additional continuous six histidines residues at the C-terminal of the protein. The purpose of this His-tag is to facilitate the purification of BmrA with the use of Ni affinity chromatography. In Ni affinity chromatography the nickel element is fixed on the resin sepharose, and works as chelating agent. On the addition of protein solution with His-tag, electrostatic interaction is formed between the protein and fixed nickel and hence protein molecules are trapped within the resin. Once bound, the interaction can be then reduced by addition of another potential partner (in our case imidazole) for nickel and thereby protein is released from the nickel and collected.

Column preparation:

In an empty plastic column of 20 ml the filter was placed on one end to close it. 20% ethanol was used to wash the column followed by another washing step with deionized water. Then 1 ml of Ni^{++}-agarose resin was poured in the column as supplied by the manufacture. The resin was washed with deionized water.

Equilibration of the column:

Into the column eighteen ml of buffer 'E' was added and column was kept on the rotor wheel at 4°C for ten minutes. This step is for the equilibration of the column before addition of protein solution.

Loading protein solution on the column:

After the equilibration of the resin, excess buffer 'E' was removed. Then the solubilized proteins solution was added into the column and left on rotor wheel for 30 min at 4°C. After 30 min of incubation this solution was allowed to pour through the column leaving the protein

bound with the resin. 20 ml of buffer ‘L’ was added into the column and left for incubation for 45 minutes followed by overnight incubation of column with buffer ‘L’. The long duration washing with buffer ‘L’ is to get rid of any protein contamination.

Elution of BmrA:

After the washing step, bound protein was released by passing 7 ml of buffer ‘E’. There was a high concentration of immidazole within the buffer which helped to dissociate the interaction between protein and Ni and hence targeted protein is released and collected in fraction of 1 ml each. 1 µl of each fraction was mixed with 5 µl of Bradford and based on visual examination, fractions with higher protein amount were pooled together.

1.10. Dialysis:

The pooled protein fractions were dialyzed against 1 L of buffer ‘D’ for two hour and then for overnight. The protein concentration of the dialyzed sample was determined by Bradford method. The protein concentration was concentrated up to 1.6 mg/ml with a vivaspin filter with a cut off of 100 kDa.

1.11. Composition of buffers:

Buffer ‘A’ :	**Buffer ‘E’ :**
50 mM Tris-HCl pH 8	50 mM Tris-HCl pH 8
5 mM MgCl2	Glycerol 15 %
1 mM DTT	100 mM NaCl
1 mM PMSF	10 mM Imidazole
Anti protease	DDM 0.05 %

Buffer ‘A°’ :	**Buffer ‘L’ :**
50 mM Tris-HCl pH 8	50 mM Tris-HCl pH 8
1.5 mM EDTA	Glycerol 15 %
1 mM DTT	100 mM NaCl
1 mM PMSF	20 mM Imidazole
Anti protease	DDM 0.05 %

Buffer 'B' :

20 mM Tris-HCl pH 8
300 mM Sucrose
1 mM EDTA

Buffer 'E °' :

50 mM Tris-HCl pH 8
Glycerol 15 %
100 mM NaCl
250 mM Imidazole
DDM 0.05 %

Buffer 'S' :

50 mM Tris-HCl pH 8
Glycerol 15 %
100 mM NaCl
10 mM Imidazole
1 mM PMSF

Buffer 'D':

50 mM Tris-HCl pH 8
Glycerol 10 %
50 mM NaCl
DDM 0.05 %

Buffer PIPES:
10 mM PIPES
60 mM $CaCl_2$
15% Glycerol

2. Purification of recombinant BmrC/BmrD:

The plasmid pET21 carrying the double gene for BmrC/BmrD was transformed into competent *E. coli* cells BL21 DE3 *ΔacrB* (Ma, Cook et al. 1995).

2.1. Plasmid vector transformation:

The plasmid vector was transformed into competent cell following the same protocol as for BmrA.

2.2. Overexpression of BmrC/BmrD:

To one liter autoclaved culture of TB medium ampicilline (75 µg/ml) was added. Then from Petri dish around 8 to 9 colonies of BL21 (DE3Δ*acrB*) carrying the transformed plasmid of BmrC/BmrD were added into culture. The culture was incubated at 37 °C for 13 hours in the shaking incubator at a speed of 225 rpm. After around 13 hours when optical density reached between 1.8-2.0, IPTG was added at final concentration of 0.7 mM and incubated again in shaking incubator at 25°C for another16 hours.

Afterwards bacteria were collected, inverted-membrane vesicles were prepared and BmrC/BmrD were purified following the same protocol used for BmrA.

3. Biochemical and analytical methods:

3.1. Protein concentration:

There are two steps in the protein purification protocol where the exact protein concentration determination is required: for the inverted membranes vesicles and at final stage of purified protein in detergent. Therefore, two methods were used Lowry method for protein concentration determination in inverted membrane vesicles and Bradford method for the purified protein solubilized in detergent. Due to the presence of sugar in buffer 'B' the Lowry method was modified and therefore will be referred to as modified Lowry method.

3.1.1. Modified Lowry method:

The Lowry method is a biochemical assay used for the determination of total protein concentration in a solution. The method can be applied to determine the concentration from 5 mg/ml to 100 mg/ml (Lowry, Rosebrough et al. 1951). In alkaline medium aromatic residues of the protein i.e. tyrosine and tryptophan tend to react with cupric sulfate-tartrate making a complex. This complex has tendency to reduce Folin-Ciocalteu reagent. The reduction of reagent results in apparent of blue color. The content of blue color could be visually noticed and then exact amount is determined by reading at 595 nm against a standard curve using BSA.

3.1.2. Bradford method:

Bradford protein concentration determination method is most frequently used in protein purification techniques to accurately determine the protein concentration. It is a short protocol requiring only Coomassie Blue G250 dye and can be performed within few minutes. Like other spectroscopic technique, the principal is based on the color change of the dye after its binding to protein and then can be read at 595 nm (Bradford 1976).

A standard curve was determined with the help of known concentrations of BSA range of 0 to 30 µg protein concentration. To determine the protein concentrations, the protein samples after the final step of purification were diluted two and five times in buffer 'D'. 30 µl of both sample protein solution and standard BSA solution were mixed with 900 µl of Coomassie Plus reagent (provided by Pierce) separately. After five minutes incubation, the absorbance of the solutions was read at 595 nm. To measure the exact concentration, the protein samples were performed in triplicate and mean protein concentration value was determined.

3.2. Protein characterization by polyacrylamide gel electrophoresis (SDS-PAGE):

SDS-PAGE (sodium dodecyl sulfate polyacrylamide gel electrophoresis) was used for the characterization and separation of protein molecules based on their molecular weight. The technique is also helpful for the profiling of proteolytic fragments of a protein originating due to the limited proteolysis.

PAGE principal is based on the movement of charged particles under electric field. Acrylamide provide the platform (in form of gel) for the migration of protein molecules and addition of SDS causes denaturation and equal charge distribution on all the molecules. Therefore, the migration of the proteins is solely based on the number of residues present and eventually on molecular weight.

3.2.1. Gel composition:

The composition of an SDS-PAGE gel consists of acrylamide, Tris-HCl, SDS, ammonium persulfate (APS) and N, N, N ', N'-tetramethylethylenediamine (TEMED).

The acrylamide is provided in solution carrying both acrylamide and bisacrylamide, its polymerization is initiated by ammonium persulfate in the presence of TEMED. The tertiary amines of the TEMED catalyze the free radical formation from the ammonium persulfate which then causes the polymerization of acrylamide. The thickness of the gel is defined by percent content of acrylamide in the final solution. In routine analysis ~12% acrylamide gel was used for the proteins below 40 kDa and 9-10% was used for the higher molecular weight.

For BmrA and BmrC/BmrD, the gel was polymerized into two parts, stacking and resolving. The stacking gel acrylamide concentration was kept at 4 %, this part of the gel is to concentrate the sample before migration on the resolving gel.

The composition of stacking gel:

Tris-HCl 100 mM pH 6.5

Acrylamide 4 % (w / v)

SDS 0.1 % (w / v)

Ammonium persulfate 0.1 % (w / v)

and TEMED 0.001 % (v / v)

The resolving gel which made the larger part of the gel was 10 % of acrylamide and Tris HCl was used at pH 8.0.

For limited proteolytic samples analysis the concentration of resolving gel was kept at 12 %.

Sample Preparation: before loading onto the gel the samples were mixed with Laemmli 4X buffer (also known as sample dilution buffer) in 3:1 ratio. The mixture was kept at 37°C for five to ten minutes and immediately loaded after the heating step. In addition to samples, markers with known molecular weight and prestained with dye were also loaded in the first well of the stacking gel. The composition of Laemmli buffer:

Tris-HCl 250 mM pH 6.8

Glycerol 40 % (v / v)

SDS 8 % (w / v)

β-mercaptoethanol 4 % (v / v)

bromophenol blue 0.001-0.04 % (w / v)

3.2.2. Coloration/decoloration:

After the samples were separated on the gel by electrophoresis, the acrylamide gel was kept in the solution of Coomassie Blue R250 , 0.25 % (w/v) dissolved in ethanol 40 % (v/v) and acetic acid 10 % (v/v). This step was performed to color the protein samples in the gel. The unrequired staining of the gel which masked the proteins samples was removed by keeping the gel in ethanol 10 % (v/v) and acetic acid 5 % (v/v) solution (Diezel, Kopperschlager et al. 1972).

3.3 Limited proteolysis of BmrA:

The limited proteolysis of wild-type BmrA was performed in apo and Vi inhibited form in detergent solubilized state and BmrA enriched membranes. The protease to substrate ratio was kept 1:1000 in both cases.

Briefly, 10 µl of freshly prepared trypsin at concentration of 10 µg/ml was added to 100 µl of concentration protein solution carrying BmrA at 1.0 mg/ml protein concentration. Aliquots of 10 µl were withdrawn after 5, 15 and 30 min. 1 µl of TFA 0.01% was added in each aliquot and quickly frozen in liquid nitrogen. To acquire the inhibited form of BmrA with Vi, 5 µl of Mg^{2+} 100 mM, 5 µl of ATP 100 mM and 2µl of Vi 70 mM were added to the protein solution prior to digestion by the protease. The aliquots for BmrA digestion in inverted membranes vesicles were withdrawn after 5, 15, 30, 60, 120 and 180 min.

The samples were then analyzed by electrophesis on a SDS PAGE gel of 12.5%. The gel was scanned after the completion of electrophoresis.

3.4. ATPase activity:

To determine the ATPase activity of BmrA, a multienzyme coupled system was used. In this system the ADP produced by the hydrolysis of the ATPase (BmrA in this case) is continuously regenerated back into ATP by the pyruvate kinase. The pyruvate kinase converts phosphoenol pyruvate into pyruvate. Lactate dehydrogenase catalyze a reaction converting pyruvate into lactate, this reaction requires NADH as cofactor and its oxidation results into NAD^+ formation. The NADH absorbs at 340 nm, as the hydrolysis of ATP is increased the rate of conversion of NADH to NAD^+ is also accelerated which leads to decrease in amount of NADH. The lower absorbance at 340 nm provides direction of the ATP hydrolysis rate by ATPase (Pullman, Penefsky et al. 1960).

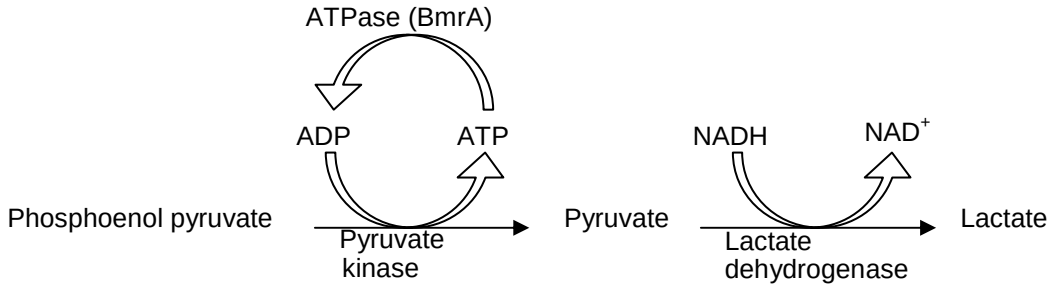

Preparation of ATP and ortho vanadate stock solutions:

100 mM ATP solution was made by dissolving the amorphous ATP (supplied by Sigma) in 100 mM Tris solution. The pH was adjusted at 8 with HCl. Tris solution protects the sharp change in pH on the dissolution of ATP, as ATP tends to hydrolyze quickly itself at acidic pH.

To prepare the saturated solution of orthovanadate, 100 mg of Na_3VO_4 was dissolved in 3 ml of deionize water. Due to low solubility, the solution was heated at 90°C and pH was adjusted at 10 with HCl. As the solution turns colorless, the concentration of vanadate is measured at 265 nm, optical density coefficient of vanadate is $2925 M^{-1}cm^{-1}$.

Both solutions of ATP and vanadate were divided into 100 µl aliquots and frozen at -20°C till further use.

Formula for rate of ATP hydrolysis:

How to calculate the activity: $OD = \varepsilon.l.c$ therefore $\Delta OD = \varepsilon.l.\Delta c$

and $\varepsilon NADH_{340nm} = 6220\ (l.mol^{-1}.cm^{-1})$

Rate of NADH disappearance (mol/min) = Δc (mol/l/min) x V(sample volume, in l)

$$\text{Rate (mol/min)} = \frac{\Delta OD}{\varepsilon . l} \times V = \frac{\Delta OD\ (min^{-1})}{6220 \times 1\ (cm)} \times 500.10^{-6}\ (\text{if } 500\ \mu l)$$

$$\text{Rate (}\mu\text{mol/min)} = \frac{\Delta OD}{\varepsilon . l} \times V = \frac{\Delta OD\ (min^{-1})}{6220 \times 1\ (cm)} \times 500$$

$$\text{Rate (}\mu\text{mol/min/mg)} = \frac{\Delta OD\ (min^{-1}) \times 500 \times 1000}{6220 \times \text{Protein (in } \mu g)} = \frac{\Delta OD\ (min^{-1}) \times 5.10^{2}}{6.22 \times \text{Protein (in } \mu g)}$$

To measure the activity of proteins in detergent, the buffer used was Tris-HCl 50 mM pH 8, NaCl 50 mM, $MgCl_2$ 5 mM , glycerol 10 % (v / v), β-mercaptoethanol 5 mM, lactate dehydrogenase 32 µg/ml (isolated from rabbit muscle, Roche), pyruvate kinase 60 µg/ml (isolated from rabbit muscle, Roche), phosphoenol pyruvate 4 mM (Roche), NADH 0.4 mM (Roche) and DDM 0.05 % (w / v) (Alexis). While monitoring the inhibitory effect of vanadate on ATPase activity of BmrA, orthovanadate 0.2-0.5 mM was added in the reaction buffer before the addition of protein. In a quartz cuvette with a thickness of 1 cm and a volume of 500 µl, 10-20 mg of protein in detergent was incubated in buffer at 30° or 37° C for 5 minutes. The reaction was triggered by adding 20 µl of ATP 100 mM to a final concentration of 4 mM and absorbance at 340 nm was followed for 10 minutes. The slope (ΔOD340nm/Δt) was calculated from 2 to 4 minutes.

3.5. Deuterated sample preparation:

3.5.1. BmrA deuteration in detergent:

ABC exporter BmrA, both wild-type and mutant E504A, were purified in dimeric state and concentrated up to 1.6 mg/ml in hydrogenated buffer. After concentrating the protein was diluted ten times in deuterated buffer. The deuterated buffer was composed of 50 mM NaCl and 0.05 % DDM in 99.9% D_2O (Sigma).

Hydrogen deuterium exchange (HDX) reaction was initiated by adding 84 µl of concentrated protein in 756 µl of deuterated buffer at 0 s. After 15, 60, 300, 600, 1800 and 3600 s, aliquots of 120 µl of deuterated samples were withdrawn and mixed with 26 µl of quench solution.

The quench solution was composed of 8 M guanidium hydrochloride (GndCl), 500 mM glycine HCl, pH 2.2. This solution was pre-cooled on ice. After mixing with quench buffer each aliquot was frozen in liquid nitrogen and kept frozen till further use.

For inhibited state of wild type BmrA, the concentrated protein solution was incubated with 5 µl of 100 mM ATP, 5 µl of 100 mM Mg^{2+} and 2.5 µl of 70 mM Vi for few minutes prior to dilution in deuteration buffer. To obtain inhibited state of BmrA mutant E504A similar amount of reagents were used as for the wild-type except that Vi was not included.

The deuterated samples for protein deuteration kinetics and peptide deuteration kinetics were prepared in similar way.

3.5.2. Deuteration of BmrA enriched inverted membrane vesicles:

To deuterate BmrA enriched membranes vesicles, 20 mM Tris HCl (pD 7.6) solution was prepared in 99.9% D_2O. For both wild-type and mutant E504A, membranes were diluted till total protein concentration of 5 mg/ml. Then, as for the experiments in detergent 84 µl solution of membranes were diluted in 756 µl of deuteration buffer to initiate the hydrogen deuterium exchange and after specific time intervals aliquots were withdrawn and frozen.

The inhibited state of mutant of BmrA mutant E504A was prepared in a similar way as to the detergent sample.

3.5.3. BmrC/BmrD deuteration in detergent:

BmrC/BmrD, in case of wild-type and mutants, was purified and concentrated up to 5 mg/ml in detergent. For wild-type apo state 40 µl of concentrated protein was diluted in 560 µl of deuterated buffer. For deuterated buffer of BmrC/BmrD, HCl 50mM pD 7.6, NaCl 300 mM and DDM 0.05 % was dissolved in 99.9 % D_2O. After 15s of dilution an aliquot of 105 µl from dilution tube was withdrawn and transferred into another tube already containing precooled 35 µl of quench solution (GndCl 7M in HCl 50 mM) and frozen in liquid nitrogen till further use. Similarly, four more aliquots after 1, 10, 30 and 60 min were mixed with quench solution and frozen.

For mutants, E592D (BmrD), E592D/D500E (BmrC/BmrD) and E592A/D500A (BmrC/BmrD), 2.5 µl of ATP 100 mM and 2.5 µl of Mg^{2+} 100 Mm were incubated with 45 µl of protein sample for 10 minutes. From incubated solution 40 µl of sample was diluted in deuteration buffer, quench mixed and frozen as for the wild type.

4. Mass spectrometry:

Similar solvents and conditions were used for peptide analysis of BmrA and BmrC/BmrD unless specified.

4.1. Liquid chromatography:

Two types of MS instruments were used: electrospray ionization (ESI) and Matrix-assisted laser desorption ionization (MALDI). But most of the analyses were performed on electrospray ionization coupled with high performance liquid chromatography (HPLC). For HPLC two kinds of typical solvent systems were used: solvent 'A' and solvent 'B'.

The solvent 'A' was composed of mass spectrometry grade water 99.97 % (v/v) (LC-MS Ultra Chromasov, Sigma Aldrich) and trifluoroacetic acid 0.03% (v/v)(Acros Organics, 99.9%). The solvent 'B' consists of acetonitrile 95 % (v/v) (LC-MS Ultra Chromasov, Sigma Aldrich), water 4.97 % (v/v) and trifluoroacetic acid 0.03% (v/v). For online desalting step of protein and peptides, protein macrotrap (Protein Macro Trap^{TM}, Michrom) and peptide microtrap (Peptide Micro Trap^{TM}, Michrom) were used, respectively. The peptides were separated exploiting hydrophobic interactions on Jupiter C18 (Phenomenex) column of 5 µm particle size.

The peptides either eluting from the immobilized pepsin column or from in solution digestion were concentrated and desalted on the peptide microtrap at flow rate of 200 µl/min of solvent 'A'. The sample loading, digestion (in case of pepsin column), concentrating and desalting, all four steps were performed in two minutes. The C18 analytical column was pre-equilibrated at 15 % of solvent 'B', the peptides eluted from microtrap were separated on analytical with help of gradient of solvent 'B' from 15% to 45% in 26 minutes. The detergent liberated after the elution of last peptide hence did not disturb the LC and MS analyses of peptides. The monoisotopic mass of each peptide was confirmed on ToF.

4.2. Mass spectrometry calibration:

The ESI-ToF was calibrated with ESI Low Concentration Tuning Mix (Agilent Technologies) molecular weight range from 118 Da to 2722 Da in positive ion mode. Similarly, ESI-TRAP was calibrated with ESI Tuning Mix (Agilent Technologies) in positive ion mode but once a month only. The MALDI-ToF instrument was calibrated with protein calibration standard (Bruker Daltonics) mass range from 757 Da to 3150 Da and from 22307 Da to 66000 Da for peptides and protein analysis respectively. The matrices used for sample preparation in

MALDI analyses were sinapinic acid (Sigma Aldrich) and α-cyano for protein and peptide analyses, respectively.

4.3. LC-MS/MS analyses:

The LC-MS/MS technique was used for the peptides mapping.

BmrA:

To identify the proteolytic fragments generated from the pepsin digestion, the MS/MS analysis of BmrA was performed on Trap Esquire 3000+ (Bruker Daltonics). The instrument was equipped with ESI source directly coupled with a manually operated HPLC (Shimadzu). The data acquisition and analysis were done with the programs Esquire Control v5.0 (Bruker) and Data Analysis v3.2 (Bruker), respectively.

The peptides were loaded and concentrated on peptide microtrap at flow rate of 200 µl/min of solvent 'A' for three minutes. The gradient 15 % to 45 % solvent 'B' in 57 min was run on pre-equilibrated C18 analytical column. The mass range was kept between 100 Da to 1500 Da.

BmrC/D:

The LC-MS/MS experiments for the peptide mapping of BmrC/BmrD were carried out on FT-ICR mass spectrometer (Bruker Daltonics). The instrument was also equipped with ESI source and directly coupled with liquid chromatography.

4.4. LC-MS analyses:

Mass Spectrometer:

The LC-MS analysis of intact protein and peptides were carried out on ESI-ToF (Time-of-Flight LC/MS 6210, Agilent Technologies). The ESI source was directly coupled with high perfoemance liquid chromatography (HPLC). Both HPLC and MS were administered through the online program Data Acquisition (Agilent).

Protein analysis:

BmrA in both detergent solubilized state and inverted membrane vesicles was loaded on the protein macrotrap and desalted at flow rate of 200 µl/min of solvent 'A'. The protein was then eluted from the trap with solvent 'B' gradient 40 % to 70 % in 15 minutes and an analytical column was used to trap the detergent or lipid so that good signal-to-noise of protein could be

achieved. To separate the detergent from protein the analytical column C4 was equilibrated 40% acetonitrile.

The mass range for data acquisition was kept between 400 to 1500 m/z. The average mass of protein was deconvoluted with Windows based program Qualitative Analysis (Agilent).

Peptide analysis:

For deuterated samples the average of each peptide was calculated in three steps. First, the raw data file of peptide was exported in CSV format from Quantitative Analysis (Agilent). Then with the help of script the CSV files were converted into simple text format. This text file was then opened in program Magtran 1.03 b2 (Amgen Inc.)(Zhang and Marshall 1998). The average mass of the peptide was calculated by calculating the centroid of isotopic envelope based on Gaussian curve for deuterated or undeuterated samples.

4.5. MALDI analysis:

The MALDI ToF analysis of intact protein BmrA was carried out by using a modified sample preparation method called ultra thin layer method. This method was shown to be useful to analyze membrane proteins in the presence of detergent (Gabant and Cadene 2008).

Different steps of sample preparation are outlined in Figure 45.

Sample preparation steps:

A saturated solution of 4HCCA (a-cyano-4-hydroxycinnamic acid) was prepared in FWI matrix solvent (consisting of 3:1:2 formic acid: water: isopropyl alcohol (v/v).

A thin layer of matrix was spread over the plate, after drying remaining moisture was wiped gently not disturbing the layer.

Protein sample was diluted in the same 4HCCA matrix saturated solution from 5 to 50 times and 20 times was found the best condition. A spot of 0.5 and 1.0 µl of the diluted sample was made on layer. The spot was then washed by 0.1%TFA and aspirated by vacuum line.

After complete dryness, the spot was ready for MALDI analysis.

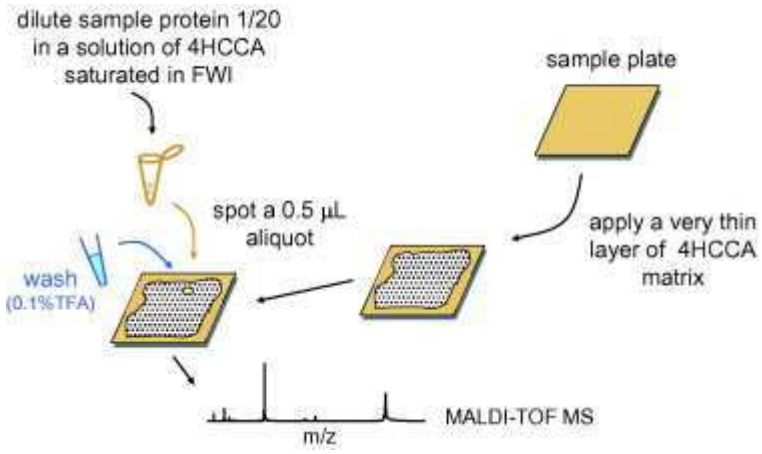

Figure 45. Ultra thin layer sample preparation (Gabant and Cadene 2008).

The method is applicable from lower to high molecular weight membrane proteins.

For peptide analysis, the digested sample was mixed with matrix 4HCCA (a-cyano-4-hydroxycinnamic acid) in 1:1 ratio. 1 µl of digest and 1 µl of matrix was mixed on the plate and left on the bench for drying. After the formation of crystal the plate was manually inserted in the MALDI ToF. The MS spectrum of MALDI-ToF was obtained with program Autoflex (Bruker Daltonics) and processed with Flex Analysis (Bruker Daltonics), respectively.

Results and Discussion

Chapter 1. H/D exchange kinetics of BmrA in apo and closed form

The initial step of characterization of BmrA by HDX-MS was to obtain peptide mapping after digestion with acid proteases pepsin and rhizopuspepsin. In beginning the typical in solution digestion of the transporter was employed and the peptides were identified on ESI-Trap mass spectrometer. BmrA is a membrane protein and sufficient amount of detergent DDM is required to keep the transporter solubilized. The final concentration of the DDM was 0.05% in the protein buffer as well as in the deuterated dilution buffer.

Fortunately, the presence of detergent did not interfere with the peptide separation or the mass spectrometric analysis. This was due to the semi hydrophobic nature of the detergent that was found to be eluted at about 40-45% of acetonitrile, after the elution of most of the peptides (Figure 46).

However, the peptide mapping obtained in solution digestion was only 34% of the total sequence, missing most of the significant regions of the transporter. The prolonged digestion time i.e. from two minutes to five minutes did not improve the sequence coverage. The use of immobilized enzyme proved to be useful for digestion of the transporter and the use of denaturants further improved the digestion and a reasonable 78% sequence coverage was obtained in the presence of 1.5 M guanidine hydrochloride (GnCl). As anticipated the transmembrane region of the transporter was not well covered as compared to the nucleotide-binding domain. However, the peptides originating from the regions of interest like ICD1, ICD2 and ABC motif were mapped. After careful identification and assignment of all peptides with the help of MS/MS data and Mascot server, each peptide was then identified on ESI ToF mass spectrometer.

The global deuteration kinetics of BmrA was determined in a detergent solubilized state or BmrA enriched membranes in order to define the effect of detergent on the transporter. The overall kinetics showed that in two different conformations the relative deuterium exchange of the transporter was found to be similar. Furthermore, limited proteolysis analyses of the protein showed that the closed conformation (vanadate inhibited or conserved glutamate mutation) is more resistant towards the enzymatic digestion as compared to the open conformation (in absence of any nucleotide), in detergent solubilized state and as well as in BmrA enriched membranes.

The influence of the conformation of BmrA on the significant regions of the protein is discussed in detail in the manuscript submitted and included within chapter 1 starting at page 11. Please note that figures' numbering within paper is in its own order different from global numbering of thesis manuscript.

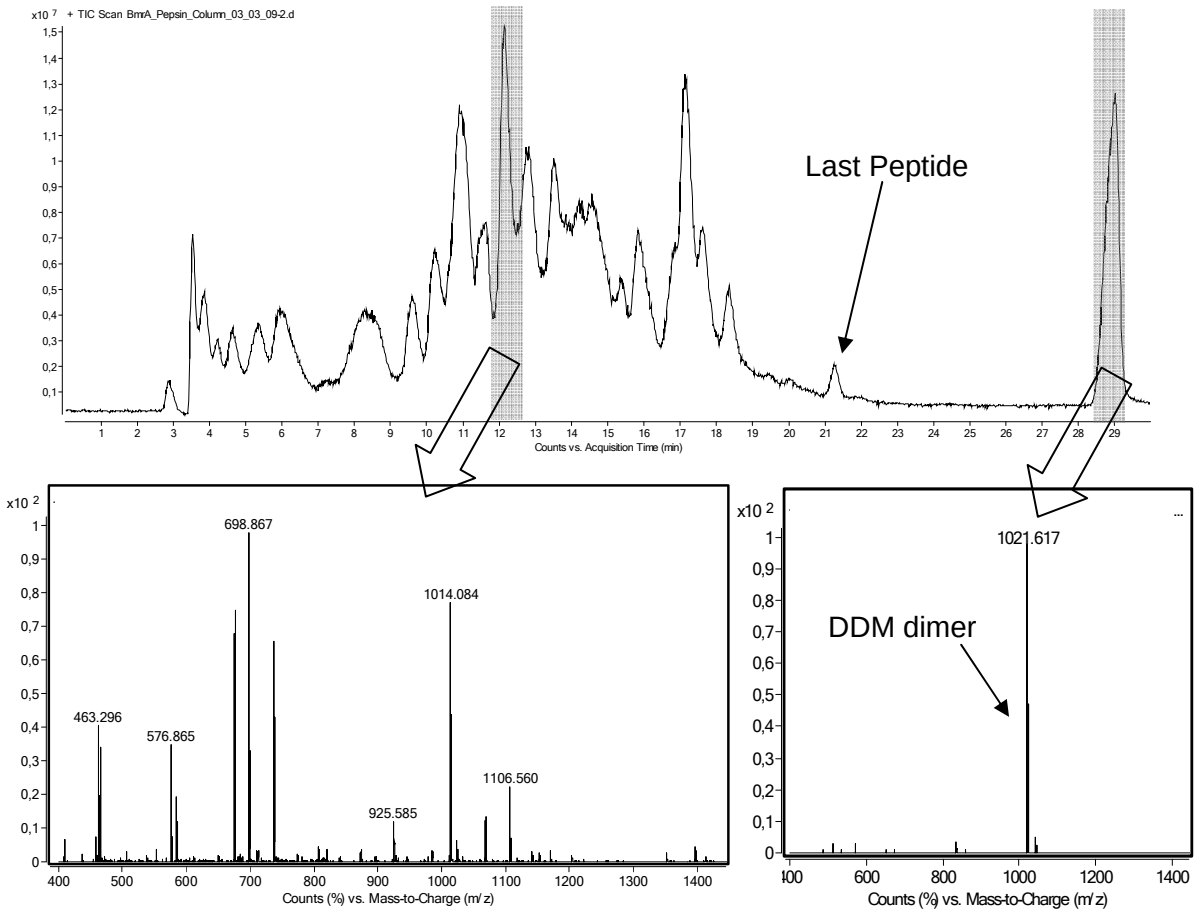

Figure 46. Chromatogram showing total ion current of the eluted peptides of BmrA. In-sets show the presence of peptides and elution of detergent at the end of the run.

The intracellular domains of a bacterial multidrug ABC transporter are highly dynamic in the resting state

Shahid Mehmood[1,2,3], Carmen Domene[4], Eric Forest[1,2,3]*& Jean-Michel Jault[1,2,3]*

[1]Institut de Biologie Structurale, Université Joseph Fourier Grenoble 1, [2]CEA Grenoble, [3]UMR-5075 CNRS, 41 rue Jules Horowitz 38027 Grenoble cedex 1, France. [4]University of Oxford, Department of Chemistry, Wellington Square, Oxford OX1 2JD, United Kingdom.

Running head: heterodimeric multidrug ABC transporter
*To whom correspondence should be addressed. Fax : 33 (0)4 38 78 54 94 ; Phone : 33 (0)4 38 78 31 19 ; E-mail : jean-michel.jault@ibs.fr; eric.forest@ibs.fr

SUMMARY

The study of membrane proteins remains a very challenging task and approaches to unravel the dynamics of these proteins are scarce. Here, we applied H/D exchange coupled to mass spectrometry to probe the motions of a bacterial multidrug ATP-Binding Cassette transporter, BmrA, in two different conformations. The closed state, outward facing conformation, was obtained using either the wild-type BmrA trapped in a vanadate-inhibited complex or the ATP-bound E504A inactive mutant, while in the resting state BmrA was expected to adopt an open inward-facing conformation. First, trypsin digestion and global H/D exchange support the existence of two very different conformations of BmrA either in membrane or in detergent. Next, local H/D exchange rates obtained for different peptides of BmrA agree with the overall 3D models of the transporter derived from each state. This shows that BmrA can cycle between an inward and outward facing conformations. However, in the resting state, peptides from the two intracellular domains, ICD1 and especially ICD2, show a much higher rate of H/D exchange than in the closed state. This shows that these two sub-domains are much more flexible in the resting state than expected from the known 3D structures of related transporters, MsbA or ABCB1. Congruent with this, molecular dynamic simulations suggest a large fluctuation of Cα position from ICD2 residues in the inward facing conformation of MsbA. These results highlight the unexpected flexibility of a multidrug ABC transporter in a resting state and underline the power of H/D exchange coupled to mass spectrometry to explore conformational changes and dynamics of large membrane proteins.

INTRODUCTION

Transport across membranes to import nutrients or export signaling molecules or noxious compounds, toxics or wastes, is an essential process in all kingdom of life, and selectivity of transport must therefore be ensured. This task is maintained by transporters, and the ATP-Binding Cassette (ABC) is one of the largest families of proteins involved in this 'checkpoint' [1, 2]. ABC transporters are found in all living species and they are powered by ATP hydrolysis to transport a wide variety of substrates. In prokaryotes, they participate in either the uptake of food supplies or the extrusion of many different compounds, some being harmful upon accumulation (e.g. antibiotics) while others can be incorporated as building block in the cell wall [3]. In man, the dysfunction of several ABC transporters causes severe pathologies such as adrenoleukodystrophy, hyperinsulinemic hypoglycemia or cystic fibrosis [4]. Other medically important ABC transporters are responsible for multidrug resistance (MDR) phenotypes. As opposed to most ABC transporters that are usually specific to one class of compounds (e.g. sugar, vitamin, or ions), multidrug transporters are capable to recognize and expel many unrelated organic compounds with quite dissimilar chemical scaffold. Thus, although their original function is dedicated to a protective role in healthy cells, the occurrence of these transporters in malignant tissues, pathogenic microorganisms or parasites confer a resistance towards the drugs used to cure the related pathologies [5]. The archetype of multidrug ABC transporters and first to be discovered is the human P-glycoprotein (also known as ABCB1); it is responsible for the failure of chemotherapeutic treatments in cancerous tissues. In bacteria, the identification of related transporters is relatively recent [6], as compared to other families of multidrug transporters that use the proton gradient as the energy source [7]. However, growing bodies of evidence support the implication of these multidrug ABC transporters in antibiotic resistance in many species [8], including recently in a *Streptococcus pneumoniae* strain isolated from a clinical setting [9]. Thus, given the prevalence of putative multidrug transporters in many bacterial genomes [10], they are now considered as a major threat jeopardizing a successful therapy.

All ABC transporters share a common architecture with two transmembrane domains (TMD) responsible for substrate translocation and two nucleotide-binding domains (NBD). In importers, these four core domains are usually borne on different polypeptides, up to four, and an additional subunit captures the substrate from the extracellular medium and delivers it to the transporter. In most exporters, these four domains are either linked into a single polypeptide (e.g. for the majority of eukaryotic transporters) or function as dimers with one NBD fused to one TMD (homo- or hetero-dimers). As opposed to the TMDs which are rather divergent in sequence and topology, the NBDs are highly conserved with several distinctive motifs, notably the Walker A and Walker B found in many ATPases and the ABC signature specific to this family [11, 12]. Tremendous progresses have been made in the past ten years to decipher the molecular mechanisms of ABC transporters by solving high-resolution 3-D structures of isolated NBDs or full-length transporters in different conformations. Hence, NBD structures have shown that during the catalytic cycle, the two NBDs interact together transiently to form a sandwich dimer in a head to tail fashion thereby trapping two ATP molecules at their interface [13-15]. In this closed conformation, that can be stabilized either by ATPase-inactive mutations [16] or by vanadate-induced ADP trapping [17], each composite ATP-binding site is made of elements from one NBD (i.e. Walker A and B motifs) while the ABC signature is provided in *trans* by the second NBD. For full-length ABC transporters, the overall structure of importers appears more compact than those of exporters with the presence in the latter of two large intracellular domains, called ICD1 and ICD2, that protrude from the TMD to interact with the NBD [18]. Importantly, while ICD1 from one monomer interacts with its own NBD, ICD2 (or ICD4 for full-length exporters) interacts with the NBD of the other monomer (or other moiety for full-length exporters) [19-21], and this has been validated by cross-linking experiments [22, 23]. Snapshots of 3-D structures and EPR spectroscopy indicate that large motions occur during the catalytic cycle of ABC exporters, with the transporter oscillating between an apo open conformation, with its two NBDs lying far apart, and an ATP-bound closed conformation with the NBDs engaged in a tight interaction [19-21, 24]. Importantly, the contact between ICDs and NBDs are always maintained in these structures, as these two domains keep the same overall conformation and interaction. Thus, this suggests that NBDs closure operates by a rigid body motion [19, 21]. On the other hand, cross-linking experiments

between ICDs and NBDs give support to alternative conformations for these two domains in different ABC exporters [22, 23, 25, 26].

To shed light on structural modifications that might occur during the mechanism of ABC transporters, we used a hydrogen/deuterium exchange (HDX) approach coupled to mass spectrometry. It revealed how different domains and sub-domains of an ABC transporter are affected in the resting *versus* the closed states. HDX has been widely used on soluble proteins to probe the accessibility of backbone amides, thus highlighting secondary structure modifications at the peptides level [27-29]. For membrane proteins, this approach is only beginning to emerge [30-34], but given their importance in the living world (i.e. one-third of proteins in each organism and about two-thirds of current medical targets), our results strengthen the benefit of using HDX to address fundamental issues about the functioning of these proteins in general. Here, it gave us access to the dynamics of BmrA, a bacterial multidrug ABC transporter strongly homologous to two related bacterial transporters, MsbA and Sav1866, and to the murine P-glycoprotein [35-37]. The results obtained extend our vision of the functioning mechanism of ABC exporters and complements the snapshots of high-resolution 3D structures. In particular, it showed for the first time that the two ICDs of BmrA behave quite differently depending on the conformational state considered. As opposed to the closed state, ICD2 and to a lower extent ICD1 become highly exchangeable in the resting state (open conformation). Therefore, this reveals a much greater flexibility of these two sub-domains than what was foreseen from the known 3-D structures of related ABC transporters.

Results

Comparison of the apo and closed conformations of BmrA in membrane and detergent.

3-D structures of MsbA and murine MDR1 solved in the presence of detergent have suggested that large conformational changes might occur during the ATPase cycle of these transporters [19, 21, 38]. To investigate this, we first checked if the presence of detergent affects the conformational changes that take place during the catalytic cycle of BmrA. Thus, global HDX was performed on the protein either purified in detergent or in its membrane environment. After overexpression in *E. coli* [36], BmrA-enriched membranes were either frozen in liquid nitrogen and kept at -80°C or solubilized in DDM detergent and purified by Ni affinity chromatography as previously described [37]. In agreement with our previous results [39], the ATPase activity of BmrA was shown to be conserved in a detergent solubilized state and sensitive to vanadate inhibition (Figure S1). Because lipids and detergents either give strong signals in mass spectrometry or disturb the protein ionization in the electrospray source [40], they must be separated from the protein before reaching the source. Previous separations involved gel electrophoresis and electroelution [41], protein precipitation and resuspension in concentrated acidic solutions [42], or size exclusion chromatography after dissolution in a chloroform/methanol/acid solution [43]. Yet, although efficient, all these methods were hardly compatible with the requirement of a fast preparation of the samples to limit as much as possible the back exchange reaction after deuterium incorporation into BmrA. Thus, chromatographic parameters were first optimized to separate membrane lipids or DDM detergent from the protein using classical reversed phase chromatography (see Materials and Methods). The electrospray mass spectra of BmrA either embedded in membrane or in a DDM solubilized state are presented in Figure 1 (panels A and B). First insets show the deconvoluted mass spectra (with close-up views in the second insets), with the mass of the major peak of 66341 ± 2 Da in membranes. Due to the cloning strategy used [37], purified BmrA was expected to contain three additional residues on its *N*-terminus (sequence MASMPT…, with the underlined residues corresponding to the beginning of the native protein) and 15 additional residues on its C-terminus including the Histidine tag (sequence …KAGVDKLAAALEHHHHHH, with the underlined residues corresponding to the end of the native protein). Thus, the deconvoluted mass obtained is in very good agreement with the calculated mass of BmrA possessing only one extra Ser amino acid on its *N*-terminus (66340 Da). Masses of a second peak (66413 Da, in membranes) are also in very good agreement with the calculated mass of BmrA with two extra amino acids on its *N*-terminus, Ala plus Ser (66411 Da). Therefore, the first methionine and sometimes also the second amino acids (Ala) of the *N*-terminus of the proteins were very likely cleaved off by proteolysis during the purification process. The other peaks of lower intensity were likely due to unidentified non-covalent adducts on both forms of BmrA. The high quality of each spectrum reflects the efficiency of the chromatographic separation upstream the electrospray source for either samples.

After incubation of each BmrA preparation in deuterated buffers for times varying from 15 s to 1 h the mass of deuterated BmrA was measured. The percentage of deuterated amides was calculated taking into account the average total number of amide hydrogens in BmrA (585 for the native protein) and the mass increase. Deuteration kinetics are presented in Figure 1C with open symbols for BmrA in its resting state in membranes (squares) or in DDM (circles). Both curves show the same behavior, the exchange steadily increasing with time. However BmrA in membranes was about half less deuterated (13-25%) than in its solubilized state (23-52%). This lower deuteration exchange in membrane could possibly reflect a more compact conformation of BmrA dimer. However, when the same experiment was performed after a prior incubation of BmrA with vanadate in the presence of ATP-Mg (closed symbols), i.e. conditions known to promote the formation of a closed dimer [17], a lower deuteration was found for BmrA either in membrane (squares) or in detergent (circles). Thus, although HDX occurs about twice faster in detergent as compared to the membrane bound BmrA, vanadate inhibition induced a significant decrease in HDX to a similar extent for both environments. Therefore, this shows that in either state, membrane bound or solubilized, BmrA can switch between two different conformations: an apo one where deuterium exchange readily occurs and a closed one more resistant to deuterium exchange.

To bring further evidence that the conformational changes observed during the catalytic cycle of BmrA are similar in detergent and membranes, the apo and closed conformations were subjected to

limited proteolysis in both environments. A clear difference of resistance against proteolysis by trypsin could be observed using SDS-PAGE (Figure 2). BmrA in the apo conformation was rapidly digested by trypsin in membranes (Figure 2A) as well as in DDM (Figure 2C, lanes 3-5). In contrast, in the closed conformation triggered by vanadate inhibition, BmrA exhibited a good resistance to this protease in both environments (Figures 2B and 2C, lanes 6-8). These results give support that regardless of its environment, DDM or membrane, BmrA can adopt two different conformations: an apo one quite sensitive to trypsin digestion and a closed one rather resistant to this protease. Because (i) a similar behavior of BmrA was seen in detergent and membrane environments (Figures 1C and 2) and (ii) a much higher deuteration level was found for the protein in detergent (Figure 1C), the next experiments involving HDX at the peptide level were carried out after purification of BmrA in the presence of DDM. Indeed, it is suitable to start from a high deuteration level if one wants to achieve a sequence coverage of the protein as large as possible. Also, the presence of *E. coli* native proteins in the membrane fraction would likely pollute the peptide signals coming from BmrA, hampering the unambiguous identification or the determination of deuterium incorporation for some of them.

Peptide mapping of BmrA.

To localize the difference in deuterium incorporation between the two conformations of BmrA, the protein digestion that must occur at low pH and low temperature and the peptides separation were optimized. This step is essential to reach a sequence coverage of the protein as large as possible with peptides as small as possible [27]. However, the DDM used for BmrA purification gave a very strong signal in MS. To enable observation of the MS signals of the peptides, a protocol previously developed in our group for another membrane protein and based on the washing off of non-ionic detergents with dichloromethane was first tried [44], but without success here. Reversed phase separation was then adjusted so that all peptides eluted before the detergent, at low temperature to limit deuterium back-exchange. For peptides sequencing using tandem mass spectrometry, the chromatographic parameters were chosen for a good separation to facilitate their identification, while the detergent still eluted after the last peptides. For the analysis of deuterated peptides, the elution times were also shortened as much as possible to limit deuterium back-exchange. Pepsin and rhizopuspepsin were used independently to digest BmrA [45]. The pepsin digestion in solution yielded only 31 peptides covering 45% of the BmrA sequence (Table 1). However the use of immobilized pepsin significantly increased the number of peptides (67) and thus the sequence coverage raised to 78%. These results were obtained in the presence of 1.5 M guanidinium hydrocholride, a denaturant concentration which was optimized after different trials between 0.5 and 4 M. The sequence coverage was lower in the TMD (60%), the majority of the identified peptides belonging to the hydrophilic intra cellular domains, ICD1 and ICD2 (Figure 3). This low coverage of the hydrophobic transmembrane helices is presumably due to the presence of the detergent that presumably afforded some protection against the protease digestion. We also noticed a similar protection against proteolysis by lipidic vesicles for hydrophobic helices in the diphtheria toxin translocation domain [46]. In contrast, the NBD sequence was almost fully covered by the pepsin digestion (98%). Immobilized rhizopuspepsin was also used for on-line digestion of BmrA. The goal was to obtain complementary sequence coverage to improve spatial resolution by the occurrence of overlapping peptides. The number of peptides and the sequence coverage were significantly lower in the TMD in comparison with immobilized pepsin (Table 1 and Figure 3). In the NBD, the coverage appeared quite complementary from the one obtained by pepsin. However, after deuteration a significant number of peptides were lost with each protease, a phenomenon that is frequently observed in HDX [47, 48]. This is due to a heterogeneous deuteration that induces a broadening of the MS signal and thus a decrease in its intensity. The loss was much higher in the case of rhizopuspepsin which was also less efficient than pepsin. Therefore, only pepsin was used in the remaining part of the study, giving 45% and 92% coverage for TMD and NBD, respectively, with a peptide average size of about 9 amino acids. Although the sequence coverage was lower for the TMD, it is noteworthy that most of the two ICDs were covered by the HDX because these two sub-domains are known to be essential for the transmission of the conformational changes between the NBD and the TMD [20, 49, 50].

Comparison of the deuterium incorporation between the apo and closed forms of BmrA for three selected peptides.

Besides the inhibition by vanadate, another way to promote the closed conformation in ABC transporter is to use catalytic inactive mutants [7, 14, 15]. For BmrA, we previously showed that the conserved glutamate residue E504 adjacent to the Walker-B motif is very likely the catalytic base for ATP hydrolysis, because mutation of this residue to Asp, Ala, Gln, Ser or Cys fully abrogated the activity [51, 52]. Thus, BmrA mutants could be trapped into a closed conformation in the presence of ATP-Mg alone [51]. Therefore, these mutations can be used as a substitute for vanadate to reach a stable closed conformation during the ATPase cycle. Deuterium incorporation was monitored as a function of time and was compared for each peptide generated from the three following forms of BmrA: wild-type in the resting state (apo form), wild-type inhibited by vanadate (in the presence of ATP-Mg) and E504A mutant in the presence of ATP-Mg. The mass spectra are presented for three selected peptides in Figure 4 after two deuteration times, 15 s and 1 h, and kinetics for all peptides are shown in Figure S2. In some cases, as exemplified in Figure 4, peptides mass spectra from the vanadate inhibited form showed two envelopes of isotopic peaks, thus giving two different kinetics, with the minor envelope corresponding to that of the wild-type. Because the inhibition of ATPase activity by vanadate was not total (~ 80% see Figure S1, and see also [39]), it is very likely that this envelope originates from BmrA dimers not inhibited among the whole population; depending on the peptide considered and on its initial intensity, this tiny envelope could be detected, or not, on the MS spectrum. In other cases, the two envelopes were too close to be deconvoluted with the Magtran software and the kinetics could not be drawn (Figure S2). In the apo conformation of wild-type BmrA, each of these peptides belonging either to the ICD2 (203-215 and 216-236) or to the NBD (372-383) showed a very fast deuterium exchange with a large shift of the isotopic envelope towards higher m/z (Figure 4). This shift was already obtained after 15 s with identical exchange after 1 h for peptides 203-215 and 216-236 while peptide 372-383 exhibited a little further shift increase between 15 s and 1 h. After vanadate inhibition and 15 s deuteration a first major envelope corresponded to a very limited deuteration whereas a second one, much smaller in intensity, corresponded to the highly deuterated form observed also for the wild-type in the apo conformation. After 1 h the first envelope shifted towards higher masses and the second one still behaved like that of the wild-type in the apo conformation. In contrast, the E504A mutant showed practically only one isotopic envelope that was always similar to the low isotopic envelope observed in the vanadate inhibited sample.

An uncommon behavior was found for peptide 501-509 including the E504 amino acid and most of the Walker B motif (Figure S3). Like several other peptides in the apo form of BmrA, it quickly reached its maximum deuteration level (at about 70%; see Figure S2). Again, the vanadate inhibited form showed the same behavior as the three previously described peptides with two isotopic envelopes. In the E504A mutant, however, the isotopic envelope shifted much faster than the main one in the vanadate inhibited form and evolved with time to HDX values similar to that of the wild-type in the apo conformation. This very specific difference between the mutant and the vanadate inhibited form could be explained by a rather flexible and accessible region in the mutant (although lower than in the apo conformation of the wild-type protein). In the case of the vanadate inhibited form and for the main isotopic peaks, there might be some additional protection afforded by the presence of vanadate (or the combination of ADP-Mg-Vi in the ATP-binding site). This masking effect would contribute to the low isotopic envelope that was not present in the E504A mutant.

Given the propensity of the E504A mutant to readily adopt the closed conformation of BmrA in the presence of ATP-Mg and the homogeneity of HDX of its peptides, the remaining part of the paper will focus only on differences between this mutant in the closed conformation (ATP-bound state) and the wild-type in the apo conformation. It is important to note that addition of ATP-Mg in the wild-type BmrA, which triggered ATP hydrolysis, gave HDX patterns for the different peptides similar to that found in the apo conformation. This is consistent with many biochemical and structural data showing that upon ATP hydrolysis, and thus in an ADP-bound state, ABC transporters reset into their resting state (i.e. an open conformation) [53, 54]. Conversely, local deuteration kinetics were also determined for the E504A mutant in the absence of any nucleotide (apo conformation) and they were found to be similar to those of the wild-type in the same conformation. Therefore, the comparison

between the E504A mutant and the wild-type BmrA highlights the two different conformations, open and closed, that occur during the catalytic cycle of this ABC transporter.

Visualization of HDX between the open and closed forms on the predicted topology and secondary structure of BmrA.

To pinpoint the local differences of HDX between the open and closed conformations of BmrA, the percentage of deuteration was plotted for each peptide at two different times, 15 s and 600 s (Figure 5). It is noteworthy that HDX is systematically higher in the wild-type apo conformation (open form) than in the mutant (closed form), except in a few cases where it is similar. Very low HDX could be observed in THM2 and THM4 for both forms showing likely a strong protection by DDM against HDX, similar to that observed against pepsin proteolysis. Interestingly, a high HDX level was quickly obtained in the *C*-terminus part of ICD1 and in all peptides identified from ICD2, for the wild-type in the apo conformation. This indicates a high accessibility and/or a low level of structuration of these sub-domains. In the closed conformation of the E504A mutant, the corresponding peptides from ICD1 were much less exchanged on a short time scale, but a longer incubation period allowed to substantially increase the exchange. For ICD2, even after a prolonged exchange time, a huge difference remained between the peptides from the wild-type and the E504A mutant. The NBD generally shows major differences between open and closed forms, particularly in the Walker A, Walker B and the ABC signature regions which are known to be involved in nucleotide binding. In contrast, some regions of the NBD notably between the Walker A and the ABC signature in the so-called α helical sub-domain [14] showed no HDX difference. This indicates that they are likely not involved in the NBD/NBD interaction triggered by ATP/Mg binding. The major differences in HDX between both protein forms can be visualized on the "heat map" presented in Figure S4. The regions in red or orange correspond to peptides with still more than 45% and 30% HDX difference, respectively, after 1h deuteration. They clearly belong to ICD1, ICD2 and NBD, domains on which we will focus below.

Influence of the BmrA conformation on HDX of the ICDs and NBDs.

To highlight the HDX data, two BmrA models previously constructed [35], and based on the X-ray structures of homologous bacterial ABC transporters were used (Figure 6). For the apo conformation of BmrA, the open form of EcMsbA was used as a template whereas the closed conformation of BmrA (mimicked by the ATP-Mg bound E504A mutant) was modeled upon the Sav1866 structure [20, 21]. In agreement with the proposed closed model, the regions participating either in NBD/NBD interaction triggered by ATP binding or in direct interaction with ATP/Mg show a rather low level of HDX. This is the case, for instance, for the peptide 372-383 that entirely covers the Walker A motif and makes direct contact with ATP (HDX of 29%), or with the peptide 479-492 encompassing the ABC signature and involved in ATP binding in *trans* upon NBD/NBD dimerization (26%). In contrast, the former peptide became much more rapidly deuterated in the apo conformation of the wild-type transporter with a high deuteration level of the Walker A motif (82%), consistent with the presence of a large accessible loop, while the peptide covering the ABC signature motif showed also a substantial increase in its exchange rate (69%). The lowest value of HDX obtained for this second peptide suggests that in the open conformation, it likely conserved an α-helical structure less prone to HDX than a loop. Thus, the exchange rates for these two peptides are in agreement with the open model used to picture the apo conformation (Figure 6, panel B). For other peptides of the NBDs known to be involved in ATP/Mg binding or NBD/NBD dimerization, similar trends were observed with a faster exchange rate in the apo conformation as compared to the ATP-bound conformation (e.g. peptide 501-509 partially encompassing the Walker B motif). Other regions of the NBDs not involved in either process (i.e. ATP binding or NBD/NBD dimerization) gave similar HDX in both conformations with, for instance, a high deuteration level consistent with a loop structure (84%) for peptide 439-447.

A different picture emerges when one focuses on ICDs. In contrast to the two models suggesting that these domains have a similar conformation in the two states, open and closed, peptides from both ICDs showed a large difference in the HDX in these two conformations. Thus, ICD2 was highly deuterated in the apo conformation, with 82% and 79% for peptides 203-215 and 216-236, respectively, whereas in the closed conformation the HDX rate significantly decreased for both

regions to 33 % and 34 %, respectively. Likewise, but to a lower extent, regions 104-114 and 115-132 from ICD1 were also fairly deuterated in the apo conformation, showing a rather high accessibility (66 and 81%, respectively) whereas this value dropped in the closed state to 27% for the former peptide, while it remained highly deuterated for the latter peptide (69%).

This difference is not simply due to a greater accessibility of the peptides from either ICDs in the resting state versus the closed state because based on the two BmrA models used here, the accessibility of these two domains is essentially unaffected upon the tight dimerization of the two NBDs (i.e. in the closed state, see Figure S5). For instance, peptides 104-114 from ICD1 and 203-215 from ICD2 are predicted to be equally accessible in either state, whereas their HDX is far greater, especially for the ICD2 peptide, in the apo conformation. Therefore, the conformation and/or flexibility of both ICDs is somehow modified to account for the faster rate of deuterium exchange observed in the resting state.

To further assess the flexibility of these two sub-domains in the 3D structures of the related transporters used to model BmrA, molecular dynamic simulations were performed on EcMsbA and Sav1866 along with that of StMsbA which was included for comparison. After reaching a plateau for the root mean square deviation of the Cα for each conformation, the fluctuation of the position of these atoms were calculated for the last 20 ns of the simulations and the results are shown in Figure 7. Clearly, a minor fluctuation was observed in the closed conformations of either Sav1866 or StMsbA whatever the Cα considered (always below 2.5 Å). In contrast, some basal fluctuations occurred throughout the sequence of EcMsbA and were much more pronounced (above 4 Å) for four areas including in particular ICD2. This suggests that this latter sub-domain must be quite flexible in this apo conformation.

Discussion

The goal of this study was to get some insights into the dynamics of a multidrug ABC transporter in two different conformations, i.e. the resting state where the transporter might adopt an open conformation and the closed state where the two NBDs interact together in a transient, ATP-bound, conformation. Overall, global H/D exchange and trypsin digestion show that either in membrane or in detergent BmrA can switch between two very different conformations during its catalytic cycle: a closed conformation rather resistant to trypsin digestion and H/D exchange and another one in the resting state quite sensitive to trypsin and more susceptible to H/D exchange. Thus, our results give support to the postulate that multidrug ABC transporters can cycle between an open, inward facing, conformation in the resting state and a closed, outward facing, ATP-bound conformation. Similar conclusions were drawn recently for the catalytic cycle of MsbA from cross-linking experiments [55] or from EPR spectroscopy [24, 56, 57]. Based on 3-D structures of ABC exporters, the transition between these two opposite conformations was proposed to operate according to a rigid body motion [21]. This entails that the same overall structure of the two monomers (or moieties) of the transporter would be maintained throughout the catalytic cycle. However, local H/D exchange obtained for BmrA clearly challenges this assumption. In fact, our results strongly suggest that in the resting state, BmrA samples different conformations. Yet, these different conformations appear to be restricted to both ICDs, mostly to ICD2 but also to ICD1 although to a lower extent. Indeed, apart for the peptides involved either in the interaction between the two NBDs or with ATP, no major changes are observed for the other peptides from either the NBD or the transmembrane helices, although limited information is available for this latter part. Therefore, the interaction between the TMD and the NBD that is secured by the two ICDs in the closed state, must become loosen in the resting state due to a greater flexibility of these ICDs. This would allow some reorientation of the whole NBD as compared to the TMD and would explain some unexpected cross-links previously observed for BmrA. Indeed, it was found that disulfide bonds were formed between ICD1 and the Q-loop of the NBD in the resting state only [25]. However, in all structures of exporters, either closed or open, ICD2 appears firmly sandwiched between ICD1 and the Q-loop thereby impeding the possible interaction between these two protein segments [19-21]. Hence, some reorganization of BmrA domains presumably occurred to allow the cross-link between ICD1 and the Q-loop [25]. Other unpredicted cross-links questioning the conformation observed in 3D structures were also reported for

two other ABC transporters, TAP1/TAP2, and Yor1p [22, 26]. These results lend support to additional conformations of these transporters with different orientations of the NBD relative to ICDs or of the two ICDs with respect to each other. It is worth mentioning that two other studies performed on homodimeric ABC transporters, LmrA and MsbA, and using either solid state NMR or EPR spectroscopy reached similar conclusions of alternative conformations (or greater flexibility) of the NBD in the resting state, as opposed to the TMD [56, 58]. In addition, to the NBD flexibility, EPR experiments also support a large conformational entropy of residues from ICD1 in the resting state of MsbA as evidenced by the large distance distribution of the spin label probe tethered to residue 115 [56]. For CFTR, although cross-link patterns support a global architecture similar to that found in Sav1866 or MDR1, Riordan and colleagues proposed that a considerable flexibility must exist at the interface of NBDs and ICDs to account for the formation of the cross-link between these two domains regardless of the length of the cross-linking reagent (from 3.9 to 24.7 Å) [23]. In addition, a recent report using a genetic screen with the yeast ABC multidrug transporter, PDR5, support the idea of a non-canonical coupling between the NBD and the TMD as being mainly achieved through ICD1 and not through ICD2 [59]. Whether this is a peculiar property of PDR5 or reflects an alternative conformation of the ICDs in this transporter remains to be investigated. Related to the former hypothesis, the ICDs of PDR5 are predicted to be shorter than those of Sav1866 or MDR [60], and this might lead to a different interaction of these domains with the NBDs. Interestingly, a molecular dynamic study of Sav1866 has revealed that in a closed conformation and among residues whose Cα show the largest displacement between the ATP and ADP+Pi bound states, some belong to ICD2 (residues 221-222) and to ICD1 (residues 110-113) [61]. Here, molecular dynamic simulations suggest that in the open-apo conformation of EcMsbA, and in contrast to the closed conformations of StMsbA or Sav1866, a large fluctuation in the position of Cα residues from ICD2 is likely to take place.

H/D exchange coupled to mass spectrometry is commonly used to probe the dynamics of soluble proteins but this technique remains trickier in the case of membrane proteins especially because detergent often reduces the sequence coverage. Up to now, the only ABC transporter for which this technique was employed was the soluble NBD1 of CFTR [62]. However, our results on BmrA emphasize how useful this technique might be especially to study membrane proteins with large extramembranous domains like the ABC family. Other membrane proteins containing large soluble domains include for instance the secondary transporter of the Resistance-Nodulation-cell Division (RND) family such as the multidrug AcrB transporter [63]. Also, primary transporter of the P-type family contains several extramembranous domains and the transport mechanism are supposed to required large conformational changes among these domains as exemplified in different structures of the archetype of this family, the Ca^{2+}-ATPase [64-66]. The use of H/D exchange coupled to mass spectrometry to unravel different conformations of these membrane proteins should shed new light on their transport mechanism.

Materials and Methods

Materials

Unless specified, chemicals and pepsin were purchased from Sigma-Aldrich. n-Dodecyl-ß-D-maltoside (DDM) was purchased from Anatrace. Recombinant protease rhizopuspepsin (Rp) was purified as previously described [45].

Site-directed mutagenesis and purification of BmrA

The E504A BmrA mutant was constructed as previously described [51]. The E504A mutant and wild-type BmrA were overexpressed as described [36] and BmrA-enriched membranes were either frozen in liquid nitrogen and kept at -80°C until used or solubilized in 1% DDM. After solubilization of the membranes, BmrA was purified by Ni affinity chromatography as previously described [37]. Protein concentrations were estimated by using a modified Lowry method [67] for BmrA-enriched membranes or the Bradford method [68] after purification. The accurate masses of the purified mutant and wild-type proteins were checked using electrospray mass spectrometry.

Limited proteolysis of BmrA

BmrA was proteolysed with trypsin at a protease/substrate ratio of 1:1000 (w/w). For BmrA solubilized in detergent a reaction mixture of 100 µl was prepared and aliquots of 10 µl were

withdrawn after 5, 15 and 30 min. To reach the vanadate-inhibited state 5 mM ATP, 5 mM $MgCl_2$ and 3 mM vanadate were added to the protein solution and incubated for 15 min at room temperature before adding trypsin. For digestion of BmrA-enriched membranes, a reaction mixture of 100 µl was prepared and aliquots of 10 µl were withdrawn after 5, 15, 30 min, 1 h, 2 h and 3 h. Each aliquot was acidified with 1 µl of 5% trifluoro acetic acid (TFA) and immediately frozen in liquid nitrogen. 12.5% SDS PAGE were run followed by Coomassie blue staining.

Pepsin digestion

The vanadate-inhibited state was prepared in the same way as for limited proteolysis experiments. The E504A mutant was incubated with 5 mM ATP and 5 mM $MgCl_2$. All protein digestions in solution were performed in an ice bath at 0 °C. Protease solutions were prepared in 500 mM glycine, pH 2.2, and cooled to 0 °C. BmrA was digested in the same buffer for 2-5 min using a protease/substrate ratio of 1:1 or 1:10 (w/w) for pepsin and recombinant type XVIII, respectively. Increase in digestion time did not have any effect on the proteolysis. On-line digestions in the presence of 0.5-4 M guanidinium chloride (GndCl) (final concentration) were also performed in an ice-bath at 0 °C using columns packed with Rp or pepsin immobilized on POROS-AL resin [45].

H/D exchange of BmrA

The vanadate-inhibited state of wild-type BmrA was prepared in the same way as for limited proteolysis experiments. The E504A mutant was first incubated for 10 min with 5 mM ATP and 5 mM $MgCl_2$. The HDX reaction was initiated by a 10 times dilution into deuterated buffer containing 50 mM NaCl and 0.05 % DDM. Time course of the HDX was followed over a 1 h period of time by sequential withdrawing of 120 µL deuterated samples which were immediately added to 26 µL of quenching buffer (8 M guanidium chloride, 500 mM glycine HCl, pH 2.2), rapidly mixed and flash-freezed in liquid nitrogen. Samples were stored in liquid nitrogen until they were analyzed.

HPLC peptide separation

Peptides obtained by in-solution or on-line digestion were loaded onto a peptide MicroTrap (Michrom Bioresources, Auburn, CA) column and desalted by washing with 0.03% TFA in water (HPLC solution A). The peptides were then separated on a reversed phase C12 column (1 X 50 mm, Jupiter; Phenomenex) using a linear gradient of 15–45% (v/v) solution B (CH_3CN 95% and TFA 0.03%) during 26 min, followed by 100 % (v/v) solution B during 20 min at a flow rate of 50 µL/min. For peptide mapping the gradient lasted 55 min instead of 26 min to improve the separation of the peptides. The column was connected to the electrospray source of mass spectrometers until 30% (v/v) B and then disconnected to avoid pollution of the electrospray source by the detergent. The column was pre-equilibrated with 15% (v/v) solution B. The valves, trap cartridge and column were cooled to 0°C by immersion in an ice-bath.

Mass spectrometric analyses of peptides

The tandem mass spectrometry (mapping) analyses were performed on an ion trap mass spectrometer (Esquire 3000+, Bruker Daltonics). The HPLC system was connected directly through a splitting T-piece to the electrospray ionization (ESI) source of the mass spectrometer. Data were processed using DataAnalysis 3.0. Tandem mass spectra were searched using Mascot, and the assignments were verified manually and by accurate mass measurements. Accurate mass measurements and the analysis of the local kinetics of deuteration were done on a time-of-flight (TOF) mass spectrometer (6210, Agilent Technologies, Santa Clara, CA) equipped with an electrospray source. Data were processed with MassHunter Qualitative Analysis, and the deconvolution and calculation of the average masses were carried out in Magtran [69].

Electrospray mass spectrometry of the full-length proteins

The molecular mass of the intact protein was measured with the same electrospray TOF mass spectrometer coupled with HPLC. Protein was loaded onto a protein MicroTrap (Michrom Bioresources, Auburn, CA) column and desalted by washing with 0.03% TFA in water (HPLC solution A). The protein and detergent were then separated on a reversed phase C18 column (1 X 50 mm, Jupiter; Phenomenex) using a linear gradient of 5-60% (v/v) solution B (95% CH_3CN and 0.03%

TFA) during 3 min, followed by 100% (v/v) solution B during 12 min at a flow rate of 50 µL/min. Protein eluted after 13 min and HPLC was quickly disconnected from the source to avoid pollution with the detergent. The deconvoluted mass was calculated with the Agilent MassHunter Qualitative Analysis software. To simplify the processing of the global deuteration data, a non deuterated average mass of 66 440 Da was calculated, taking into account the different forms of BmrA and of its adducts.

ATPase activity

To measure the ATPase activity of BmrA in detergent, an enzymatic coupled assay system was used [70], in the presence of 0.05% DDM and as described previously [71]. The activity was measured in the presence of 10-20 µg of BmrA and followed at 37°C for 10 min. When vanadate was present, it was added at a final concentration of 3 mM from a 100 mM stock solution (see [71]).

Calculation of accessibility areas of peptides

The accessibility area of BmrA peptides was calculated with the help of naccess. This software calculates the accessible area of a protein structure in a PDB format then, based on accessibility of each atom, the total access area of a residue is determined. The program is based on the calculation method of Lee and Richardson [72]. In order to compare the accessibility values with HDX MS data the mean accessibility area of individual peptides was determined. Taking into account that region from residue 325 to residue 332 is the most accessible in both models, the values of other peptides were normalized considering the peptide 325-332 as a 100% accessible region.

Molecular Dynamics simulations

MD trajectories were simulated with the version 2.7 of NAMD [73], using the CHARMM27 force field with CMAP corrections [74], and the TIP3 (Transferable Intermolecular 3-point) model for water molecules [75]. All the simulations were performed in the NpT ensemble. The pressure was maintained at 1 atm using a Nose-Hoover Langevin piston control [76], with period of 100 fs and damping time constant of 50 fs. Temperature was maintained at 300 K by coupling to a Langevin thermostat, with damping coefficient of 5 ps^{-1}. Electrostatic interactions were treated by the Particle Mesh Ewald algorithm [77], with grid spacing lower than 1 Å. Smoothed cut-off (10-12 Å) was used for the van der Waals interactions. Equations of motion were integrated with a time step of 2 fs. The SETTLE algorithm was used to restraint hydrogen atoms [78].

Three systems were considered: (i) the Sav1866 multidrug transporter from *S. aureus* at 3.0 Å in an outward-facing conformation reflecting the ATP-bound state [20], (ii**)** the MsbA lipid 'flippase' either from *E. coli* in the open apo-conformation at 5.3 Å, or (iii) from *S. typhimurium* in the outward-facing conformation at 3.7 Å [21]. The structures were defined according to PDB files 2HYD, 3B5W and 3B60 respectively together with the crystallographic water molecules. Only the Cα-trace structure is available in 3B5W. Missing backbone and side-chain atoms were predicted using MAXSPROUT [79] and SCWRL [80]. An acetyl group was attached to the N-terminus residue to mimic the preceding peptide bond and the C-terminal carboxylate was protonated. Default ionization states at pH 7 were set, except for buried residues whose ionization states were determined using WHATIF [81] and visual inspection. The proteins were centred in the x-y plane with the permeation pathway aligned to the z-axis, and embedded in a pre-equilibrated bilayer of 569 DOPC molecules. The upper layer of the lipid membrane was aligned to the centre of mass along z of the aromatic residues of the extracellular side (Phe158, Phe157, Tyr39, Tyr268 in Sav1866, and Trp165, Trp66, Tyr162, Tyr168, Phe157, Phe265, Phe272 in MsbA). Lipid molecules closer than 1.2 Å to protein atoms were removed. Sodium and chloride ions were added to neutralize the system (up to a final concentration of 150 mM). The final systems contain ~195,000 atoms in the Sav1866 simulation (~41800 TIP3P water molecules, 360 DMPC lipids, 61Cl^- and 59Na^+), ~202,000 atoms in the simulation of MsbA PDB 3B60 (~42,800 TIP3P water molecules, 402 DMPC lipids, 55Cl^- and 63Na^+), and ~244 atoms in the simulation of MsbA PBD 3B5W (~53500 TIP3P water molecules, 472 DMPC lipids, 71Cl^- and 79Na^+).

In order to equilibrate the atoms around the transporters, 2000 steps of energy minimization and 1 ns of MD were performed with restraints applied to the backbone atoms of the protein. Restraints were initially set to 10 kcal*mol^{-1}*$Å^{-2}$, and gradually reduced to zero. Unrestrained MD simulation followed

for ~82 ns (MsbA 3B5W), ~88 ns (MsbA 3B60), and ~93 ns (Sav1866). The atomic systems used for the analyses were from the last 20 ns of the unrestrained MD. A significant drift that stabilizes at 6.7±0.2 Å after 60 ns and remains constant until the end of the simulation is observed in the RMSD of MsbA (3B5W). The RMSD values of the MsbA (3B60) and Sav1866 simulations reached a plateau in less than 3 ns with average values of 2.4±0.1 Å and 1.9±0.1 respectively.

Acknowledgments
We thank Dr. Serge Crouzy for his help with the naccess software.

Funding statements
Higher Education Commission of Pakistan is acknowledged for supporting doctoral fellowship to SM. This work was initiated thanks to the previous financial support from the 'Agence Nationale de la Recherche', grant N°: ANR-06-Blan-0420 and ANR-PCV06-135269, and to the current support of this agency, grant N°: ANR-09-PIRI-0002-01(both to JMJ).

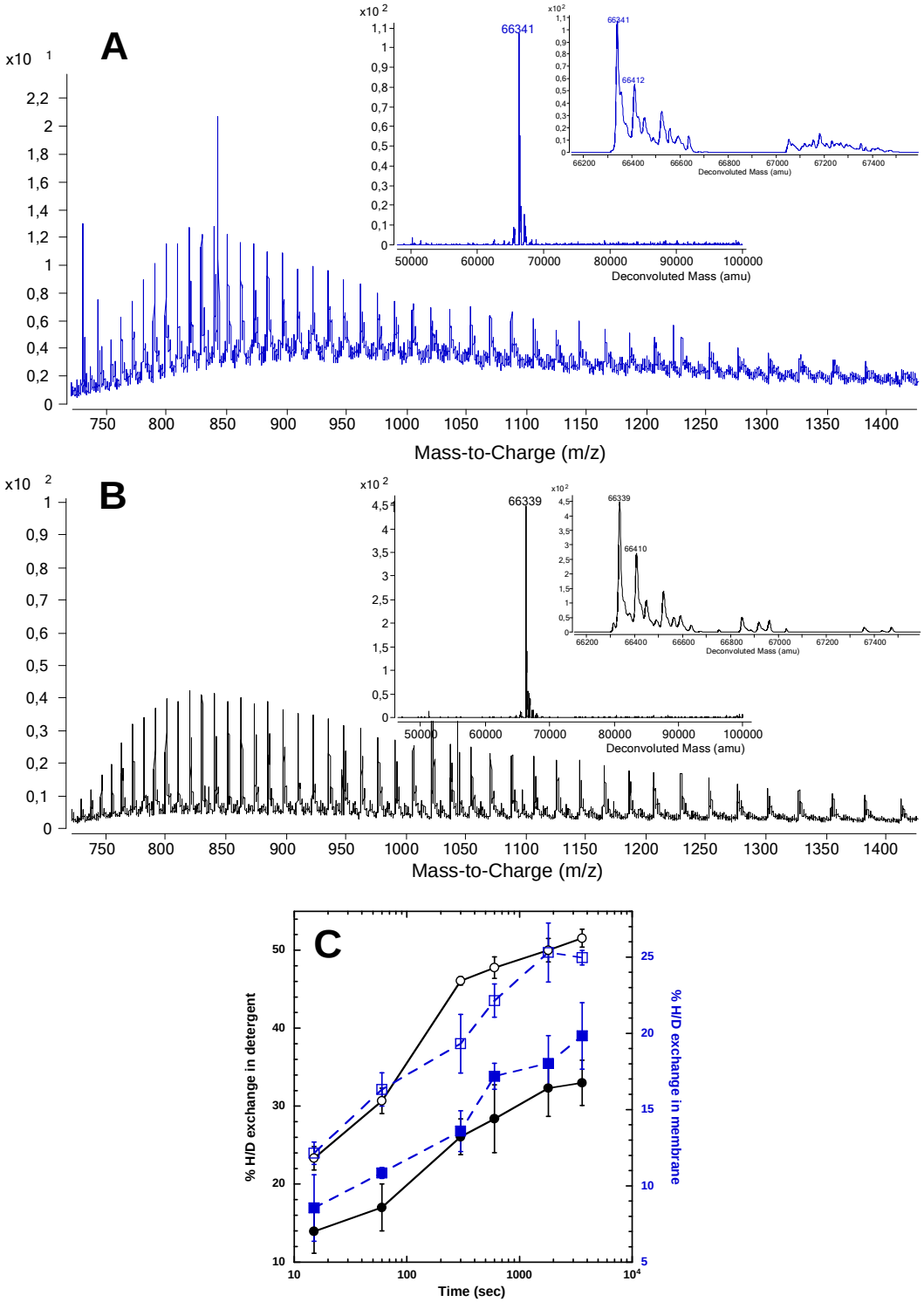

Figure 1. Raw mass spectra and global H/D exchange of BmrA-enriched membranes or BmrA purified in detergent. Raw mass spectrum of BmrA in membranes (***A***) or BmrA purified in DDM (***B***). Deconvoluted mass spectra are presented in first insets with a close-up view in the second insets. (***C***) Global deuteration kinetics of apo BmrA in membranes (open square) or purified in DDM (open circle), or of vanadate-inhibited BmrA in membrane (full square) or purified in DDM (full circle). Standard deviations for two separate experiments are shown by vertical bars.

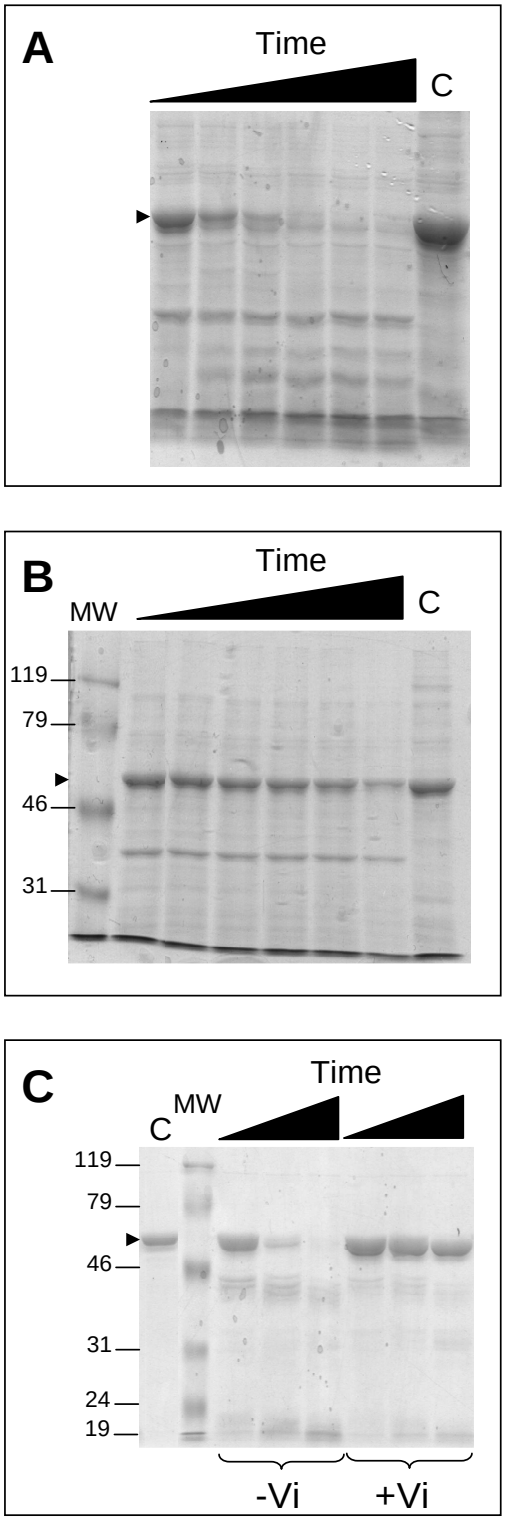

Figure 2. SDS-PAGE of BmrA-enriched membranes or BmrA purified in DDM and after limited proteolysis with trypsin. BmrA in membranes in the apo conformation (***A***) or in the vanadate-inhibited conformation (***B***) and after incubation with trypsin for 5 min, 15 min, 30 min, 1 h, 2 h and 3 h (from left to right lanes); (***C***) BmrA purified in detergent in the apo conformation (lanes 3-5), and in the vanadate-inhibited conformation (lanes 6-8) and after incubation with trypsin for 5, 15 and 30 min (from left to right lanes). *C* is the control lane with no trypsin added with the black arrowhead showing the position of the full-length BmrA. The masses of the molecular weight markers (MW) are indicated in kDa.

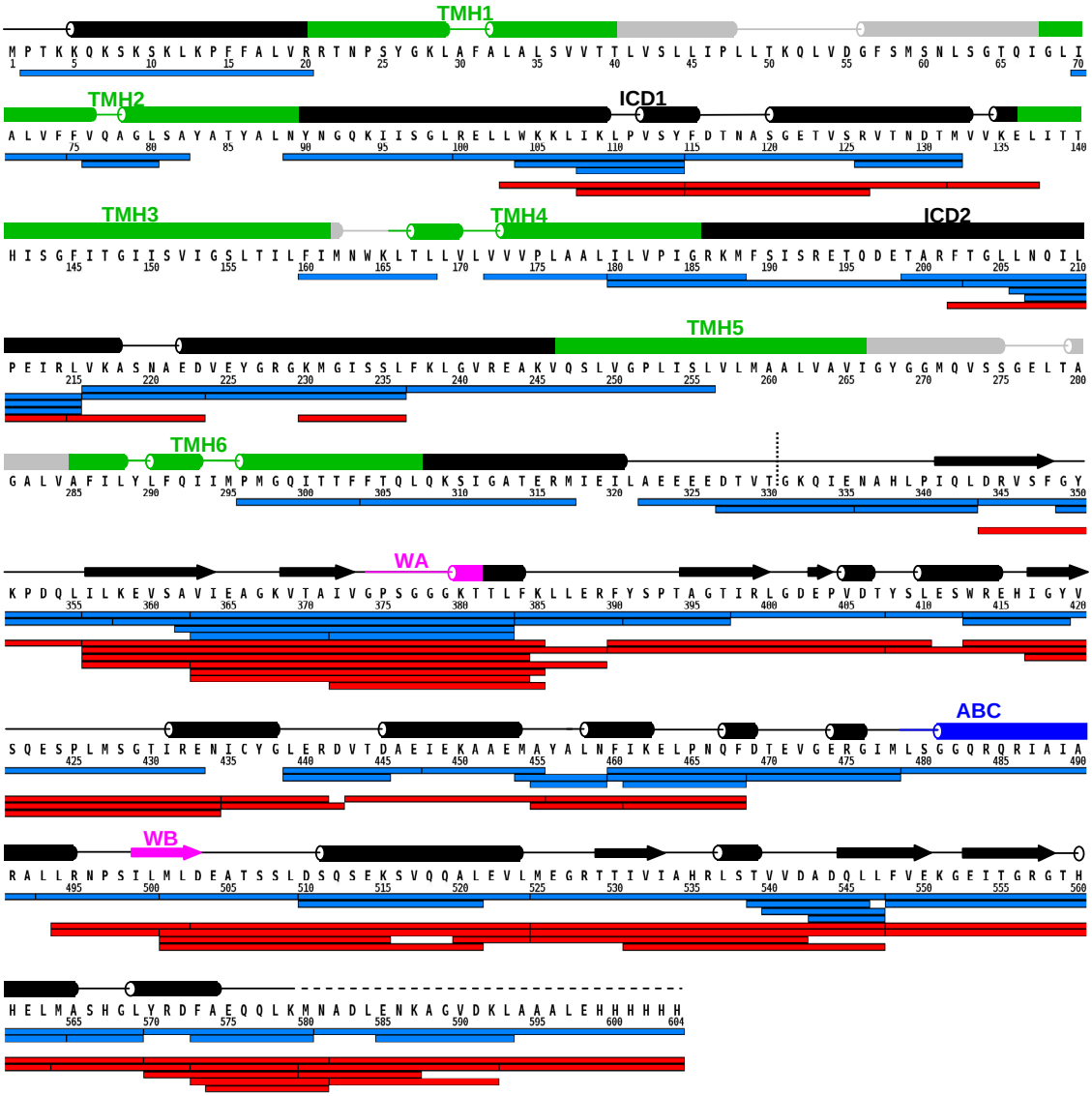

Figure 3. Peptide mapping of BmrA using immobilized pepsin (blue) or immobilized rhizopuspepsin (red). The predicted secondary structure (cylinders for α-helices and arrows for β-strands) and topology of BmrA based on the Sav1866 3-D structure is shown above the sequence with the specific regions: Walker A (WA) and B (WB) motifs and the ABC signature. The transmembrane helices 1 to 6 (TMH1 to 6) are shown in green colour and the position of the intracellular domains 1 and 2 (ICD1 and ICD2, respectively) are indicated. The extracellular parts of BmrA are shown in grey colour. The boundary between the TMD and the NBD is shown by a vertical dotted line.

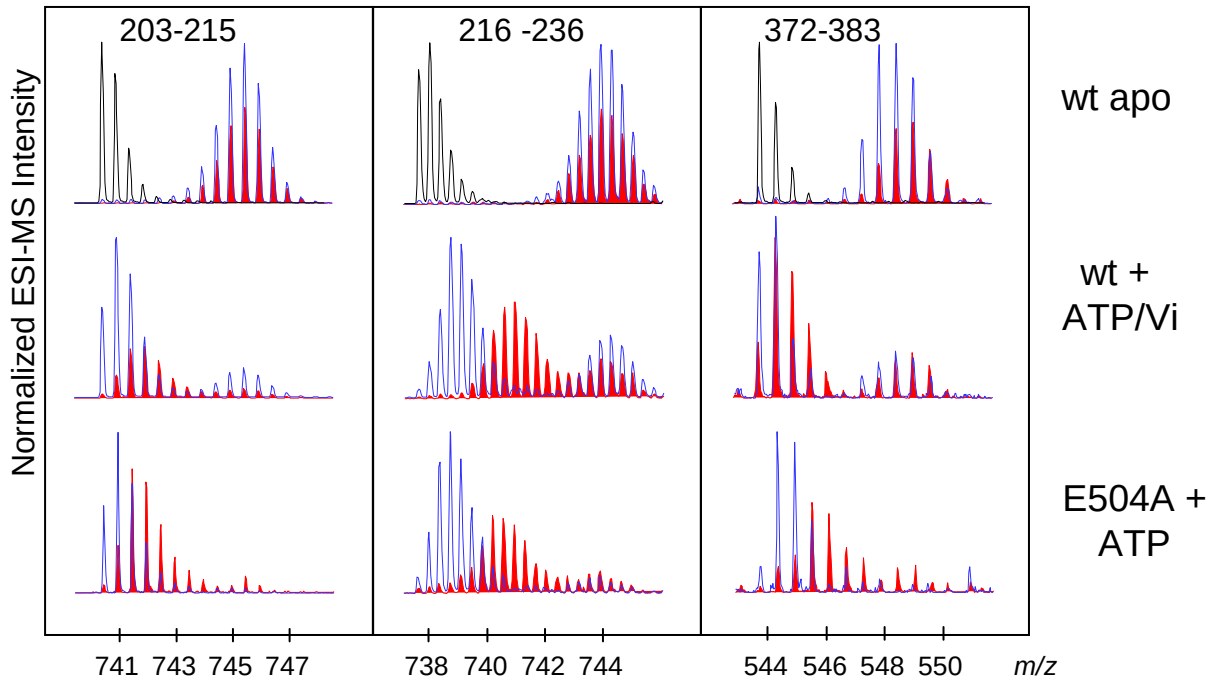

Figure 4. Isotopic profiles of three selected peptides at different deuteration times. The mass spectra of three peptides, two from ICD2 (203-215 and 216-236) or one from the NBD (372-383) are shown before (black line) or after 15 s (blue line) and 3600 s (red line) deuteration of BmrA. These peptides were from the wild-type BmrA in the apo (wt apo) or vanadate-inhibited states (wt + ATP/Vi) or from the E504A mutant incubated in the presence of ATP (E504A + ATP).

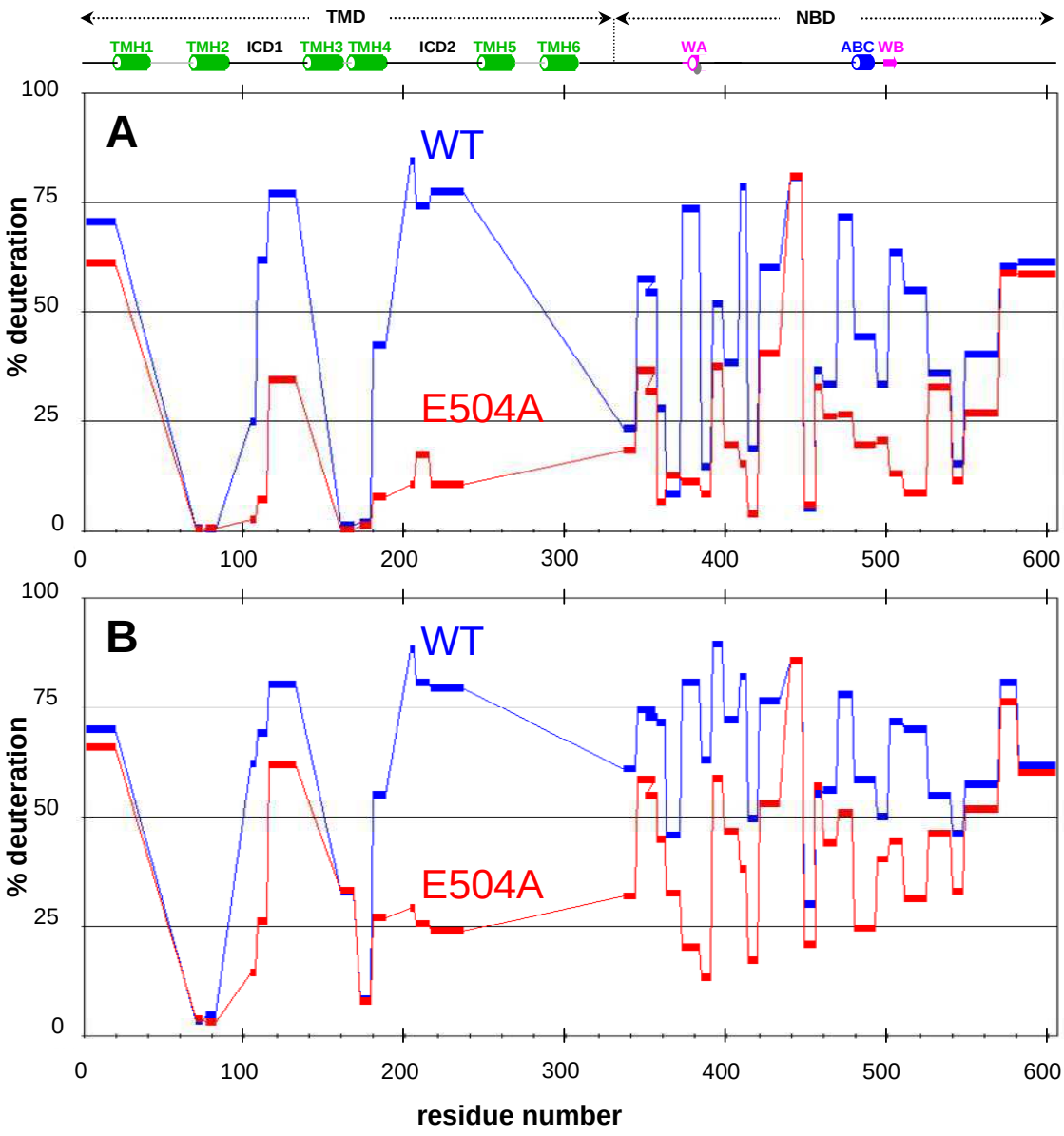

Figure 5. HDX profile of wild-type BmrA and the E504A mutant. The wild-type BmrA in the apo state (blue bars) and the E504A mutant in the ATP-bound state (red bars) were submitted to HDX, and the results obtained after 15 s (***A***) and 600 s of deuteration (***B***) are shown. The topology prediction and specific motifs in the NBD of BmrA are displayed above the graphs (see legend to Figure 3).

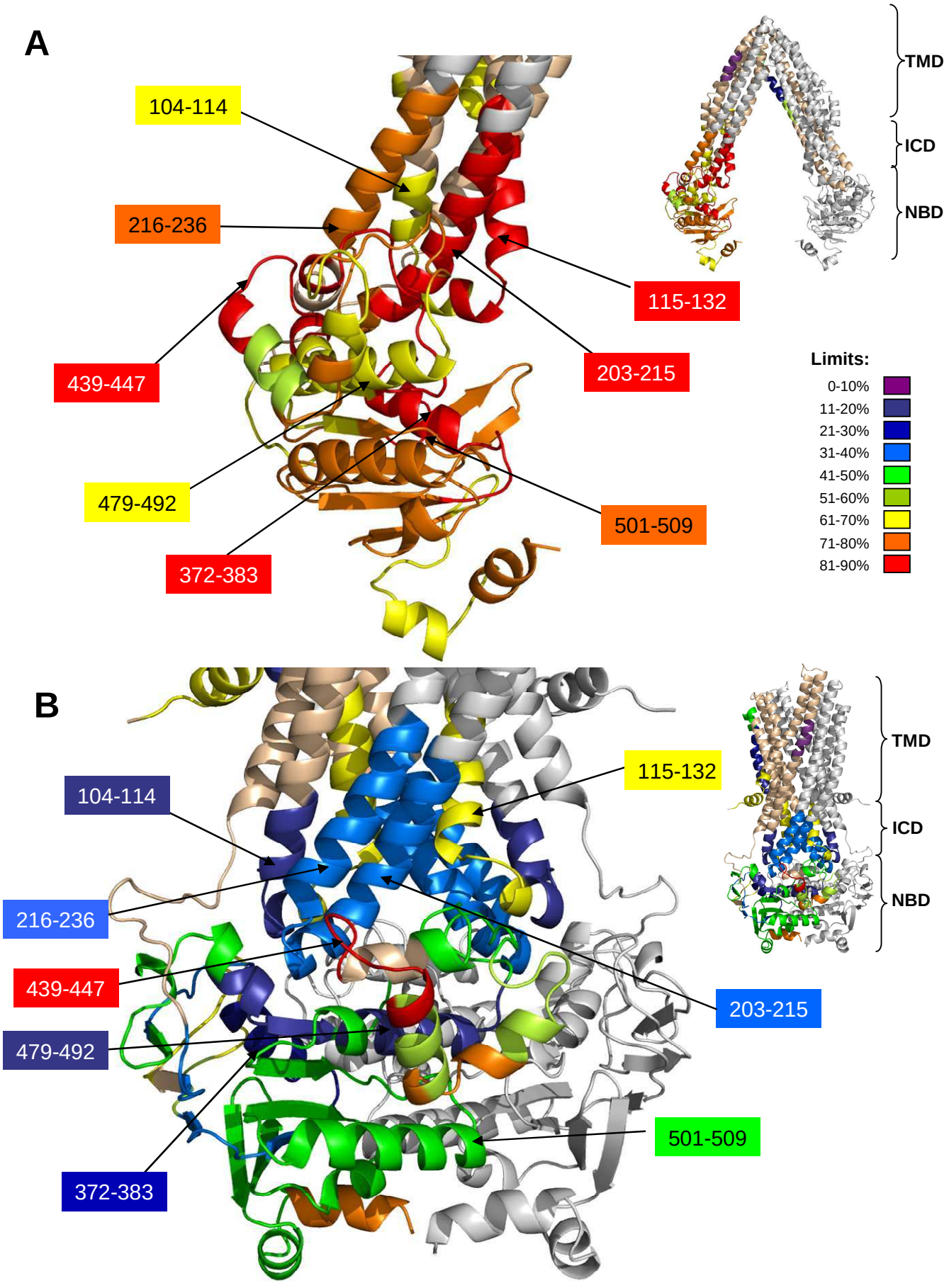
A
104-114
216-236
115-132
439-447
203-215
479-492
501-509
372-383
TMD
ICD
NBD
Limits:
0-10%
11-20%
21-30%
31-40%
41-50%
51-60%
61-70%
71-80%
81-90%
B
104-114
115-132
216-236
439-447
203-215
479-492
501-509
372-383
TMD
ICD
NBD

Figure 6. HDX of different peptides from the ICDs and the NBD of BmrA depicted on BmrA 3-D models. The inserts show BmrA modelled in the open apo conformation (***A***) or in the closed ATP-bound conformation (***B***) and the close-up views are restricted to the ICD1 and the NBD from one monomer together with ICD2 from the second monomer. One subunit was drawn in wheat colour and the other in light gray. In each conformation, specific regions are drawn with rainbow colours determined by their percentage of deuterium exchange after 600 s of deuteration (scale of deuterium exchange shown as insert). Selected regions are also shown with arrows.

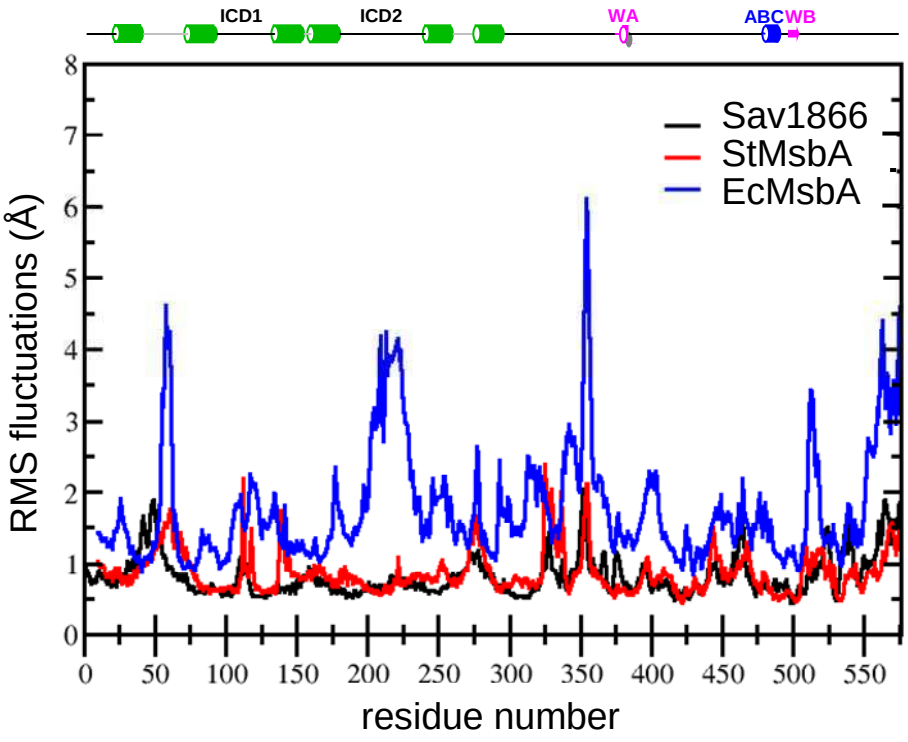

Figure 7. Root mean square fluctuation of the Cα of Sav1866, StMsbA and EcMsbA. Molecular dymanics simulations were performed on each structure and, once equilibrium was reached, the Root Mean Square (RMS) fluctuation in Å was calculated for the last 20ns, and is shown as a function of the residue number. The predicted topology of BmrA is also shown on top of the figure for comparison using the same color-coding as in Figure 3.

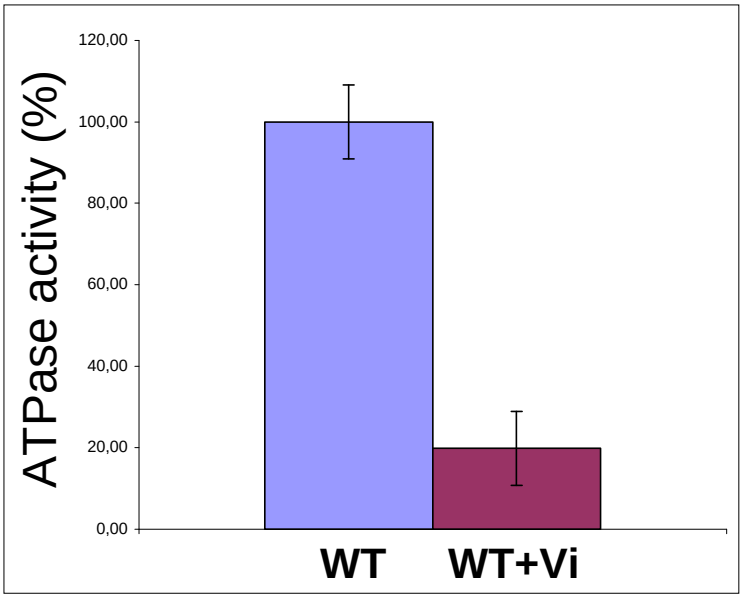

Figure S1. ATPase activity of the wild-type BmrA. 10-20 µg of BmrA were injected into an ATPase assay medium in the absence (blue bar, WT) or presence of 3 mM vanadate (purple bar, WT + Vi).

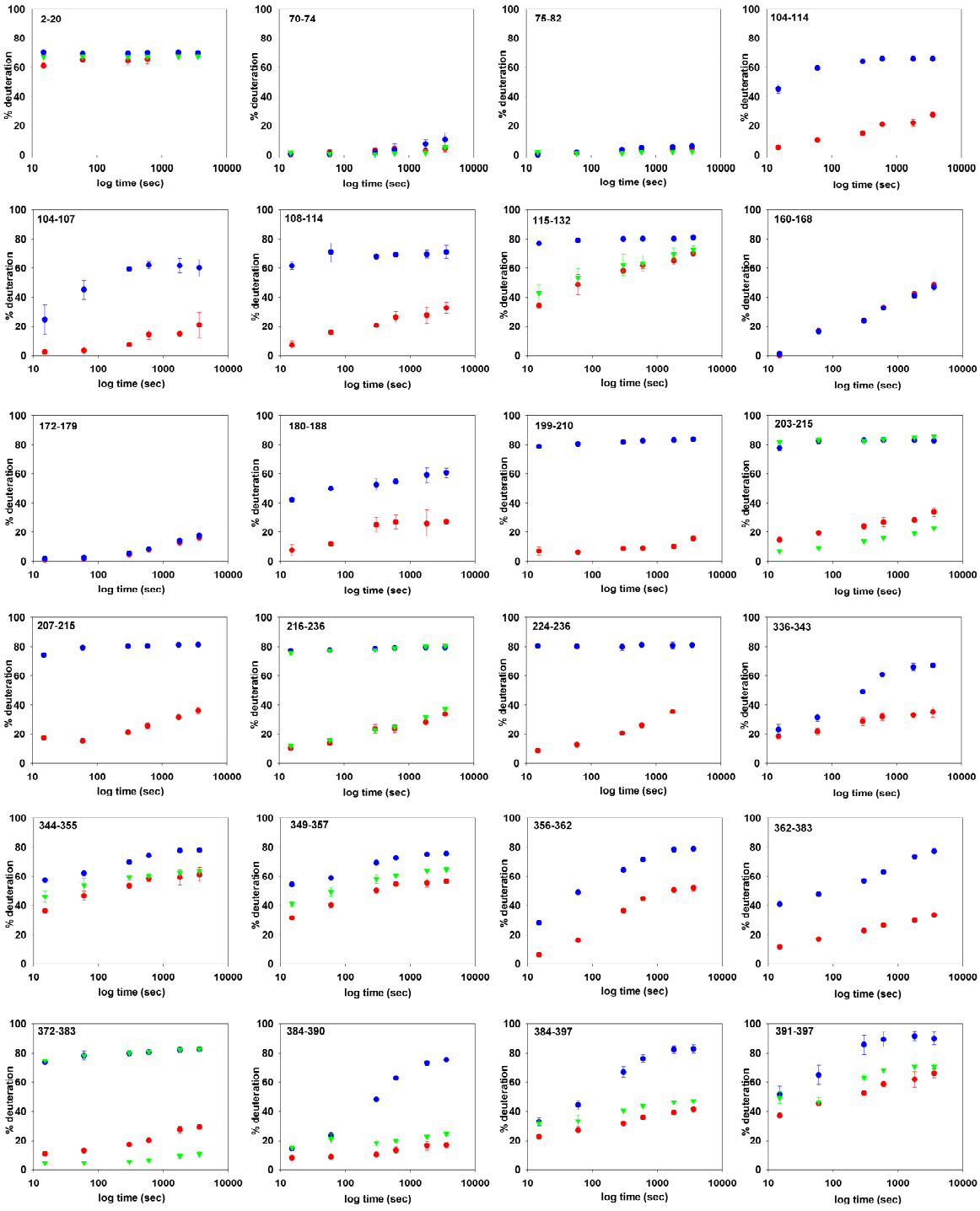

Figure S2. HDX kinetics of all BmrA peptides identified after digestion with immobilized pepsin. The percentage of deuteration is plotted against different deuteration times for the wild-type BmrA in the apo state (blue circles), in the vanadate-inhibited state (green circles) or in the mutated (E504A) form (red circles). Standard deviations (for two experiments) are shown by vertical bars ; in many cases, bars are so small that they are hidden by the symbols.

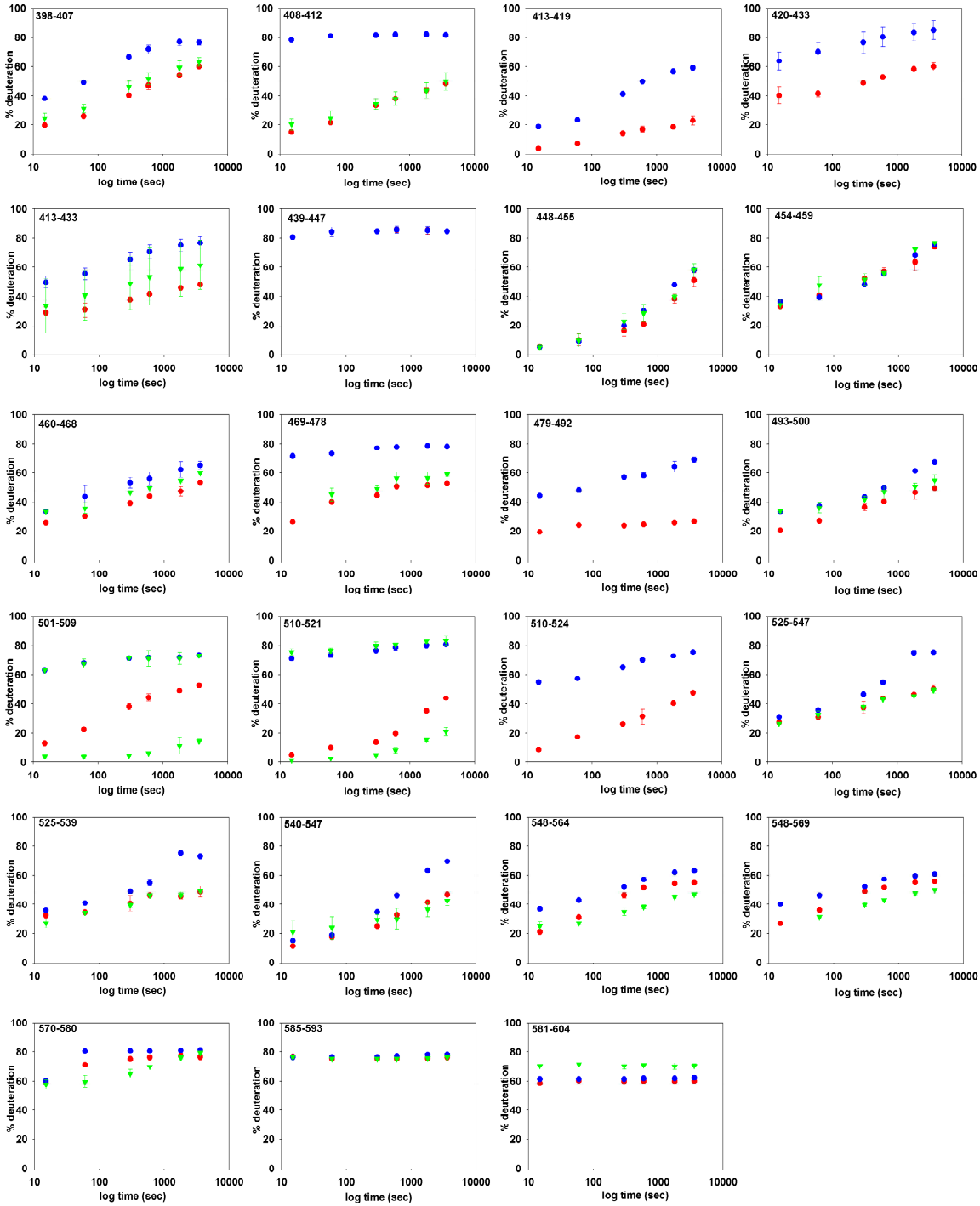

Figure S2 (following part)

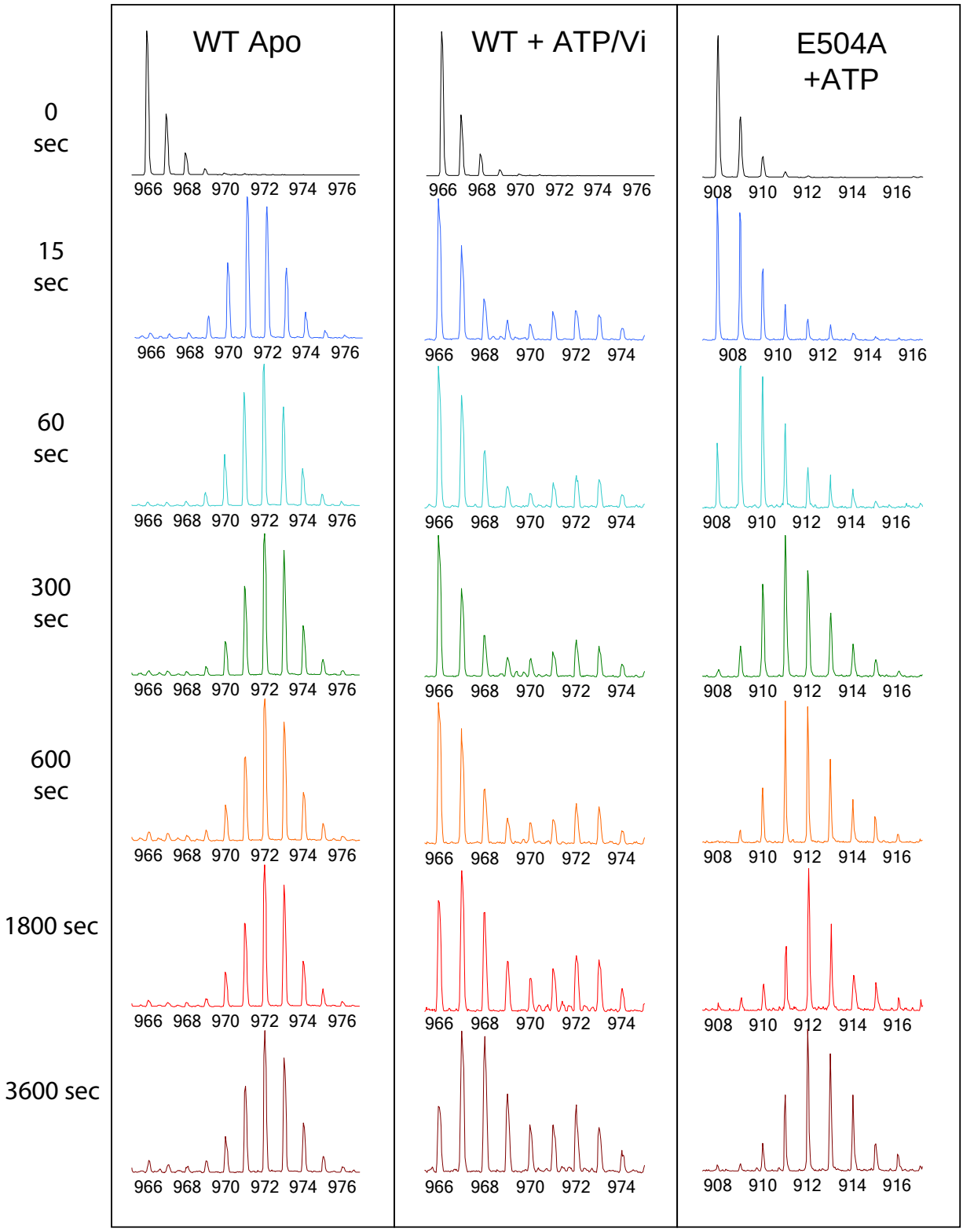

Figure S3. Evolution of the isotopic envelope of peptide 501-509 at different deuteration times for the wild-type BmrA in the apo state (WT Apo) or in the vanadate-inhibited state (WT + ATP/Vi) or for the E504A mutant (E504A + ATP). Please note that this peptide contains the mutated residue in the mutant form accounting for the mass difference observed.

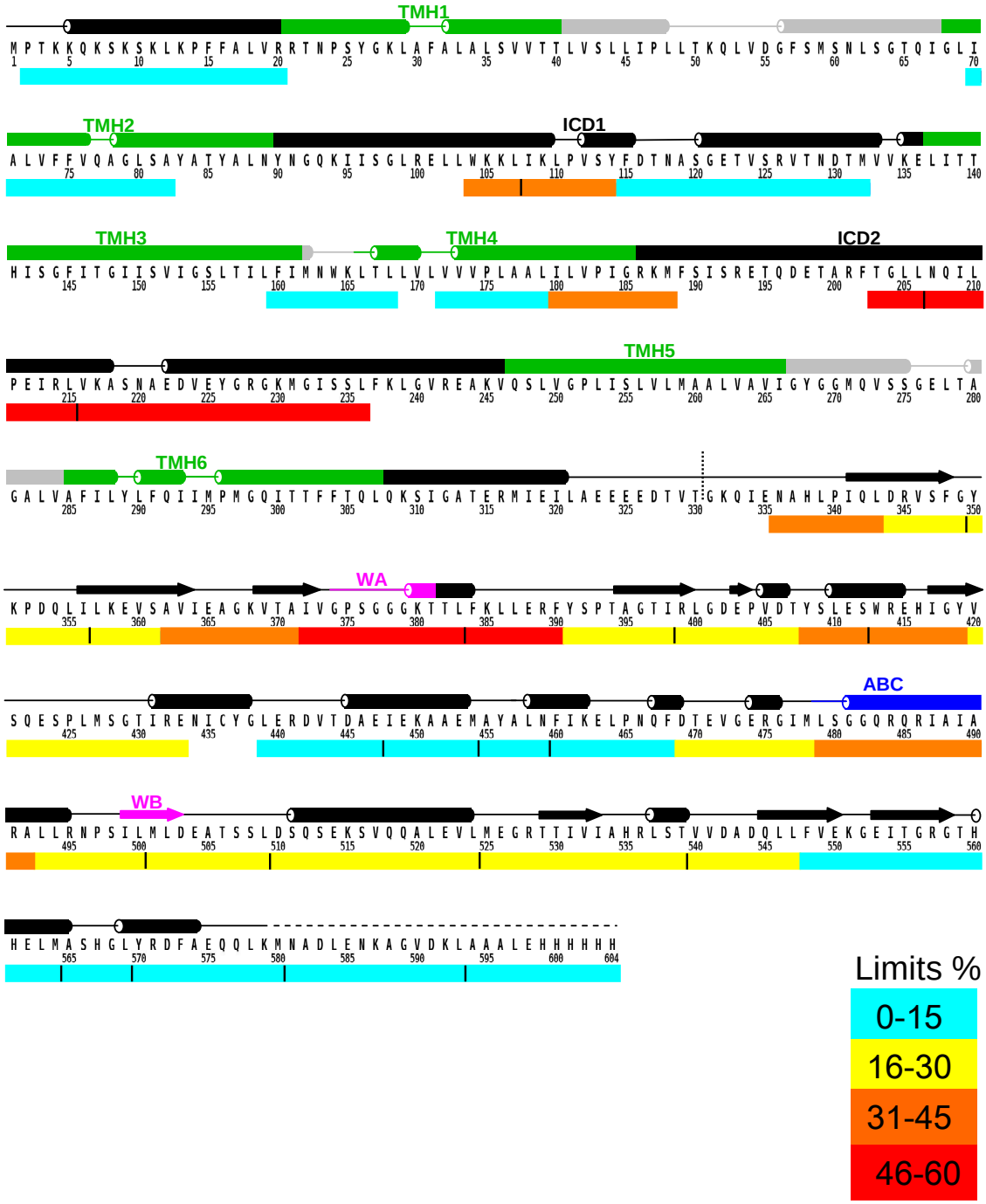

Figure S4. Heat map showing the difference in deuterium incorporation between the apo conformation (wild-type in the resting state) and the closed conformation (E504A in the presence of ATP) after 1 h deuteration. The predicted secondary structure and topology of BmrA (see legend to Figure 3) is indicated above the sequence with the colour legend shown as an insert.

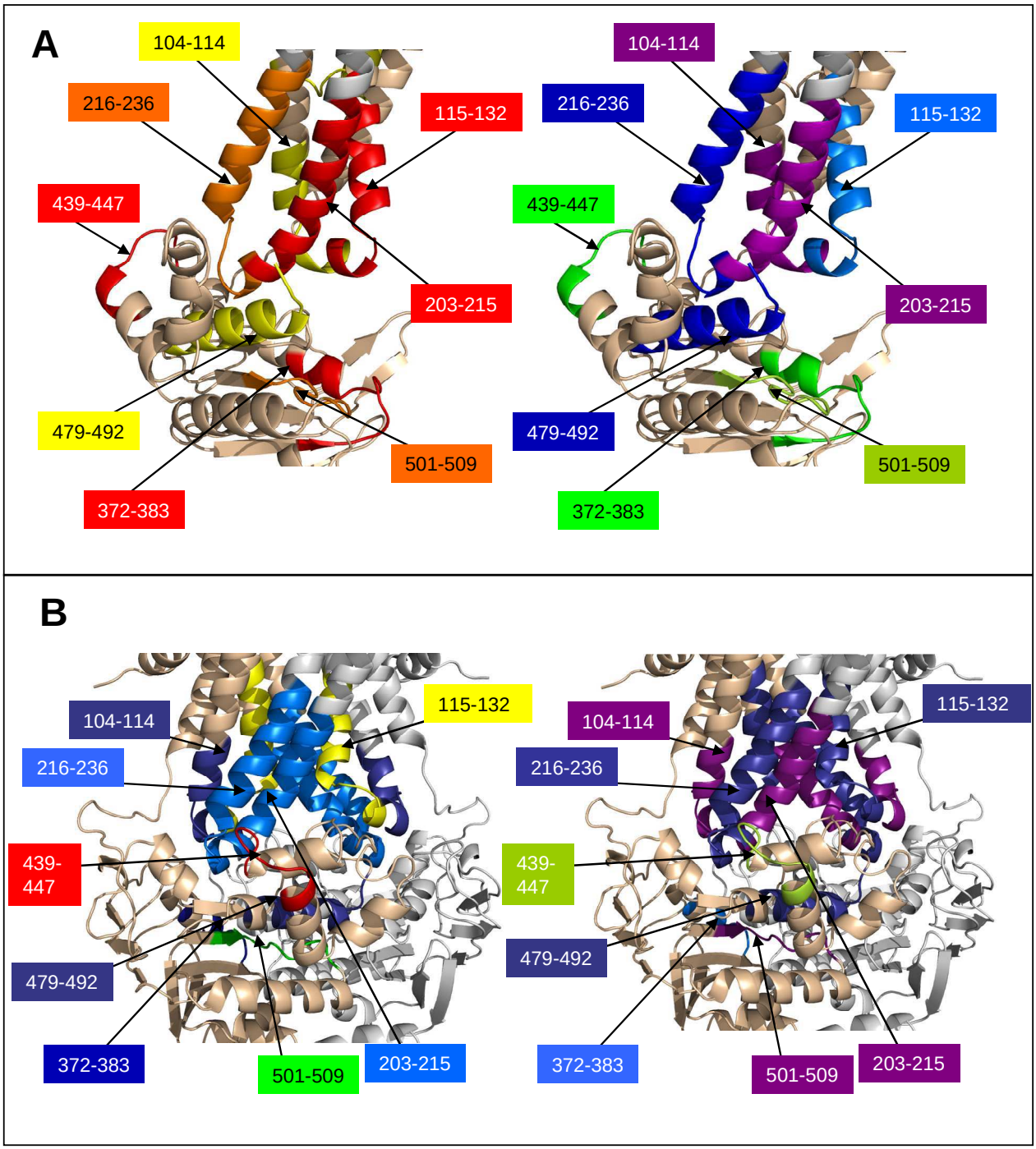

Figure S5. Comparison of deuterium incorporation and accessibility areas in both conformations of BmrA, open (***A***) or closed (***B***). The left panels are identical to those shown in Figure 6 for the HDX except that only the selected peptides are coloured according to the deuterium exchange scale. The right panels show the accessibility of the corresponding peptides deduced from each BmrA model.

		BmrA	TMD	NBD
Pepsin Column	**%Coverage**	78	60	98
	Peptides	67	24	43
	Average	7.0	8.0	6.4
Pepsin Solution	**%Coverage**	45	11	82
	Peptides	31	3	28
	Average	8.7	12.6	8.3
XVIII Column	**%Coverage**	50	10	84
	Peptides	52	8	44
	Average	5.8	8.0	5.4
HDX	**%Coverage**	67.5	45	92
	Peptides	44	15	29
	Average	9.3	9.0	9.3

Table 1. Sequence coverage, number of peptides and average size of the peptides for BmrA and for its domains TMD and NBD obtained in different digestion conditions and after deuteration and digestion with immobilized pepsin.

References

1. Davidson, A.L., et al., *Structure, function, and evolution of bacterial ATP-binding cassette systems.* Microbiol Mol Biol Rev, 2008. **72**(2): p. 317-64.
2. Rees, D.C., E. Johnson, and O. Lewinson, *ABC transporters: the power to change.* Nat Rev Mol Cell Biol, 2009. **10**(3): p. 218-27.
3. Cuthbertson, L., V. Kos, and C. Whitfield, *ABC transporters involved in export of cell surface glycoconjugates.* Microbiol Mol Biol Rev, 2010. **74**(3): p. 341-62.
4. Borst, P. and R.O. Elferink, *Mammalian abc transporters in health and disease.* Annu Rev Biochem, 2002. **71**: p. 537-92.
5. Ernst, R., et al., *Multidrug efflux pumps: substrate selection in ATP-binding cassette multidrug efflux pumps--first come, first served?* Febs J, 2010. **277**(3): p. 540-9.
6. van Veen, H.W., et al., *Multidrug resistance mediated by a bacterial homolog of the human multidrug transporter MDR1.* Proc Natl Acad Sci U S A, 1996. **93**(20): p. 10668-72.
7. Oldham, M.L., et al., *Crystal structure of a catalytic intermediate of the maltose transporter.* Nature, 2007. **450**(7169): p. 515-21.
8. Lubelski, J., W.N. Konings, and A.J. Driessen, *Distribution and Physiology of ABC-Type Transporters Contributing to Multidrug Resistance in Bacteria.* Microbiol Mol Biol Rev, 2007. **71**(3): p. 463-76.
9. Garvey, M.I., et al., *Overexpression of patA and patB, which encode ABC transporters, is associated with fluoroquinolone resistance in clinical isolates of Streptococcus pneumoniae.* Antimicrob Agents Chemother, 2011. **55**(1): p. 190-6.
10. Paulsen, I.T., *Multidrug efflux pumps and resistance: regulation and evolution.* Curr Opin Microbiol, 2003. **6**(5): p. 446-51.
11. Geourjon, C., et al., *A common mechanism for ATP hydrolysis in ABC transporter and helicase superfamilies.* Trends Biochem Sci, 2001. **26**(9): p. 539-44.
12. Seeger, M.A. and H.W. van Veen, *Molecular basis of multidrug transport by ABC transporters.* Biochim Biophys Acta, 2009. **1794**(5): p. 725-37.
13. Chen, J., et al., *A tweezers-like motion of the ATP-binding cassette dimer in an ABC transport cycle.* Mol Cell, 2003. **12**(3): p. 651-61.
14. Smith, P.C., et al., *ATP binding to the motor domain from an ABC transporter drives formation of a nucleotide sandwich dimer.* Mol Cell, 2002. **10**(1): p. 139-49.
15. Zaitseva, J., et al., *H662 is the linchpin of ATP hydrolysis in the nucleotide-binding domain of the ABC transporter HlyB.* Embo J, 2005. **24**(11): p. 1901-10.
16. Zaitseva, J., et al., *Functional characterization and ATP-induced dimerization of the isolated ABC-domain of the haemolysin B transporter.* Biochemistry, 2005. **44**(28): p. 9680-90.
17. Urbatsch, I.L., et al., *P-glycoprotein catalytic mechanism: studies of the ADP-vanadate inhibited state.* J Biol Chem, 2003. **278**(25): p. 23171-9.
18. Parcej, D. and R. Tampe, *ABC proteins in antigen translocation and viral inhibition.* Nat Chem Biol, 2010. **6**(8): p. 572-80.
19. Aller, S.G., et al., *Structure of P-glycoprotein reveals a molecular basis for poly-specific drug binding.* Science, 2009. **323**(5922): p. 1718-22.
20. Dawson, R.J. and K.P. Locher, *Structure of a bacterial multidrug ABC transporter.* Nature, 2006. **443**(7108): p. 180-5.
21. Ward, A., et al., *Flexibility in the ABC transporter MsbA: Alternating access with a twist.* Proc Natl Acad Sci U S A, 2007. **104**(48): p. 19005-19010.
22. Oancea, G., et al., *Structural arrangement of the transmission interface in the antigen ABC transport complex TAP.* Proc Natl Acad Sci U S A, 2009. **106**(14): p. 5551-6.

23. Serohijos, A.W., et al., *Phenylalanine-508 mediates a cytoplasmic-membrane domain contact in the CFTR 3D structure crucial to assembly and channel function.* Proc Natl Acad Sci U S A, 2008. **105**(9): p. 3256-61.
24. Borbat, P.P., et al., *Conformational Motion of the ABC Transporter MsbA Induced by ATP Hydrolysis.* PLoS Biol, 2007. **5**(10): p. e271.
25. Dalmas, O., et al., *The Q-loop Disengages from the First Intracellular Loop during the Catalytic Cycle of the Multidrug ABC Transporter BmrA.* J Biol Chem, 2005. **280**(44): p. 36857-36864.
26. Pagant, S., et al., *Mapping of interdomain interfaces required for the functional architecture of Yor1p, a eukaryotic ATP-binding cassette (ABC) transporter.* J Biol Chem, 2008. **283**(39): p. 26444-51.
27. Zhang, Z. and D.L. Smith, *Determination of amide hydrogen exchange by mass spectrometry: a new tool for protein structure elucidation.* Protein Sci, 1993. **2**(4): p. 522-31.
28. Hoofnagle, A.N., K.A. Resing, and N.G. Ahn, *Protein analysis by hydrogen exchange mass spectrometry.* Annu Rev Biophys Biomol Struct, 2003. **32**: p. 1-25.
29. Wales, T.E. and J.R. Engen, *Hydrogen exchange mass spectrometry for the analysis of protein dynamics.* Mass Spectrom Rev, 2006. **25**(1): p. 158-70.
30. Hebling, C.M., et al., *Conformational analysis of membrane proteins in phospholipid bilayer nanodiscs by hydrogen exchange mass spectrometry.* Anal Chem, 2010. **82**(13): p. 5415-9.
31. Konermann, L., J. Pan, and Y.H. Liu, *Hydrogen exchange mass spectrometry for studying protein structure and dynamics.* Chem Soc Rev, 2011. **40**(3): p. 1224-34.
32. Zhang, J., et al., *Hydrogen/deuterium exchange reveals distinct agonist/partial agonist receptor dynamics within vitamin D receptor/retinoid X receptor heterodimer.* Structure, 2010. **18**(10): p. 1332-41.
33. Zhang, X., et al., *Dynamics of the beta2-adrenergic G-protein coupled receptor revealed by hydrogen-deuterium exchange.* Anal Chem, 2010. **82**(3): p. 1100-8.
34. Rey, M., et al., *Conformational dynamics of the bovine mitochondrial ADP/ATP carrier isoform 1 revealed by hydrogen/deuterium exchange coupled to mass spectrometry.* J Biol Chem, 2010. **285**(45): p. 34981-90.
35. Do Cao, M.A., et al., *Probing the conformation of the resting state of a bacterial multidrug ABC transporter, BmrA, by a site-directed spin labeling approach.* Protein Sci, 2009. **18**(7): p. 1507-20.
36. Steinfels, E., et al., *Highly efficient over-production in E. coli of YvcC, a multidrug-like ATP-binding cassette transporter from Bacillus subtilis.* Biochim Biophys Acta, 2002. **1565**(1): p. 1-5.
37. Steinfels, E., et al., *Characterization of YvcC (BmrA), a Multidrug ABC Transporter Constitutively Expressed in Bacillus subtilis.* Biochemistry, 2004. **43**(23): p. 7491-7502.
38. Gutmann, D.A., et al., *Understanding polyspecificity of multidrug ABC transporters: closing in on the gaps in ABCB1.* Trends Biochem Sci, 2010. **35**(1): p. 36-42.
39. Ravaud, S., et al., *The ABC transporter BmrA from Bacillus subtilis is a functional dimer when in a detergent-solubilized state.* Biochem J, 2006. **395**(2): p. 345-53.
40. Barnidge, D.R., et al., *Extraction method for analysis of detergent-solubilized bacteriorhodopsin and hydrophobic peptides by electrospray ionization mass spectrometry.* Anal Biochem, 1999. **269**(1): p. 1-9.
41. le Maire, M., et al., *Electrospray ionization mass spectrometry on hydrophobic peptides electroeluted from sodium dodecyl sulfate-polyacrylamide gel electrophoresis*

application to the topology of the sarcoplasmic reticulum Ca2+ ATPase. Anal Biochem, 1993. **214**(1): p. 50-7.
42. Whitelegge, J.P., C.B. Gundersen, and K.F. Faull, *Electrospray-ionization mass spectrometry of intact intrinsic membrane proteins.* Protein Sci, 1998. **7**(6): p. 1423-30.
43. Whitelegge, J.P., et al., *Toward the bilayer proteome, electrospray ionization-mass spectrometry of large, intact transmembrane proteins.* Proc Natl Acad Sci U S A, 1999. **96**(19): p. 10695-8.
44. Rey, M., et al., *Effective removal of nonionic detergents in protein mass spectrometry, hydrogen/deuterium exchange, and proteomics.* Anal Chem, 2010. **82**(12): p. 5107-16.
45. Rey, M., et al., *Recombinant immobilized rhizopuspepsin as a new tool for protein digestion in hydrogen/deuterium exchange mass spectrometry.* Rapid Commun Mass Spectrom, 2009. **23**(21): p. 3431-8.
46. Man, P., et al., *Accessibility changes within diphtheria toxin T domain when in the functional molten globule state, as determined using hydrogen/deuterium exchange measurements.* Febs J, 2010. **277**(3): p. 653-62.
47. Marcoux, J., et al., *p47phox molecular activation for assembly of the neutrophil NADPH oxidase complex.* J Biol Chem, 2010. **285**(37): p. 28980-90.
48. Melnyk, R.A., et al., *Structural determinants for the binding of anthrax lethal factor to oligomeric protective antigen.* J Biol Chem, 2006. **281**(3): p. 1630-5.
49. Hrycyna, C.A., *Molecular genetic analysis and biochemical characterization of mammalian P-glycoproteins involved in multidrug resistance.* Semin Cell Dev Biol, 2001. **12**(3): p. 247-56.
50. Kwan, T. and P. Gros, *Mutational analysis of the P-glycoprotein first intracellular loop and flanking transmembrane domains.* Biochemistry, 1998. **37**(10): p. 3337-50.
51. Orelle, C., et al., *The Conserved Glutamate Residue Adjacent to the Walker-B Motif Is the Catalytic Base for ATP Hydrolysis in the ATP-binding Cassette Transporter BmrA.* J Biol Chem, 2003. **278**(47): p. 47002-8.
52. Orelle, C., et al., *Conformational change induced by ATP binding in the multidrug ATP-binding cassette transporter BmrA.* Biochemistry, 2008. **47**(8): p. 2404-12.
53. Lu, G., et al., *ATP hydrolysis is required to reset the ATP-binding cassette dimer into the resting-state conformation.* Proc Natl Acad Sci U S A, 2005. **102**(50): p. 17969-74.
54. Zaitseva, J., et al., *A structural analysis of asymmetry required for catalytic activity of an ABC-ATPase domain dimer.* Embo J, 2006. **25**(14): p. 3432-43.
55. Doshi, R., B. Woebking, and H.W. van Veen, *Dissection of the conformational cycle of the multidrug/lipidA ABC exporter MsbA.* Proteins, 2010. **78**(14): p. 2867-72.
56. Zou, P., M. Bortolus, and H.S. McHaourab, *Conformational cycle of the ABC transporter MsbA in liposomes: detailed analysis using double electron-electron resonance spectroscopy.* J Mol Biol, 2009. **393**(3): p. 586-97.
57. Zou, P. and H.S. McHaourab, *Alternating access of the putative substrate-binding chamber in the ABC transporter MsbA.* J Mol Biol, 2009. **393**(3): p. 574-85.
58. Siarheyeva, A., et al., *Probing the molecular dynamics of the ABC multidrug transporter LmrA by deuterium solid-state nuclear magnetic resonance.* Biochemistry, 2007. **46**(11): p. 3075-83.
59. Ananthaswamy, N., et al., *The signaling interface of the yeast multidrug transporter Pdr5 adopts a cis conformation, and there are functional overlap and equivalence of the deviant and canonical Q-loop residues.* Biochemistry, 2010. **49**(21): p. 4440-9.

60. Rutledge, R.M., et al., *Toward understanding the mechanism of action of the yeast multidrug resistance transporter Pdr5p: a molecular modeling study.* J Struct Biol. **173**(2): p. 333-44.
61. Oliveira, A.S., A.M. Baptista, and C.M. Soares, *Conformational changes induced by ATP-hydrolysis in an ABC transporter: A molecular dynamics study of the Sav1866 exporter.* Proteins, 2011. **79**(6): p. 1977-90.
62. Lewis, H.A., et al., *Structure and dynamics of NBD1 from CFTR characterized using crystallography and hydrogen/deuterium exchange mass spectrometry.* J Mol Biol, 2010. **396**(2): p. 406-30.
63. Murakami, S., et al., *Crystal structures of a multidrug transporter reveal a functionally rotating mechanism.* Nature, 2006. **443**(7108): p. 173-9.
64. Sorensen, T.L., J.V. Moller, and P. Nissen, *Phosphoryl transfer and calcium ion occlusion in the calcium pump.* Science, 2004. **304**(5677): p. 1672-5.
65. Toyoshima, C., *How Ca2+-ATPase pumps ions across the sarcoplasmic reticulum membrane.* Biochim Biophys Acta, 2009. **1793**(6): p. 941-6.
66. Toyoshima, C. and T. Mizutani, *Crystal structure of the calcium pump with a bound ATP analogue.* Nature, 2004. **430**(6999): p. 529-35.
67. Bensadoun, A. and D. Weinstein, *Assay of proteins in the presence of interfering materials.* Anal Biochem, 1976. **70**(1): p. 241-50.
68. Bradford, M.M., *A rapid and sensitive method for the quantitation of microgram quantities of protein utilizing the principle of protein-dye binding.* Anal Biochem, 1976. **72**: p. 248-54.
69. Zhang, Z. and A.G. Marshall, *A universal algorithm for fast and automated charge state deconvolution of electrospray mass-to-charge ratio spectra.* J Am Soc Mass Spectrom, 1998. **9**(3): p. 225-33.
70. Jault, J.M., et al., *Alteration of apparent negative cooperativity of ATPase activity by alpha-subunit glutamine 173 mutation in yeast mitochondrial F1. Correlation with impaired nucleotide interaction at a regulatory site.* J Biol Chem, 1991. **266**(13): p. 8073-8.
71. Galian, C., et al., *Optimized purification of a heterodimeric ABC transporter in a highly stable form amenable to 2-D crystallization.* PLoS One, 2011. **6**(5): p. e19677.
72. Lee, B. and F.M. Richards, *The interpretation of protein structures: estimation of static accessibility.* J Mol Biol, 1971. **55**(3): p. 379-400.
73. Phillips, J.C., et al., *Scalable molecular dynamics with NAMD.* J Comput Chem, 2005. **26**(16): p. 1781-802.
74. MacKerell, A.D., et al., *All-atom empirical potential for molecular modeling and dynamics studies of proteins.* Journal of Physical Chemistry B 1998. **102**: p. 3586-3616.
75. Jorgensen, W.L., et al., *Comparison of simple potential functions for simulating liquid water.* J. Chem. Phys., 1983. **79**: p. 926-935.
76. Feller, S.E., et al., *Constant-pressure molecular dynamics simulation- the langevin piston method.* Journal of Chemical Physics 1995. **103**: p. 4613-4621.
77. Essmann, U., et al., *A smooth particle mesh Ewald method.* J. Chem. Phys. , 1995. **103**: p. 8577-8593.
78. Miyamoto, S. and P.A. Kollman, *Settle - An analytical version of the Shake and Rattle algorithm for wigid water molecules.* Journal of Computational Chemistry 1992. **13**: p. 952-962.
79. Holm, L. and C. Sander, *Database algorithm for generating protein backbone and side-chain co-ordinates from a C alpha trace application to model building and detection of co-ordinate errors.* J Mol Biol, 1991. **218**(1): p. 183-94.

80. Canutescu, A.A., A.A. Shelenkov, and R.L. Dunbrack, Jr., *A graph-theory algorithm for rapid protein side-chain prediction.* Protein Sci, 2003. **12**(9): p. 2001-14.
81. Vriend, G., *WHAT IF: a molecular modeling and drug design program.* J Mol Graph, 1990. **8**(1): p. 52-6, 29.

Chapter 2. H/D exchange kinetics of BmrA mutant K380R

Comparative HDX analysis between wild-type apo and closed form of BmrA due to inactive catalytic glutamate next to the Walker 'B' motif clearly highlighted the difference of the conformation of transporter and as well as the dynamics of intracellular domains which was not anticipated with static X-ray structures. We extended our investigations with the mentioned technique to monitor the effect of the inactivation of the Walker 'A' critical lysine residue on the dynamics of the transporter. The lysine residue was shown to be required for the hydrolysis of ATP in presence of Mg^{2+}. The significance of this residue in BmrA was earlier realized showing that the mutation of lysine into alanine or arginine makes the transporter unable to hydrolyze ATP. However, the effect of these mutations was different from conserved glutamate which is next to Walker 'B' motif. As described in introduction, BmrA wild-type or mutants are able to form a regular ring shape structures. It was shown that addition of ATP/Mg^{2+} to wild-type BmrA leads to a large conformational change distorting regular ring shaped structure. In case of Walker 'A' motif mutant (K380R or K380A) the addition of ATP/Mg^{2+} did not affect the rings (Orelle, Gubellini et al. 2008).

The purpose of applying HDX kinetics to K380R mutant was primarily to monitor the dynamics of ICD1 and ICD2 and compare it to wild-type and/or with the closed state of transporter.

2.1. Conformation of BmrA mutant K380R in 0.5 mM ATP/Mg^{2+}:

As it was discussed for wild-type apo or mutant E504A, the protein was deuterated at time intervals from 15 s to 3600 s. The deuteration exchange was performed after incubation of transporter in 5 mM ATP and 5 mM Mg^{2+} for 5 min. The protein was diluted ten times in deuterated buffer making final concentration of ATP and Mg^{2+} 0.5 mM in deuterated buffer.

For apo conformation the peptides from ICDs e.g. 203-215, got highly deuterated as it was discussed earlier. In the case of K380R mutant in the presence of ATP and Mg^{2+}, two populations of the peptide were observed at 15 s deuteration time: one undeuterated and another highly deuterated exactly mimicking the closed and apo form of BmrA deuteration, respectively (Figure. 47). The undeuterated population of peptide tends to disappear with increasing deuteration time and after 10 min the peptide was more than 80 % deuterated.

The deuteration kinetics of ICDs and particularly ICD2 led us to conclude that initial 5 mM (0.5 mM in deuteration buffer) concentration of ATP/Mg^{2+} was not enough to limit the dynamics of the transporter. Therefore, the mutant K380R was incubated in the presence of 50 mM ATP/Mg^{2+} for 5 min and then labeled by diluting ten fold in deuterated buffer (5 mM in deuteration buffer).

The deuteration kinetics was followed from 15 s to 300 s. To underline the effect of initial high concentration of ATP/Mg^{2+}, wild type of BmrA was also incubated with 50 mM ATP/Mg^{2+} and deuterated (5 mM in deuteration buffer). However, peptides of wild-type BmrA in presence of 5 mM ATP/Mg^{2+} showed similar kinetics as it was found for the closed form BmrA mutant E504A. The closed form mimicking behavior of wild-type in presence of 5 mM ATP/Mg^{2+} might be due to the fact that most of the wild-type BmrA molecules were in a closed state in the presence of high nucleotide concentration. Since the mutant K380R lacks ATPase activity therefore to compare the difference due to nucleotide, the wild-type BmrA was incubated with 50 mM ADP/Mg^{2+} (5 mM in deuteration buffer).

The HDX kinetics of different regions of wild-type BmrA and mutant BmrA K380R in the presence of 5 mM ADP/Mg^{2+} and 5 mM ATP/Mg^{2+} respectively, are discussed.

2.2. Conformation of BmrA wild - type + 5 mM ADP/Mg^{2+} and mutant K380R + 5 mM ATP/Mg^{2+}:

Figure 48 shows the deuterium exchange level of different regions of BmrA on its sequence in mapped form for three conditions wild-type apo, wild - type + 5 mM ADP/Mg^{2+} and mutant K380R + 5 mM ATP/Mg^{2+}. Figure 49 shows the raw kinetics data for all three mentioned conditions. The results described in the following sections are based on these figures unless otherwise specified.

2.2.1. Transmembrane region:

The peptides originating from transmembrane region (peptides 70-74 and 73-80) showed low deuterium exchange even after one hour of deuteration as it was shown for WT apo or E504A due to the protection of the region by detergent. Another peptide, 172-179 from transmembrane helix 4 showed low deuterium exchange as it was found for peptide 70-74 or 73-80.

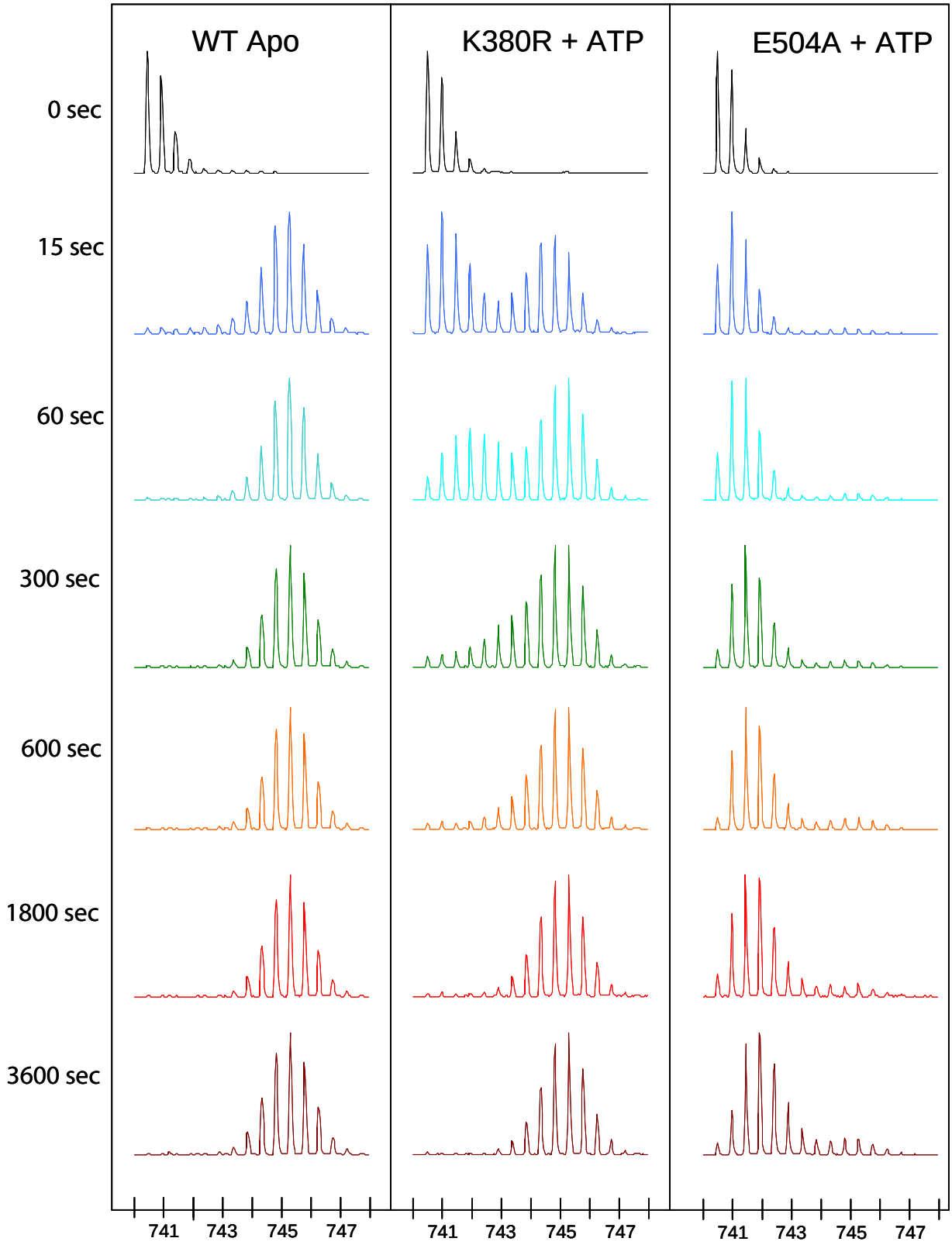

Figure 47. The HDX kinetics of peptide 203-215 of BmrA is shown. Left panel shows the wild-type apo, central panel shows the mutant K380R at incubation in 0.5 mM ATP/Mg^{2+} and right panel shows mutant E504A at 0.5 mM ATP/Mg^{2+}.

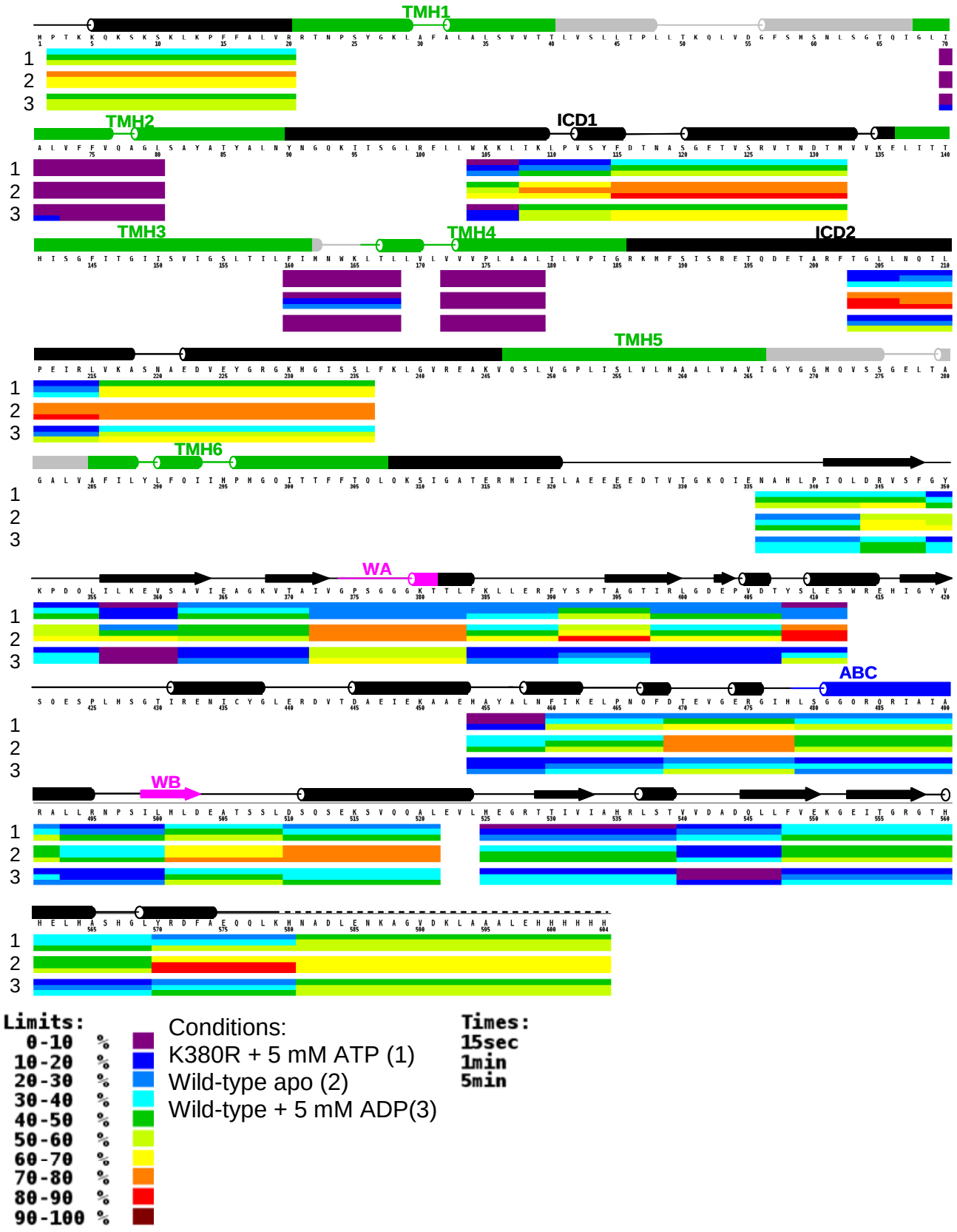

Figure 48. The deuteration kinetics results obtained after incubation of BmrA wild-type apo, K380R mutant + 5 mM ATP/Mg^{2+} and wild-type BmrA + 5 mM ADP/Mg^{2+} in deuterated buffer for 15, 60 and 300s are mapped as heat map on sequence of BmrA. Predicted secondary structure elements are also shown.

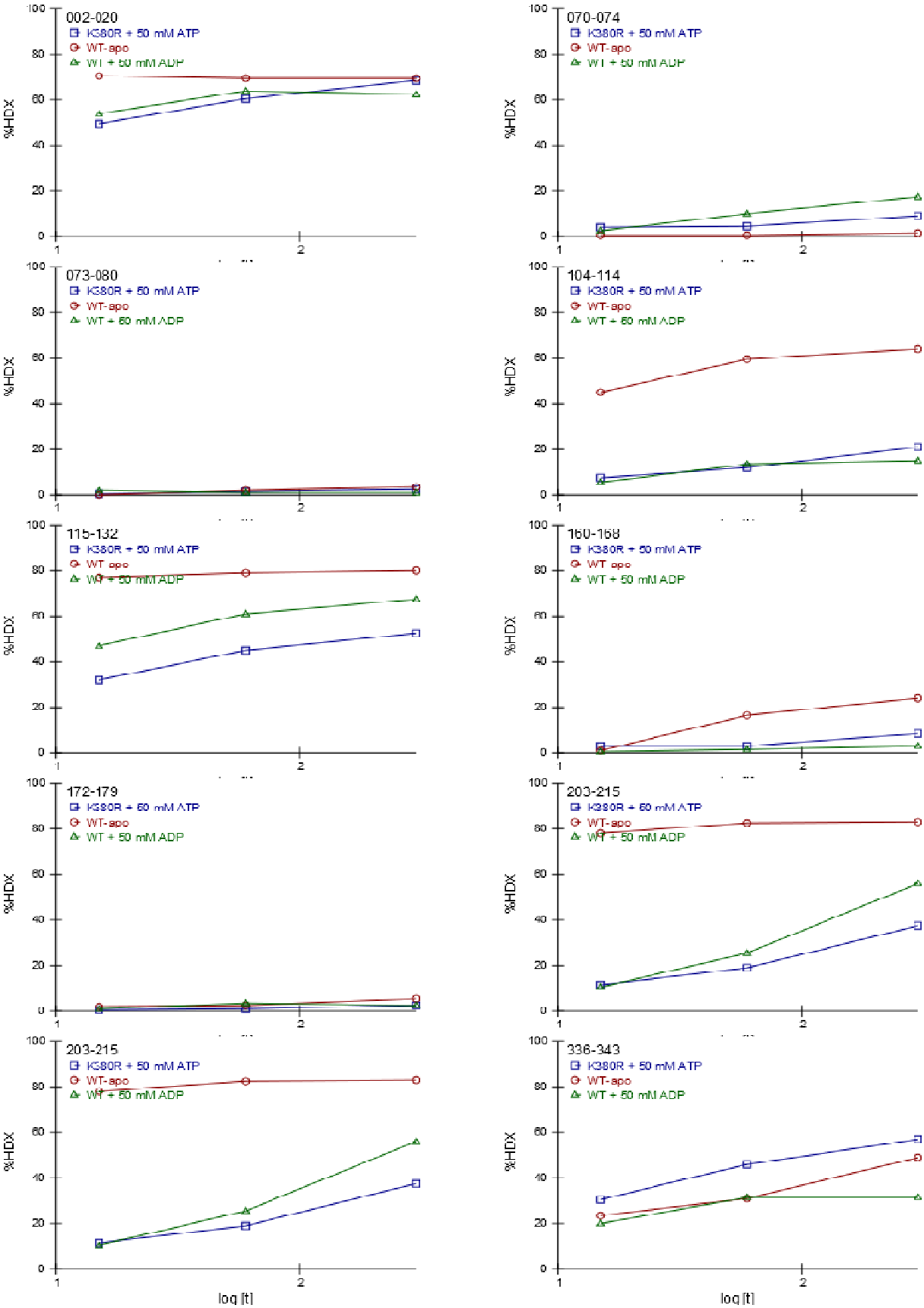

Figure 49. HDX plots of the all identified peptides of BmrA. Hydrogen/deuterium exchange of WT-apo, WT + 5 mM ADPMg^{2+} and mutant K380R + 5 mM ATP/Mg^{2+} kinetics are plotted against time (Part I). Two series of experiments were performed and average value is plotted here.

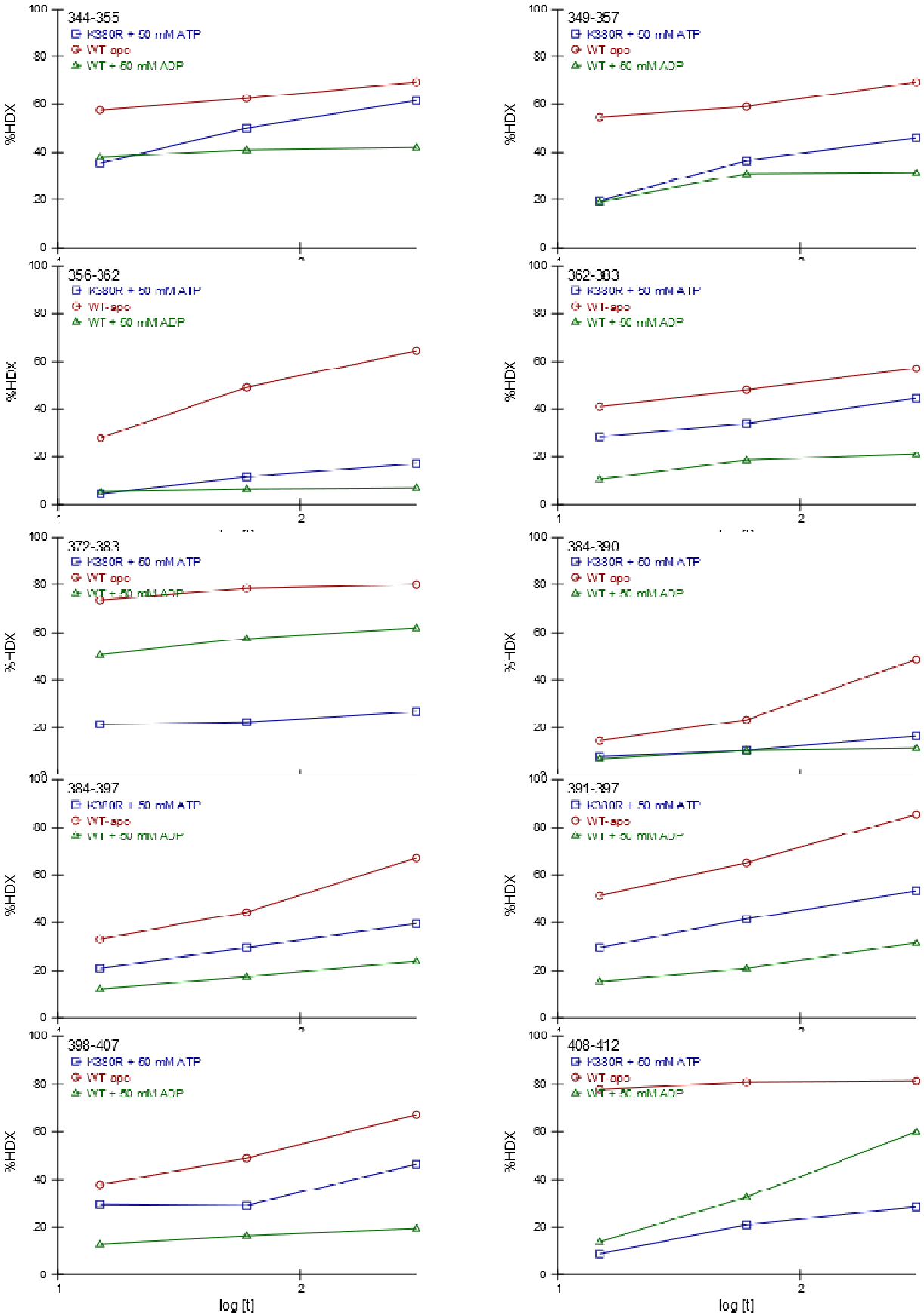

Figure 49. HDX plots of the all identified peptides of BmrA. Hydrogen/deuterium exchange of WT-apo, WT + 5 mM ADPMg^{2+} and mutant K380R + 5 mM ATP/Mg^{2+} kinetics are plotted against time (Part II).

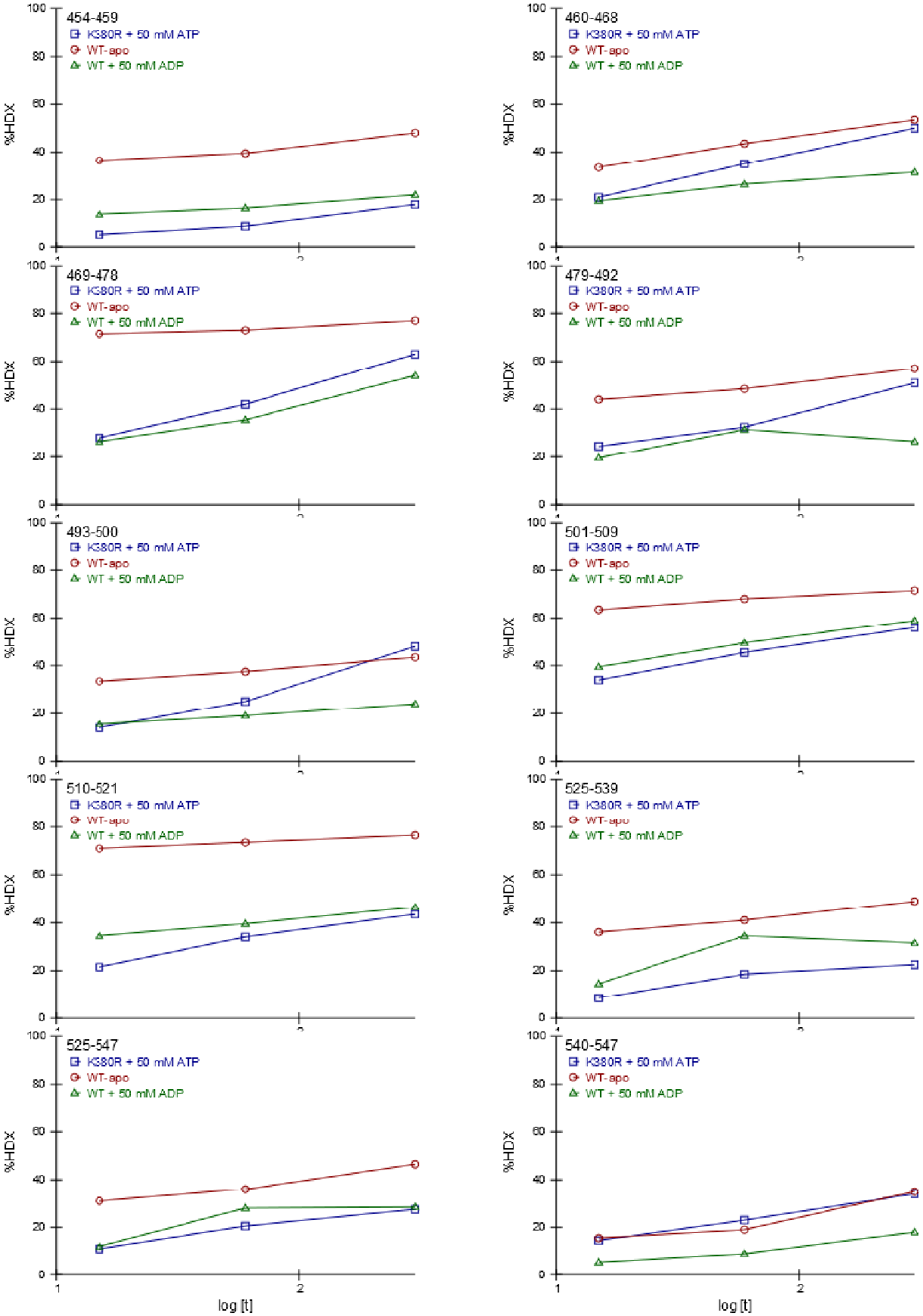

Figure 49. HDX plots of the all identified peptides of BmrA. Hydrogen/deuterium exchange of WT-apo, WT + 5 mM ADPMg^{2+} and mutant K380R + 5 mM ATP/Mg^{2+} kinetics are plotted against time (Part III).

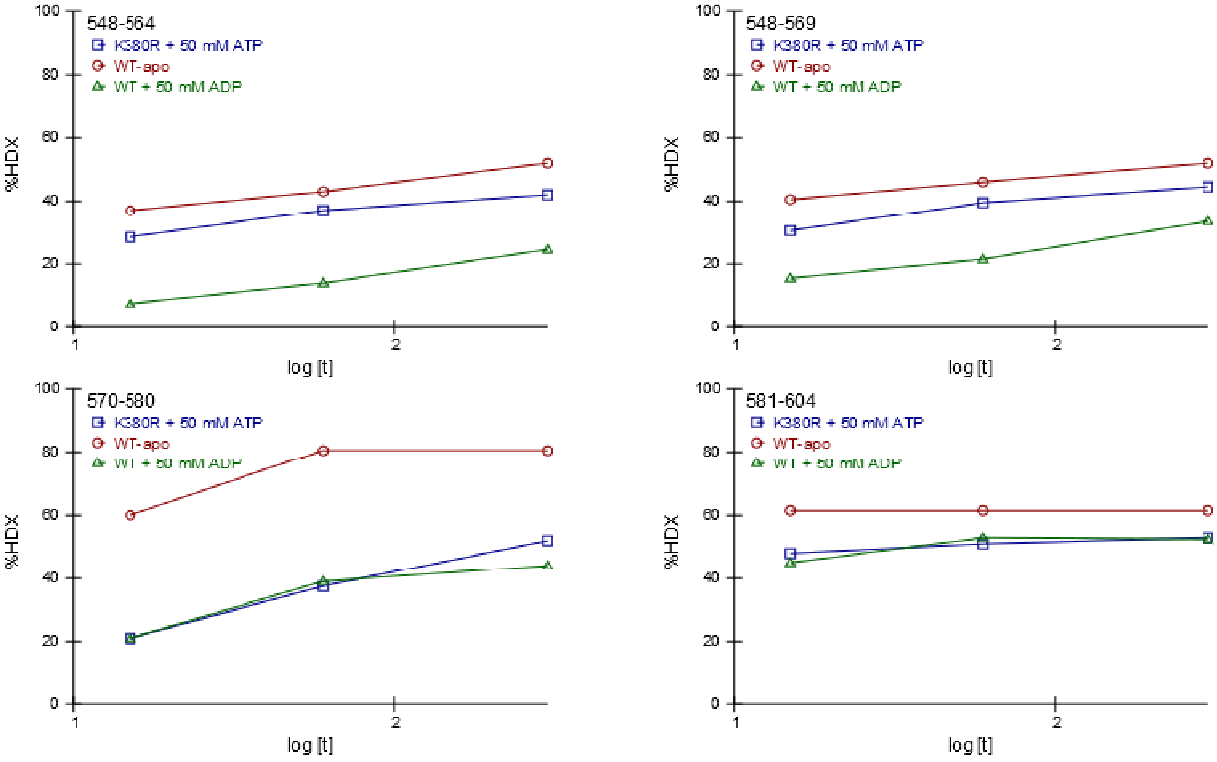

Figure 49. HDX plots of the all identified peptides of BmrA. Hydrogen/deuterium exchange of WT-apo, WT + 5 mM ADPMg^{2+} and mutant K380R + 5 mM ATP/Mg^{2+} kinetics are plotted against time (Part IV).

2.2.2. Intracellular domains:

To investigate the difference between the dynamics of ICD1 of wild-type/mutant apo and K380R mutant in presence of ATP/Mg^{2+}, peptides 104-114 and peptides 115-132 were analyzed. In peptide 115-132, after 15 s of deuteration, 16% higher exchange was found for wild-type+5 mM ADP/Mg^{2+} as compared to mutant K380R+5 mM ATP/Mg^{2}. The deuteration difference was constant after one min and five min of deuteration. The second peptide of ICD1 i.e. 104-114 showed lower deuteration exchange in both cases. The minimum exchange was found 7 % and 6 % in wild-type+5 mM ADP/Mg^{2+} and K380R+5 mM ADP/Mg^{2+} respectively and after 5 min, the maximum deuteration found was 20 % and 15 %. Although difference of deuteration level of both peptides of ICD1 in two conditions (wild-type + ADP 5 mM and K380R + 5mM ADP) was not large, in comparison with wild-type apo, both forms were significantly less deuterated, showing that dynamics of ICD1 was decreased (Figure 50). The significant and unusual *trans*- interaction of ICD2 was described in detail earlier. The domain was well covered with peptide 203-215 and peptide 216-236 from N-terminal to C-terminal end respectively. The peptide 203-215 was found one to be of the most intense and very nicely separated peptide eluting at almost the end of the chromatographic run. Peptide

203-215 showed slight difference between two conditions, the overall exchange rate and difference in exchange rate was low at the beginning i.e. 10% in WT+5 mM ADP/Mg^{2+} and 11% in K380R+5 mM ATP/Mg^{2+} so the difference was not significant at 15 s. However, with the increasing time, the difference of exchange was also found to be increased reaching 7% and 18% after 1 min and 5 min, respectively. But in wild-type apo form, the level of deuteration was very high more than 70% even after 15 s. This indicated that for the above mentioned peptides the movement of ICD2 was restricted in presence of nucleotide both for mutant and wild-type. Whereas peptide 203-215 showed some significant difference of the deuteration levels in both conditions for two deuteration times, the other peptide, 216-236, showed large difference for first deuteration point only. But in comparison to wild-type, kinetics of peptide 216-236, the deuteration level was much lower for all three time points in two conditions.

2.2.3. Nucleotide-binding domain:

Three significant regions of nucleotide-binding domains which are directly involved in ATP binding and hydrolysis were analyzed by HDX: Walker 'A', Walker 'B' and signature motif.

Walker 'A':

Walker 'A' consists of conserved GPSGGGKTT sequence and peptide 372-383 comprises on IVGPSGGGKTTL sequence in BmrA. Therefore, it precisely shows changes taking place on Walker 'A' motif. The HDX occurs at moderate pace and with increase of time, the deuterium exchange content and the difference between wild-type + 5 mM ADP/Mg^{2+} and K380R + 5 mM ATP/Mg^{2+} was also increased slightly.

The difference of deuterium exchange was very high between wild-type apo and mutant K380R in presence of 5 mM ATP/Mg^{2+}.

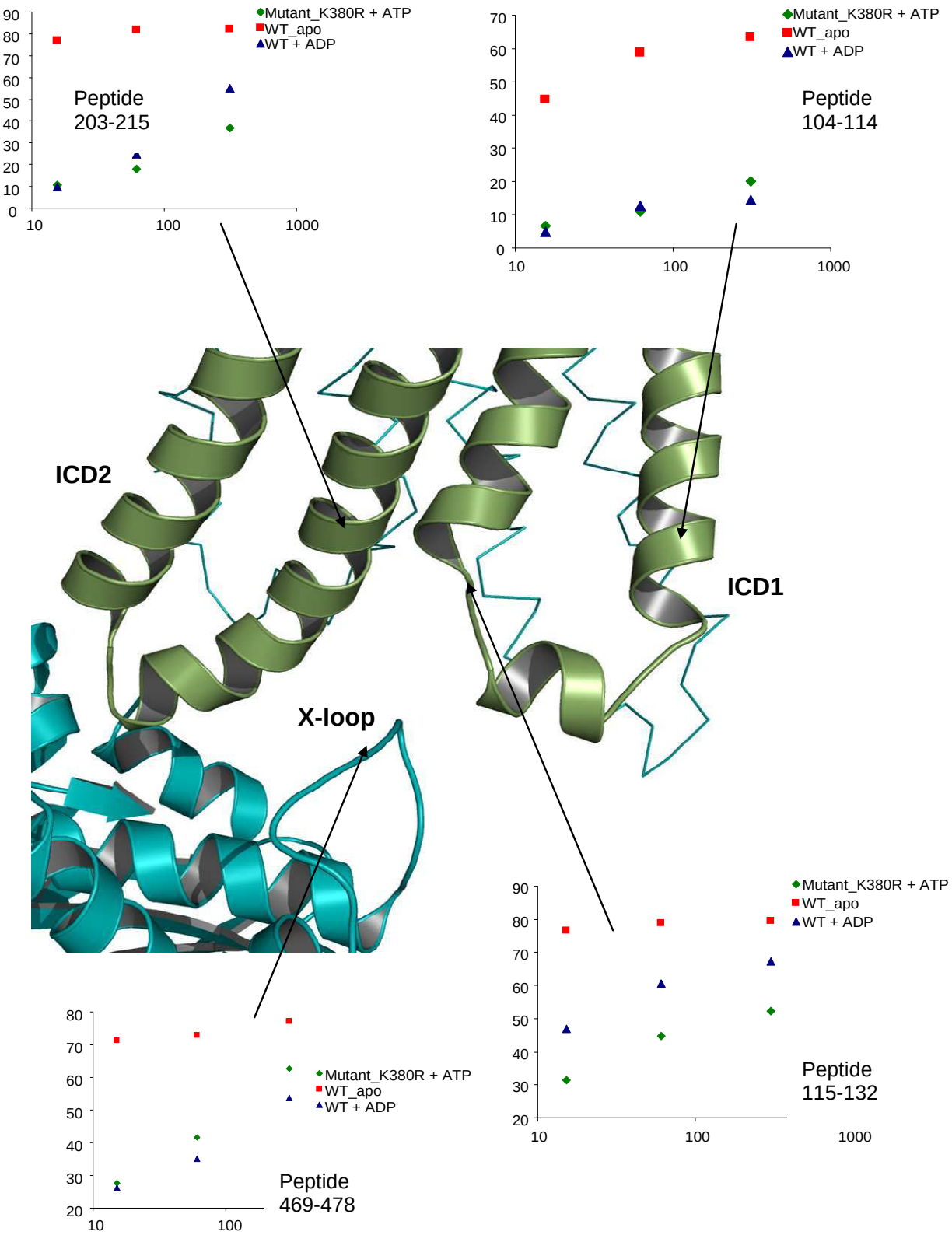

Figure 50. HDX kinetics of ICD1, ICD2 and x-loop are shown on BmrA 3D model based on Sav1866. The interaction of ICD1 and ICD2 of *cis*- subunit with NBD of *trans*- subunit is focused. Part of the ICDs of *cis*- subunit are shown in green color and ribbon view, part of ICDs of *trans*- subunit are show as wire in cyan color. Part of NBD of *trans*- subunit is shown as ribbon in carton. The NBD of *cis*- subunit is not shown.

X-loop:

The interaction site of ICD1 and ICD2, on nucleotide-binding domain was identified for the first time in Sav1866 and named as X-loop (Dawson and Locher 2006). It is a short stretch of few amino acids (TEVG**E**RG in Sav1866) with conserved glutamate (underlined). This conserved glutamate is found in nucleotide-binding domains of ABC exporters only. Peptide 469-478 in BmrA spans the region of X-loop. In apo form of wild-type BmrA, the deuteration level was found 71 % and 77 % at 15 s and 300 s, respectively. The deuterium content of the mutant K380R + 5 mM ATP/$Mg^{2+}$and wild-type + 5 mM ADP/Mg^{2+} was less compared to wild-type form. This peptide is one of the fewer examples where the deuteration level of mutant K380R + 5 mM ATP/Mg^{2+} was found higher compared with WT+5 mM ADP/Mg^{2} (Figure 50).

Signature motif:

Highly conserved within nucleotide-binding domain of ABC transporters, signature motif is identified by the presence of LSGGQ residues. Peptide 479-492 covers the entire motif. In wild-type apo, the deuterium exchange of peptide was found moderate in comparison with other peptides. In the K380R mutant and wild-type in the presence of ATP/Mg^{2+} and ADP/Mg^{2+} respectively, showed less exchange compared with wild-type apo form. No difference was observed between mutant K380R+ATP/Mg^{2+} and wild-type/ADP+Mg^{2+} at 15 s and 60 s. At 300 s, the mutant was found more deuterated.

Walker 'B' motif:

Peptide 501-509 covers part of Walker 'B' motif and catalytic glutamate. Again the difference between mutant K380R+ATP/Mg^{2+} and wild-type/ADP+Mg^{2+} was not high but when compared with wild-type apo form, both were significantly less deuterated at 15 s, 60 s and 300 s. But this difference is smaller than the one found for Walker 'A' motif.

2.3. Conclusion:

Our results on BmrA mutant K380R showed that the overall dynamics of this transporter was restricted in presence of moderate concentration of nucleotide. It has been previously shown that this mutant is unable to adopt a closed conformation in presence of nucleotide. Therefore, the hydrogen–deuterium exchange kinetics coupled with mass spectrometry of this BmrA mutant in presence of ATP/Mg^{2+}, shows the dynamics of BmrA in open conformation but not freely moving state. The high deuteration of ICD1 and ICD2 in BmrA apo form was also possibly due to disengagement from the nucleotide-binding as we found in closed form of BmrA both ICDs and x-loop were less deuterated . A similar kind of behavior of ICDs and x-loop in mutant K380R +ATP/Mg^{2+} indicated that due to the presence of nucleotide, the mentioned regions are much more folded than in the apo/open conformation.

Lower deuteration on Walker 'A' motif of mutant showed that mutant is still able to bind to ATP. Higher deuteration level on Walker 'A' motif of wild-type in the presence of ADP might be due to a lower affinity comparatively to that of the wild-type for ADP.

There are two possible reasons of lower deuteration level on signature motif: first the ATP binding to Walker 'A' motif introduced local conformational rearrangement of signature motif. Secondly, in the closed form of ABC transporters, signature motif provides the complement site during ATP hydrolysis which indicates that it has some affinity for ATP and therefore it was less deuterated in open form in presence of ATP.

The mechanisms proposed for ATP hydrolysis by ABC exporters describe that binding of ATP to Walker 'A' motif of NBD acts as a platform and then Walker 'B' and catalytic glutamate mainly contributes to ATP hydrolysis. Our results on open state of BmrA mutant in presence of ATP showed less deuterium exchange on Walker 'B' motif compared to apo state. The difference of deuterium exchange in two conditions for Walker 'B' motif was lower than the difference found for Walker 'A' motif in same conditions. This is in accordance with the proposed mechanism of ATP hydrolysis and that Walker 'A' has higher affinity for ATP compared to Walker 'B' motif.

Chapter 3. H/D exchange kinetics of ABC hetero-dimer BmrC/BmrD

The results obtained on the dynamics of BmrA led us to continue following the HDX kinetics of another ABC transporter identified by our group. The hetero-dimeric ABC exporter BmrC/BmrD shares many features with BmrA. The same detergent DDM is required to solubilize hetero-dimer and the concentration of detergent also remains similar i.e. 0.05 %. In contrast being a hetero-dimer it contains two different subunits BmrC and BmrD with molecular weight of 67 kDa and 77 kDa, respectively.

3.1. Peptide mapping:

To optimize the peptide mapping of the BmrC/BmrD, four strategies were applied to digest the hetero-dimer: immobilized pepsin, immobilized pepsin in the presence of 1.5 M guanidinium hydrochloride, immobilized rhizopuspepsin and pepsin in solution. In all cases typical HDX digestion conditions were followed. The MS/MS analyses of the peptides, obtained with any digestion enzymes, were performed on FT-ICR mass spectrometer coupled with LC. The high mass accuracy, due to high resolution of FT-MS, made possible quick identification and assignment of the eluted peptides. Peptide mapping MS/MS experiments on FT-MS were performed by Petr Man in Prague.

The immobilized pepsin digestion in the presence of 1.5 M guanidinium hydrochloride was found to be the best condition both for BmrC and BmrD. In the case of BmrC 68 peptides were identified providing coverage of 73 % sequence. Among these 68 peptides, 22 peptides (50 % sequence coverage) were from the transmembrane domain; in contrast the coverage for NBD region was 98 % with 46 peptides. Consistent with digestion condition for BmrC, the best digestion condition was found when BmrD was digested with immobilized pepsin in presence of 1.5 M guanidinium hydrochloride. 68 peptides were identified from BmrD covering 66% of the protein sequence: 58 % of the transmembrane region and 91 % of the nucleotide-binding domain. The number of peptides identified from transmembrane domain and nucleotide-binding domain were 25 and 43, respectively. It is noteworthy that for both BmrC and BmrD subunits, the coverage was found better in the nucleotide-binding region and poor in the transmembrane domain owing presumably to protection by detergent. The peptide mapping obtained for both subunits with the FT-ICR mass spectrometer was required to be checked on in-house available Time-of-Flight (ToF) mass spectrometer. As the digestion with immobilized pepsin in the presence of guanidinium hydrochloride was found to be the best condition, therefore only this condition was used for ToF and for subsequent HDX experiments. Few peptides were unrecognized with the ToF mass spectrometer compared with FT-MS and signal intensity for some other peptides was not strong enough to be used for

HDX experiments. Thus, 50 peptides (67 % sequence coverage) from BmrC and 53 peptides (63 % sequence coverage) from BmrD were indentified on ToF (Figures 51 & 52). Tables 7 & 8 show the summary of number of peptides and sequence coverage identified with both FT-MS and ToF-MS.

Table 7. Sequence coverage in percent, number of peptides and average size of peptide obtained from BmrC in different conditions on FT-ICR. Last three lines show the peptides recognized on ToF.

		BmrC	**TMD**	**NBD**
Pepsin Column+(GndCl)	**% Coverage**	73	55	97
	Peptides	68	23	45
	Average	6.5	8.1	5.2
Pepsin Column	**% Coverage**	66	42	97
	Peptides	64	14	50
	Average	6.2	10.8	5
Rhizopuspepesin Column	**% Coverage**	57	19	85
	Peptides	53	11	42
	Average	6.5	6.2	5
Pepsin in solution	**% Coverage**	57	33	85
	Peptides	62	18	44
	Average	5.5	6.5	4.8
ToF MS (pepsin column + GndCl)	**% Coverage**	67	50	88
	Peptides	50	20	30
	Average	8.1	9	7.2

Table 8. Sequence coverage in percent, number of peptides and average size of peptide obtained from BmrD in different conditions on FT-ICR. Last three lines show the peptides recognized on ToF.

		BmrD	TMD	NBD
Pepsin Column+(GndCl)	**% Coverage**	65	58	91
	Peptides	71	25	46
	Average	6.3	10	5.1
Pepsin Column	**% Coverage**	64	47	81
	Peptides	66	20	46
	Average	6.7	10.1	4.5
Rhizopuspepesin Column	**% Coverage**	58	41	89
	Peptides	63	20	43
	Average	6.3	8.8	5.3
Pepsin in solution	**% Coverage**	58	42	88
	Peptides	61	14	47
	Average	6.5	9.6	4.8
ToF MS (pepsin column + GndCl)	**% Coverage**	63	49	88
	Peptides	53	21	32
	Average	8.1	10	7

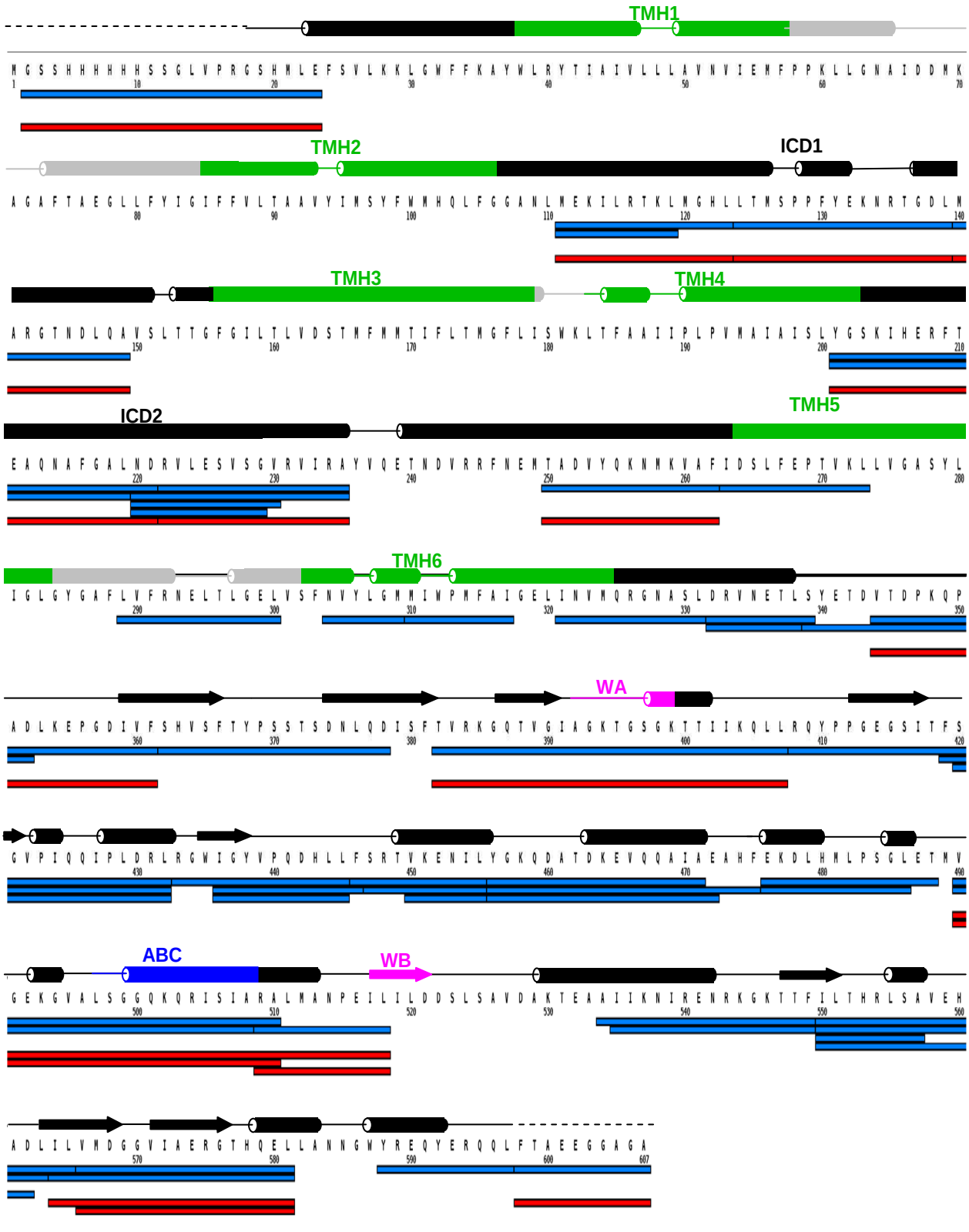

Figure 51. Peptide mapping of BmrC. Peptides recognized after on-column digestion by pepsin on ToF (after MS/MS assignment) and peptides used for HDX-MS studies are shown in blue and red color, respectively. Predicted secondary structural elements and conserved motifs are also indicated on sequence.

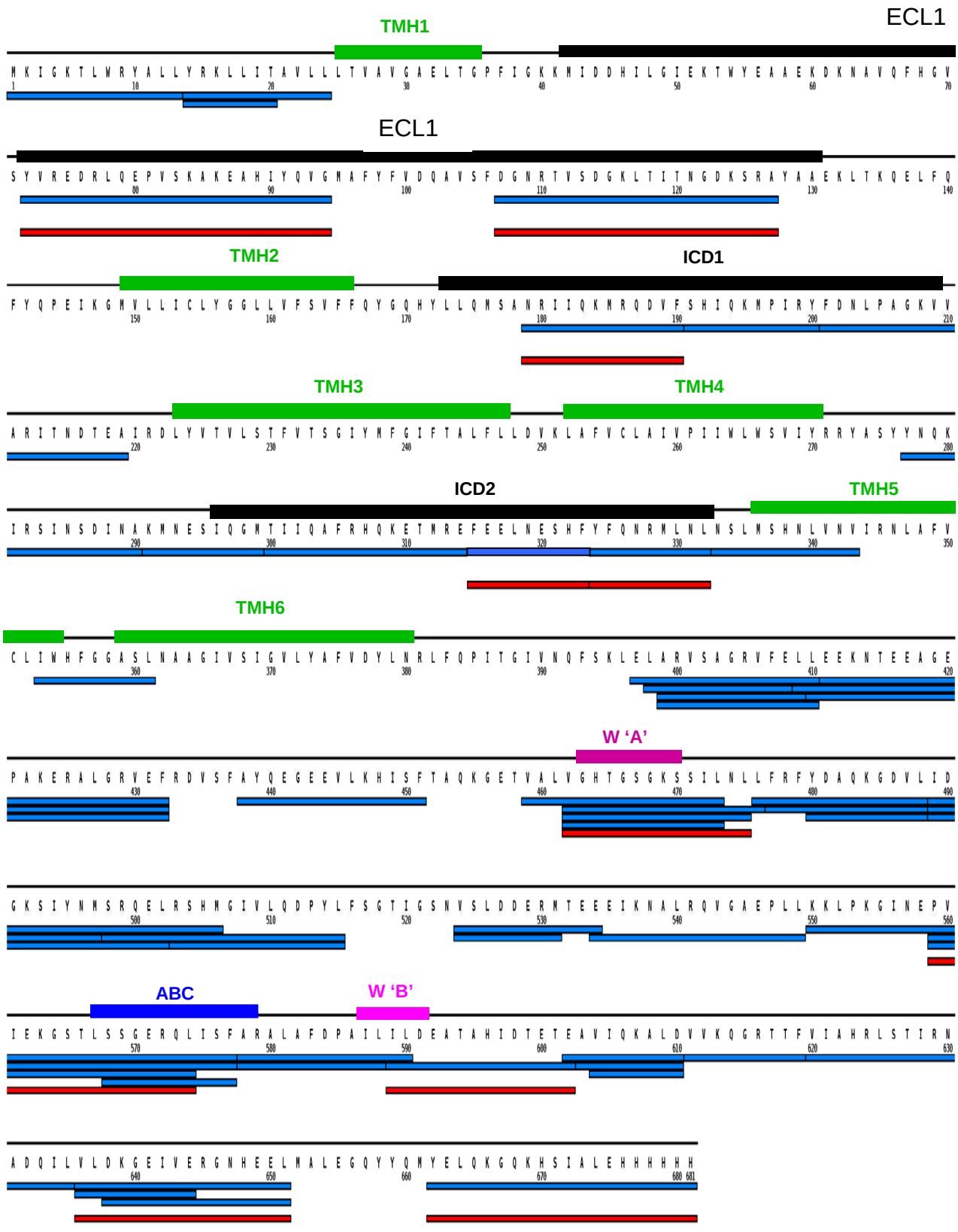

Figure 52. Peptide mapping of BmrD subunit. Peptides recognized on ToF (after MS/MS assignment) are shown in red color and peptides used for HDX-MS are shown in blue color. The predicted region of transmembrane helices and conserved motifs are also indicated according to Gallian et al (Galian, Manon et al. 2011).

3.2. H/D exchange kinetics of BmrC/BmrD apo form:

Here it is noteworthy that BmrC/BmrD is a high molecular weight complex made up of two proteins of 66 kDa and 77 kDa. It was expected that the presence of a large number of peptides would hinder the analysis of kinetics data due to some overlapping.

We, therefore, limited the analysis for the peptides to interesting regions only rather than screening all the peptides irrespective of their origin (Figures 51 & 52).

3.2.1. The intracellular domains of wild-type BmrC/BmrD are highly dynamic:

To determine the kinetics of BmrC/BmrD, the transporter complex was deuterated for five time intervals ranging from 15 s to 3600 s. The intracellular domain (ICD1) of BmrC which is predicted to connect the transmembrane helix 2 with transmembrane helix 3 was well covered with three peptides: 111-123, 124-139 and 140-149 (Figure 51). In beginning, all three peptides show similar deuterium exchange level i.e. ~70 % deuteration at 15 s. Peptides 124-139 and 140-149 did not show any significant change after longer time of deuteration incubation, in contrast peptide 111-123 showed a progressive increase in deuteration level reaching more than 90 % after 3600 s (Figure 53). Peptides 201-221, 222-235 and 250-262 are predicted to belong to the intracellular domain two (ICD2) of BmrC subunit. Both peptides 222-235 and 250-262 showed EX1 HDX kinetics (Part: Introduction, Chapter 5. H/D Exchange) explained later in detail. EX1 also indicates high dynamic nature of a protein region. Comparatively, lower deuteration exchange was observed for peptide 201-221 at the beginning and a slight increase in deuterium exchange was found with increase in deuteration time (Figure 53).

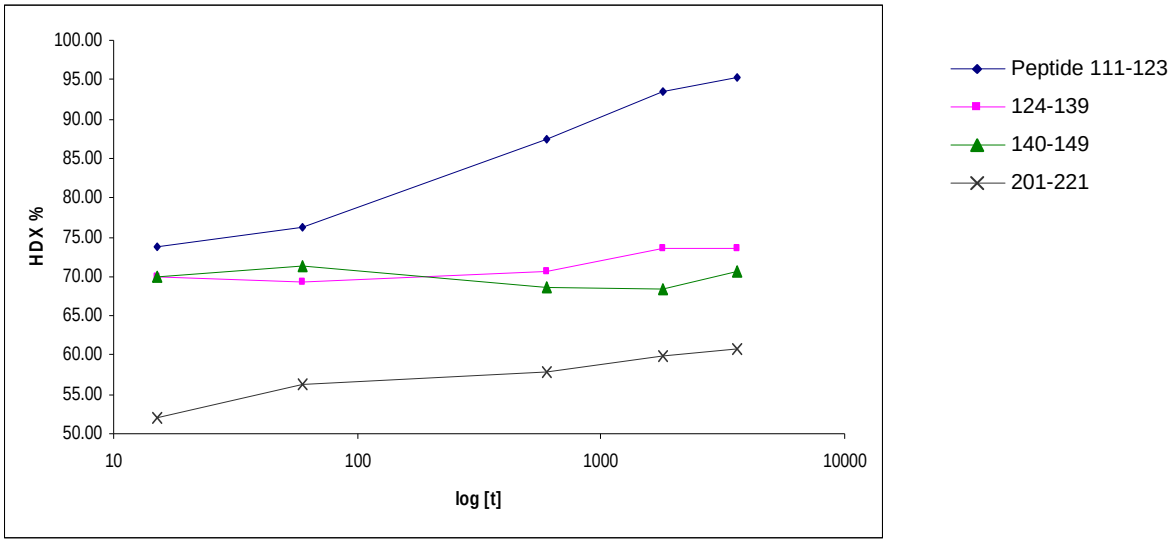

Figure 53. H/D exchange kinetics of peptides from ICD1 and ICD2 of BmrC.

According to predicted topology of BmrD, ICD1 would be between amino acids 170 and 220. Two peptides were identified from the mentioned region but due to low signal-to-noise ratio, it was difficult to follow the deuterium exchange kinetics except for peptide 179-190. This peptide showed very high deuterium level right from the beginning of deuteration and, exceeding 90 % after 3600 s. Part of predicted ICD2 of BmrD was covered by two short peptides, 315-323 and 324-332. In C-terminal part of ICD2, very high deuteration level was observed ranging between 70 – 80 %. The N-terminal part of ICD2, peptide 315-323 retained deuterium exchanged level from 15 to 3600 s but it was lesser than compared to peptide 324-332.

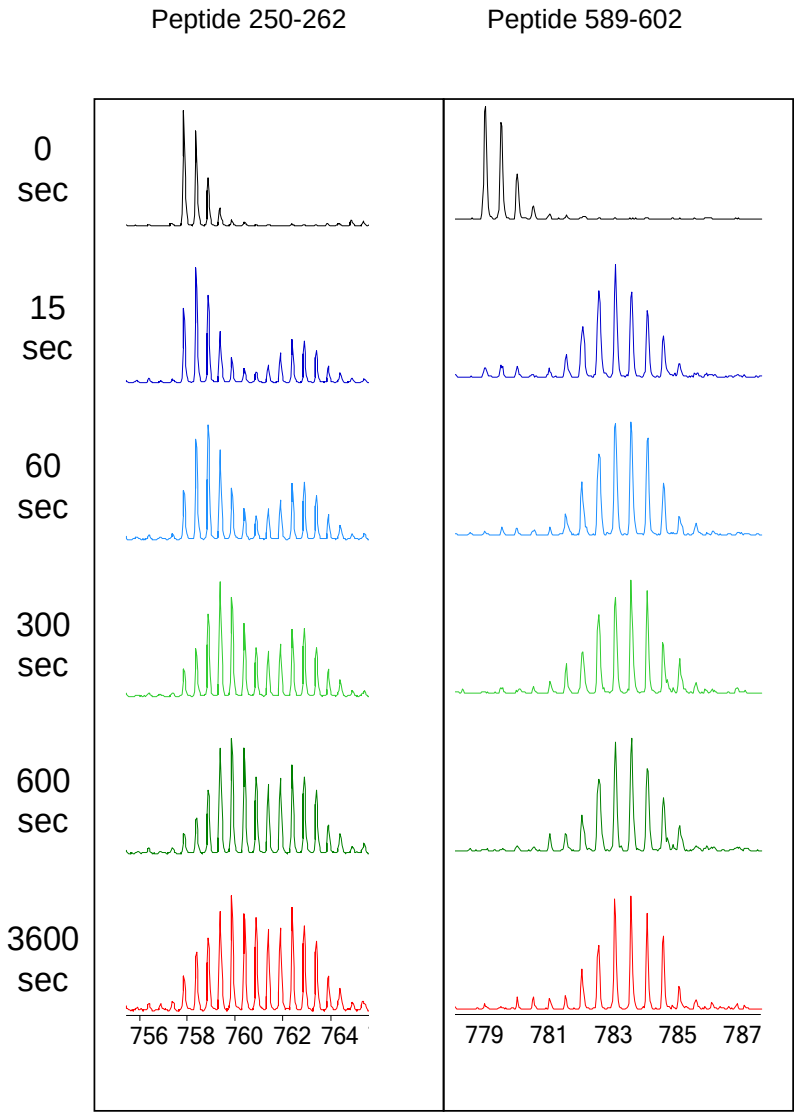

Figure 54. EX1 and EX2 kinetics examples are shown for the peptide 250-262 and peptide 589-602, respectively.

3.2.2. ICD2 of BmrC showed EX1 kinetics:

The use of EX1 kinetics can be helpful to determine the folding/unfolding events of the interested protein in physiological conditions (Weis, Wales et al. 2006). Two peptides of BmrC were identified showing EX1 kinetics, both from ICD2, one example peptide 250-262, is shown in Figure 54. The EX1 kinetics for mentioned region of BmrC indicated that there is local unfolding takes place in apo state of transporter. For the same region in BmrA (apo form), very high deuterium level was observed. Most of the amide hydrogens of ICD2 of BmrA were exchange for deuterium in short time showing possible unstructured form of mention domain. In the case of ICD2 of BmrC, the local unfolding indicates that ICDs of ABC exporters in solution might exist in irregular secondary structure fashion.

3.3. H/D exchange kinetics difference between apo and closed form of BmrC/BmrD:

From HDX kinetics studies of BmrA apo/closed form, we learnt that a significant difference of kinetics is present for NBDs interacting regions i.e. Walker 'A', signature motif, etc. and for ICDs which was not anticipated from the high resolution structures of ABC exporters. After characterizing the HDX kinetics of BmrC/BmrD complex in its apo form, the next step was to determine the kinetics of BmrC/BmrD in its closed form.

As described for BmrA, the closed form can be obtained by inhibiting with vanadate or mutation of catalytic glutamate residue after the Walker 'B' motif. Within ABC hetero-dimers, the mentioned catalytic residue is found only in BmrD. In the smaller subunit the, BmrC, corresponding residue is an aspartic acid residue.

The inhibition of BmrC/BmrD by vanadate was incomplete as it was found for BmrA. Earlier, in the course of BmrC/BmrD characterization, it was found that mutation of conserved glutamate at position 592 of BmrD subunit into aspartate abolished the ATPase activity of transporter. To verify that conserved E592 is responsible for ATPase activity, the corresponding aspartate of BmrC subunit at position 500 was mutated into glutamate. This new double mutant, E592D in BmrD subunit / D500E in BmrC, did not show any ATPase activity as well confirming that glutamate of BmrD is exclusively responsible for hydrolytic activity of transporter (Carmen Galian's thesis). Mutations of the corresponding residues in hetero-dimer TmrA/TmrB also ended up with similar conclusion (Zutz, Hoffmann et al. 2011).

Table 9. Different mutants used for HDX analyses of BmrC/BmrD are shown. The HDX kinetics results obtained for the wild-type BmrC/BmrD apo form and mutant E592A/D500A + 5 mM ATP/Mg^{2+} are described. To indicate the number of aspartate the sequence of BmrC was considered without the N-ter His-tag.

	Conserved glutamate in BmrD ILILDE	Conserved aspartate in BmrC ILILDD
Single mutation	ILILDD E592D	ILILDD
Double mutation	ILILDD E592D	ILILDE D500E
Double drastic mutation	ILILDA E592A	ILILDA D500A

Therefore, we expected that closed form of BmrC/BmrD could be obtained by addition of ATP/Mg^{2+} in mutants. Preliminary HDX kinetic analyses of BmrC/BmrD single (E592D) or double mutants (E592D/D500E) in the presence of 5 mM ATP/Mg^{2+} (0.5 mM in deuterated buffer) showed two populations for the peptides from important regions like ICD1, ICD2 and NBDs interacting regions, one example is shown in Figure 55. This is important to mention here, that these two populations were due to incomplete inhibition exhibiting EX2 kinetics different from EX1. This led us to the conclusion that two species of mass envelopes were possibly arising from some residual ATPase activity of these mutants as previously used ATPase activity analyses technique was not sensitive enough to measure very low ATPase activity.

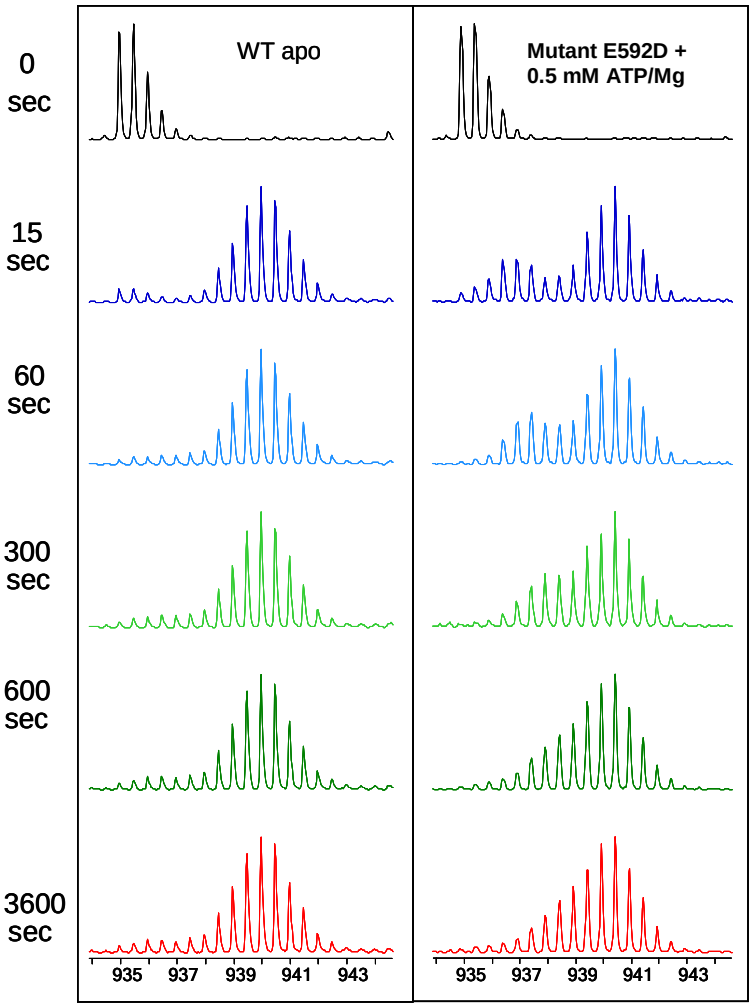

Figure 55. H/D exchange kinetics for peptide 124-139, an example of significant peptides from BmrC subunit. Whereas, the peptide showed fast deuterium exchange in wild-type apo, in mutant (single mutation in BmrD subunit: E592D) addition of ATP/Mg^{2+} resulted in two populations after deuterium showing that inhibition was not complete.

3.3.1. The closed form of BmrC/BmrD is not as tight as that found with BmrA:

Based on the conclusion of single (E592) or double mutant (E592D/D500A) HDX kinetics, the conserved glutamate of BmrD and aspartate of BmrC were mutated into alanine. It was anticipated that mutation of catalytic residue(s) into alanine would totally abolished any residual ATPase activity if any activity was still present in previous mutants. The ATPase activity of this newly made double mutant is undetermined yet.

The double alanine mutant (E592A/D500A) transporter complex was incubated with 5 mM ATP/Mg^{2+} for five minutes and then diluted in D_2O for several time intervals ranging from 15 s to 3600 s and local HDX kinetics were determined. With this mutant again two populations of deuterated masses were found. The very similar kinetics behavior obtained with this mutant confirmed that the closed form of BmrC/BmrD is not as tight as compared to BmrA and two

populations found in earlier mutants were also due to loose closure of the complex in this inhibited state. Determination of ATPase with radiolabeled 8-azido-ATP, where very low level ATPase activity can be monitored, it can confirm that it is still capable to hydrolyze ATP.

Though two isotopic envelopes due to presence of two populations induced more complication for data analysis, it was overcome by determination of average mass based on both envelopes.

3.3.2. Dynamics of closed form/inhibited state of BmrC/BmrD mutant (E592A/D500A):

As for the previous BmrC/BmrD mutants and BmrA mutant E504A mutant, this newly prepared BmrC/BmrD double alanine mutant (E592A/E500D) was incubated with 5 mM ATP/Mg^{2+} and ten fold diluted in deuterated buffer (0.5 mM ATP/Mg^{2+} in deuterated buffer). The overall local kinetics data showed that closed form of BmrC/BmrD is less dynamic compared to its open form. The difference of kinetics exchange between two conformations (apo and closed) in significant regions is smaller compared to the difference that were observed in two forms (apo and closed) of BmrA but this might be due to the presence of two populations. There are some regions e.g. C-terminal part of both subunits which did not show any difference in exchange kinetics. The following described results refer to Figures 56A and B.

3.3.2.1. Intracellular domains:

Both intracellular domains (ICD1 and ICD2) of BmrC showed less exchange in closed form. Among three peptides of ICD1, peptide 111-123 was the least deuterated i.e. ~35 % at 15 s and ~45 % after 3600 s. When compared with apo/open form mentioned peptide showed the highest difference in comparison with two other peptides. Two other peptides 124-139 and 140-149 were almost equally deuterated in apo/open state (about 70 % at any time) in closed form and these peptides maintained their similar deuterium exchange pattern but deuterium content was ~20 % less at any time. Peptide 201-221 of ICD2 of BmrC showed ~25 % deuteration at 15 s, which is 25 % less compared to apo/open state of same peptide, however with the increased time deuteration, difference between the two forms was significantly decreased to only 10 %. Two more peptides from ICD2 of BmrC, 222-235 and 250-262, are not discussed for their closed form because no difference could be observed in two states due to presence of EX1 kinetics of their apo form.

A large decrease in deuterium level was found for peptide 179-190 in closed form in comparison with apo/open. This is the only peptide from BmrD ICD1, therefore the information on this region exclusively rely on it. Two peptides identified from ICD2 also showed less deuterium level. Peptide 315-323 was 30 % deuterated which is half of the deuterium content compared with apo/open state at 15 s. Both level of deuteration of this peptide and its difference with apo/open state was unchanged after 3600 s. The other peptide of ICD, 324-332, showed high difference in deuterium level compared to apo/open state which was reduced with the time increasing. The H/D exchange kinetics data of ICDs from both monomers show that the close or inhibited state of protein had decreased their dynamics compared to apo state and overall behavior of ICDs in apo or closed form in ABC homo-dimer and hetero-dimer is similar.

3.2.2.2. Predicted large extracellular loop of BmrD:

Pairwise sequence alignment and secondary structure prediction tools showed that the additional 94 residues found in BmrD form an extracellular loop (ECL1) connecting TMH1 and TMH2 of transmembrane domain (Galian, Manon et al. 2011) (Figure 52). Although there is no 3D structure of ABC hetero-dimer exporter available, Cysteine cross-linking and homology model of TAP1/TAP2 based on Sav1866 also indicated the presence of additional residues between TMH1 and TMH2 of both TAP1 and TAP2(Oancea, O'Mara et al. 2009). The role of this loop is not identified in functioning of ABC transporters yet. In BmrD, the loop was partially covered by two peptides: 72-94 and 107-127. In case of peptide 107-127 high deuterium level was found form the beginning of deuteration and a progressive increase was observed for longer time of deuteration reaching 80 % (Figure 56 B). The other peptide identified from ECL1 was 72-94. This peptide also showed high deuterium level at 15 s reaching ~70 % after 3600 s of deuteration. The kinetics of both peptides did not vary in apo/open or close state of transporter.

3.2.2.3. Nucleotide-binding domain:

The different regions of nucleotide-binding domain of BmrC and BmrD double alanine mutant were investigated by H/D exchange in the presence of ATP/Mg^{2+} and the deuterium level of mentioned regions was compared with the H/D exchange kinetics of apo conformation of the wild-type. Though two populations (EX2 kinetics) were observed due to incomplete inhibition as discussed earlier, the average of two envelopes was calculated which showed less deuterium level for both subunits BmrC and BmrD.

Peptide 382-407 which covers the Walker ‘A’ motif of BmrC, in apo conformation showed moderate deuterium exchange which was reduced in closed form. The deuterium level was ~15 % and ~35 % at 15 and 3600 s, respectively showing the decrease of ~35 % and ~25 % less deuteration compared to apo conformation. The conserved ABC motif ‘LSGGQ’ begins at residue 497 in BmrC. A long peptide 490-518 covers the mentioned conserved region, but due to presence of an overlapping peptide 509-518, the deuterium exchange kinetics of 490-508 could be calculated. The region showed fast deuterium exchange ~80 % at 15 s in apo conformation and remained constant with increasing time. In closed state the deuterium level was found around ~50 % which was ~30 % less compared to apo conformation. Like apo conformation, the level of deuterium remained constant after one hour of deuteration, thus the difference was also ~30 % after the mentioned time of deuteration.

Walker ‘A’ motif of BmrD was covered by peptide 462-475. In apo conformation the deuterium exchange was found to be ~45 % at 15 s and slow progress was observed reaching 55 % after 3600 s. In closed form the deuterium exchange was reduced to~25 % at 15 s and ~35 % after 3600 s, thus throughout the course of exchange the difference in two conditions was constant and as 20 %. Peptide 559-577 covered the conserved ABC signature motif of BmrD subunit, the peptide showed ~50 % deuterium exchange at 15 s and with increasing time the deuterium level was also found to be increasing reaching ~75 % after 3600 s of deuteration. The difference in deuterium level of closed and apo stat for same peptide was less in beginning of deuteration but gradual increase in difference was observed at higher deuteration times. Peptide 589-602 covering C-terminal part of Walker ‘B’ motif including catalytic glutamate showed ~60 % deuterium exchange at 15 s. The level of deuterium uptake was not changed throughout the deuteration experiment. In closed state, the same peptide showed less deuterium level which could be quantified as ~24 % and ~15 % after 15 s and 3600 s of deuteration.

Both NBDs of ABC transporters take part in ATP hydrolysis. In hetero-dimers, the catalytic activity is retained within one subunit but complementary interactions with other subunit provide efficient hydrolysis activity. Low H/D exchange kinetics of most of the regions of both NBDs in closed confirm the active involvement of both subunits in hetero-dimer, BmrC/BmrD.

Some C-terminal peptides of NBDs of BmrC and BmrD did not show any difference in deuterium exchange in two states. The level of difference was not changed in the mentioned regions validating their no contribution in ATP hydrolysis.

3.4. Conclusion:

Our results on ABC hetero-dimer BmrC/BmrD show that intracellular domains of both domains are highly dynamic in the resting. The dynamics of mentioned domain reduces on the closure/interaction of the nucleotide-binding domains. The predicted extracellular loop of BmrD is also dynamic in the resting state and closure of nucleotide-binding domains did not have effect on its movement. The interaction between two subunits in inhibited state is not strong might be due to asymmetry founding hetero-dimer in comparison with homo-dimeric ABC exporters. Though in wild-type BmrC/BmrD, the BmrD acts as catalytic subunit, the hydrolysis of ATP is contributed by both subunits by interacting together because lowered deuterium exchange was observed for ATP binding regions of both subunits. The dynamics of C-terminal end of both NBDs remained unchanged in apo/open or closed states.

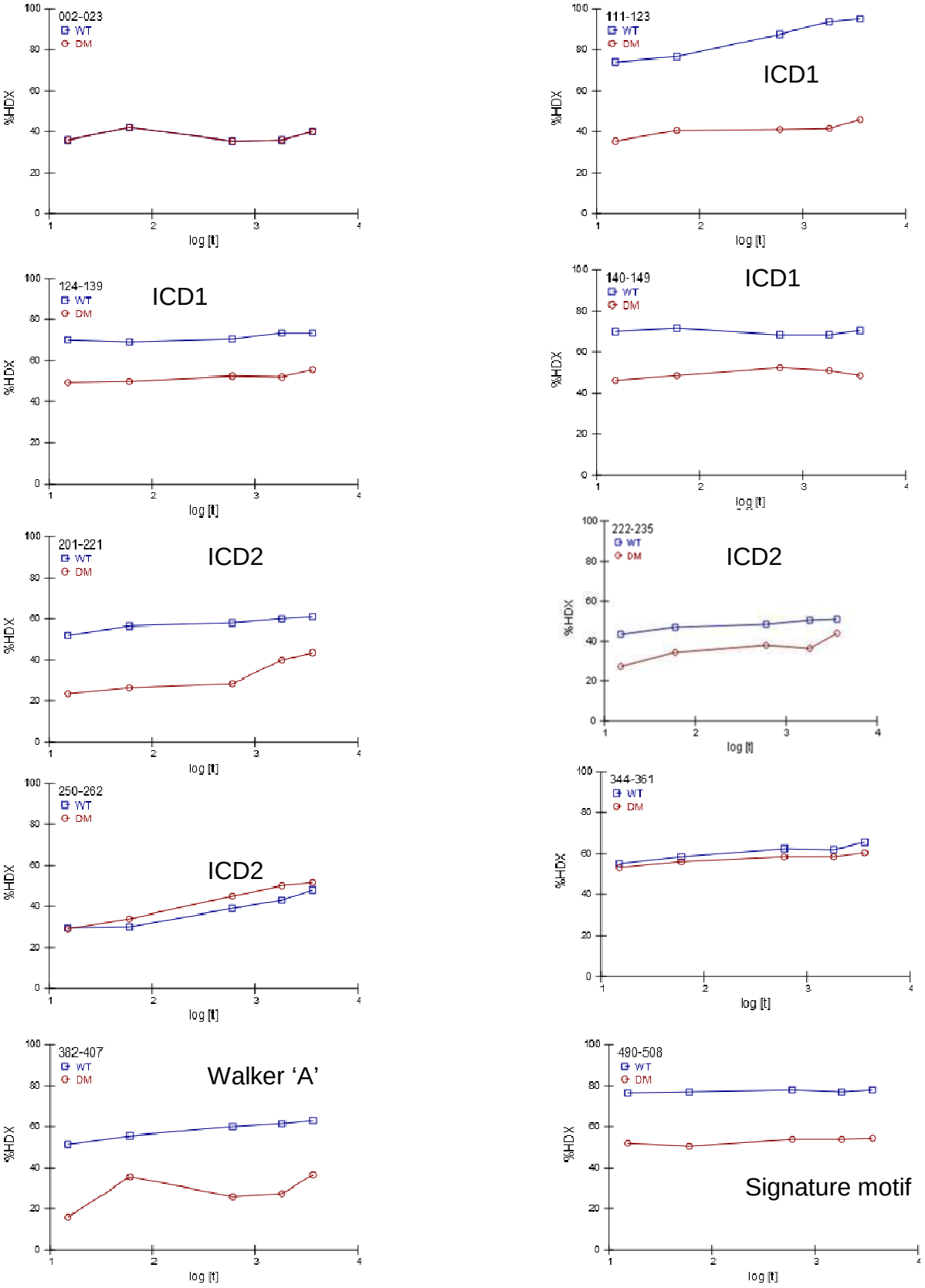

Figure 56-A. Kinetics plots of selected peptides of BmrC wild-type apo (WT) are presented in blue and double mutant (E592A and D500A)(DM) in red color. The double mutant was deuterated in presence of 0.5 mM ATP/Mg^{2+}. For peptide 222-235 and 250-262 the average of two envelopes are shown in apo form (Part I).

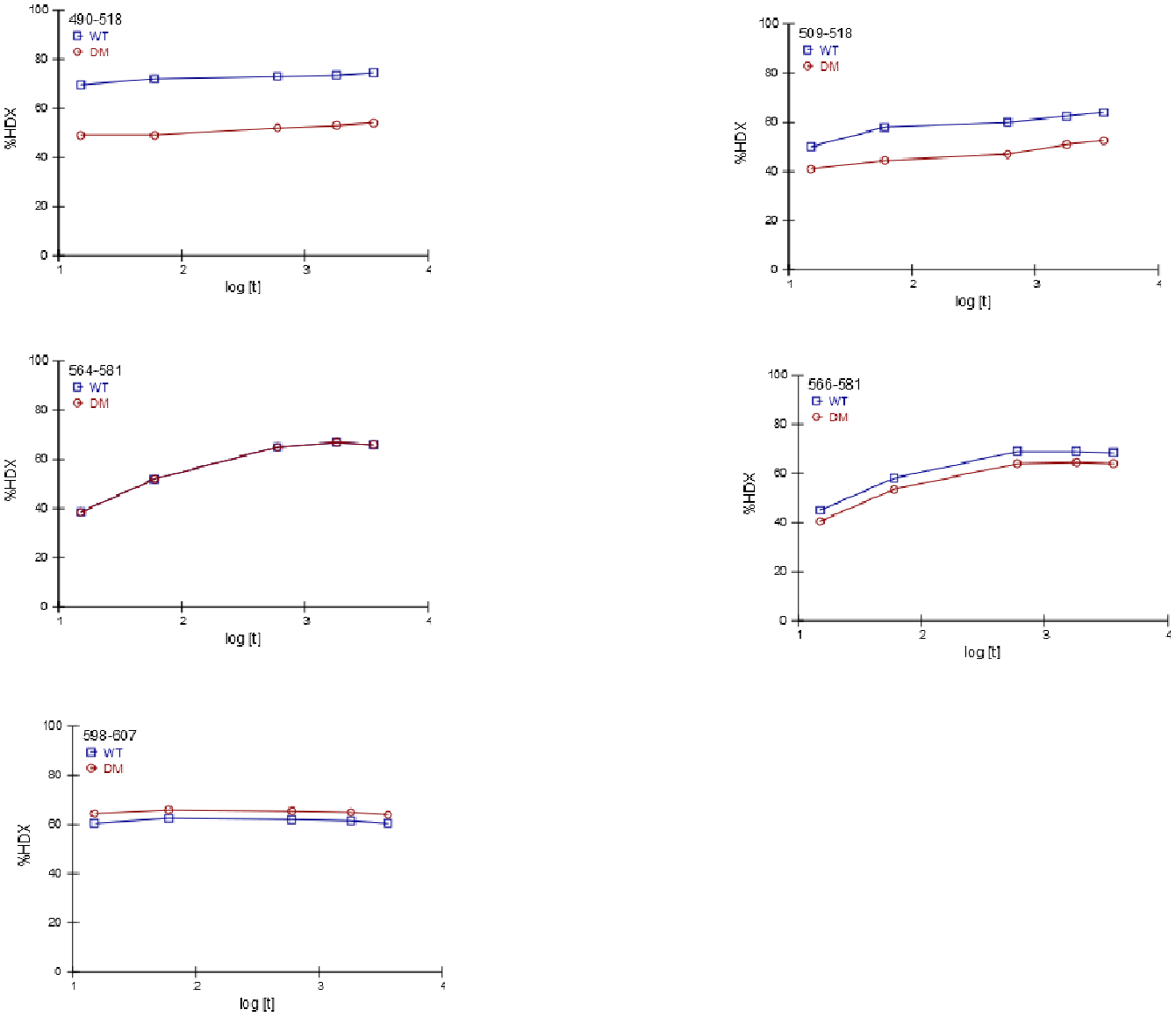

Figure 56-A. Kinetics plots of selected peptides of BmrC wild-type apo (WT) in are presented in blue and double mutant (E592A and D500A)(DM) in red color. The double mutant was deuterated in presence of 0.5 mM ATP/Mg^{2+} (Part II).

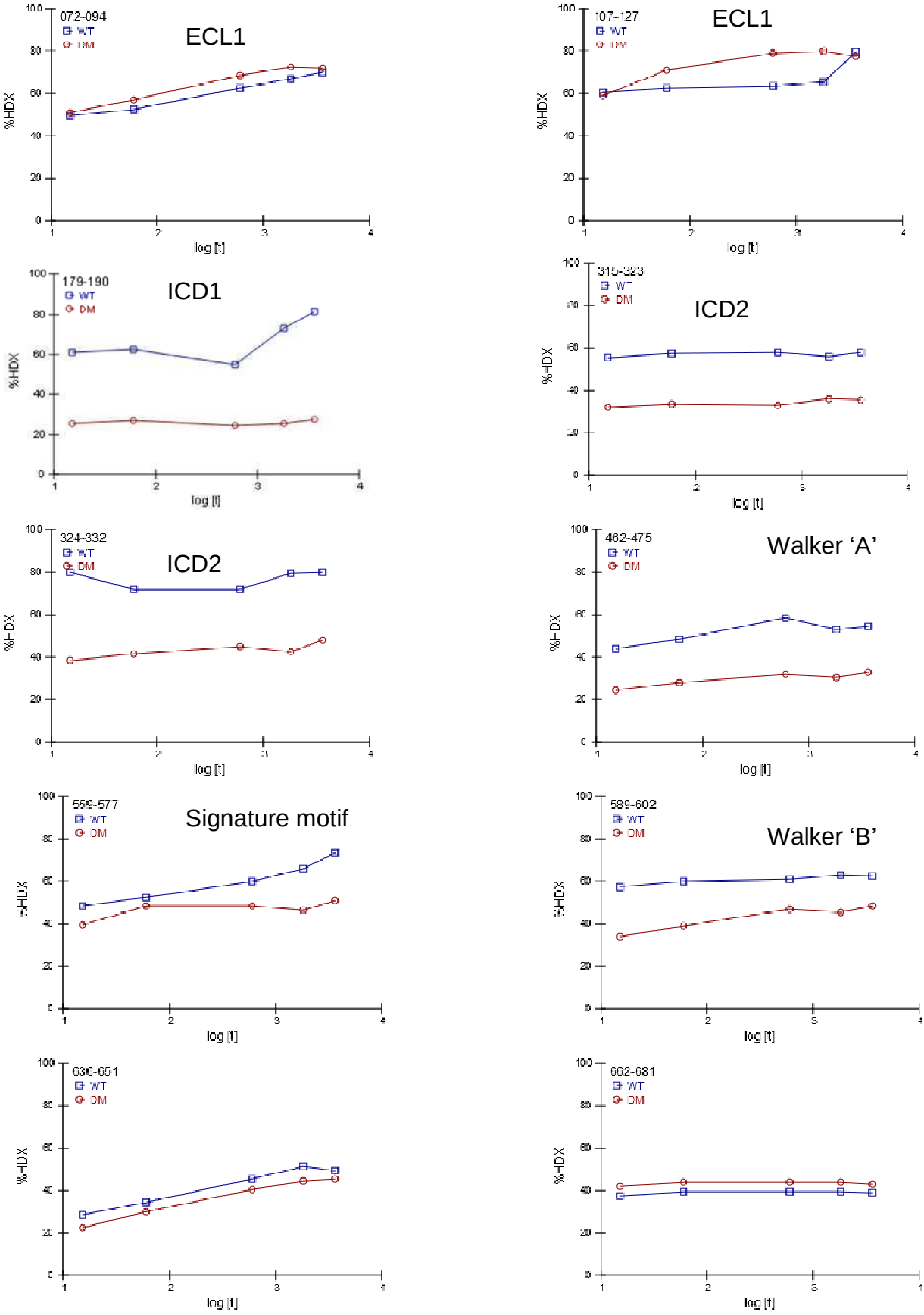

Figure 56-B. Kinetics plots of selected peptides of BmrD wild-type apo (WT) in are presented in blue and double mutant (E592A and D500A)(DM) in red color. The double mutant was deuterated in presence of 0.5 mM ATP/Mg^{2+}.

Chapter 4. H/D exchange kinetics of a prokaryotic homologue of ligand-gated ion channel GLIC

4.1. Introduction

4.1.1. Ligand-gated ion channel superfamily:

In higher organisms, the activities of the body are controlled by brain. The orders from the brain are carried to the target organ with the help of different kinds of intermediates. Nerve cells are one of the mean of this transport of information. The transmission of information across nerve cells is mediated by neurotransmitters, stored in synaptic vesicles (Figure 57). With the change in active potential of nerve cell, these vesicles are ruptured releasing neurotransmitters. The neurotransmitters bind with the receptors (these receptors are linked with intrinsic channels) present on post synaptic end. The neurotransmitters act as ligand for the postsynaptic receptor and their binding causes the opening or closing of intrinsic channel. Therefore, these are also called as ligand-gated ion channels (LGIC) or receptor-coupled ion channels. The opening/closing of channel causes the initiation/blockage of ions transfer. The binding sites of neurotransmitter and ion conductance channel are distant, therefore the binding of neurotransmitter allosterically controls the passage of ions.

The mean of selectivity to ions and ligand is provided by ion channels and receptor, respectively.

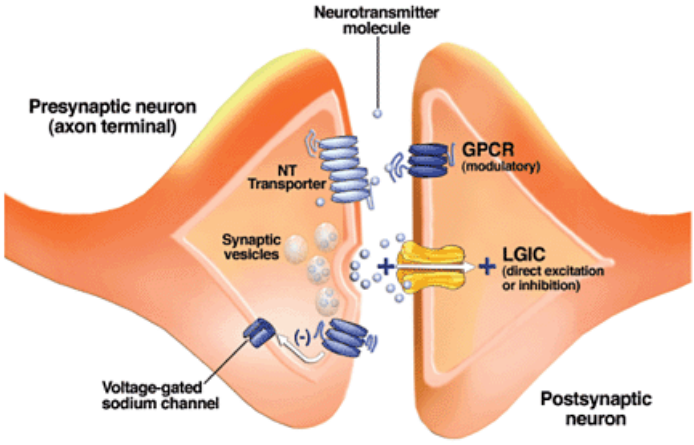

Figure 57. A schematic presentation of LGIC within a synapse between neuron (Web link:http://www.niaaa.nih.gov/Resources/GraphicsGallery/Neuroscience/PublishingImages/synapsebetween_neurons.gif)

The LGICs organize themselves in polymeric form within the membrane. The number of subunits is not constant and minimal three subunits are joined with one another, forming a pore. The topology of individual subunit is shown in Figure 58. Based on the number of components, LGICs are divided into three superfamilies (Le Novere and Changeux 1999; Collingridge, Olsen et al. 2009).

- Cys-loop receptor superfamily
- Glutamate cationic receptor superfamily
- ATP gated channel superfamily

Cys-loop receptor superfamily:

The channels of Cys-loop receptor superfamily are composed of five subunits arranged in homo or hetero-pentameric fashion.

This is the largest family of receptor-coupled ion channels identified by the presence of a stretch of conserved residues in each monomer. The conserved motif generally carries cysteine residues on both its C-ter and N-ter side. These two cysteine residues form a disulfide bridge in addition to a loop formed by conserved residues therefore giving the Cys-loop receptor superfamily name (Sine and Engel 2006).

The members of Cys-loop receptor superfamily consists of both positive and negative ions conducting channels. The ligands acting on the receptor part of Cys-loop super-family include acetylcholine, 5-HT3 (5-hydroxytryptamine; 5-HT3 receptors), glycine and GABA (gamma-aminobutyric acid; GABAA receptors). Both excitatory and inhibitory functions are mediated by these channels (Bocquet, Prado de Carvalho et al. 2007).

The binding of ligand to the receptor and transmission of information to channel for passage of ions through LGICs show that these are highly organized complex transmembrane protein assemblies. The mechanism of their functioning and ligand binding site can be understood by obtaining the data on structural information of these receptors. Once the mechanism is understood, putative drugs can be synthesize and used to target these receptors as they are related to several chronic diseases like Alzheimers and Parkinson's (Connolly and Wafford 2004; Cederholm, Schofield et al. 2009). One of the examples of Cys-loop ligand gated ion channels, the nicotinic acetylcholine receptor from the electric organ of the *Torpedo* was obtained at low resolution by electro microscopy (Miyazawa, Fujiyoshi et al. 2003).

Glutamate cationic receptor superfamily:

The members of Glutamate cationic receptor superfamily possess four subunits giving rise to homo-tetramer or hetero-tetramer. The available structure of receptor shows that two dimers, dimerize together giving rise to a tetramer(Tichelaar, Safferling et al. 2004). Unlike Cys-loop receptor superfamily, Glutamate cationic receptor superfamily perform only excitatory synaptic transmission. The channels linked to Glutamate cationic receptors can mediate the transport of cations only (Traynelis, Wollmuth et al. 2010).

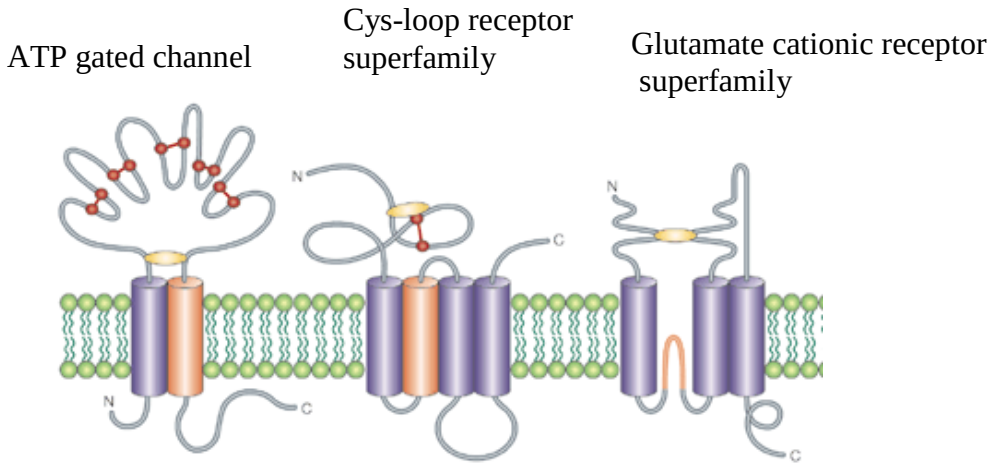

Figure 58. The topology of individual subunit of different ligand-gated ion channels (Khakh 2001).

ATP gated ion channel:

ATP gated ion channel receptors possess three subunits. Each subunit can be divided into three parts: two transmembranes and one extracellular domain. The extracellular domain links the two transmembrane domains. Extracellular ATP and protons act as ligand for the receptor and channels generally show selectivity towards monovalent cation like Na^+, K^+ (Khakh 2001; North 2002).

4.1.2. Ligand-gated ion channels in bacteria:

The completion of prokaryotic and eukaryotic genome sequencing projects prompted scientists to identify the prokaryotic homologues of the proteins already characterized in higher organisms. With careful sequence analysis, Tasneem *et al* showed the presence of ligand-gated ion channel homologues in several bacterial species and more than 20 proteins have been identified as homologous to Cys-loop ligand gated ion channels in prokaryotes (Tasneem, Iyer et al. 2005; Corringer, Baaden et al. 2010).

After identification of eukaryotic ligand-gated ion channels genes in prokaryotes, attempts were made to clone and overexpress the identified genes and determine the functional properties of expressed proteins. Bocquet *et al* showed for the first time that the proteins from *Gloeobacter violaceus* are able to form a channel which is cation-selective. They also showed that channel is activated at low pH concluding that protons act as ligand for channel (Bocquet, Prado de Carvalho et al. 2007).

With the characterization of homologous proteins in bacteria, the next step was to study the structure of these complex machines at high resolution (Miyazawa, Fujiyoshi et al. 2003; Hilf and Dutzler 2009b).

4.1.3. Structures of prokaryotic homologues of cys-loop ion channels:

Recently high resolution structures of two pentameric ligand-gated ion channel (pLGIC) from *Erwinia chrysanthemi* (ELIC) and *Gloeobacter violaceus* (GLIC) have been solved. Whereas, ELIC was crystallized at physiological pH, GLIC could be crystallized at pH 4.6 only. There are two structures of GLIC published back to back, solved in similar conditions and showing same structural arrangement. Both, GLIC and ELIC structures show similar quaternary structural arrangement of pentamers but ELIC and GLIC showed apparently the so-called closed and open conformations, respectively (Hilf and Dutzler 2008; Bocquet, Nury et al. 2009; Hilf and Dutzler 2009a). The difference found within two structures can explain the mechanism of receptor functioning.

4.1.3.1 GLIC structure:

The prokaryotic homologue of Cys-loop ligand-gated ion channel, GLIC, is constituted of five identical subunits giving rise to a homo-pentameric complex. Each subunit can be divided into two main parts: extracellular domain and transmembrane domain

Extracellular domain:

The extracellular domain which is responsible for the binding of ligand mainly consists of β-structural elements. There are two β-sheets comprising five inner and three outer β strands connected by loops of varied length. The two β-sheets tightly interact together giving rise to a β-sandwich (Figure 59). The overall structure of extracellular domain was found in correlation with nicotine acetylcholine-binding protein whose structure was solved in year 2001(Brejc, van Dijk et al. 2001).

Transmembrane domain:

Like other membrane proteins, transmembrane domain traverses the lipid bilayer. Each domain consists of four α-helices which are numbered from M1 to M4. M2 helix of each of the five subunits forms pore region of the channel. Whereas, M1 and M3 stabilize the pore by making strong interaction with corresponding helix of adjacent subunit, M4 is the outer most helix. The helices are connected by short loops and arranged in a presumably round shape (Figure 59).

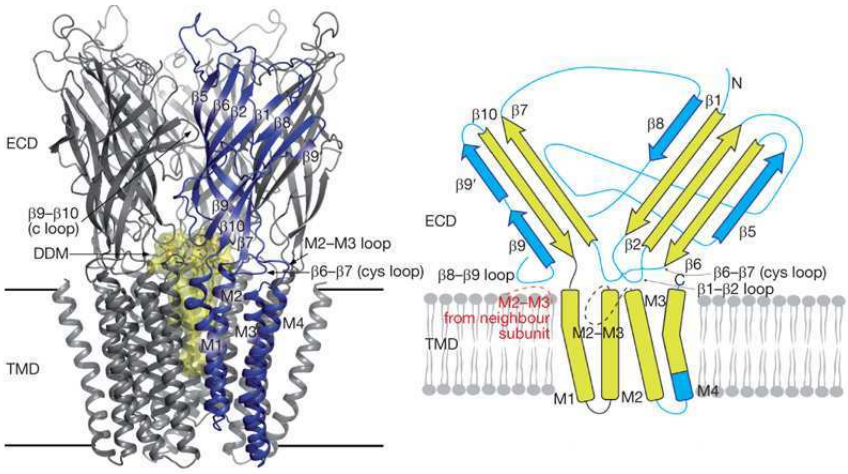

Figure 59. Left: Ribbon representation of GLIC from the plane of lipid bilayer. The structure was solved at 2.9Å. Detergent (dodecyl-D-maltoside, DDM) bound molecules are shown in space filling presentation of yellow color. Right: Topological presentation of extracellular domain (ECD) and transmembrane domain. ECD consists of three outer and five inner strands. The regions which are common in GLIC and ELIC are shown in yellow color(Bocquet, Nury et al. 2009).

4.1.3.2. Difference between ELIC and GLIC structures:

As described earlier both GLIC and ELIC share similar structural features but structural arrangement of specific regions is different. Within the two strands of extracellular domain a twist is observed when viewed from the plane crossing between the strands. When viewed from the membrane plan this twist is made and increases this proximity between strands of other subunits.

The different orientation of M2 in two structures is a major contributing factor for their open and closed states. The M2 helix with other helices forms the pore region, a way for translocation of ions. M2 helix is shown as twisted out of the plan of central axis of channel in GLIC on its C-terminal side and ELIC M2 helix does not change its orientation throughout its length, showing apparent closed conformation.

The region involved in making the interface between transmembrane and extracellular domain was previously shown as the binding site of the ligands (Grutter, de Carvalho et al. 2005; Lee and Sine 2005). At structural level, this region lies between conserved β1-β2 and β6-β7 loops from the ECD and M2-M3 loop of TMD. In GLIC structure, β1- β2 loop of ECD is in more open or freely existing away from the M2-M3 loop of TMD. M2-M3 loop itself adopts a position away from the central core (Figure 60). Similar behavior observed for β6- β7 of ECD, the famous cys-loop, known for binding ligands and named the superfamily, so providing a larger space compared with ELIC structure.

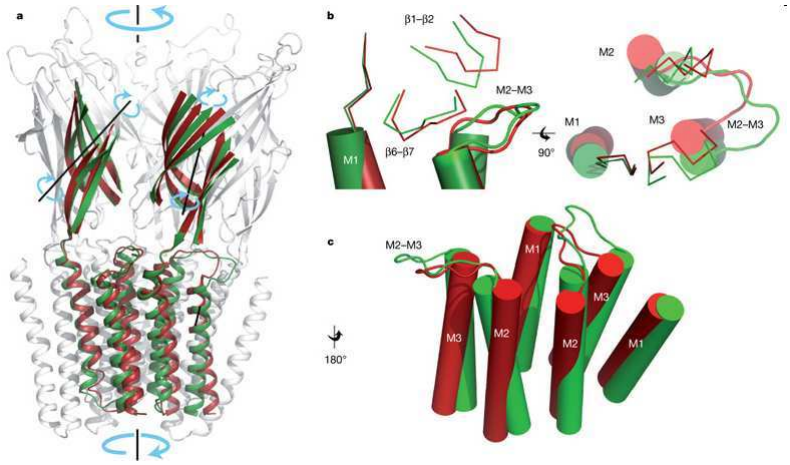

Figure 60. Side view of GLIC and ELIC superimposition in green and red color, respectively (Bocquet, Nury et al. 2009).

4.2. Materials and Methods:

4.2.1. Peptide mapping:

GLIC protein was expressed and purified as previously described (Bocquet, Prado de Carvalho et al. 2007; Bocquet, Nury et al. 2009). The purified protein was concentrated up to 8.5 mg/ml. The peptide mapping was obtained either with online pepsin digestion with pepsin, rhizopuspepsin or in-solution pepsin. For in-solution pepsin digestion, 1:2 protein to enzyme ratio was. Briefly 2 µl of GLIC protein solution (300 mM NaCl, 20 mM Tris HCl pH 7.2, 0.02% DDM) was diluted in 80 µl of cold hydrogenated buffer (300 mM NaCl and 0.02% DDM) and kept on ice. 10 µl of 3.4 mg/ml pepsin solution in 50 mM HCl was added to diluted protein sample. After addition, the mixture was left on ice for 2 minutes and then loaded on the peptide micro-trap.

Varied protein to enzyme ratio, longer incubation time or digestion at ambient temperature did not improve peptide digestion.

4.2.2. Deuterated sample preparation:

Deuteration at pH 7.0:

The pH of protein solution was adjusted to 7.0. In 200 µl of deuterated buffer, 10 µl of concentrated protein (8.5 mg/ml) was diluted. For GLIC deuteration buffer 300 mM NaCl and DDM 0.02 % was dissolved in 99.9 % D_2O. After 15 s of dilution an aliquot of 40 µl from dilution tube was withdrawn and transferred into another tube already containing precooled 10 µl of quench solution (pepsin 3 mg/ml in 50 mM HCl) and frozen in liquid nitrogen till further use. Similarly, four more aliquots after 60, 180 and 270 s were mixed with quench solution and frozen.

Deuteration at pH 4.6:

The pH of protein solution was adjusted to 4.6. In 200 µl of deuterated buffer (50 mM sodium acetate, 300 mM NaCl and DDM 0.02 % in 99.9 % D_2O), 10 µl of concentrated protein (8.5 mg/ml) was diluted. After 63 min, 4 h and 12 min, 12 h and 33 min and after 18 h and 50 min, aliquots of 7 µl of quench solution (pepsin 4.5 mg/ml in 50 mM HCl). The longer incubation time at pH 4.6 was for the correction of amide exchange as it was found slower with decrease in pH, one order of magnitude per pH unit (Zhang and Smith 1993). The ratio between incubation times of two conditions was 251 calculated by taking antilog of pH difference.

pH difference between two conditions: 7.0 – 4.6 = 2.4

Antilog of 2.4 = 251

Time at pH 7.0: 15 s

Required time at pH 4.6 equivalent to 15 s at pH 7.0: 15 X 251 = 3765 s or 63 min

The MS and MS/MS conditions and peptide analyses were performed as described in Materials and Methods section for BmrC/BmrD.

4.3. Results:

4.3.1. The transmembrane region of GLIC is strongly protected:

Several acid proteases were used for GLIC hydrolysis including pepsin, and rhizopuspepsin. The purpose of using multiple enzymes is to improve the sequence coverage and precise information of region of interest (Cravello, Lascoux et al. 2003; Marcoux, Man et al. 2010). We have previously shown that immobilization of these acid protease (Rey, Man et al. 2009) is another strategy for optimized digestion of membrane proteins (Rey, Man et al. 2010).

GLIC complex was digested as described in Materials and Methods section. The peptides eluted from hydrolysate were analyzed by tandem mass spectrometry. The tandem mass spectrometry allowed the identification of peptides on protein sequence. The separated or combined use of enzymes pepsin, enzyme XVIII and rhizopuspepsin generated 107 unique peptides exclusively covering extracellular domain. The in-solution digestion by pepsin was found the best digestion condition generating 83 peptides (59 % sequence coverage) and was followed in all the experiments. The transmembrane domain was very poorly covered; only one peptide was identified maybe due to strong protection of transmembrane helices offered by detergent. Another reason is probably given by the very strong interaction between

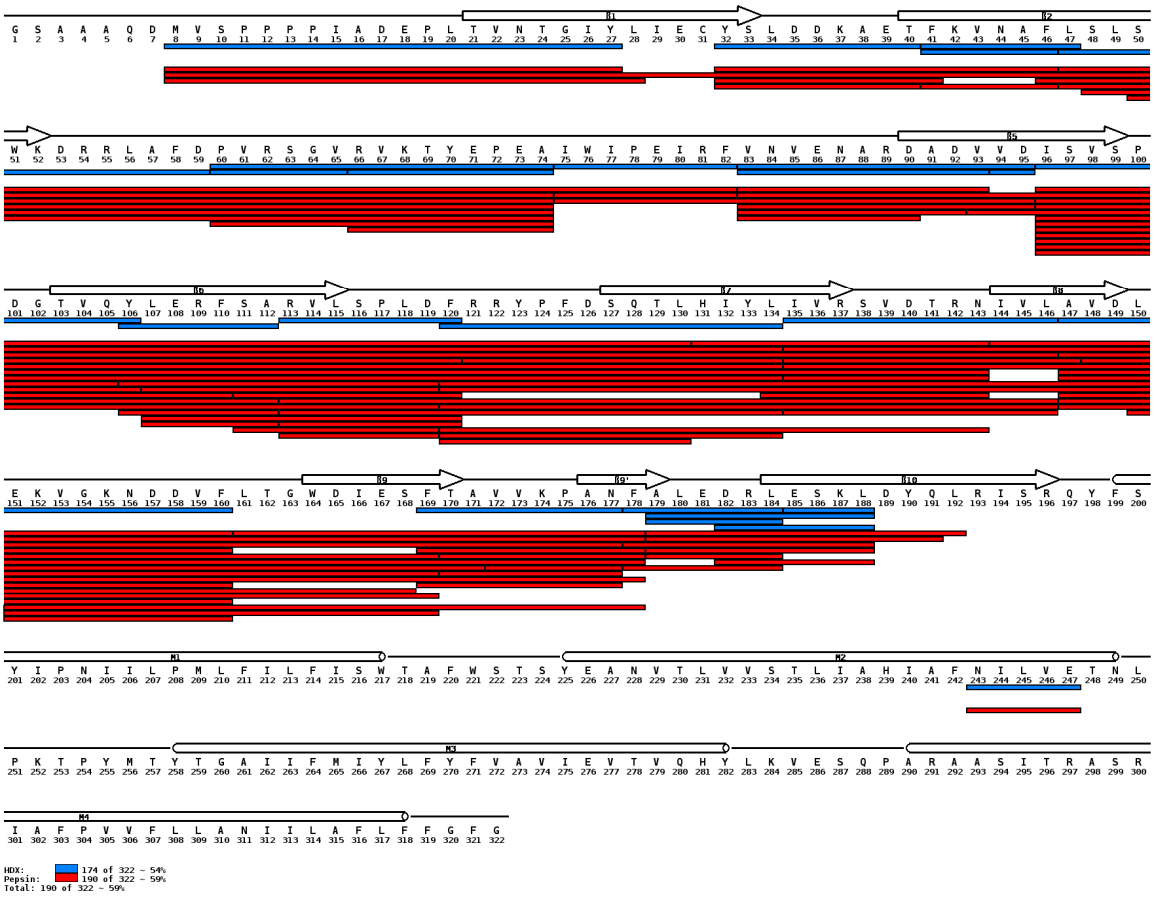

Figure 61. The peptides eluting from pepsin in-solution digestion are mapped in red and peptides used for HDX-MS are shown in blue color on GLIC sequence. Peptide mapping was obtained on FT-MS.

transmembrane helices. After identification of peptides on MS and due to low signal-to-noise ratio of deuterated samples, only 24 peptides were used for HDX-MS studies covering 54% sequence (Figure 61).

The HDX kinetics of some other peptides was possible to monitor at pH 7.0 but impossible at pH 4.6 may be due to longer incubation time in deuterated buffer which caused protein precipitation. Peptide mapping MS/MS experiments on FT-MS were performed by Petr Man in Prague.

4.3.2. The dynamics of GLIC at pH 4.6 and pH 7.0:

The conformational dynamics of GLIC at pH 4.6 and pH 7.0 was probed by HDX-MS. To analyze the behavior of precise regions of channel at different pH, local deuteration kinetics were determined. For pH 4.6, the protein was incubated in deuterated buffer (pH 4.6) between 63 min and 19 h and then digested by pepsin. Likewise for pH 7.0, the deuterated buffer at pH

7.0 was used and incubation from 15 to 270 s was performed. For all the peptides except one the HDX kinetics curves were found higher at pH 4.6 as compared to pH 7.0; however in most cases the difference was decreased with increasing deuteration incubation time (Figures 62 & 63).

4.3.3. The outer surface of ECD is highly exchangeable at pH 4.6 & pH 7.0:

The outer surface of each ECD is mainly composed of three β-strands made up of β7, β9, β9′ and β10, connected by short loops. β7 is covered by two peptides, 120-134 and 135-146 on N-terminal and C-terminal ends, respectively. Peptide 135-146 showed higher exchange of deuterium reaching 60% after 270 s at pH 4.6. At pH 7.0, exchange was slightly lower at shorter time as compared to pH 4.6 but at the final point of deuteration, no difference was found between both conditions. This is consistent with structure of GLIC showing β7 as part of outer sheet. Other two outer strands of ECD, β9′ and β10 showed higher deuteration exchange level from the least to maximum time of deuteration. Peptide 169-177, partially contributing both to β9 and β9′, is the only example where at final deuteration point, exchange was found slightly higher at pH 7.0 as compared to pH 4.6. Thus, change in pH had affected the deuterium exchange behavior of ECD outer surface.

4.3.4. The interface between ECD and TMD showed the highest exchange difference:

The TMD and ECD interaction region are one of the examples where structures of GLIC and ELIC showed difference in arrangement in high resolution structures. The N-terminal part of β6- β7 loop and β6 itself was covered by two peptides: 106-112 and 113-120. Peptide 113-120 showed low deuterium exchange (15 %) at first point of deuterium incubation at pH 7.0. After 270 s, the deuterium level was not changed significantly (~20 %). At pH 4.6, the same peptide was highly deuterated after first incubation time with ~70 % deuterium exchange; the content of exchange was unchanged for other time points. Thus peptide 113-120 showed a large difference in deuterium exchange between at pH 4.6 and pH 7.0 for all deuteration points from 15 s to 270 s. The other peptide 106-112 which is not part of interaction region loop rather showed similar deuterium exchange behavior as it was found for peptide 113-120 except it showed moderate exchange at first point of deuteration i.e. ~40% and with the increase of time, a progressive increase was observed reaching to ~70%. The progressive increase in peptide 106-112, might be due to the presence of a regular secondary structure. The difference in deuterium content for two peptides between two conditions was ~60 % after longest time of deuterium incubation.

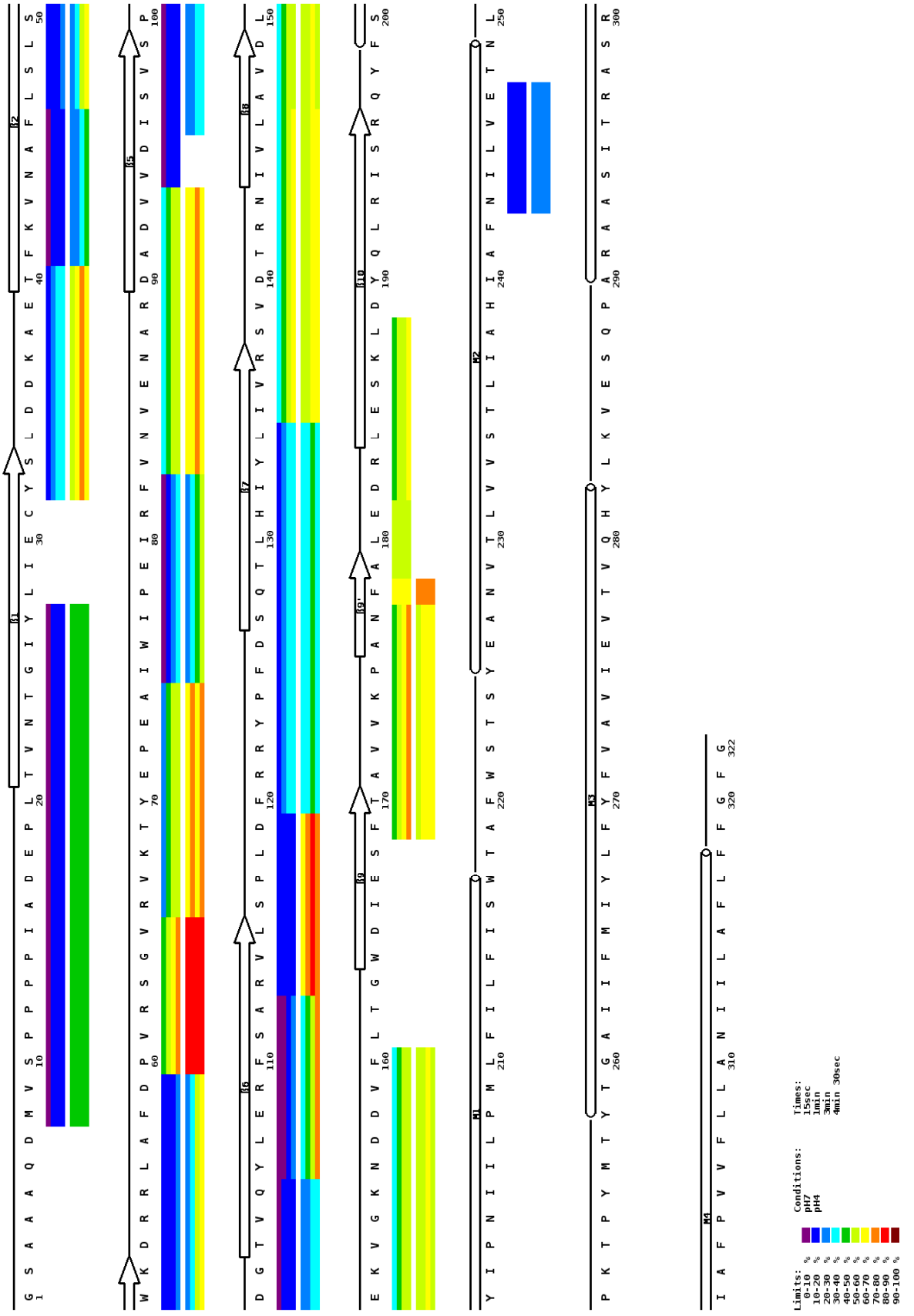

Figure 62. Heap map showing the deuterium exchange kinetics on GLIC sequence, secondary structure elements are also shown. Two separate wide lines show the deuterium exchange at pH 7.0 and pH 4.6. Within each line the deuterium content is colored from 15 s to 270 s.

Another part of ECD involved in interaction interface between ECD and TMD, is a loop connecting β1 with β2. The region was covered precisely with a short peptide 32-40 exactly showing the information of this region. As observed for peptide of β6- β7 loop, this peptide also showed higher deuterium exchange (~60 %) at first point of incubation at pH 4.6 which was slightly increased with the deuterium incubation time. For the same peptide, at pH 7.0, ~20 % of deuterium exchange was observed that increased to ~35 % at maximum deuteration time. Therefore, difference of deuterium content between two conditions was always about ~35%.

β1- β2 loop is followed by β2 sheet, the difference of deuterium content was also higher in this sheet. Though owing to specific secondary structure the deuterium content was not high even though difference could be observed.

4.4. Conclusion:

The X-ray crystallography is unarguably the best mean to provide the structural information of proteins which has extended its role in membrane proteins as well. However, due to specific experimental conditions and large sample requirement etc. sometimes the protein structure in varied condition is never obtained.

The x-ray structure of GLIC was solved after crystallization the protein at pH 4.6 but at physiological pH no structural data is available for GLIC. The structure of closely related protein ELIC was possible to obtain at pH7.0 which showed different arrangement of M2 helix of pore region and loops of the ECD and TMD interface, as compared to GLIC.

We applied HDX-MS technique on GLIC at pH 4.6 and pH 7.0. First, quick information was obtained that the transmembrane region of protein is strongly resistant against acid proteases. This is probably due to protection of TMD by detergent and/or strong interaction of subunits. In our experience the protein is not very stable at pH 4.6 for long time at room temperature. The signal-to-noise ratio of deuterated protein samples at this pH for long time was very poor which resulted in loss of many peptides.

The HDX-MS results obtained at pH 4.6 were verified by its correlation with three dimensional structure at pH 4.6. The comparison of HDX kinetics results obtained at pH 4.6 and pH 7.0 indicated that at pH 7.0 GLIC also adopts the so-called closed conformation similar to that one observed for ELIC structure.

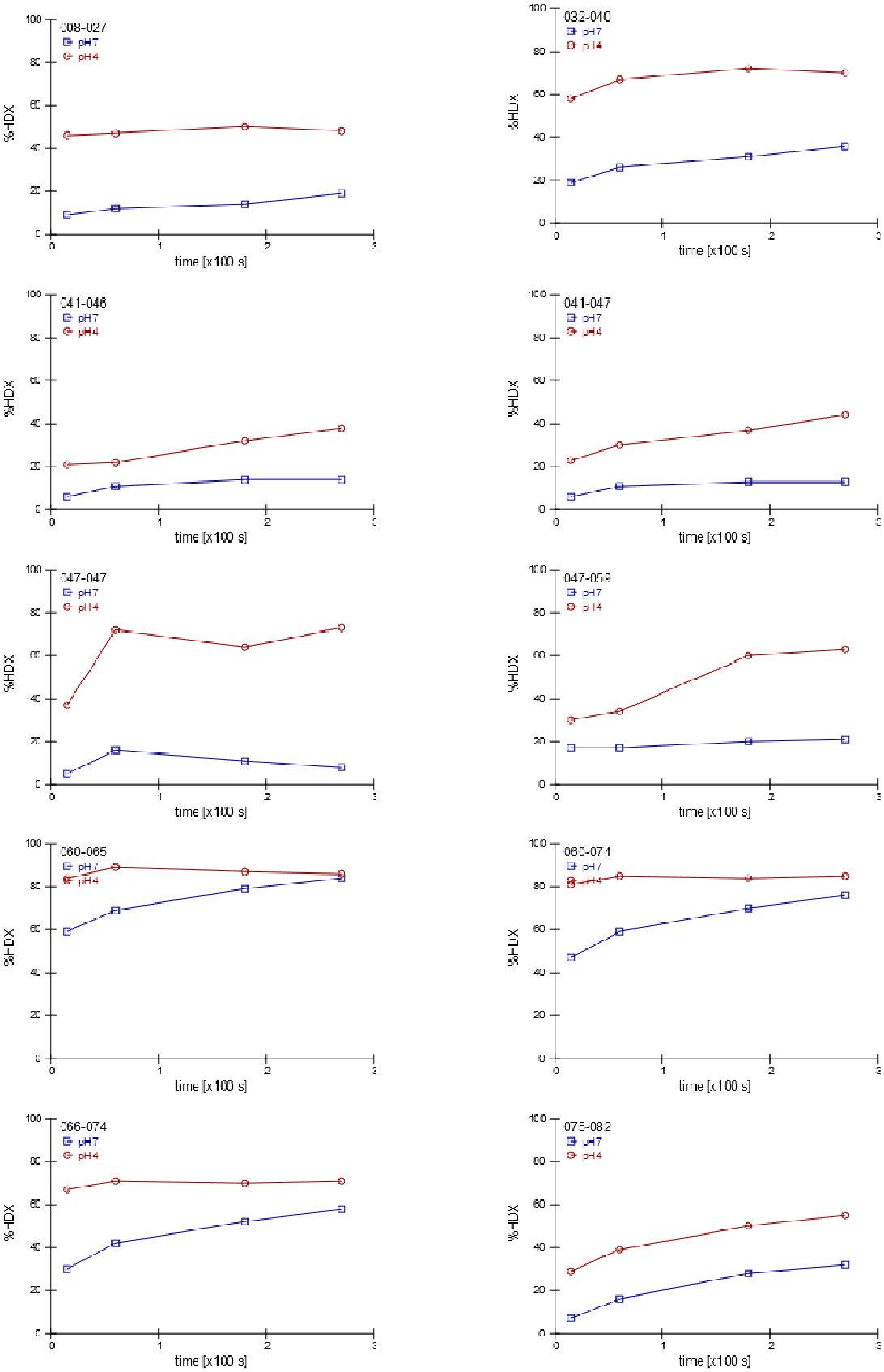

Figure 63. H/D exchange kinetics plots of GLIC peptides (Part I).

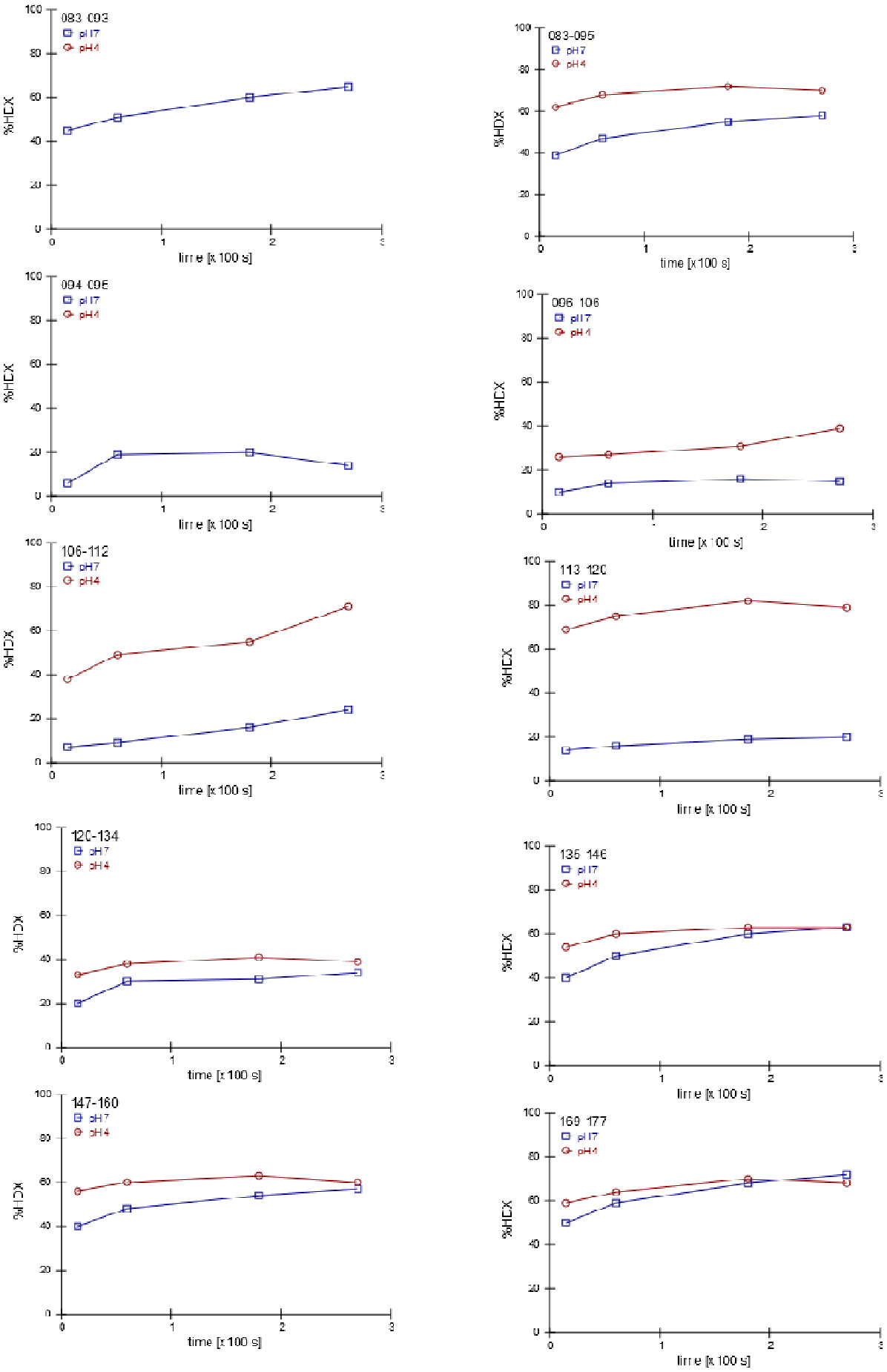

Figure 63. H/D exchange kinetics plots of GLIC peptides (Part II).

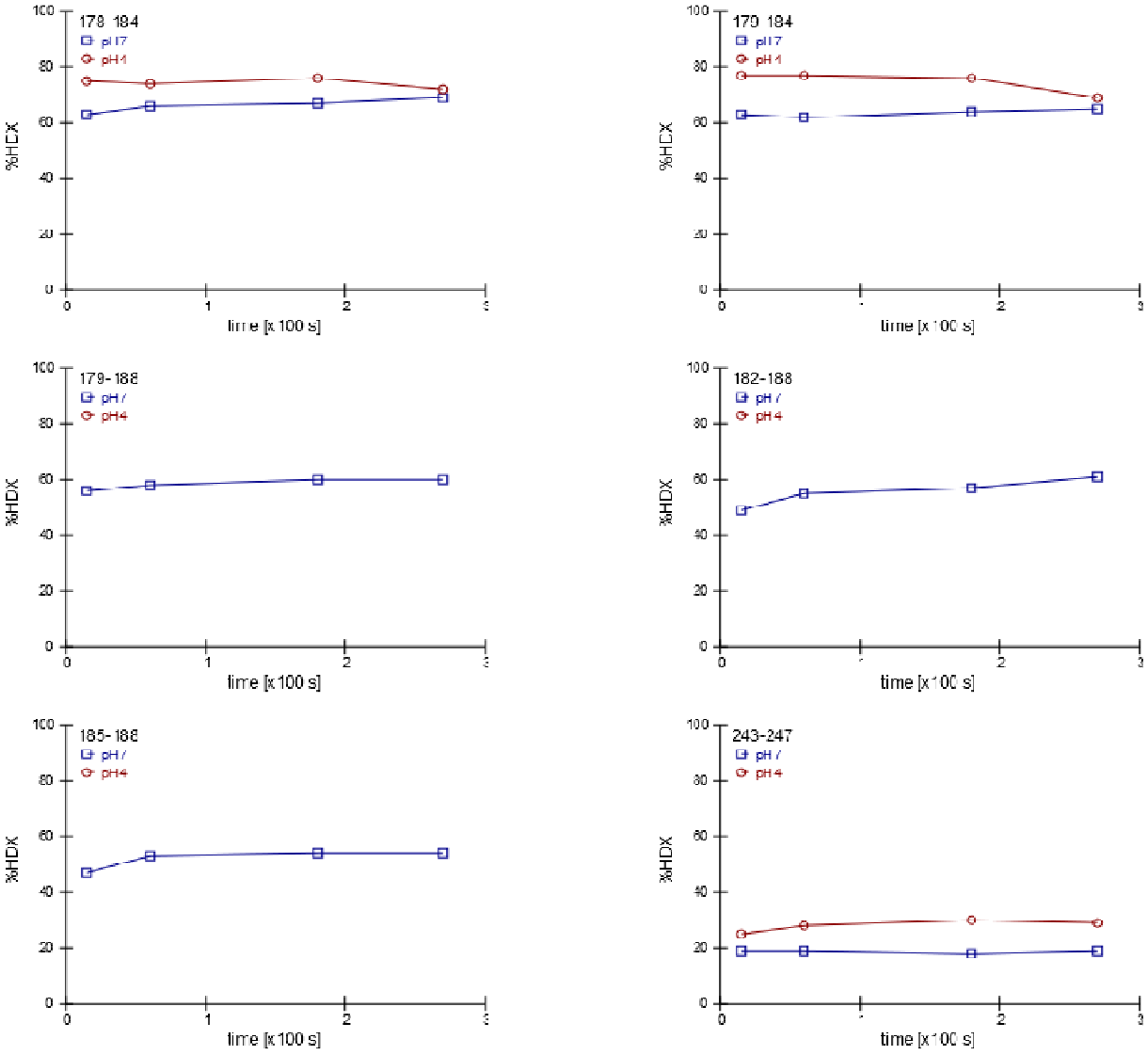

Figure 63. H/D exchange kinetics plots of GLIC peptides (Part III).

General Conclusion and Outlook

The investigation of conformational changes in proteins requires use of different biophysical techniques. In this PhD thesis work, for the first time, hydrogen-deuterium exchange coupled to mass spectrometry was applied to study ABC transporters and pentameric ligand-gated ion channel (pLGIC). The major emphasis was on two different ABC transporters: BmrA and BmrC/BmrD. In addition a pLGIC, GLIC, was also characterized at two different pH.

The ABC transporters are present in all form of life in varying number, involved in vital functions. Their dysfunction is known to be associated with several diseases like cystic fibrosis in humans. Some ABC exporters are involved in multidrug transport and show poly-specificity to substrates. They are overexpressed in response to chemotherapy treatment of cancer. In bacteria they are one of the causes of antibiotic resistance.

A question directly related to membrane protein is the effect of detergent on their stability and conformation. For BmrA we showed both with help of HDX - MS and limited proteolysis experiments that protein is more dynamic in detergent as compared to lipid bilayer in apo form. But at the same time it is protected in similar extent in both conditions in its closed form.

The structures of other ABC exporters solved at high resolution in presence or absence of nucleotides showed different conformations. But in all cases the *trans*- interaction of ICD2 is kept. Our H/D exchange kinetics results on apo conformation of BmrA raised the question of this interaction and showed their highly dynamic nature in solution. We also suggested that possibly ICDs exist in unstructured conformation for transporter in its apo form. The kinetics of ICD2 obtained in the presumably closed form were in agreement with the BmrA models based on closed structure of homologue ABC exporter thus validating our results.

Another aspect of ABC transporter related to our study is physiological existing state of NBDs in apo form. We clearly showed that the NBDs of two subunits are highly dynamic and are possibly not associated with one another in absence of nucleotide. The addition of different drugs which are known to be transported by ABC transporters did not affect dynamics of NBDs. We also confirmed that dynamics of NBDs were reduced on addition of ATP/Mg^{2+} due to their tight interaction in mutant lacking ATPase activity.

The dynamics of different regions of BmrA was also reduced in its resting state but not freely moving due to mutation on Walker ‘A’ motif.

ABC hetero-dimer showed, BmrC/BmrD, similar H/D exchange kinetics results as found for BmrA in apo conformation: highly dynamic nature of predicted ICDs and well non-interacting NBDs. But closed form of hetero-dimer mutant on addition of ATP/Mg^{2+} was not as stable as found for homo-dimer BmrA. The predicted extracellular loop of BmrD was not found to be affected in presence or absence of nucleotide.

The structures of ligand-gated ion channels at high resolution have been emerging recently like GLIC or ELIC. The H/D exchange kinetics of GLIC obtained at pH 4.6 were in correlation with its apparently open conformation. For the same protein, results obtained at pH 7.0 showed less deuteration for particular region confirming a possible closed form. The kinetics at pH 7.0 was found to be in accordance with the structure of homologue protein ELIC.

The HDX-MS technique is expanding its application on membrane protein characterization like recent example of ADP/ATP carrier and GPCR receptors. The work performed during this thesis showed possible application of mentioned technique on ABC proteins and ligand-gated ion channels as well. For ABC hetero-dimer BmrC/BmrD, the analogue of ATP (for example AMP-PNP) could be used to verify the proposed mechanism of cooperative binding of ATP in two subunits. Since both subunits are different in their amino acid sequence, the AMP-PNP concentration required for binding on one subunit can be determined by its H/D-exchange kinetics in varied AMP-PNP concentrations.

In this study the coverage of peptide mapping was good but not optimum for characterized protein. This problem can be overcome by different digestion techniques and new acid proteases. Especially good coverage of transmembrane region can provide information about drug binding site in case of ABC exporters. In GLIC this can be helpful to determine the differential kinetics of pore region particularly M2 helix.

The finding of different acid proteases can be helpful for characterization of proteins with better resolution at short peptide size level. The time required for the HDX experiment can be reduced by development of automatically controlled robotic methods (under construction in our group). The robotic methods will be helpful for reproducibility of data. The further reduction of time, required for the processing of large data generated by HDX-MS experiments can be achieved by developing more precise computer based programs.

References

Abramson, J., I. Smirnova, et al. (2003). "Structure and mechanism of the lactose permease of Escherichia coli." Science 301(5633): 610-5.
Akama, H., M. Kanemaki, et al. (2004). "Crystal structure of the drug discharge outer membrane protein, OprM, of Pseudomonas aeruginosa: dual modes of membrane anchoring and occluded cavity end." J Biol Chem 279(51): 52816-9.
Allen, H. K., J. Donato, et al. (2010). "Call of the wild: antibiotic resistance genes in natural environments." Nat Rev Microbiol 8(4): 251-9.
Aller, S. G., J. Yu, et al. (2009). "Structure of P-glycoprotein reveals a molecular basis for poly-specific drug binding." Science 323(5922): 1718-22.
Antoniou, T. and K. A. Gough (2005). "Early-onset pentamidine-associated second-degree heart block and sinus bradycardia: case report and review of the literature." Pharmacotherapy 25(6): 899-903.
Arakawa, Y. (1999). "[Functional and molecular classification of beta-lactamases]." Nihon Saikingaku Zasshi 54(3): 639-49.
Bai, Y., J. S. Milne, et al. (1993). "Primary structure effects on peptide group hydrogen exchange." Proteins 17(1): 75-86.
Barrera, N. P., N. Di Bartolo, et al. (2008). "Micelles protect membrane complexes from solution to vacuum." Science 321(5886): 243-6.
Beavis, R. C. and B. T. Chait (1989a). "Cinnamic acid derivatives as matrices for ultraviolet laser desorption mass spectrometry of proteins." Rapid Commun Mass Spectrom 3(12): 432-5.
Beavis, R. C. and B. T. Chait (1989b). "Matrix-assisted laser-desorption mass spectrometry using 355 nm radiation." Rapid Commun Mass Spectrom 3(12): 436-9.
Bebrone, C. (2007). "Metallo-beta-lactamases (classification, activity, genetic organization, structure, zinc coordination) and their superfamily." Biochem Pharmacol 74(12): 1686-701.
Begum, A., M. M. Rahman, et al. (2005). "Gene cloning and characterization of four MATE family multidrug efflux pumps from Vibrio cholerae non-O1." Microbiol Immunol 49(11): 949-57.
Benesch, J. L. P. and B. T. Ruotolo (2011). "Mass spectrometry: come of age for structural and dynamical biology." Curr Opin Struct Biol 21(5): 641-649.
Biemans-Oldehinkel, E., M. K. Doeven, et al. (2006). "ABC transporter architecture and regulatory roles of accessory domains." FEBS Lett 580(4): 1023-35.
Bjorland, J., M. Sunde, et al. (2001). "Plasmid-borne smr gene causes resistance to quaternary ammonium compounds in bovine Staphylococcus aureus." J Clin Microbiol 39(11): 3999-4004.
Blair, J. M. and L. J. Piddock (2009). "Structure, function and inhibition of RND efflux pumps in Gram-negative bacteria: an update." Curr Opin Microbiol 12(5): 512-9.
Bocquet, N., H. Nury, et al. (2009). "X-ray structure of a pentameric ligand-gated ion channel in an apparently open conformation." Nature 457(7225): 111-114.
Bocquet, N., L. Prado de Carvalho, et al. (2007). "A prokaryotic proton-gated ion channel from the nicotinic acetylcholine receptor family." Nature 445(7123): 116-9.
Bodnar, W. M., R. K. Blackburn, et al. (2003). "Exploiting the complementary nature of LC/MALDI/MS/MS and LC/ESI/MS/MS for increased proteome coverage." J Am Soc Mass Spectrom 14(9): 971-9.
Borderie, D., A. Hernvann, et al. (2001). "Tetracyclines inhibit nitrosothiol production by cytokine-stimulated osteoarthritic synovial cells." Inflamm Res 50(8): 409-14.
Boslego, J. W., E. C. Tramont, et al. (1987). "Effect of spectinomycin use on the prevalence of spectinomycin-resistant and of penicillinase-producing Neisseria gonorrhoeae." N Engl J Med 317(5): 272-8.

Bradford, M. M. (1976). "A rapid and sensitive method for the quantitation of microgram quantities of protein utilizing the principle of protein-dye binding." Anal Biochem 72: 248-54.
Brejc, K., W. J. van Dijk, et al. (2001). "Crystal structure of an ACh-binding protein reveals the ligand-binding domain of nicotinic receptors." Nature 411(6835): 269-276.
Brier, S., D. Lemaire, et al. (2004). "Identification of the protein binding region of S-trityl-L-cysteine, a new potent inhibitor of the mitotic kinesin Eg5." Biochemistry 43(41): 13072-82.
Brown, M. H., I. T. Paulsen, et al. (1999). "The multidrug efflux protein NorM is a prototype of a new family of transporters." Mol Microbiol 31(1): 394-5.
Brown, R. S. and J. J. Lennon (1995). "Mass resolution improvement by incorporation of pulsed ion extraction in a matrix-assisted laser desorption/ionization linear time-of-flight mass spectrometer." Anal Chem 67(13): 1998-2003.
Bush, K. (1989). "Classification of beta-lactamases: groups 2c, 2d, 2e, 3, and 4." Antimicrob Agents Chemother 33(3): 271-6.
Bush, K. and G. A. Jacoby (2010). "Updated functional classification of beta-lactamases." Antimicrob Agents Chemother 54(3): 969-76.
Bush, K., G. A. Jacoby, et al. (1995). "A functional classification scheme for beta-lactamases and its correlation with molecular structure." Antimicrob Agents Chemother 39(6): 1211-33.
Cadene, M. and B. T. Chait (2000). "A robust, detergent-friendly method for mass spectrometric analysis of integral membrane proteins." Anal Chem 72(22): 5655-8.
Campbell, E. A., N. Korzheva, et al. (2001). "Structural mechanism for rifampicin inhibition of bacterial rna polymerase." Cell 104(6): 901-12.
Cederholm, J. M., P. R. Schofield, et al. (2009). "Gating mechanisms in Cys-loop receptors." Eur Biophys J 39(1): 37-49.
Chami, M., E. Steinfels, et al. (2002). "Three-dimensional structure by cryo-electron microscopy of YvcC, an homodimeric ATP-binding cassette transporter from Bacillus subtilis." J Mol Biol 315(5): 1075-85.
Chang, A. B., R. Lin, et al. (2004). "Phylogeny as a guide to structure and function of membrane transport proteins." Mol Membr Biol 21(3): 171-81.
Chang, G., C. B. Roth, et al. (2006). "Retraction." Science 314(5807): 1875.
Chen, J., G. Lu, et al. (2003). "A tweezers-like motion of the ATP-binding cassette dimer in an ABC transport cycle." Mol Cell 12(3): 651-61.
Chen, J., Y. Morita, et al. (2002). "VmrA, a member of a novel class of Na(+)-coupled multidrug efflux pumps from Vibrio parahaemolyticus." J Bacteriol 184(2): 572-6.
Chen, Y. J., O. Pornillos, et al. (2007). "X-ray structure of EmrE supports dual topology model." Proc Natl Acad Sci U S A 104(48): 18999-9004.
Chung, Y. J. and M. H. Saier, Jr. (2001). "SMR-type multidrug resistance pumps." Curr Opin Drug Discov Devel 4(2): 237-45.
Clatworthy, A. E., E. Pierson, et al. (2007). "Targeting virulence: a new paradigm for antimicrobial therapy." Nat Chem Biol 3(9): 541-8.
Collingridge, G. L., R. W. Olsen, et al. (2009). "A nomenclature for ligand-gated ion channels." Neuropharmacology 56(1): 2-5.
Connolly, C. N. and K. A. Wafford (2004). "The Cys-loop superfamily of ligand-gated ion channels: the impact of receptor structure on function." Biochem Soc Trans 32(Pt3): 529-34.
Cooks, R. G., I. Howe, et al. (1969). "Structure and Fragmentation Mechanisms of Organic Ions in Mass Spectrometer." Organic Mass Spectrometry 2(2): 137-&.

Cornish, T. J. and R. J. Cotter (1993). "A curved-field reflectron for improved energy focusing of product ions in time-of-flight mass spectrometry." Rapid Commun Mass Spectrom 7(11): 1037-40.

Corringer, P. J., M. Baaden, et al. (2010). "Atomic structure and dynamics of pentameric ligand-gated ion channels: new insight from bacterial homologues." Journal of Physiology-London 588(4): 565-572.

Cotte-Rodriguez, I., Y. Zhang, et al. (2011). Ionization Methods in Protein Mass Spectrometry. Protein and Peptide Mass Spectrometry in Drug Discovery, John Wiley & Sons, Inc.: 1-42.

Cotter, R. J., B. D. Gardner, et al. (2004). "Tandem time-of-flight mass spectrometry with a curved field reflectron." Anal Chem 76(7): 1976-81.

Cravello, L., D. Lascoux, et al. (2003). "Use of different proteases working in acidic conditions to improve sequence coverage and resolution in hydrogen/deuterium exchange of large proteins." Rapid Commun Mass Spectrom 17(21): 2387-93.

Creese, A. J. and H. J. Cooper (2007). "Liquid chromatography electron capture dissociation tandem mass spectrometry (LC-ECD-MS/MS) versus liquid chromatography collision-induced dissociation tandem mass spectrometry (LC-CID-MS/MS) for the identification of proteins." J Am Soc Mass Spectrom 18(5): 891-7.

Dalmas, O., M. A. Do Cao, et al. (2005). "Time-resolved fluorescence resonance energy transfer shows that the bacterial multidrug ABC half-transporter BmrA functions as a homodimer." Biochemistry 44(11): 4312-21.

Dalmas, O., C. Orelle, et al. (2005). "The Q-loop disengages from the first intracellular loop during the catalytic cycle of the multidrug ABC transporter BmrA." J Biol Chem 280(44): 36857-64.

Dang, S., L. Sun, et al. (2010). "Structure of a fucose transporter in an outward-open conformation." Nature 467(7316): 734-8.

Das, D., Q. S. Xu, et al. (2007). "Crystal structure of the multidrug efflux transporter AcrB at 3.1A resolution reveals the N-terminal region with conserved amino acids." J Struct Biol 158(3): 494-502.

Davidson, A. L., E. Dassa, et al. (2008). "Structure, function, and evolution of bacterial ATP-binding cassette systems." Microbiol Mol Biol Rev 72(2): 317-64, table of contents.

Dawson, R. J., K. Hollenstein, et al. (2007). "Uptake or extrusion: crystal structures of full ABC transporters suggest a common mechanism." Mol Microbiol 65(2): 250-7.

Dawson, R. J. and K. P. Locher (2006). "Structure of a bacterial multidrug ABC transporter." Nature 443(7108): 180-5.

Dawson, R. J. and K. P. Locher (2007). "Structure of the multidrug ABC transporter Sav1866 from Staphylococcus aureus in complex with AMP-PNP." FEBS Lett 581(5): 935-8.

Dean, M., A. Rzhetsky, et al. (2001). "The human ATP-binding cassette (ABC) transporter superfamily." Genome Res 11(7): 1156-66.

Deng, Y., H. Pan, et al. (1999). "Selective Isotope Labeling Demonstrates That Hydrogen Exchange at Individual Peptide Amide Linkages Can Be Determined by Collision-Induced Dissociation Mass Spectrometry." J Am Chem Soc 121(9): 1966-1967.

Deng, Y. and D. L. Smith (1998). "Identification of unfolding domains in large proteins by their unfolding rates." Biochemistry 37(18): 6256-62.

Diezel, W., G. Kopperschlager, et al. (1972). "An improved procedure for protein staining in polyacrylamide gels with a new type of Coomassie Brilliant Blue." Anal Biochem 48(2): 617-20.

Dixon, R. A. and I. Chopra (1986). "Polymyxin B and polymyxin B nonapeptide alter cytoplasmic membrane permeability in Escherichia coli." J Antimicrob Chemother 18(5): 557-63.

Doeven, M. K., R. Abele, et al. (2004). "The binding specificity of OppA determines the selectivity of the oligopeptide ATP-binding cassette transporter." J Biol Chem 279(31): 32301-7.
Doyle, L. A. and D. D. Ross (2003). "Multidrug resistance mediated by the breast cancer resistance protein BCRP (ABCG2)." Oncogene 22(47): 7340-58.
Doyle, L. A., W. Yang, et al. (1998). "A multidrug resistance transporter from human MCF-7 breast cancer cells." Proc Natl Acad Sci U S A 95(26): 15665-70.
Dozzo, P. and H. E. Moser (2010). "New aminoglycoside antibiotics." Expert Opin Ther Pat 20(10): 1321-41.
Drew, D., M. M. Klepsch, et al. (2008). "The structure of the efflux pump AcrB in complex with bile acid." Mol Membr Biol 25(8): 677-82.
Drlica, K. and X. Zhao (1997). "DNA gyrase, topoisomerase IV, and the 4-quinolones." Microbiol Mol Biol Rev 61(3): 377-92.
Durante-Mangoni, E., A. Grammatikos, et al. (2009). "Do we still need the aminoglycosides?" Int J Antimicrob Agents 33(3): 201-5.
Dye, C. (2006). "Global epidemiology of tuberculosis." Lancet 367(9514): 938-40.
Eicher, T., L. Brandstatter, et al. (2009). "Structural and functional aspects of the multidrug efflux pump AcrB." Biol Chem 390(8): 693-9.
Eitinger, T., D. A. Rodionov, et al. (2011). "Canonical and ECF-type ATP-binding cassette importers in prokaryotes: diversity in modular organization and cellular functions." FEMS Microbiol Rev 35(1): 3-67.
El Zoeiby, A., F. Sanschagrin, et al. (2003). "Structure and function of the Mur enzymes: development of novel inhibitors." Mol Microbiol 47(1): 1-12.
Englander, S. W. and N. R. Kallenbach (1983). "Hydrogen exchange and structural dynamics of proteins and nucleic acids." Q Rev Biophys 16(4): 521-655.
Everberg, H., N. Gustavasson, et al. (2008). "Enrichment of membrane proteins by partitioning in detergent/polymer aqueous two-phase systems." Methods Mol Biol 424: 403-12.
Fang, J., K. D. Rand, et al. (2011). "False EX1 signatures caused by sample carryover during HX MS analyses." Int J Mass Spectrom 302(1-3): 19-25.
Fenn, J. B. (2003). "Electrospray wings for molecular elephants (Nobel lecture)." Angew Chem Int Ed Engl 42(33): 3871-94.
Fenn, J. B., M. Mann, et al. (1989). "Electrospray ionization for mass spectrometry of large biomolecules." Science 246(4926): 64-71.
Fenn, J. B., M. Mann, et al. (1990). "Electrospray ionization–principles and practice." Mass Spectrom Rev 9(1): 37-70.
Fenyo, D., Q. Wang, et al. (2007). "MALDI sample preparation: the ultra thin layer method." J Vis Exp(3): 192.
Ferguson, P. L., J. Pan, et al. (2006). "Hydrogen/Deuterium Scrambling during Quadrupole Time-of-Flight MS/MS Analysis of a Zinc-Binding Protein Domain." Anal Chem 79(1): 153-160.
Fetsch, E. E. and A. L. Davidson (2002). "Vanadate-catalyzed photocleavage of the signature motif of an ATP-binding cassette (ABC) transporter." Proc Natl Acad Sci U S A 99(15): 9685-90.
Frommberger, M., P. Schmitt-Kopplin, et al. (2004). "A simple and robust set-up for on-column sample preconcentration--nano-liquid chromatography--electrospray ionization mass spectrometry for the analysis of N-acylhomoserine lactones." Anal Bioanal Chem 378(4): 1014-20.
Gabant, G. and M. Cadene (2008). "Mass spectrometry of full-length integral membrane proteins to define functionally relevant structural features." Methods 46(2): 54-61.

Galian, C., F. Manon, et al. (2011). "Optimized purification of a heterodimeric ABC transporter in a highly stable form amenable to 2-D crystallization." PLoS One 6(5): e19677.
Garcia, M. C. (2005). "The effect of the mobile phase additives on sensitivity in the analysis of peptides and proteins by high-performance liquid chromatography-electrospray mass spectrometry." J Chromatogr B Analyt Technol Biomed Life Sci 825(2): 111-23.
Geourjon, C., C. Orelle, et al. (2001). "A common mechanism for ATP hydrolysis in ABC transporter and helicase superfamilies." Trends Biochem Sci 26(9): 539-44.
Gerber, S., M. Comellas-Bigler, et al. (2008). "Structural basis of trans-inhibition in a molybdate/tungstate ABC transporter." Science 321(5886): 246-50.
Gottesman, M. M., S. V. Ambudkar, et al. (2009). "Structure of a multidrug transporter." Nat Biotechnol 27(6): 546-7.
Griffiths, W. J., A. P. Jonsson, et al. (2001). "Electrospray and tandem mass spectrometry in biochemistry." Biochem J 355(Pt 3): 545-61.
Grinius, L. L. and E. B. Goldberg (1994). "Bacterial multidrug resistance is due to a single membrane protein which functions as a drug pump." J Biol Chem 269(47): 29998-30004.
Grutter, T., L. P. de Carvalho, et al. (2005). "Molecular tuning of fast gating in pentameric ligand-gated ion channels." Proc Natl Acad Sci U S A 102(50): 18207-12.
Guilhaus, M. (1995). "Special feature: Tutorial. Principles and instrumentation in time-of-flight mass spectrometry. Physical and instrumental concepts." J Mass Spectrom 30(11): 1519-1532.
Hagman, C., Y. O. Tsybin, et al. (2006). "Solution-phase deuterium/hydrogen exchange at a specific residue using nozzle-skimmer and electron capture dissociation mass spectrometry." Rapid Commun Mass Spectrom 20(4): 661-5.
Hall, M. D., M. D. Handley, et al. (2009). "Is resistance useless? Multidrug resistance and collateral sensitivity." Trends Pharmacol Sci 30(10): 546-56.
Halquist, M. S. and H. Thomas Karnes (2010). "Quantitative liquid chromatography tandem mass spectrometry analysis of macromolecules using signature peptides in biological fluids." Biomed Chromatogr 25(1-2): 47-58.
Hardouin, J. (2007). "Protein sequence information by matrix-assisted laser desorption/ionization in-source decay mass spectrometry." Mass Spectrom Rev 26(5): 672-682.
Harvey, D. J. (2009). "Analysis of carbohydrates and glycoconjugates by matrix-assisted laser desorption/ionization mass spectrometry: An update for 2003-2004." Mass Spectrom Rev 28(2): 273-361.
He, X., P. Szewczyk, et al. (2010). "Structure of a cation-bound multidrug and toxic compound extrusion transporter." Nature 467(7318): 991-4.
Hebling, C. M., C. R. Morgan, et al. (2010). "Conformational analysis of membrane proteins in phospholipid bilayer nanodiscs by hydrogen exchange mass spectrometry." Anal Chem 82(13): 5415-9.
Higgins, C. F. (1992). "ABC transporters: from microorganisms to man." Annu Rev Cell Biol 8: 67-113.
Higgins, C. F. (2007). "Multiple molecular mechanisms for multidrug resistance transporters." Nature 446(7137): 749-757.
Higgins, C. F., R. Callaghan, et al. (1997). "Structure of the multidrug resistance P-glycoprotein." Semin Cancer Biol 8(3): 135-42.
Higgins, C. F. and K. J. Linton (2004). "The ATP switch model for ABC transporters." Nat Struct Mol Biol 11(10): 918-926.

Hilf, R. J. C. and R. Dutzler (2008). "X-ray structure of a prokaryotic pentameric ligand-gated ion channel." Nature 452(7185): 375-379.
Hilf, R. J. C. and R. Dutzler (2009a). "Structure of a potentially open state of a proton-activated pentameric ligand-gated ion channel." Nature 457(7225): 115-118.
Hilf, R. J. C. and R. Dutzler (2009b). "A prokaryotic perspective on pentameric ligand-gated ion channel structure." Curr Opin Struct Biol 19(4): 418-424.
Holland, I. B. and M. A. Blight (1999). "ABC-ATPases, adaptable energy generators fuelling transmembrane movement of a variety of molecules in organisms from bacteria to humans." J Mol Biol 293(2): 381-99.
Hollenstein, K., R. J. P. Dawson, et al. (2007). "Structure and mechanism of ABC transporter proteins." Current Opinion in Structural Biology 17(4): 412-418.
Hollenstein, K., D. C. Frei, et al. (2007). "Structure of an ABC transporter in complex with its binding protein." Nature 446(7132): 213-6.
Hooper, D. C. (2000). "Mechanisms of action and resistance of older and newer fluoroquinolones." Clin Infect Dis 31 Suppl 2: S24-8.
Hooper, D. C. (2002). "Fluoroquinolone resistance among Gram-positive cocci." Lancet Infect Dis 2(9): 530-8.
Hu, Q., R. J. Noll, et al. (2005). "The Orbitrap: a new mass spectrometer." J Mass Spectrom 40(4): 430-43.
Huang, Y., M. J. Lemieux, et al. (2003). "Structure and mechanism of the glycerol-3-phosphate transporter from Escherichia coli." Science 301(5633): 616-20.
Hung, L. W., I. X. Wang, et al. (1998). "Crystal structure of the ATP-binding subunit of an ABC transporter." Nature 396(6712): 703-7.
Hvorup, R. N., B. A. Goetz, et al. (2007). "Asymmetry in the structure of the ABC transporter-binding protein complex BtuCD-BtuF." Science 317(5843): 1387-90.
Isenbarger, T. A., C. E. Carr, et al. (2008). "The most conserved genome segments for life detection on Earth and other planets." Orig Life Evol Biosph 38(6): 517-33.
Jacoby, G. A. and L. S. Munoz-Price (2005). "The new beta-lactamases." N Engl J Med 352(4): 380-91.
Janin, J., R. P. Bahadur, et al. (2008). "Protein-protein interaction and quaternary structure." Q Rev Biophys 41(2): 133-80.
Jones, P. M., M. L. O'Mara, et al. (2009). "ABC transporters: a riddle wrapped in a mystery inside an enigma." Trends Biochem Sci 34(10): 520-31.
Juliano, R. L. and V. Ling (1976). "A surface glycoprotein modulating drug permeability in Chinese hamster ovary cell mutants." Biochim Biophys Acta 455(1): 152-62.
Kaatz, G. W., F. McAleese, et al. (2005). "Multidrug resistance in Staphylococcus aureus due to overexpression of a novel multidrug and toxin extrusion (MATE) transport protein." Antimicrob Agents Chemother 49(5): 1857-64.
Kabsch, W. and C. Sander (1983). "Dictionary of protein secondary structure: pattern recognition of hydrogen-bonded and geometrical features." Biopolymers 22(12): 2577-637.
Kadaba, N. S., J. T. Kaiser, et al. (2008). "The high-affinity E. coli methionine ABC transporter: structure and allosteric regulation." Science 321(5886): 250-3.
Kaltashov, I. A., C. E. Bobst, et al. (2009). "H/D exchange and mass spectrometry in the studies of protein conformation and dynamics: is there a need for a top-down approach?" Anal Chem 81(19): 7892-9.
Katta, V. and B. T. Chait (1991). "Conformational changes in proteins probed by hydrogen-exchange electrospray-ionization mass spectrometry." Rapid Commun Mass Spectrom 5(4): 214-7.

Kebarle, P. and L. Tang (1993). "From Ions in Solution to Ions in the Gas-Phase - the Mechanism of Electrospray Mass-Spectrometry." Anal Chem 65(22): A972-A986.
Kebarle, P. and U. H. Verkerk (2009). "Electrospray: from ions in solution to ions in the gas phase, what we know now." Mass Spectrom Rev 28(6): 898-917.
Kelleher, N. L., H. Y. Lin, et al. (1999). "Top Down versus Bottom Up Protein Characterization by Tandem High-Resolution Mass Spectrometry." J Am Chem Soc 121(4): 806-812.
Kerfoot, S. A. and M. L. Gross (2011). Chemical Footprinting for Determining Protein Properties and Interactions. Protein and Peptide Mass Spectrometry in Drug Discovery, John Wiley & Sons, Inc.: 175-211.
Khakh, B. S. (2001). "Molecular physiology of p2x receptors and atp signalling at synapses." Nat Rev Neurosci 2(3): 165-174.
Ko, D. C., M. D. Gordon, et al. (2001). "Dynamic movements of organelles containing Niemann-Pick C1 protein: NPC1 involvement in late endocytic events." Mol Biol Cell 12(3): 601-14.
Koestler, M., D. Kirsch, et al. (2008). "A high-resolution scanning microprobe matrix-assisted laser desorption/ionization ion source for imaging analysis on an ion trap/Fourier transform ion cyclotron resonance mass spectrometer." Rapid Commun Mass Spectrom 22(20): 3275-85.
Konermann, L., J. Pan, et al. (2011). "Hydrogen exchange mass spectrometry for studying protein structure and dynamics." Chem Soc Rev 40(3): 1224-34.
Konermann, L. and D. A. Simmons (2003). "Protein-folding kinetics and mechanisms studied by pulse-labeling and mass spectrometry." Mass Spectrom Rev 22(1): 1-26.
Koronakis, V., A. Sharff, et al. (2000). "Crystal structure of the bacterial membrane protein TolC central to multidrug efflux and protein export." Nature 405(6789): 914-9.
Krugel, H., A. Licht, et al. (2010). "Cervimycin C resistance in Bacillus subtilis is due to a promoter up-mutation and increased mRNA stability of the constitutive ABC-transporter gene bmrA." FEMS Microbiol Lett 313(2): 155-63.
Kuroda, T. and T. Tsuchiya (2009). "Multidrug efflux transporters in the MATE family." Biochim Biophys Acta 1794(5): 763-768.
Kwart, H., L. P. Kuiin, et al. (1954). "The Rates and Equilibria of Hydrogen-Deuterium Exchange in Hydroxylic Compounds." J Am Chem Soc 76(23): 5998-6001.
Lam, V. H., J. H. Lee, et al. (2011). "Pathways of transport protein evolution: recent advances." Biol Chem 392(1-2): 5-12.
Law, C. J., P. C. Maloney, et al. (2008). "Ins and outs of major facilitator superfamily antiporters." Annu Rev Microbiol 62: 289-305.
Le Novere, N. and J. P. Changeux (1999). "The Ligand Gated Ion Channel Database." Nucleic Acids Res 27(1): 340-2.
Lee, W. Y. and S. M. Sine (2005). "Principal pathway coupling agonist binding to channel gating in nicotinic receptors." Nature 438(7065): 243-7.
Lewinson, O., J. Adler, et al. (2006). "Promiscuity in multidrug recognition and transport: the bacterial MFS Mdr transporters." Mol Microbiol 61(2): 277-84.
Linton, K. J. (2007). "Structure and function of ABC transporters." Physiology (Bethesda) 22: 122-30.
Locher, K. P., A. T. Lee, et al. (2002). "The E. coli BtuCD structure: a framework for ABC transporter architecture and mechanism." Science 296(5570): 1091-8.
Lowry, O. H., N. J. Rosebrough, et al. (1951). "Protein measurement with the Folin phenol reagent." J Biol Chem 193(1): 265-75.
Ma, D., D. N. Cook, et al. (1995). "Genes acrA and acrB encode a stress-induced efflux system of Escherichia coli." Mol Microbiol 16(1): 45-55.

Ma, Y., A. Erkner, et al. (2002). "Hedgehog-mediated patterning of the mammalian embryo requires transporter-like function of dispatched." Cell 111(1): 63-75.
Maden, B. E. (2000). "Tetrahydrofolate and tetrahydromethanopterin compared: functionally distinct carriers in C1 metabolism." Biochem J 350 Pt 3: 609-29.
Magalhaes, J. V., J. Liu, et al. (2007). "A gene in the multidrug and toxic compound extrusion (MATE) family confers aluminum tolerance in sorghum." Nat Genet 39(9): 1156-61.
Maliepaard, M., G. L. Scheffer, et al. (2001). "Subcellular localization and distribution of the breast cancer resistance protein transporter in normal human tissues." Cancer Res 61(8): 3458-64.
Man, P., C. Montagner, et al. (2007). "Defining the interacting regions between apomyoglobin and lipid membrane by hydrogen/deuterium exchange coupled to mass spectrometry." J Mol Biol 368(2): 464-72.
March, R. E. (1997). "An Introduction to Quadrupole Ion Trap Mass Spectrometry." J Mass Spectrom 32(4): 351-369.
March, R. E. (2009). "Quadrupole ion traps." Mass Spectrom Rev 28(6): 961-89.
Marcoux, J., P. Man, et al. (2010). "p47phox molecular activation for assembly of the neutrophil NADPH oxidase complex." J Biol Chem 285(37): 28980-90.
Marcoux, J., E. Thierry, et al. (2009). "Investigating alternative acidic proteases for H/D exchange coupled to mass spectrometry: plasmepsin 2 but not plasmepsin 4 is active under quenching conditions." J Am Soc Mass Spectrom 21(1): 76-9.
Marcsisin, S. R. and J. R. Engen (2010). "Hydrogen exchange mass spectrometry: what is it and what can it tell us?" Anal Bioanal Chem 397(3): 967-72.
Marquardt, J. L., E. D. Brown, et al. (1994). "Kinetics, stoichiometry, and identification of the reactive thiolate in the inactivation of UDP-GlcNAc enolpyruvoyl transferase by the antibiotic fosfomycin." Biochemistry 33(35): 10646-51.
Marshall, A. G., C. L. Hendrickson, et al. (1998). "Fourier transform ion cyclotron resonance mass spectrometry: a primer." Mass Spectrom Rev 17(1): 1-35.
Maw, M. A., B. Kennedy, et al. (1997). "Mutation of the gene encoding cellular retinaldehyde-binding protein in autosomal recessive retinitis pigmentosa." Nat Genet 17(2): 198-200.
McLuckey, S. A. and J. L. Stephenson, Jr. (1998). "Ion/ion chemistry of high-mass multiply charged ions." Mass Spectrom Rev 17(6): 369-407.
Medzihradszky, K. F. (2005). "Peptide sequence analysis." Methods Enzymol 402: 209-44.
Mikesh, L. M., B. Ueberheide, et al. (2006). "The utility of ETD mass spectrometry in proteomic analysis." Biochim Biophys Acta 1764(12): 1811-1822.
Miranker, A., C. V. Robinson, et al. (1993). "Detection of transient protein folding populations by mass spectrometry." Science 262(5135): 896-900.
Miroux, B. and J. E. Walker (1996). "Over-production of proteins in Escherichia coli: mutant hosts that allow synthesis of some membrane proteins and globular proteins at high levels." J Mol Biol 260(3): 289-98.
Miyazawa, A., Y. Fujiyoshi, et al. (2003). "Structure and gating mechanism of the acetylcholine receptor pore." Nature 423(6943): 949-955.
Morita, Y., K. Kodama, et al. (1998). "NorM, a putative multidrug efflux protein, of Vibrio parahaemolyticus and its homolog in Escherichia coli." Antimicrob Agents Chemother 42(7): 1778-82.
Mueller, D. R., H. Voshol, et al. (2007). "LC-MALDI MS and MS/MS - an efficient tool in proteome analysis." Subcell Biochem 43: 355-80.
Murakami, S. (2008). "Multidrug efflux transporter, AcrB--the pumping mechanism." Curr Opin Struct Biol 18(4): 459-65.

Murakami, S., R. Nakashima, et al. (2006). "Crystal structures of a multidrug transporter reveal a functionally rotating mechanism." Nature 443(7108): 173-9.
Murakami, S., R. Nakashima, et al. (2002). "Crystal structure of bacterial multidrug efflux transporter AcrB." Nature 419(6907): 587-93.
Neu, H. C. and T. D. Gootz (1996). "Antimicrobial Chemotherapy."
Newstead, S., D. Drew, et al. (2011). "Crystal structure of a prokaryotic homologue of the mammalian oligopeptide-proton symporters, PepT1 and PepT2." Embo J 30(2): 417-26.
Nikaido, H. (2009). "Multidrug resistance in bacteria." Annu Rev Biochem 78: 119-46.
Nikaido, H., M. Basina, et al. (1998). "Multidrug efflux pump AcrAB of Salmonella typhimurium excretes only those beta-lactam antibiotics containing lipophilic side chains." J Bacteriol 180(17): 4686-92.
Nikaido, H. and Y. Takatsuka (2009). "Mechanisms of RND multidrug efflux pumps." Biochim Biophys Acta 1794(5): 769-781.
Nishino, K. and A. Yamaguchi (2001). "Analysis of a complete library of putative drug transporter genes in Escherichia coli." J Bacteriol 183(20): 5803-12.
North, R. A. (2002). "Molecular physiology of P2X receptors." Physiol Rev 82(4): 1013-67.
Nury, H., C. Dahout-Gonzalez, et al. (2006). "Relations between structure and function of the mitochondrial ADP/ATP carrier." Annu Rev Biochem 75: 713-41.
Oancea, G., M. L. O'Mara, et al. (2009). "Structural arrangement of the transmission interface in the antigen ABC transport complex TAP." Proc Natl Acad Sci U S A 106(14): 5551-6.
Oldham, M. L. and J. Chen (2011). "Snapshots of the maltose transporter during ATP hydrolysis." Proc Natl Acad Sci U S A 108(37): 15152-6.
Oldham, M. L., A. L. Davidson, et al. (2008). "Structural insights into ABC transporter mechanism." Curr Opin Struct Biol 18(6): 726-733.
Oldham, M. L., D. Khare, et al. (2007). "Crystal structure of a catalytic intermediate of the maltose transporter." Nature 450(7169): 515-21.
Orelle, C., O. Dalmas, et al. (2003). "The conserved glutamate residue adjacent to the Walker-B motif is the catalytic base for ATP hydrolysis in the ATP-binding cassette transporter BmrA." J Biol Chem 278(47): 47002-8.
Orelle, C., F. Gubellini, et al. (2008). "Conformational Change Induced by ATP Binding in the Multidrug ATP-Binding Cassette Transporter BmrA " Biochemistry 47(8): 2404-2412.
Paizs, B. and S. Suhai (2005). "Fragmentation pathways of protonated peptides." Mass Spectrom Rev 24(4): 508-48.
Pan, J., J. Han, et al. (2009). "Hydrogen/deuterium exchange mass spectrometry with top-down electron capture dissociation for characterizing structural transitions of a 17 kDa protein." J Am Chem Soc 131(35): 12801-8.
Pan, J., J. Han, et al. (2010). "Characterizing short-lived protein folding intermediates by top-down hydrogen exchange mass spectrometry." Anal Chem 82(20): 8591-7.
Parry, C. M. (2003). "Antimicrobial drug resistance in Salmonella enterica." Curr Opin Infect Dis 16(5): 467-72.
Pascal, B. D., M. J. Chalmers, et al. (2007). "The Deuterator: software for the determination of backbone amide deuterium levels from H/D exchange MS data." BMC Bioinformatics 8: 156.
Perichon, B. and P. Courvalin (2000). "Update on vancomycin resistance." Int J Clin Pract Suppl(115): 88-93.

Perkins, D. N., D. J. C. Pappin, et al. (1999). "Probability-based protein identification by searching sequence databases using mass spectrometry data." Electrophoresis 20(18): 3551-3567.
Perry, R. H., R. G. Cooks, et al. (2008). "Orbitrap mass spectrometry: Instrumentation, ion motion and applications." Mass Spectrom Rev 27(6): 661-699.
Peter-Katalinic, J. (2005). "Methods in enzymology: O-glycosylation of proteins." Methods Enzymol 405: 139-71.
Petsko, G. A. (2007). "And the second shall be first." Genome Biol 8(2): 103.
Pinkett, H. W., A. T. Lee, et al. (2007). "An inward-facing conformation of a putative metal-chelate-type ABC transporter." Science 315(5810): 373-7.
Pittenauer, E. and G. Allmaier (2009). "High-energy collision induced dissociation of biomolecules: MALDI-TOF/RTOF mass spectrometry in comparison to tandem sector mass spectrometry." Comb Chem High Throughput Screen 12(2): 137-55.
Poole, K. (2001). "Multidrug resistance in Gram-negative bacteria." Curr Opin Microbiol 4(5): 500-8.
Poutanen, M., L. Salusjärvi, et al. (2001). "Use of matrix-assisted laser desorption/ionization time-of-flight mass mapping and nanospray liquid chromatography/electrospray ionization tandem mass spectrometry sequence tag analysis for high sensitivity identification of yeast proteins separated by two-dimensional gel electrophoresis." Rapid Commun Mass Spectrom 15(18): 1685-1692.
Procko, E. and R. Gaudet (2009). "Antigen processing and presentation: TAPping into ABC transporters." Curr Opin Immunol 21(1): 84-91.
Pullman, M. E., H. S. Penefsky, et al. (1960). "Partial resolution of the enzymes catalyzing oxidative phosphorylation. I. Purification and properties of soluble dinitrophenol-stimulated adenosine triphosphatase." J Biol Chem 235: 3322-9.
Raut, J. S., S. Akella, et al. (2009). "Catastrophic drop breakup in electric field." Langmuir 25(9): 4829-34.
Ravaud, S., M. A. Do Cao, et al. (2006). "The ABC transporter BmrA from Bacillus subtilis is a functional dimer when in a detergent-solubilized state." Biochem J 395(2): 345-53.
Reece, R. J. and A. Maxwell (1991). "DNA gyrase: structure and function." Crit Rev Biochem Mol Biol 26(3-4): 335-75.
Rees, D. C., E. Johnson, et al. (2009). "ABC transporters: the power to change." Nat Rev Mol Cell Biol 10(3): 218-27.
Reiber, D. C., T. A. Grover, et al. (1998). "Identifying proteins using matrix-assisted laser desorption/ionization in-source fragmentation data combined with database searching." Anal Chem 70(4): 673-683.
Ren, Q. and I. T. Paulsen (2005). "Comparative analyses of fundamental differences in membrane transport capabilities in prokaryotes and eukaryotes." PLoS Comput Biol 1(3): e27.
Ren, Q. and I. T. Paulsen (2007). "Large-scale comparative genomic analyses of cytoplasmic membrane transport systems in prokaryotes." J Mol Microbiol Biotechnol 12(3-4): 165-79.
Rey, M., P. Man, et al. (2009). "Recombinant immobilized rhizopuspepsin as a new tool for protein digestion in hydrogen/deuterium exchange mass spectrometry." Rapid Commun Mass Spectrom 23(21): 3431-8.
Rey, M., P. Man, et al. (2010). "Conformational dynamics of the bovine mitochondrial ADP/ATP carrier isoform 1 revealed by hydrogen/deuterium exchange coupled to mass spectrometry." J Biol Chem 285(45): 34981-90.

Rey, M., H. Mrazek, et al. (2010). "Effective removal of nonionic detergents in protein mass spectrometry, hydrogen/deuterium exchange, and proteomics." Anal Chem 82(12): 5107-16.
Richards, F. M. and C. E. Kundrot (1988). "Identification of structural motifs from protein coordinate data: secondary structure and first-level supersecondary structure." Proteins 3(2): 71-84.
Rodgers, R. P., F. M. White, et al. (1998). "Resolution, elemental composition, and simultaneous monitoring by Fourier transform ion cyclotron resonance mass spectrometry of organosulfur species before and after diesel fuel processing." Anal Chem 70(22): 4743-4750.
Romanov, V., U. H. Verkerk, et al. (2009). "Threshold collision-induced dissociation measurements using a ring ion guide as the collision cell in a triple-quadrupole mass spectrometer." Anal Chem 81(16): 6805-12.
Rose, G. D., P. J. Fleming, et al. (2006). "A backbone-based theory of protein folding." Proc Natl Acad Sci U S A 103(45): 16623-33.
Rose, G. D. and R. Wolfenden (1993). "Hydrogen bonding, hydrophobicity, packing, and protein folding." Annu Rev Biophys Biomol Struct 22: 381-415.
Sadygov, R. G., H. Liu, et al. (2004). "Statistical models for protein validation using tandem mass spectral data and protein amino acid sequence databases." Anal Chem 76(6): 1664-71.
Saier, M. H., Jr. (2003). "Tracing pathways of transport protein evolution." Mol Microbiol 48(5): 1145-56.
Saiz, L. and J. M. Vilar (2008). "Protein-protein/DNA interaction networks: versatile macromolecular structures for the control of gene expression." IET Syst Biol 2(5): 247-55.
Sarkadi, B., L. Homolya, et al. (2006). "Human multidrug resistance ABCB and ABCG transporters: participation in a chemoimmunity defense system." Physiol Rev 86(4): 1179-236.
Scheffers, D. J. and M. G. Pinho (2005). "Bacterial cell wall synthesis: new insights from localization studies." Microbiol Mol Biol Rev 69(4): 585-607.
Schneider, M. C., B. E. Prosser, et al. (2009). "Neisseria meningitidis recruits factor H using protein mimicry of host carbohydrates." Nature 458(7240): 890-3.
Schuldiner, S. (2009). "EmrE, a model for studying evolution and mechanism of ion-coupled transporters." Biochim Biophys Acta 1794(5): 748-62.
Seeger, M. A., A. Schiefner, et al. (2006). "Structural asymmetry of AcrB trimer suggests a peristaltic pump mechanism." Science 313(5791): 1295-8.
Selkoe, D. J. (2003). "Folding proteins in fatal ways." Nature 426(6968): 900-4.
Selwyn, S. (1979). "Pioneer work on the 'penicillin phenomenon', 1870-1876." J Antimicrob Chemother 5(3): 249-55.
Shakil, S., R. Khan, et al. (2008). "Aminoglycosides versus bacteria--a description of the action, resistance mechanism, and nosocomial battleground." J Biomed Sci 15(1): 5-14.
Sharon, M. and C. V. Robinson (2007). The role of mass Spectrometry in structure elucidation of dynamic protein complexes. Annu Rev Biochem. Palo Alto, Annual Reviews. 76: 167-193.
Sharoni, M., S. Steiner-Mordoch, et al. (2005). "Exploring the binding domain of EmrE, the smallest multidrug transporter." J Biol Chem 280(38): 32849-55.
Sheppard, D. N. and M. J. Welsh (1999). "Structure and function of the CFTR chloride channel." Physiol Rev 79(1 Suppl): S23-45.

Shi, Y. and J. Wu (2007). "Structural basis of protein-protein interaction studied by NMR." J Struct Funct Genomics 8(2-3): 67-72.
Sine, S. M. and A. G. Engel (2006). "Recent advances in Cys-loop receptor structure and function." Nature 440(7083): 448-55.
Siuzdak, G. (2006). The Expanding Role of Mass Spectrometry in Biotechnology, Second Edition, MCC Press.
Slysz, G. W., C. A. Baker, et al. (2009). "Hydra: software for tailored processing of H/D exchange data from MS or tandem MS analyses." BMC Bioinformatics 10: 162.
Smith, R. D., J. A. Loo, et al. (1991). "Principles and practice of electrospray ionization—mass spectrometry for large polypeptides and proteins." Mass Spectrom Rev 10(5): 359-452.
Sommer, H., H. A. Thomas, et al. (1951). "The Measurement of e/M by Cyclotron Resonance." Phys Rev 82(5): 697.
Spizek, J. and T. Rezanka (2004). "Lincomycin, cultivation of producing strains and biosynthesis." Appl Microbiol Biotechnol 63(5): 510-9.
Steinfels, E., C. Orelle, et al. (2004). "Characterization of YvcC (BmrA), a multidrug ABC transporter constitutively expressed in Bacillus subtilis." Biochemistry 43(23): 7491-502.
Studier, F. W., A. H. Rosenberg, et al. (1990). "Use of T7 RNA polymerase to direct expression of cloned genes." Methods Enzymol 185: 60-89.
Suchanova, B. and R. Tuma (2008). "Folding and assembly of large macromolecular complexes monitored by hydrogen-deuterium exchange and mass spectrometry." Microb Cell Fact 7: 12.
Sweet, S. M. and H. J. Cooper (2007). "Electron capture dissociation in the analysis of protein phosphorylation." Expert Rev Proteomics 4(2): 149-59.
Sweet, S. M. and H. J. Cooper (2009). "On-line liquid chromatography electron capture dissociation for the characterization of phosphorylation sites in proteins." Methods Mol Biol 527: 191-9, x.
Syka, J. E. P., J. A. Marto, et al. (2004). "Novel linear quadrupole ion trap/FT mass spectrometer: Performance characterization and use in the comparative analysis of histone H3 post-translational modifications." J Proteome Res 3(3): 621-626.
Szakacs, G., J. K. Paterson, et al. (2006). "Targeting multidrug resistance in cancer." Nat Rev Drug Discov 5(3): 219-34.
Tanaka, K. (2003). "The origin of macromolecule ionization by laser irradiation (Nobel lecture)." Angew Chem Int Ed Engl 42(33): 3860-70.
Tanaka, K., H. Waki, et al. (1988). "Protein and polymer analyses up to m/z 100 000 by laser ionization time-of-flight mass spectrometry." Rapid Commun Mass Spectrom 2(8): 151-153.
Tang, J., M. Luo, et al. (2010). "The crystal structure of hexamer RraA from Pseudomonas aeruginosa reveals six conserved protein-protein interaction sites." Protein J 29(8): 583-90.
Tang, X., J. E. Bruce, et al. (2006). "Characterizing electrospray ionization using atmospheric pressure ion mobility spectrometry." Anal Chem 78(22): 7751-60.
Tarassov, K., V. Messier, et al. (2008). "An in vivo map of the yeast protein interactome." Science 320(5882): 1465-70.
Tasneem, A., L. M. Iyer, et al. (2005). "Identification of the prokaryotic ligand-gated ion channels and their implications for the mechanisms and origins of animal Cys-loop ion channels." Genome Biol 6(1): R4.

Taylor, P., T. T. Talley, et al. (2007). "Structure-guided drug design: conferring selectivity among neuronal nicotinic receptor and acetylcholine-binding protein subtypes." Biochem Pharmacol 74(8): 1164-71.
Then, R. L. (2004). "Antimicrobial dihydrofolate reductase inhibitors--achievements and future options: review." J Chemother 16(1): 3-12.
Thevenon-Emeric, G., J. Kozlowski, et al. (1992). "Determination of amide hydrogen exchange rates in peptides by mass spectrometry." Anal Chem 64(20): 2456-8.
Tichelaar, W., M. Safferling, et al. (2004). "The Three-dimensional Structure of an Ionotropic Glutamate Receptor Reveals a Dimer-of-dimers Assembly." J Mol Biol 344(2): 435-42.
Tornroth-Horsefield, S., P. Gourdon, et al. (2007). "Crystal structure of AcrB in complex with a single transmembrane subunit reveals another twist." Structure 15(12): 1663-73.
Torres, C., C. Galian, et al. (2009). "The YheI/YheH heterodimer from Bacillus subtilis is a multidrug ABC transporter." Biochim Biophys Acta 1788(3): 615-22.
Traynelis, S. F., L. P. Wollmuth, et al. (2010). "Glutamate Receptor Ion Channels: Structure, Regulation, and Function." Pharmacol Rev 62(3): 405-496.
Tsuchida, A., T. Yamauchi, et al. (2005). "Nuclear receptors as targets for drug development: molecular mechanisms for regulation of obesity and insulin resistance by peroxisome proliferator-activated receptor gamma, CREB-binding protein, and adiponectin." J Pharmacol Sci 97(2): 164-70.
Tsuda, M., T. Terada, et al. (2009). "Targeted disruption of the multidrug and toxin extrusion 1 (mate1) gene in mice reduces renal secretion of metformin." Mol Pharmacol 75(6): 1280-6.
Ubarretxena-Belandia, I., J. M. Baldwin, et al. (2003). "Three-dimensional structure of the bacterial multidrug transporter EmrE shows it is an asymmetric homodimer." Embo J 22(23): 6175-81.
Vaara, M. (1993). "Antibiotic-supersusceptible mutants of Escherichia coli and Salmonella typhimurium." Antimicrob Agents Chemother 37(11): 2255-60.
van der Heide, T. and B. Poolman (2002). "ABC transporters: one, two or four extracytoplasmic substrate-binding sites?" EMBO Rep 3(10): 938-43.
van Heijenoort, J. (2001). "Formation of the glycan chains in the synthesis of bacterial peptidoglycan." Glycobiology 11(3): 25R-36R.
Walker, J. E., M. Saraste, et al. (1982). "Distantly related sequences in the alpha- and beta-subunits of ATP synthase, myosin, kinases and other ATP-requiring enzymes and a common nucleotide binding fold." Embo J 1(8): 945-51.
Wang, H., E. W. Lee, et al. (2008). "Membrane topology of the human breast cancer resistance protein (BCRP/ABCG2) determined by epitope insertion and immunofluorescence." Biochemistry 47(52): 13778-87.
Ward, A., C. L. Reyes, et al. (2007). "Flexibility in the ABC transporter MsbA: Alternating access with a twist." Proc Natl Acad Sci U S A 104(48): 19005-10.
Weber, G. F., S. Ashkar, et al. (1996). "Receptor-ligand interaction between CD44 and osteopontin (Eta-1)." Science 271(5248): 509-12.
Weis, D. D., J. R. Engen, et al. (2006). "Semi-automated data processing of hydrogen exchange mass spectra using HX-Express." J Am Soc Mass Spectrom 17(12): 1700-3.
Weis, D. D., T. E. Wales, et al. (2006). "Identification and characterization of EX1 kinetics in H/D exchange mass spectrometry by peak width analysis." J Am Soc Mass Spectrom 17(11): 1498-509.
Wells, J. M. and S. A. McLuckey (2005). "Collision-induced dissociation (CID) of peptides and proteins." Methods Enzymol 402: 148-85.

West, G. M., E. Y. Chien, et al. (2011). "Ligand-Dependent Perturbation of the Conformational Ensemble for the GPCR beta(2) Adrenergic Receptor Revealed by HDX." Structure 19(10): 1424-32.
Wiley, W. C. and I. H. McLaren (1955). "Time-of-Flight Mass Spectrometer with Improved Resolution." Rev Sci Instrum 26(12): 1150-1157.
Wilkinson, A. J., and K. H. G. Verschueren. (2003). "Crystal structures of periplasmic solute-binding proteins in ABC transport complexes illuminate their function." In I. B. Holland, S. P. C. Cole, K. Kuchler, and C. F. Higgins (ed.), ABC proteins: from bacteria to man. Academic Press, London, United Kingdom.: 187-207.
Wilm, M., A. Shevchenko, et al. (1996). "Femtomole sequencing of proteins from polyacrylamide gels by nano-electrospray mass spectrometry." Nature 379(6564): 466-9.
Wright, G. D. (2005). "Bacterial resistance to antibiotics: enzymatic degradation and modification." Adv Drug Deliv Rev 57(10): 1451-70.
Wu, B., E. Y. Chien, et al. (2010). "Structures of the CXCR4 chemokine GPCR with small-molecule and cyclic peptide antagonists." Science 330(6007): 1066-71.
Wu, C. C. and J. R. Yates, 3rd (2003). "The application of mass spectrometry to membrane proteomics." Nat Biotechnol 21(3): 262-7.
Xu, C. and B. Ma (2006). "Complexity and scoring function of MS/MS peptide de novo sequencing." Comput Syst Bioinformatics Conf: 361-9.
Yang, H. and D. L. Smith (1997). "Kinetics of cytochrome c folding examined by hydrogen exchange and mass spectrometry." Biochemistry 36(48): 14992-9.
Yao, X. J., G. Velez Ruiz, et al. (2009). "The effect of ligand efficacy on the formation and stability of a GPCR-G protein complex." Proc Natl Acad Sci U S A 106(23): 9501-6.
Yerushalmi, H. and S. Schuldiner (2000). "An essential glutamyl residue in EmrE, a multidrug antiporter from Escherichia coli." J Biol Chem 275(8): 5264-9.
Yin, Y., X. He, et al. (2006). "Structure of the multidrug transporter EmrD from Escherichia coli." Science 312(5774): 741-4.
Yinon, J. and D. G. Hwang (1984). "Metabolic studies of explosives. 1--EI and CI mass spectrometry of metabolites of 2,4,6-trinitrotoluene." Biomed Mass Spectrom 11(11): 594-600.
Yu, E. W., G. McDermott, et al. (2003). "Structural basis of multiple drug-binding capacity of the AcrB multidrug efflux pump." Science 300(5621): 976-80.
Yusibov, V. and S. J. Streatfield (2010). "Plant-produced microbial vaccines: Alexander V. Karasev, editor: Current topics in microbiology and immunology 2009; v. 332." Hum Vaccin 6(9).
Zaitseva, J., S. Jenewein, et al. (2005). "H662 is the linchpin of ATP hydrolysis in the nucleotide-binding domain of the ABC transporter HlyB." EMBO J 24(11): 1901-1910.
Zhang, Z. and A. G. Marshall (1998). "A universal algorithm for fast and automated charge state deconvolution of electrospray mass-to-charge ratio spectra." J Am Soc Mass Spectrom 9(3): 225-33.
Zhang, Z. and D. L. Smith (1993). "Determination of amide hydrogen exchange by mass spectrometry: a new tool for protein structure elucidation." Protein Sci 2(4): 522-31.
Zolnerciks, J. K., C. Wooding, et al. (2007). "Evidence for a Sav1866-like architecture for the human multidrug transporter P-glycoprotein." Faseb J 21(14): 3937-48.
Zutz, A., J. Hoffmann, et al. (2011). "Asymmetric ATP hydrolysis cycle of the heterodimeric multidrug ABC transport complex TmrAB from Thermus thermophilus." J Biol Chem 286(9): 7104-15.

Abstract

Some ATP-Binding Cassette exporters are known to be responsible for resistance against a broad spectrum of antibiotics and chemotherapeutic drugs in bacteria and mammalian cells.
Amide hydrogen deuterium exchange coupled to mass spectrometry (HDX-MS) was applied to investigate the conformational changes in two different bacterial ABC exporters, BmrA and BmrC/BmrD, in the presence and absence of nucleotide. Local H/D exchange kinetics showed highly dynamic nature of ICDs in apo form which was not anticipated from X-ray structure of the homologue proteins. In outward facing (closed form) conformation the movement of ICDs were largely reduced for both transporters. The H/D exchange kinetics of closed form were determined by applying H/D exchange on mutants unable to hydrolyze nucleotides or on wild-type inhibited by vanadate. The dynamics of NBDs particularly for those regions which interact during ATP hydrolysis were also reduced in closed form as compared to open one. The addition of different drugs which are known to be transported by ABC transporters did not affect dynamics of NBDs.
We further applied H/D exchange kinetics on a prokaryotic homologue of pentameric ligand-gated ion channel (pLGIC) GLIC. Local H/D exchange kinetics were in full agreement with the available structure and change in pH showed differences in deuterium level for interacting regions of the subunits.

Des exporteurs « ATP-Binding Cassette » (ABC) sont connus pour être responsables de la résistance contre un large spectre d'agents antibiotiques ou chimiothérapeutiques chez les bactéries et les cellules de mammifères.
L'échange hydrogène / deutérium associé à la spectrométrie de masse (HDX-MS) a été utilisé pour caractériser les changements conformationnels de deux exporteurs ABC bactériens, BmrA et BmrC/BmrD, en présence et en absence de nucléotide. Les cinétiques locales d'HDX ont montré la nature hautement dynamique des domaines intra-cellulaires (ICDs) dans la forme apo, ce qui n'était pas attendu d'après les structures cristallographiques aux rayons X des protéines homologues. Dans la conformation ouverte vers l'extérieur (« outward facing »), domaines fixant les nucléotides (NBDs) interagissant, le mouvement des ICDs sont largement réduits pour les deux transporteurs. Les cinétiques d'HDX MS dans la conformation « outward facing » ont été déterminées en appliquant cette technique sur des mutants incapables d'hydrolyser les nucléotides et sur la forme sauvage inhibée au vanadate. La dynamique des NBDs, en particulier pour les régions qui interagissent au cours de l'hydrolyse de l'ATP, a été aussi diminuée dans la conformation « outward facing » comparativement à celle ouverte vers l'intérieur. L'ajout de différents agents connus pour être transportés par des transporteurs ABC n'a pas affecté la dynamique des NBDs.
Par ailleurs, nous avons aussi appliqué l'HDX MS à la protéine GLIC, un homologue procaryote d'un « ligand-gated ion channel » pentamérique (pLGIC). Les cinétiques locales d'HDX sont en plein accord avec la structure cristallographique disponible et le changement de pH révèle des différences de deutération dans les régions d'interaction des sous-unités.